AMR Unit of Mineral Processing

ANTS Anthropogenic Material Cycles

RWTH AACHEN UNIVERSITY

OPEN ACCESS

SBSC 2024

10th Sensor-Based Sorting & Control

Kathrin Greiff,
Alexander Feil,
Lars Weitkämper,
Nils Kroell,
Tabea Scherling,
Devrim Gürsel,
Vincent Merz (eds.)

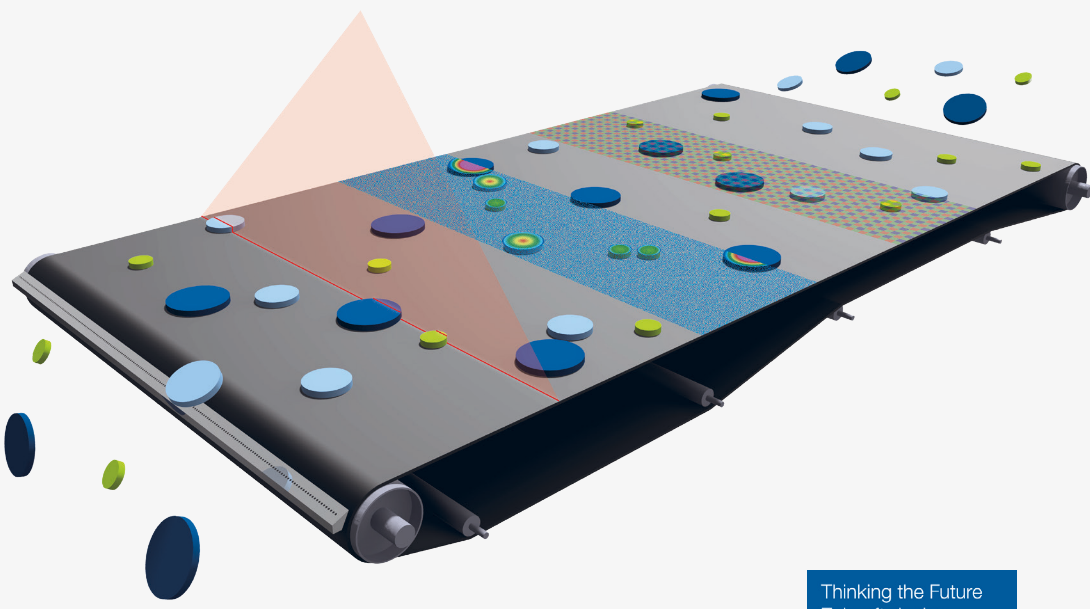

Thinking the Future
Zukunft denken

Sensor-Based Sorting & Control

Kathrin Greiff, Alexander Feil, Lars Weitkämper, Nils Kroell, Tabea Scherling, Devrim Gürsel, Vincent Merz (eds.)

10th Sensor-Based Sorting & Control 2024

Shaker Verlag
Aachen 2024

Bibliographic information published by the Deutsche Nationalbibliothek
The Deutsche Nationalbibliothek lists this publication in the Deutsche Nationalbibliografie; detailed bibliographic data are available in the Internet at http://dnb.d-nb.de.

Shaker Verlag 2024

Print-ISBN 978-3-8440-9278-3
PDF-ISBN 978-3-8440-9413-8
ISSN 2942-2507
eISSN 2942-2515
https://doi.org/10.2370/9783844094138

Shaker Verlag GmbH • Am Langen Graben 15a • 52353 Düren
Phone: 0049/2421/99011-0 • Telefax: 0049/2421/99011-9
Internet: www.shaker.de • e-mail: info@shaker.de

SBSC 2024

10th Sensor-Based Sorting & Control

Scientific Direction:
Prof. Dr. rer. nat. Kathrin Greiff; Dr.-Ing. Alexander Feil; Dr.-Ing. Nils Kroell, Tabea Scherling, M. Sc.; Devrim Gürsel, M. Sc.; and Vincent Merz, M. Sc. (eds.)

A joint conference of Department of Anthropogenic Material Cycles (ANTS) and the Unit of Mineral Processing (AMR) of RWTH Aachen University. March 13. – 14., 2024 in Aachen, Germany.

Acknowledgements:
This proceeding was made possible thanks to the dedicated efforts of the scientific staff of the ANTS and AMR.

Preface

Dear participants of the SBSC 2024,

A crucial challenge for our generation and those to come is the mindful and sustainable utilization of finite resources within the planetary boundaries. In addition to other industries, this also appears to be especially important for the mining and recycling sectors. Over the past four decades, the advent of sensor technologies and the utilization of machine and deep learning methods has been a catalyst for significant advancements in both sectors, which will be discussed among the expert audience of the SBSC 2024.

A key focus of our conference is the accelerating pace of digitalization and its impact on sensor technology applications. As shown by the contributions of SBSC 2024, we are witnessing an increased focus on the increased exploitation of existing and new data streams and the utilization of sensor technologies both for novel applications as well as the sensor-based sorting of new material flows.

Another highlight of SBSC 2024 is the new panel discussion themed "Closing the Implementation Gap." In this panel, we will discuss with experts from different disciplines and with different perspectives how the transition of technical innovations into practical applications in the sensor-based sorting and control space can be accelerated to meet global challenges and enhance a sustainable development.

As we gather at SBSC 2024, we extend our gratitude to all participants, speakers, and contributors. Your presence and insights are what transform SBSC 2024 into a hub of knowledge and innovation. This conference is not just about sharing advancements; it is about fostering a community committed to the responsible and sustainable use of technology in our industries. Thank you for being a part of SBSC 2024. Here's to another year of new advancements and inspiring exchanges in the world of sensor-based technologies!

Kathrin Greiff, Alexander Feil, Lars Weitkämper, Nils Kroell, Tabea Scherling, Devrim Gürsel, and Vincent Merz

Content

Data Mining Within a Lightweight Packaging Waste Sorting Plant: Long-Term Insights into the Data of a Sensor-Based Sorter

Nikolai Kuhn[1]*, Sabine Schlögl[1], Gerald Koinig[1], Alexia Tischberger-Aldrian[1]

1 Montanuniversität Leoben, Chair of Waste Processing Technology and Waste Management, Leoben, Austria

* Corresponding Author: Franz-Josef Str. 18, 8700 Leoben, nikolai.kuhn@unileoben.ac.at

Keywords: Data Mining, Sensor-based Sorting, Sensor-based Material Flow Characterization, Plant Optimization, Lightweight Packaging Waste, Plastic Recycling

Abstract

Sensor-based material flow monitoring has great potential in sorting plants in general, an implementation based on the data of a sensor-based sorter (SBS) provides an economic advantage compared to the use of additional sensors. In this work, we provide insights into the data stream collected by a SBS positioned at the beginning of the sorting cascade for 3D-shaped particles in a sorting plant for lightweight packaging waste in Austria. The data was analyzed in three regards: A first analysis identifies plant downtimes within a year and allocates them to events such as weekends or public holidays. A second analysis presents the composition of the lightweight packaging material over a year. Here, the mean of the dominating fractions is 45.1% for PET, 16.1% for PE, and 15.4% for PP. Lastly, we examine the seasonal variability of the material composition. Here, no major changes in the composition in terms of mean and standard deviation were observed. Only the share of clear PET bottles increases in summer, whereas a lower share of blue PET bottles at the same time compensates the overall share of PET bottles. The results of this

research indicate the variety of possible applications for monitoring based on SBS data to improve the operational efficiency of the plant.

1 Introduction

Lightweight packaging waste is a heterogeneous mixture in many respects and differs, in material type, particle size, and particle mass. This heterogeneity stems primarily from their wide range of applications and packaged goods. Furthermore, the composition of waste depends also on socio-economic factors such as consumption habits, place of residence, education, but also from systemic influences caused by the collection system and charging scheme for the disposal of other post-consumer wastes (Dehoust & Christiani, 2012; Langner et al., 1998). The basis for recycling is material with a high degree of purity, which can be obtained by sorting the heterogeneous waste in sorting plants (Letcher, 2020). For efficient plant operation, extensive knowledge of the waste composition is important. Typically, such waste characterization is carried out by manual sorting (Langner et al., 1998). However, this is relatively time-consuming, requires a lot of personnel, and is hence often limited to the input and output of a plant. Alternatively, sensors can be used to automate the characterization (Kroell et al., 2023a; Kroell et al., 2024, Schlögl et al., 2022a; Schlögl et al., 2023). This enables gathering inline information from any desired position within a plant at comparatively low costs. For this purpose, either sensors that are already installed, as in sensor-based sorters (SBS), or additional sensors can be used. While the former do not have to be purchased and installed from scratch, the data they collect is only available in most systems in a form that is analyzed in the context of the respective sorting task. It is therefore the more economical solution but poses some challenges regarding implementation and interpretation.

In this research paper, we present insights into a lightweight packaging waste sorting plant in Austria with focus on the material flow over a year and the material composition within the selected periods. This data is of interest to the public, non-governmental organizations, and researchers, but is currently only collected by private actors in Austria and is not made publicly accessible. The latest publicly available study describing the composition of lightweight packaging waste by type of plastic in Austria is based on extrapolation and refers to the reference year 2013 and was published by van Eygen et al. in 2018. In addition, the collection system for lightweight packaging waste in Austria will be harmonized on a federal level from

2025 with the expectation that a higher collection rate will be achieved. Additionally, a deposit system for disposable PET beverage bottles will be introduced in 2025. As a result, the most relevant target fraction of lightweight packaging sorting plants in terms of both economics and mass (Neubauer et al., 2021) will no longer exist. Both measures must be seen in the context of stricter legal targets for plastics recycling within the European Union and pose challenges for the operators of lightweight packaging waste sorting plants. The SBS data not only has the potential to be used for monitoring the plant and, if necessary, optimization or control, but also to provide reliable data for other stakeholders to make plastics recycling more transparent.

In this paper we identify plant downtimes within a year and allocate them to events such as weekends or public holidays, present the composition of the lightweight packaging material according to the sensor data over a year. Furthermore, we examine the seasonal variability of the material composition according to the sensor data through comparison of the mean composition for the months January, March, May, July, September, and November.

2 Materials and Methods

The analyzed data was automatically collected from a SBS equipped with sensors sensitive within the visible and near-infrared range of light. The sorter is part of an Austrian lightweight packaging waste sorting plant and positioned at the beginning of the sorting cascade of 3Dshaped particles. The target fraction of the aggregate are clear PETbottles. The data has a temporal resolution of one minute, totaling at 283,734 measurements. Each measurement contains the pixel sums of the material classes PE, PP, PET bottle clear, PET bottle color, PET bottle blue, PET bottle green, PET blister, PVC, PS, liquid packaging board, cellulose, and other for every pixel that couldn't be assigned to any of the material classes mentioned above.

Data handling and visualization was performed using Matlab, Version 9.13.0.2105380 (R2022b) Update 2 and Microsoft Excel Version 2311. Depending on the respective query, the data was aggregated into different bins (hours, days, weeks, month) and then analyzed according to material composition. In this context, it needs to be noted that for some days only few measurements were available. This stems from the fact that data was only stored when the SBS was in operation. In case the conveyor belt occupancy was low, it is also possible that only a few pixels were recorded within a minute. For example, this could take place when other aggregates malfunction or the plant was seizing or starting operation. Hence, the data aggregation from a time window of a minute to a time window of at least an hour enables the reduction of extremes that result from different incidents, such as input material with high shares of certain, unfavorable, products, overload of the SBS, sudden SBS or plant downtimes, material blockages etc.

3 Results and Discussion

The investigated data represents the material flow through the SBS over one year by material class. The data was examined regarding the material flow through the SBS by material class, the material composition over a year, and potential seasonal variations.

3.1 Material Flow Through the SBS by Material Class

Fig. 1 shows the material flow through the SBS, subdivided by the respective material shares, and based on a daily mean. The material proportions are relatively constant, with a peak of PE in end of February and a peak of PP in mid-May and mid-September. The average PE concentration on that day in February was 24%, which is 9 percentage points above the annual mean. The PP peak in May resulted from the fact that only a few measurements were stored on this day. These measurements contained low shares across all material classes except PP. The PP peak in September is analogous and stems from an average PP concentration exceeding the annual mean of 15% by 4 percentage points.

Plant downtimes can be identified as empty columns in Fig. 1. In addition, downtimes can be associated with events such as weekends or public holidays such as Easter, Christmas, or the Austrian national holiday, which is indicated by arrows at the top of the figure. Several conclusions can be drawn from this. Since the observed downtimes correspond to known events, the timestamps appear to be reliable enough for further analysis within shorter time periods such as months, weeks or even days. As SBS usually operate as black boxes with unknown classification algorithms and settings, this first analysis is a necessary validation of the data stream.

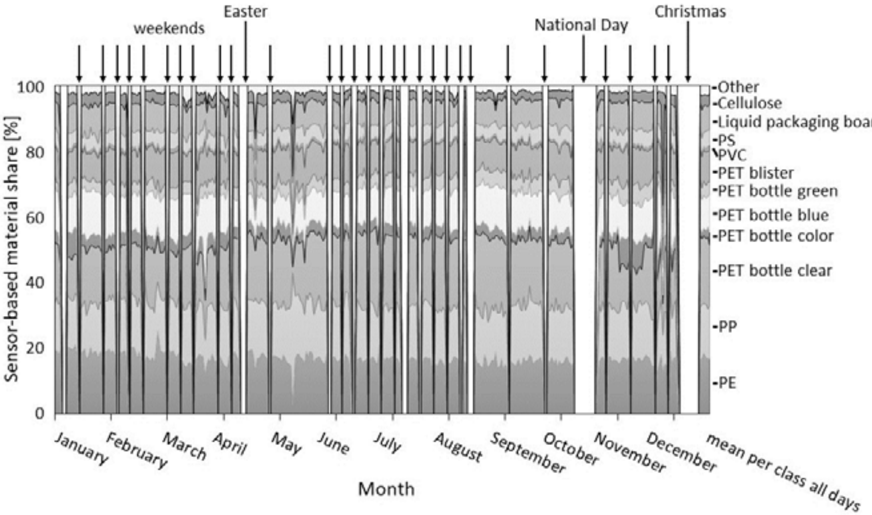

Fig. 1. Sensor-based material shares of the SBS over a year. Downtimes are indicated by arrows on top of the figure. The data was aggregated by day. The examined fractions are PE, PP, PET bottle clear, PET bottle color, PET bottle blue, PET bottle green, PET blister, PVC, PS, Liquid packaging board, Cellulose, and other.

The analysis of SBS data over longer periods allows for monitoring the operation of the plant and investigation of patterns that indicate possible anomalies or correlations. Examples of this could be the origin of the input material, the feeding of the plant, the plant throughput, or the setting of certain aggregates upstream of the SBS. Further, SBS data enables automated monitoring of the general operation of a plant in shorter periods of time. This results from the fact that possible material blockages can be observed, as no material passes the SBS even though the plant control system indicates a running plant. Ultimately, this could lead to an improved operational efficiency of the plant.

3.2 Material Composition Over a Year

In this section, we present the sensor-based material shares aggregated by week visualized in Fig. 2. As mentioned in Section 2, the aggregation by week reduces outliers. The dominant fractions PET, PE and PP show the highest variability, especially PET bottles clear and PET bottles blue. Smaller fractions such as PVC, PS, liquid packaging board and cellulose show less variability.

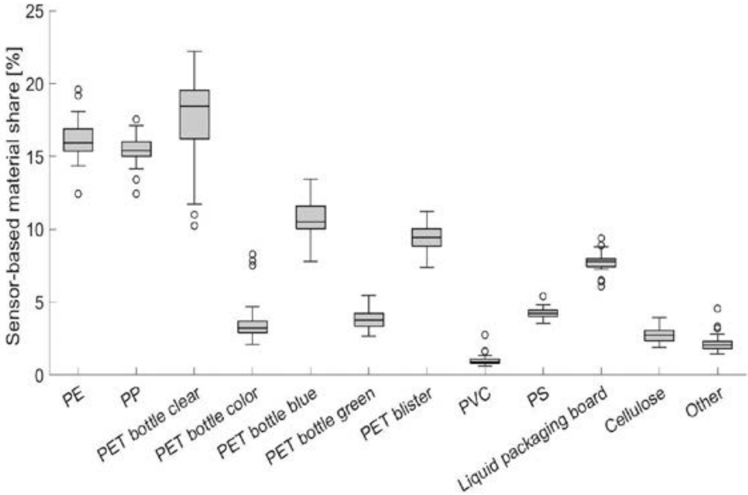

Fig. 2. Sensor-based material shares over one year by detected material classes of the SBS. The data was aggregated by week. The examined fractions are PE, PP, PET bottle clear, PET bottle color, PET bottle blue, PET bottle green, PET blister, PVC, PS, Liquid packaging board, Cellulose, and other.

Additionally, the mean values for the respective fractions were calculated: PE 16.1 %, PP 15.4 %, PET bottle clear 17.7 %, PET bottle color 3.6 %, PET bottle blue 10.6 %, PET bottle green 3.8 %, PET blister 9.4 %, PVC 1.0 %, PS 4.2 %, liquid packaging board 7.8 %, cellulose 2.7 %, other 2.1%.
It is important to note that these values are based on the pixels recorded by the camera of the SBS. Manually sorting and weighing the same material would likely result in different material shares. One reason for that are different grammages as the camera cannot determine the specific mass of a particle. However, a conversion from pixel areas to mass is possible, as described by Kroell et al (2023b).

Nevertheless, special peculiarities inherent to sensor-based monitoring and control based on SBS data must be considered. These include systematic errors, such as the non-detection of soot-colored particles or overlapping particles, but also errors based on the undisclosed classification algorithm of the sorting machine (Küppers et al., 2020, Schlögl et al., 2022a). In this data set, for example, the analyzed data was also classified on an object-level. For example, plastic bottles made of PET with PE labels and PE lids are fully classified as PET. Since the SBS was used to sort clear PET bottles, it is also likely that those pixels of the material class PET clear are weighed accordingly in the sorting engine. This hypothesis is proven by Schlögl et al. (2023), as they identified an overrepresentation of PET, PE, and PP data, when comparing the SBS data with an external NIR sensor.

Despite these inherent errors of SBS data, there is a high potential for the detection of anomalies during the operation of the plant. For example, strong deviations from the average composition could indicate problems with the input (e.g., incorrect declaration) or problems with upstream aggregates (e.g., a ballistic separator not well configured). For both cases the utilization of relative data is sufficient.

3.3 Seasonal Material Composition Over a Year

Sampling guidelines for waste characterization emphasize the temporal variability of different types of waste (e.g., Langner et al., 1998; CEN/TR 15310-1:2006; LAGA PN 98, 2001; Moser, 2004; Zwisele, 2004). Langner et al. (1998) imply, that this variability for lightweight packaging waste plays a minor role compared to residual waste or bio waste. However, there is hardly any publicly available data on the variability of lightweight packaging waste. Potential drivers for seasonal variability on the composition of lightweight packaging waste could be changed consumption patterns such as an increased consumption of certain goods (like ice cream in summer or gingerbread in winter) or changes in the waste generation (e.g., increased amounts due to holidays or tourism). Tab. 1. contains mean and standard deviation for the material fractions classified by the SBS for the months January, March, May, July, September, and November.

Tab. 1: Mean and standard deviation for the material share of the examined fractions PE, PP, PET bottle clear, PET bottle color, PET bottle blue, PET bottle green, PET blister, PVC, PS, Liquid packaging board, Cellulose, and other for the months January, March, May, July, September, and November.

Material		Jan	Mar	May	Jul	Sep	Nov
PE	**Mean [%]**	18.0	16.7	16.5	15.8	15.3	15.9
	Std [%]	*10.9*	*8.9*	*8.6*	*9.1*	*8.2*	*8.6*
PP	**Mean [%]**	14.1	15.5	16.1	15.2	16.4	15.4
	Std [%]	*8.6*	*7.9*	*7.6*	*7.7*	*8.7*	*7.9*
PET bottle clear	**Mean [%]**	15.1	14.7	18.7	19.4	19.3	14.3
	Std [%]	*8.2*	*7.1*	*8.1*	*8.9*	*8.4*	*7.8*

Material		Jan	Mar	May	Jul	Sep	Nov
PET bottle color	**Mean [%]**	4.6	3.8	3.6	3.3	2.8	5.3
	Std [%]	*3.7*	*2.5*	*2.3*	*2.4*	*2.3*	*4.1*
PET bottle blue	**Mean [%]**	12.0	11.5	8.7	10.2	11.4	10.5
	Std [%]	*6.4*	*5.8*	*3.9*	*5.7*	*5.4*	*5.6*
PET bottle green	**Mean [%]**	3.3	3.4	3.6	3.8	4.6	4.8
	Std [%]	*2.6*	*2.5*	*2.4*	*2.5*	*2.9*	*3.5*
PET blister	**Mean [%]**	8.4	9.4	10.6	9.4	8.9	10.1
	Std [%]	*5.4*	*5.0*	*4.7*	*5.0*	*4.6*	*5.2*
PVC	**Mean [%]**	1.0	1.3	1.0	0.8	0.9	1.0
	Std [%]	*2.8*	*3.7*	*2.4*	*2.0*	*2.4*	*3.7*
PS	**Mean [%]**	4.1	4.3	4.7	4.0	4.3	4.3
	Std [%]	*6.3*	*4.9*	*4.7*	*4.3*	*4.3*	*5.0*
Liquid packaging board	**Mean [%]**	8.3	8.0	7.7	7.2	7.6	8.1
	Std [%]	*5.0*	*4.1*	*4.1*	*4.0*	*4.2*	*4.4*
Cellulose	**Mean [%]**	3.3	2.8	2.7	2.3	2.2	2.8
	Std [%]	*5.9*	*4.0*	*4.0*	*3.6*	*3.3*	*3.9*
Other	**Mean [%]**	2.3	3.0	2.0	1.8	2.0	1.8
	Std [%]	*5.0*	*5.1*	*4.0*	*4.1*	*3.0*	*3.2*

Despite the high temporal resolution at two-month intervals, at first glance there are no major changes in the composition in terms of mean and standard deviation. Smaller peculiarities are a higher proportion of PE in January (18 % compared to the usual 15.3 - 16.7 %), an increased proportion of clear PET bottles in May, July, and September (18.7 - 19.4 %) compared to the usual range of 14.3 - 15.1 %. Furthermore, there is an increase in colored PET bottles between September (2.8 %) and November (5.3 %). Moreover, a lower proportion of blue PET bottles in May (8.7 %) compared to the usual 10.2 - 12.0 %.

The increased proportion of PE in January could be due to a higher proportion of film, which is generated by the increased consumption during the Christmas period and may end up in the 3D-cascade due to possible overloading of the plant. This information could be relevant for plant operation, as an increased PE content may suggest reducing the throughput to ensure constant quality of the output fractions. A theory for the increased proportion of clear PET bottles during the summer months could be an increased liquid consumption due to the higher summer temperatures.

However, this trend cannot be observed in the other PET bottle fractions. For blue PET bottles even the opposite trend can be observed. To investigate possible reasons and correlations more in-depth analyses is required. The use of SBS data to investigate the variation in material flow composition over the course of a year could be of interest not only to individual plant operators, but also to other stakeholders in the waste management sector. In this way, a nationwide comparison of the material flow composition could be realized with minimal personnel costs. This could efficiently close the knowledge gap concerning variability in lightweight packaging waste.

4 Outlook

With this article, we were able to provide insight into the data stream collected by a single SBS in a sorting plant for lightweight packaging waste. However, the analyses presented are only based on a part of the data collected by such an aggregate. For example, it would be also possible to extract additional information like conveyor belt load or grain size distribution.

Furthermore, the data was only analyzed for longer, continuous periods (months or the entire year). When shorter periods are considered, it could be possible to improve the monitoring of the plant through the detection of possible anomalies or to find unknown correlations between the material input, plant operation and plant output.

Moreover, it is also possible to combine the data recorded by several SBS in one plant. With this, further information on interdependencies of plant aggregates could be investigated. Linking SBS data in this way could be used by plant operators for better, automated monitoring of plant operation and dynamic plant control.

Nevertheless, the aforementioned peculiarities inherent to sensor-based monitoring and control based on SBS data must not be ignored in the interpretation. In this context, the problem of converting pixels to masses due to the high heterogeneity of the waste, as well as alteration of the data by the algorithm optimized for sorting, should be mentioned. To analyze the extent of this problem in practice, SBS data in different systems from different manufacturers would have to be analyzed and compared. The authors also recommend evaluating whether it is possible to access the original sensor data before changes are made by weighting or object detection to use it for material flow monitoring. This would allow the sensor data to better represent the actual material flow composition.

The ongoing analysis is promising for SBS data to have a relevant role in material flow monitoring and process control in the sorting plants of the future.

5 Acknowledgement

The authors disclose receipt of the following financial support: The project “EsKorte” was funded by the Austrian Research Promotion Agency within the program “Production of the Future” under grant agreement 877341. The project “circPLAST-mr” is funded by the Austrian Research Promotion Agency within the program “Energy of the Future, circular economy 2021 (KP)“ under grant agreement 4238670.

References

CEN/TR 15310-1:2006. Characterization of waste - Sampling of waste materials - Part 1: Guidance on selection and application of criteria for sampling under various conditions (CEN/TR 15310-1:2006). Brussels. European Committee for Standardization.

Dehoust, G., & Christiani, J. (2012). Analyse und Fortentwicklung der Verwertung-squoten für Wertstoffe: Sammel- und Verwertungsquoten für Verpackungen und stoffgleiche Nichtverpackungen als Lenkungsinstrument zur Ressourcenschonung (TEXTE 40/2012). https://www.bmuv.de/fileadmin/Daten_BMU/Pools/Forschungsdatenbank/fkz_3711_33_316_verwertungsquote_wertstoffe_bf.pdf

Kroell, N., Chen, X., Küppers, B., Schlögl, S., Feil, A., & Greiff, K. (2024). Near-infrared-based quality control of plastic pre-concentrates in lightweight-packaging waste sorting plants. In Resources, Conservation and Recycling (Vol. 201, p. 107256). Elsevier BV. https://doi.org/10.1016/j.resconrec.2023.107256

Kroell, N., Chen, X., Küppers, B., Lorenzo, J., Maghmoumi, A., Schlaak, M., Thor, E., Nordmann, C., & Greiff, K. (2023a). Near-infrared-based determination of mass-based material flow compositions in mechanical recycling of post-consumer plastics: Technical feasibility enables novel applications. In Resources, Conservation and Recycling (Vol. 191, p. 106873). Elsevier BV. https://doi.org/10.1016/j.resconrec.2023.106873

Kroell, N., Chen, X., Küppers, B., Lorenzo, J., Maghmoumi, A., Schlaak, M., Thor, E., Nordmann, C., & Greiff, K. (2023b). Near-infrared-based determination of mass-based material flow compositions in mechanical recycling of post-consumer plastics: Technical feasibility enables novel applications. In Resources, Conservation and Recycling (Vol. 191, p. 106873). Elsevier BV. https://doi.org/10.1016/j.resconrec.2023.106873

Küppers, B., Schlögl, S., Friedrich, K., Lederle, L., Pichler, C., Freil, J., Pomberger, R., Vollprecht, D. (2020). Influence of material alterations and machine impairment on throughput related sensor-based sorting performance. In Waste Management & Research: The Journal for a Sustainable Circular Economy, 39(1), 122–129. Sage Publications . https://doi.org/10.1177/0734242x20936745

LAGA PN 98. (2001). Richtlinie für das Vorgehen bei physikalischen und chemischen Untersuchungen im Zusammenhang mit der Verwertung/Beseitigung von Abfällen.

Langner, G., Albrecht, J., Ohst, E., & Herberg, B. von der. (1998). Richtlinie Abfallanalytik: Richtlinie zur einheitlichen Abfallanalytik in Sachsen.

Letcher, T. (Ed.). (2020). Plastic Waste and Recycling: Environmental Impact, Societal Issues, Prevention, and Solutions (1st). Elsevier. https://doi.org/10.1016/B978-0-12-817880-5.20001-7

Moser, G. (2004). Methodology for the Analysis of Solid Waste (SWA-Tool). https://www.wien.gv.at/meu/fdb/pdf/swa-tool-759-ma48.pdf

Neubauer, C., Stoifl, B., Tesar, M., & Thaler, P. (2021). Sortierung und Recycling von Kunststoffabfällen in Österreich: Status 2019. Vienna. https://www.umweltbundesamt.at/fileadmin/site/publikationen/rep0744_hauptteil.pdf

Schlögl, S., Kamleitner, J., Kroell, N., Chen, X., Tischberger-Aldrian, A. (2023). Developing a prediction model in a lightweight packaging waste sorting plant using sensor-based sorting data combined with data of external near-infrared and LiDAR sensors. [Manuscript submitted for publication]

Schlögl, S., Kamleitner, J., Kroell, N., Chen, X. (2022a). Implementierung von Sensor-based Material flow Monitoring in einer Kunststoffsortieranlage. In Pomberger, R.; Adam, J.; Altendorfer, M.; Bouvier-Schwarz, T.; Haslauer, P.; Kandlbauer, L.; Khodier, K.; Koinig, G.; Kuhn, N.; Lasch, T.; Mhaddolkar, N.; Nigl, T.; Rutrecht, B.; Sarc, R.; Sattler, T.; Schlögl, S.; Stipanovic, H.; Tischberger-Aldrian, A.; Viczek, S. (Eds.). Vorträge-Konferenzband zur 16. Recy & DepoTech-Konferenz (pp. 353-358). DGS Druck- und Graphikservice. ISBN: 978-3-200-08675-3.

Schlögl, S.; Küppers, B. (2022b). Quantifying the Delabelling Performance using Sensor-based Material Flow Monitoring. In Greiff, K.; Wotruba, H.; Feil, A.; Kroell, N.; Chen, X.; Gürsel, D.; Merz, V. (Eds.). 9th Sensor-Based Sorting / Control 2022 (pp. 55-70). Shaker Verlag. https.//doi.org/10.2730/9783844085457.

van Eygen, E., Laner, D., & Fellner, J. (2018). Circular economy of plastic packaging: Current practice and perspectives in Austria. Waste Management (New York, N.Y.), 72, 55–64. https://doi.org/10.1016/j.wasman.2017.11.040

Zwisele, B. (2004). Entwicklung einer neuen Probenahmemethode für heterogene Abfälle geringer Schüttdichte. Zugl.: Berlin, Techn. Univ., Diss., 2004. Rhombos-Verlag.

Particle-Specific Deflection Windows for Optical Sorting by Uncertainty Quantification

Marcel Reith-Braun[1]*, Kevin Liang[2], Florian Pfaff[1], Georg Maier[2], Robin Gruna[2], Albert Bauer[3], Harald Kruggel-Emden[3], Thomas Längle[2], Jürgen Beyerer[2], and Uwe D. Hanebeck[1]

1 Intelligent Sensor-Actuator-Systems Laboratory, Karlsruhe Institute of Technology, 76131 Karlsruhe, Germany
2 Fraunhofer IOSB, Institute of Optronics, System Technologies and Image Exploitation, 76131 Karlsruhe, Germany
3 Chair of Mechanical Process Engineering and Solids Processing, Technische Universität Berlin, 10587 Berlin, Germany

* Corresponding Author: Karlsruhe Institute of Technology, 76131 Karlsruhe, Germany, marcel.reith-braun@kit.edu

Keywords: sensor-based sorting, deflection windows, uncertainty quantification, first-passage time, constant-velocity model, constant-acceleration model

Abstract

In current state of the art sensor-based sorting systems, the length of the deflection windows, i.e., the period of nozzle activation and the number of nozzles to be activated, is commonly determined solely by the size of the particles. However, this comes at the cost of the sorting process not accounting for model discrepancies between actual and presumed particle motion, as well as for situations where the available information does not allow for precise determination of nozzle activations. To achieve a desired sorting accuracy, in practice, one is therefore usually forced to enlarge the deflection window to a certain degree, which increases the number of falsely co-deflected particles and compressed air consumption.

In this paper, we propose incorporating the uncertainty of the prediction of particle motion of *each individual particle* into the determination of the deflection windows. The method is based on the *predictive tracking* approach for optical sorting, which tracks the particles while they move toward the nozzle array based on images of an area-scan camera. Given the extracted motion information from the tracking, we propose an approximation for the distribution of arrival time and location of the particle at the nozzle array assuming nearly constant-velocity or nearly constant-acceleration particle motion behavior. By evaluating the quantile function of both distributions, we obtain a confidence interval for the arrival time and location based on prediction uncertainty, which we then combine with the particle size to form the final deflection window. We apply our method to a real sorting task using a pilot-scale chute sorter. Our results obtained from extensive sorting trials show that sorting accuracies can be remarkably improved compared with state-of-the-art industrial sorters and enhanced even further compared with predictive tracking while having the potential to reduce compressed air consumption.

1 Introduction

The aim of data processing in sensor-based sorters with pneumatic separation is essentially to determine a deflection window, i.e., to decide when, how long, and which nozzles to activate to eject a particle of an undesired class. Usually, the period of nozzle activation and the number of nozzles to be activated are determined based on the size of the respective particle (Maier et al., 2021). Therefore, although the location of the deflection window depends on the individual particle motion, its size does not. Hence, current algorithms for sensor-based sorting are unable to account for model discrepancies between actual and presumed particle motion, as well as for situations where the available information does not allow for precise determination of nozzle activations. For example, for a particle moving unusually slowly, the predicted deflection window may be too short to cover the period in which the particle passes the nozzle array, while for a particle moving strictly according to the assumed motion, it may be larger than required. This inability leads to the risk of both, particles not being ejected and falsely co-deflected particles, as well as unnecessarily high consumption of compressed air.

In practice, one is therefore usually forced to enlarge the deflection window by a fixed, often experimentally determined, amount. This amount can be viewed as an average deviation (w.r.t. all particles) or uncertainty within the forecast of particle motion. Explicitly including such a margin is thus often essential for achieving a desired sorting accuracy. However, enlarging the deflection window comes with the drawback that in turn the number of falsely co-deflected particles as well as the compressed air consumption is increased. Given that around 70 % of the operating costs of a pneumatic sorter are attributable to compressed air generation (Gülcan & Gülsoy, 2018), larger deflection windows constitute a major cost factor, and their reduction bears enormous potential for improvement.

To address this problem, we propose incorporating the uncertainty of the prediction of particle motion of *each individual particle* into the determination of the deflection windows. The basic idea is that when the uncertainty for a particular particle is low, i.e., it is indicated that the prediction is accurate, the deflection window for that particle can be decreased, while it should be enlarged when the uncertainty is high.

Our proposed method for particle-specific deflection windows builds upon the *predictive tracking* (Maier et al., 2021; Pfaff, 2019; Pfaff et al., 2015) approach for optical sorting. While the current state of the art in the industry primarily relies on line-scan-camera-based prediction, i.e., the particles are captured by a line-scan camera shortly before they arrive at the nozzle ar-ray, predictive tracking shows significant improvements compared with line-scan-camera-based sorters (Maier, 2022; Maier et al., 2021, 2023). This is mainly because line-scan-based approaches assume a constant velocity, common to all particles, along the transport direction and zero velocity per-pendicular to the transport direction to estimate a particle's arrival time and location at the nozzle array. It therefore often fails to capture the individual particle movement correctly. Predictive tracking on the other hand uses an area-scan camera along with a multitarget tracking (MTT) algorithm to track the particles' center points while the particles are moving. In its original ver-sion, it then predicts the center points' time and location of arrival at the nozzle array based on the extracted particle-individual motion information. Since no uncertainties are considered in this step, the size of the final de-flection windows is still not dependent on the individual particle's motion, although their location is typically estimated more accurately than using a line-scan-based approach.

To incorporate uncertainties in the prediction process of predictive tracking, the key concept that we are pursuing is to derive the distributions of the particle arrival time and location at the nozzle array. These distributions explicitly encode the uncertainty inherent in the prediction, which otherwise is invisible but still present. Based on these distributions, we then find the deflection windows as the confidence intervals for a desired confidence level , that is, we determine the deflection windows such that with probability , the particle arrives within the respective confidence interval (see Fig. 1).

From a mathematical perspective, the problem of finding the arrival time distribution of the particle center at the nozzle array can be viewed as a first-passage time problem. Here, the particle motion is described by a stochastic process, and we are interested in the distribution in the time domain that describes when the particle arrives at the nozzle array for the first time. Although first-passage time problems constitute an old and challenging class of mathematical problems, feasible approximations can be derived under some additional assumptions, as we recently proposed in (Reith-Braun, Thumm, et al., 2023). Fortunately, these assumptions are usually fulfilled by models describing particle motion in sorting tasks. For the distribution of the location of the particle's center at the nozzle array, in this paper, we propose a linearization approach for approximation of the distribution of the stochastic process describing the particle motion orthogonal to the transport direction at the first-passage time. Since it is known that incorporating particle extents into the determination of the deflection window yields better results (Maier et al., 2021; Udoudo, 2010), we then show how the above methods can be used to estimate the arrival time distributions of the particle front and back, as well as of the location of the upper and lower particle edge location during the particle's passage of the nozzle array. Finally, we show how to obtain deflection windows from these distributions using some approximations for the corresponding confidence intervals.

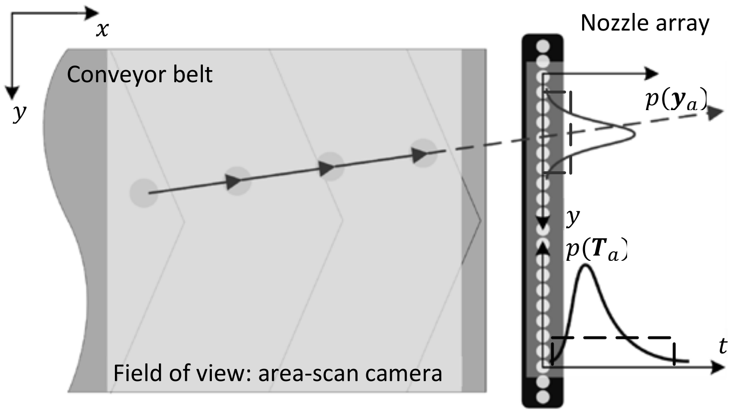

Fig. 1. Outline of our proposed method for the optical sorting problem. Particles are transported to a nozzle array (here illustrated by a conveyor belt) while being observed by an area-scan camera. We assume (nearly) constant-velocity motion behavior and track the particles with a Kalman filter. Using an estimated particle state (here the last state in the camera's field of view), we aim to estimate the distribution of the arrival time of the particle at the nozzle array (lower distribution, a distribution in the time domain) and the distribution of the particle's location (upper distribution, a distribution along the -coordinate) when passing the array of nozzles. Based on these distributions, we then calculate confidence intervals (depicted by dashed lines) used as deflection windows.

Our contributions are: First, we propose a general methodology to obtain particle-specific deflection windows based on the assumption of constant-velocity (CV) or constant-acceleration (CA) particle motion behavior. Second, we show how the distribution of the location of the particle center along the nozzle array can be approximated. Third, we propose a method to incorporate particle extents into the determination of particle-specific deflection windows and finally, we demonstrate how the parameters of the method can be determined. We evaluate our methods using numerical simulations and by applying them to a pilot-scale chute sorter in extensive sorting trials.

2 Background and Related Work

2.1 Motion Models for Describing Particle Motion

Here, we briefly describe the stochastic processes for describing particle motion that we consider in this study.

2.1.1 Constant-Velocity Model

The continuous-time (nearly) constant-velocity model, also known as the white-noise acceleration model (Bar-Shalom et al., 2001), is the Gaussian process with state $\underline{x}(t) = [x(t) \quad \dot{x}(t)]^T$, where $x(t)$ denotes the position (evolving with time t) and $\dot{x}(t)$ the velocity component, mean function

$$\hat{\underline{x}}(t) = [\hat{x}^{t_0} + \hat{\dot{x}}^{t_0}(t - t_0) \quad \hat{\dot{x}}^{t_0}] \text{ ,}$$

and covariance function $\mathrm{Cov}\{x(t)\}$ equal to

$$S\begin{bmatrix} \frac{(t-t_0)^3}{3} & \frac{(t-t_0)^2}{2} \\ \frac{(t-t_0)^2}{2} & t - t_0 \end{bmatrix} + \begin{bmatrix} \Sigma_{xx}^{t_0} + 2\Sigma_{x\dot{x}}^{t_0}(t - t_0) + \Sigma_{\dot{x}\dot{x}}^{t_0}(t - t_0)^2 & \Sigma_{x\dot{x}}^{t_0} + \Sigma_{\dot{x}\dot{x}}^{t_0}(t - t_0) \\ \Sigma_{x\dot{x}}^{t_0} + \Sigma_{\dot{x}\dot{x}}^{t_0}(t - t_0) & \Sigma_{\dot{x}\dot{x}}^{t_0} \end{bmatrix} .$$

Here, t_0 denotes the initial time, $[\hat{x}^{t_0} \quad \hat{\dot{x}}^{t_0}]^T$ is the mean of the state at t_0, and $\Sigma_{xx}^{t_0}$, $\Sigma_{x\dot{x}}^{t_0}$ and $\Sigma_{\dot{x}\dot{x}}^{t_0}$ are the respective entries of the state covariance matrix at t_0. The power spectral density S determines the amount of additional noise introduced between time t_0 and t. The CV model is linear and Markov w.r.t. the state variables. In the sense of Newtonian dynamics, the CV model has the interpretation of a freely moving particle influenced only by zero-mean white-noise random forces, with the amount of randomness controlled by S.

2.1.2 White-Noise Plus Constant Acceleration Model

The continuous-time white-noise plus constant acceleration (WN-CA) model is an extension of the CV model in which the mean function is given by

$$\hat{\underline{x}}(t) = \left[\hat{x}^{t_0} + \hat{\dot{x}}^{t_0}(t - t_0) + \frac{1}{2}a_c(t - t_0)^2 \quad \hat{\dot{x}}^{t_0} + a_c(t - t_0)\right] \text{ ,}$$

and the state and covariance function remain the same as for the CV model. Here, a_c has the interpretation of a known, constant acceleration acting on the particle in addition to zero-mean white-noise random forces. For instance, a_c can model the influence of gravity *g* in free fall ($a_c = g$) or on an inclined plane ($a_c = g \sin \alpha$, with α being the slope angle).

The discrete-time counterparts of both motion models can be obtained from the continuous-time models by fixing $\Delta t = t - t_0$ to the time difference between two consecutive time steps and treating $\underline{x}(\Delta t)$ as initial state for time step $k = 1$ and so on, i.e. $\underline{x}_{k=1} = \underline{x}(\Delta t) \mid \underline{x}^{t_0} \triangleq \underline{x}_k$, $k \in \mathbb{N}_0$, with $\underline{x}_0 = \underline{x}^{t_0}$.

2.2 Algorithms for Optical Sorting

While the current industrial state of the art is line-scan-camera-based prediction, in our previous works (Pfaff, 2019; Pfaff et al., 2015), we showed that sorting accuracy can be improved with the help of the predictive tracking paradigm. In predictive tracking, an MTT algorithm is employed on the center coordinates of the particles while they are moving. For this, an area-scan camera observes typically the last 15 to 30 cm in front of the nozzle array. In a second step, the extracted motion information is then used to precisely activate the nozzles (referred to as the prediction phase). For estimating the particle states during the MTT, multiple Kalman filters, one for each particle, using CV or CA motion models are deployed. For this, independent motion models in the transport direction, in the following referred to as the -direction, and orthogonal to the transport direction, referred to as the -direction, are used. At the end of the MTT, we are thus provided with precise estimations of the individuals particles' positions, velocities, and possibly accelerations (if a CA model is used) in the form of their expectations and covariances.

The prediction of the estimated particles' time of arrival and location at the nozzle array is then again accomplished with motion models inspired by physics, such as CV or CA models. To this end, the motion models use the expectation of the estimated particle states from the Kalman filters at the last time step before the beginning of the prediction phase. An important difference is that while in MTT, time-discrete versions of the CV or CA models are used, in the prediction of particles' time of arrival and location at the nozzle array, predictive tracking uses their time-continuous counterparts. In addition, all uncertainties are ignored, i.e., only the mean function of the time-continuous CV or CA model is used. Here, using time-continuous models allows for being independent of the camera frequency and thus being able to provide more precise nozzle activations.

Extensions to predictive tracking include incorporating orientation estimation in the MTT (Pfaff, 2019), and the use of more accurate, physically-inspired (Pfaff, 2019; Pfaff et al., 2020) and data-driven models. Latter includes the use of recurrent neural networks and multilayer perceptrons that replace the Kalman filters and the motion models as well as combinations of physically-inspired and data-driven models (Pollithy et al., 2020; Thumm et al., 2022). An experimental evaluation of some of these ideas using a lab-scale optical sorter can be found in (Maier et al., 2023). An image-based rather than a midpoint-based approach was persuaded by (Reith-Braun, Bauer, et al., 2023). Here, the sorting problem was framed as a video-forecasting task and solved using a convolutional long short-term memory network. As the approach can be trained in an unsupervised fashion, it allows sorting with a minimum of operator setup and supervision.

All algorithms eventually need to transform the information about the estimated particle arrival time and location at the nozzle array into a deflection window. This is either accomplished by targeting the particle center or, more commonly, by incorporating information about the particle extent, usually in the form of a bounding box (Maier, 2022; Maier et al., 2021; Udoudo, 2010). If the bounding box is extracted from a line-scan camera image, i.e., is in the temporal-spatial domain, it can be directly used as a deflection pattern after only minor post-processing. If the bounding box is extracted from an area-scan camera image, such as in predictive tracking, the length along the transport direction must be additionally converted to a time span by dividing by an estimated, potentially particle-dependent velocity. It is also common to use a modified version of the bounding box, e.g., by adding an offset or by multiplication with a factor. For example, an offset in -direction may account for the spatial resolution of the nozzle array (Maier et al., 2021). In general, larger deflection windows considerably improve the reliable deflection of unwanted particles. However, they also increase compressed air consumption and the number of falsely co-deflected particles. The parameters therefore need to be tuned carefully, e.g., be preliminary experiments, and a proper choice may additionally depend on the particle type (Maier, 2022; Maier et al., 2021). A scheme for determining proper parameters based on recorded particle tracks and their deviations was proposed in (Maier, 2022).

2.3 First-Passage Time Problems

The first-passage time is defined as the event $T_a = \inf\{t > t_0 : x(t) = a\}$, i.e., the first time $t > t_0$, a particle moving according to a stochastic process $x(t)$ reaches a fixed boundary $a \in \mathbb{R}$. In general, solving this problem, known as a first-passage time problem, is a challenging task, with solutions only known for very few process–boundary pairs (Blake & Lindsey, 1973; Nobile et al., 1985). An important general observation is that the event $T_a < t$ is equivalent to the event that the maximum of the process within the time range $[t_0, t)$, $m_t = \sup_{t_0 \leq s < t} x(s)$ is greater than or equal to a, i.e., $T_a < t \Leftrightarrow m_t \geq a$. Furthermore, it holds that

$$\mathbb{P}(\boldsymbol{T}_a < t) = \mathbb{P}(\boldsymbol{x}(t) > a) + \mathbb{P}(\boldsymbol{T}_a < t, \boldsymbol{x}(t) \leq a) , \quad (1)$$

that is, to have a first-passage time smaller than t, a particle must be either located above a at time t or, if not, must have crossed the boundary at some time $T_a < t$. However, $\mathbb{P}(T_a < t, x(t) \leq a)$ in general is intractable.

In (Reith-Braun, Thumm, et al., 2023), we proposed two methods to approximate the distribution of T_a, the first-passage time distribution (FPTD), under some additional assumptions on the process-boundary pair, such as that there is a dominant drift that causes a first-passage almost surely. These assumptions are usually fulfilled by motion models that, e.g., describe technical transport processes. The best proven method, referred to as *no-return approximation*, uses the relation (1) and additionally assumes that once a particle has crossed the boundary, it cannot return to a position smaller than a (hence, the name) – a condition that is usually satisfied in technical transport processes. Consequently, $\mathbb{P}(T_a < t, x(t) \leq a) = 0$ and $\mathbb{P}(T_a < t) = \mathbb{P}(x(t) > a)$ (for a mathematical more rigorous treatment of the above assumption and the domain in which the approximation is valid, we refer to (Reith-Braun, Thumm, et al., 2023)). Note that $x(t)$ represents the first component of the state vector $\underline{x}()$, and we are thus interested w.l.o.g. in the first-passage of the first state component w.r.t. a. An approximation of the FPTD can then be derived by differentiating the above relation w.r.t. t. Moreover, it is possible to find an expression for the quantile function analytically and to compute the moments numerically. The no-return approximation shows good alignment with Monte Carlo simulation for small and medium noise levels, i.e., high and medium signal-to-noise ratios.

3 Methodology

We now present how the required distributions for obtaining deflection windows can be approximated. The first part of the section focuses on the distribution of the particle's location at the nozzle array, whereas the second part shows how the particle extent can be included in the determination of the deflection windows.

3.1 The Distribution of the Particle Location at the Nozzle Array at the First Passage

For the distribution of the particle's center location along the nozzle array, we require the distribution of the process orthogonal to the transport direction at the time of the first passage. Therefore, we define the random variable $\mathrm{y_a} = \{\mathrm{y(t) : t = T_a}\}$, i.e., the -location at the first passage. Note that in addition to the uncertainties inherent to the process $\mathrm{y(t)}$, an additional source of uncertainty is that time itself is random, with distribution given by the FPTD.

We propose a linearization approach to approximate the distribution of $\mathrm{y_a}$ that is valid for linear Gaussian state space models, such as the CV or CA model and their variants, referred to as *Gauß-Taylor approximation* (a similar method for approximation of the FPTD was proposed in (Reith-Braun, Thumm, et al., 2023)). For this, we first set up the motion equation $\underline{\mathrm{y}}(\mathrm{T_a})$ in y-direction at $\mathrm{T_a}$**,** using $\underline{\mathrm{y}}(\hat{\mathrm{T}}_\mathrm{a})$ with $\hat{\mathrm{T}}_\mathrm{a} = \mathrm{E}\{\mathrm{T_a}\}$ as initial state and neglecting additional noise (here, $\mathrm{E}\{\cdot\}$ denotes the expectation operator). Subsequently, we linearize the motion equation using a first-order Taylor series expansion at $\hat{\mathrm{T}}_\mathrm{a}$ and $\mathrm{E}\{\underline{\mathrm{y}}(\hat{\mathrm{T}}_\mathrm{a})\}$, and, from the linearization, calculate the approximate mean and variance for the distribution of $\mathrm{y(t)}$ at the first passage. This results in $\mathrm{E}\{\mathrm{y_a}\}$ $\mathrm{E}\{\underline{\mathrm{y}}(\hat{\mathrm{T}}_\mathrm{a})\}$ and variance

$$\mathrm{Var}\{\boldsymbol{y}_a\} \approx \left(\frac{\partial}{\partial \boldsymbol{T}_a}\boldsymbol{y}(\boldsymbol{T}_a)\Big|_{\substack{\boldsymbol{T}_a=\hat{T}_a \\ \underline{\boldsymbol{y}}(\hat{T}_a)=\mathrm{E}\{\underline{\boldsymbol{y}}(\hat{T}_a)\}}}\right)^2 \mathrm{Var}\{\boldsymbol{T}_a\}$$

$$+\left(\nabla_{\underline{\boldsymbol{y}}(\hat{T}_a)}\boldsymbol{y}(\boldsymbol{T}_a)\Big|_{\substack{\boldsymbol{T}_a=\hat{T}_a \\ \underline{\boldsymbol{y}}(\hat{T}_a)=\mathrm{E}\{\underline{\boldsymbol{y}}(\hat{T}_a)\}}}\right)^{\mathrm{T}} \mathrm{Cov}\left\{\underline{\boldsymbol{y}}(\hat{T}_a)\right\}\left(\nabla_{\underline{\boldsymbol{y}}(\hat{T}_a)}\boldsymbol{y}(\boldsymbol{T}_a)\Big|_{\substack{\boldsymbol{T}_a=\hat{T}_a \\ \underline{\boldsymbol{y}}(\hat{T}_a)=\mathrm{E}\{\underline{\boldsymbol{y}}(\hat{T}_a)\}}}\right).$$

For instance, for the CV and the CA model, we have $\mathrm{Var}\{y_a\} \approx \mathrm{Var}\{y(\hat{T}_a)\} + \mathrm{E}\{\dot{y}(\hat{T}_a)\}^2\,\mathrm{Var}\{T_a\}$. We then assume a Gaussian density for the distribution of the arrival location y_a.

3.2 Deflection Windows Including Particle Extents

So far, we considered the particles as point masses, i.e., they were fully described by their center points. However, for a more realistic model, we need to take the particles' extents into account. We now propose a method for including particle extents in the determination of the deflection windows.

3.2.1 Temporal Deflection Windows

We propose to determine the temporal deflection windows based on the marginal distributions of the particle front arrival time $T_{(a-l/2)}$ and the particle back arrival time $T_{(a+l/2)}$, where l denotes the length of the particle in transport direction. Here, we assume that l does not change much (e.g., due to rotations) while passing the nozzle array. Particle extents may be then included by solving

$$\mathbb{P}\left(\boldsymbol{T}_{a-\frac{l}{2}} < t_{\text{start}}\right) = \frac{1-q}{2}\,, \qquad \mathbb{P}\left(\boldsymbol{T}_{a+\frac{l}{2}} < t_{\text{end}}\right) = \frac{1+q}{2}$$

for t_{start} and t_{end}, respectively, where t_{start} and t_{end} describe the lower and upper bound of the time interval within which the nozzles should be open. As before, $q\epsilon(0,1)$ denotes a desired confidence level with which one may wish to eject the particles. Solving the above equation essentially requires the quantile, or percent-point function (PPF), of the FPTD of $T_{(a-l/2)}$ and $T_{(a+l/2)}$, which is available for the no-return approximation.

3.2.2 Spatial Deflection Windows

For the derivation of the spatial deflection windows, i.e., the dimension of the window along the nozzle array, we introduce two new random variables, namely the upper and the lower particle edge location during the particle's passage of the nozzle array. These are defined by

$$\boldsymbol{y}_{\min} = \min\left\{\boldsymbol{y}(t) - \frac{b}{2} : \boldsymbol{T}_{a-\frac{l}{2}} < t < \boldsymbol{T}_{a+\frac{l}{2}}\right\},$$
$$\boldsymbol{y}_{\max} = \max\left\{\boldsymbol{y}(t) + \frac{b}{2} : \boldsymbol{T}_{a-\frac{l}{2}} < t < \boldsymbol{T}_{a+\frac{l}{2}}\right\}.$$

Here, b is the particle width orthogonal to the transport direction (we again assume that b, l do not change much). We then may again determine the deflection windows by solving

$$\mathbb{P}(\boldsymbol{y}_{\min} < y_{\text{low}}) = \frac{1-q}{2}, \qquad \mathbb{P}(\boldsymbol{y}_{\max} < y_{\text{up}}) = \frac{1+q}{2}$$

for $\mathrm{y}_{\mathrm{low}}$ and y_{up} that describe the lower and upper bounds of the spatial deflection window. This means we require the PPFs of $\mathrm{y}_{\min}$ and $\mathrm{y}_{\max}$.

However, note that deriving the distributions of $\mathrm{y}_{\min}$ and $\mathrm{y}_{\max}$ itself requires solving an additional first-passage time problem, due to the equivalence of maximum and first-passage time problems. For this reason, to render the problem feasible, we introduce the additional assumption that the process $\mathrm{y(t)}$ is either monotonously increasing or monotonously decreasing in $\mathrm{t} \in (\mathrm{T}_{(\mathrm{a-l/2})}, \mathrm{T}_{(\mathrm{a+l/2})})$. Incorporating this assumption yields

$$\boldsymbol{y}_{\min} = \min\left\{\boldsymbol{y}_{a-\frac{l}{2}}, \boldsymbol{y}_{a+\frac{l}{2}}\right\} - \frac{b}{2}, \qquad \boldsymbol{y}_{\max} = \max\left\{\boldsymbol{y}_{a-\frac{l}{2}}, \boldsymbol{y}_{a+\frac{l}{2}}\right\} + \frac{b}{2}.$$

Using a similar argument as for the no-return approximation, one can approximate the distribution of $\mathrm{y}_{\min}$ and $\mathrm{y}_{\max}$ by the lower and upper bound

$$\mathbb{P}(\boldsymbol{y}_{\min} < y_1) \geq \max\left\{\mathbb{P}\left(\boldsymbol{y}_{a+\frac{l}{2}} < y_1 + \frac{b}{2}\right), \mathbb{P}\left(\boldsymbol{y}_{a-\frac{l}{2}} < \mathrm{y}_1 + \frac{b}{2}\right)\right\}, \tag{2}$$

$$\mathbb{P}(\boldsymbol{y}_{\max} < y_2) \leq \min\left\{\mathbb{P}\left(\boldsymbol{y}_{a+\frac{l}{2}} < y_2 - \frac{b}{2}\right), \mathbb{P}\left(\boldsymbol{y}_{a-\frac{l}{2}} < \mathrm{y}_2 - \frac{b}{2}\right)\right\}, \tag{3}$$

respectively, where the distributions of $y_{a+l/2}$ and $y_{a-l/2}$ can be approximated with the method described in Sec. 3.1. The interpretation of the above formula is that, since we cannot reasonably assume that the process is either de- or increasing, one considers each case separately and decides on the one with a higher probability. However, we cannot expect that the approximations are close to the true distributions on the entire support of y_{min} and y_{max}. On the other hand, our experiments suggest that they are close to the true distribution in the technically relevant regions, i.e., for small probabilities $\mathbb{P}(y_{min} < y_1)$ and high probabilities $\mathbb{P}(y_{max} < y_2)$.

As an approximation for the PPF of y_{min} and y_{max} for small confidence levels q_1 and high confidence levels q_2, we use

$$y_1 = -\frac{b}{2} + \min\left\{y_1^1 : \mathbb{P}\left(\boldsymbol{y}_{a-\frac{l}{2}} < y_1^1\right) = q_1,\ y_1^2 : \mathbb{P}\left(\boldsymbol{y}_{a+\frac{l}{2}} < y_1^2\right) = q_1\right\},$$

$$y_2 = \frac{b}{2} + \max\left\{y_2^1 : \mathbb{P}\left(\boldsymbol{y}_{a-\frac{l}{2}} < y_2^1\right) = q_2,\ y_2^2 : \mathbb{P}\left(\boldsymbol{y}_{a+\frac{l}{2}} < y_2^2\right) = q_2\right\},$$

that is, we use the smallest value of y_1 and y_2 the highest value of that satisfy (2) and (3) since our bounds will reach q_1, q_2 after, respectively before $\mathbb{P}(y_{min} < y_1)$ and $\mathbb{P}(y_{max} < y_2)$. The PPFs, $q \rightarrow \{y: \mathbb{P}(y_{(a-l/2)} < y) = q\}$ and $q \rightarrow \{y: \mathbb{P}(y_{(a+l/2)} < y) = q\}$ can be easily approximated using the Gauß-Taylor method presented in Sec. 3.1.

4 Experimental System and Employed Algorithms

For our experiments, we use the pilot-scale optical chute sorter displayed in Fig. 2. The sorter has a chute width of 700 mm and is equipped with a Baumer VLXT-50C.I Bayer RGB area-scan camera with a maximum resolution of 2448 2048 pixels. The system can use transmitted light for transparent objects and reflected light for opaque objects. The resolution of the installed nozzle array is 1000 Hz in the temporal domain and approximately 5.2 mm in the spatial domain, i.e., we can activate the nozzles in discrete steps of 1 ms and each nozzle covers approximately 5.2 mm along the nozzle array.

The employed algorithm implements predictive tracking, as well as line-scan-camera-based sorting. For the latter, the line-scan camera is simulated using the area-scan camera by reducing the height of the image acquisition to a row of 1808 2 pixels, allowing a frame rate of 5000 fps. For predictive tracking, a frame rate of 250 fps and a resolution of 1808 952 pixels is used, which corresponds to a camera field of view of approximately 628 331 mm. For tracking, a time-discrete WN-CA model is used to model the particle motion in the transport direction, while a time-discrete CV model is used for the -direction. The slope angle for the WN-CA model was 41.5°, although the chute has a slope of 55°. The difference between both accounts for friction forces acting on the particles and was determined experimentally.

The original version of predictive tracking, i.e., the version without considering prediction uncertainties for the deflection window, uses the mean function of the time-continuous WN-CA model with the same slope angle as before to determine the time of arrival and the mean function of the time-continuous CV model to determine the location of arrival. We use this version for comparison with our new method (in the remainder of the paper simply referred to as predictive tracking). In line-scan-camera-based sorting and the original version of predictive tracking, the size of a deflection window is determined based on the size and velocity of the respective particle, plus a fixed enlargement (as explained in Sec. 2.2). In our newly proposed version of predictive tracking (hereinafter referred to as *adaptive deflection*), the size of the deflection window is determined by the uncertainty of the motion prediction of the particle’s front and back and uppermost and lowermost edge, as described in the previous section.

Fig. 2. Image of the sorting system. The material is fed into the system via a vibration feeder and a chute (on the right in the image). It is perceived by an area-scan camera, which is located at the top left of the image. Below the chute is an array of compressed air nozzles that separate the material.

5 Evaluation

Our evaluation consists of two parts: We first demonstrate the power of our approximation schemes by a numerical verification and then, after some parameter tuning, compare the adaptive deflection method with line-scan-based prediction and predictive tracking in sorting experiments. For both parts, we consider the pilot-scale optical chute sorter presented in the previous section (respectively, a simple, geometric model of it, for the numerical verification) and recycling glass particles having diameters in the range of 6 to 30 mm.

5.1 Numerical Verification of the Derived Distributions

We demonstrate the soundness of our approximations introduced in Sec. 3 by comparing them with Monte Carlo simulations. For this, we consider the example of a virtual particle moving perfectly according to the WN-CA model in the transport direction and according to the CV model orthogonal to the transport direction. For the state distribution used as input of our approximations and all parameters of the methods, we use the values obtained by tracking a typical particle from our sorting task and the same parameters as for the final sorting experiments.

The Monte Carlo simulation uses the discrete-time counterparts of the motion models with very small time increments. In each time step, it checks if the particle center, front, and back have already crossed the nozzle array. Likewise, the particle center, uppermost, and lowermost edge locations are recorded within the period when the particle passes the nozzle array. From this information, we then extract histograms used as (approximate) ground truth for comparison with our approximations.

The results for the approximation of the FPTD and the -position at the first arrival are displayed in Fig. 3. The approximations are generally very close to the Monte Carlo histograms, with no differences in PDF and CDF visually recognizable. For comparison, the plots also show uniform distributions corresponding to the conventional case where a point prediction (in this case from predictive tracking) is used with a window length equal to the particle length divided by an estimate of the particle velocity in the -direction or the particle width, respectively, and no additional enlargement. Note that our approximations capture the true distributions way more precisely, but at this point do not account for the particle extents.

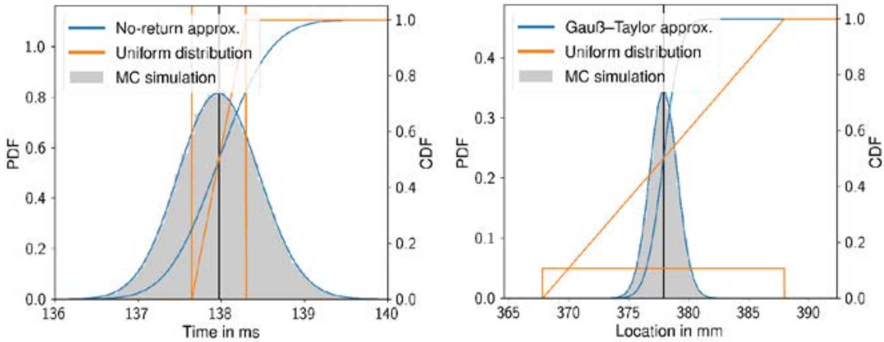

Fig. 3. The PDF and CDF of the first-arrival time distribution (left) and the distribution of the particle location along the nozzle array (right) of a typical particle from our sorting experiments. "No-return approx." denotes the similarly named approach from (Reith-Braun, Thumm, et al., 2023) for approximate FPTD. "Gauß-Taylor approx." denotes the approach proposed in Sec. 3.1 for approximation of the -location at the arrival time. "Uniform distribution" denotes the conventional approach, i.e., using a point prediction (in this case from predictive tracking, visualized by the black vertical line) for the particle arrival time and location and a window length with no additional enlargement. The shaded parts (denoted "MC simulation") display histograms of the respective distributions obtained by Monte Carlo simulations.

The results of our proposed methods for considering particle extents are visualized in Fig. 4. Again, the approximations are able to capture the true distributions for the particle under consideration with high precision. For comparison, again the same conventional approach as in Fig. 3 is displayed. Note, however, that it is here described by Dirac distributions (instead of uniform distributions), since we are now considering the particle's front and back arrival time, and its uppermost and lowermost edge location, respectively. Note that our approximation for a reasonably high always yields larger deflection windows than the ones from the conventional approach without additional enlargement, since the prediction uncertainty then adds up with the particle size. However, when the deflection windows of the conventional method are additionally enlarged, the approximation can also yield smaller deflection windows than the conventional method even if high values of are used.

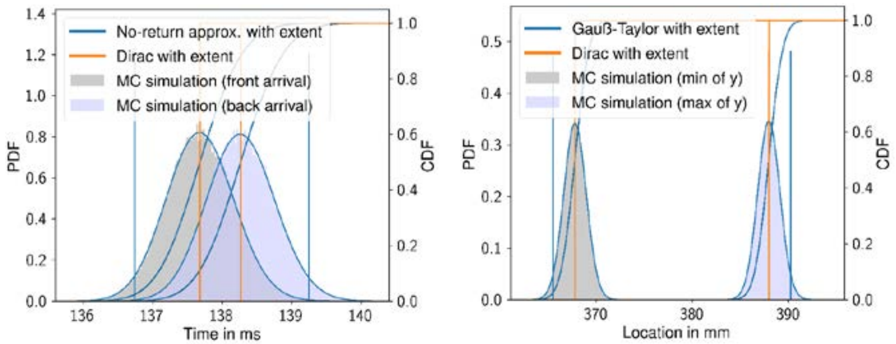

Fig. 4. The PDF and CDF of the front and back arrival time distribution (left) and the distribution of the minimum and maximum particle edge location at the nozzle array (right) of a typical particle from our sorting experiments. "No-return approx. with extents" denotes the approach described in Sec. 3.2.1. Likewise, "Gauß-Taylor with extents" denotes the approach described in Sec. 3.2.2. "Dirac with extents" denotes the usual approach, i.e., using a point prediction (in this case from predictive tracking) for the particle front and back arrival and the minimum and maximum particle edge, respectively. The shaded parts (denoted "MC simulation") display histograms of the respective distributions obtained by Monte Carlo simulations.

5.2 Sorting Experiments

The mass flow to be sorted consists of a mixture of glass recycling of 500 g white and 75 g stained glass. These particle types can be easily distinguished visually so that misclassifications can be precluded, and the sorting results are directly indicative of the effectiveness of the underlying algorithm for optical sorting. The goal of our sorting trails was to eject stained glass. The approximate mass flow during the experiments was 170 g/s. In total, we conducted five sorting trails for each of the three methods: line-scan prediction, predictive tracking, and adaptive deflection. In the following, we first describe our evaluation metrics and how we obtained the parameters of our methods, before finally presenting the sorting results.

5.2.1 Metrics

For evaluation of the sorting accuracy, we consider the true negative rate $\mathrm{TNR} = \mathrm{TN}/(\mathrm{FP} + \mathrm{TN})$ and the true positive rate $\mathrm{TPR} = \mathrm{TP}/(\mathrm{TP} + \mathrm{FN})$, where positive particles are those that should not be ejected (white glass, in our case). A high TNR thus indicates a high purity of the non-ejected fraction (there are only a few unwanted particles left), whereas a high TPR indicates a high purity of the ejected fraction (there are only a few co-deflected particles). As a measure for evaluating the compressed air consumption, we record the nozzle time, i.e., the cumulate time for which the nozzles were opened.

5.2.2 Preliminary Sorting Experiments and Parameter Tuning

The parameters of our new approach are the power spectral densities S (in x- and y-direction) and the confidence levels q (temporal and spatial). For simplicity, we assume the same value of S in both directions. Furthermore, we use the same S for the motion models in the Kalman filters of the MTT part of predictive tracking. For the confidence levels, we chose the same $q = 0{,}95$ for all confidence intervals. Note that strictly speaking, this does not imply that we wish to eject 95 % of all unwanted particles since we apply q to the temporal and spatial deflection window independently. It remains to find a suitable value for the power spectral density S. In general, this is a difficult task. There exist multiple approaches to learning the noise from data in the literature, e.g., expectation maximization (Ghahramani & Hinton, 1996), dual (Nelson, 2000), or ensemble Kalman filtering methods (Stroud & Bengtsson, 2007), each of which has their pros and cons (see also the survey by (Zhang et al., 2016)). Yet, the choice of S has a large influence on the size of the obtained deflection widows, and therefore we require a convenient method.

Here we propose to tune S using a calibration method, i.e., we wish to choose such that 95 % of all unwanted particles appear at the nozzle array within the corresponding confidence interval. For this, we record a data set of particle tracks of the unwanted class and track the particles until they have crossed the nozzle array (for this purpose, we adjust the camera field of view, so that we can observe the nozzle array). Using the recorded tracks, we then conduct “virtual” sorting experiments, whereby we run the algorithm with a specific S and count the number of hits within the confidence interval. In this step, to obtain a more accurate estimation of the particles’ time and location of arrival at the nozzle array (respectively its front, back, and upper and lower boundary), we use a linear interpolation between the last measurement before and the first measurement after the nozzle array, similar to the concept of a virtual nozzle (see e.g., (Pfaff et al., 2015; Reith-Braun, Bauer, et al., 2023)). We then perform a line search to find the desired value of S.

To ensure a proper comparison of the approaches, we chose the length of the enlargement of the deflection windows of the line-scan and conventional predictive tracking method so that a similar nozzle time as for the adaptive deflection approach with $q = 0{,}95$ was achieved. This is to compensate for the effect that we can generally achieve a higher TNR with a longer nozzle time. Finally, this resulted in an amount of 1.6 ms and 3.47 mm by which the deflection windows were enlarged.

5.2.3 Sorting Results

Our sorting results are visualized along with the nozzle times in Fig. 5. All three approaches yield high TNRs in the range of 90 to 100 % and high TPRs of approximately 99 % and higher. Comparing the TNR, predictive tracking achieves, as expected, on average slightly higher accuracies than line-scan-based prediction. Our new method improves on the results of predictive tracking and achieves by far the highest TNR (with an average of 96.7 %, compared with 94.6 and 94.0 % for predictive tracking and line-scan-based prediction). In addition, it also shows the lowest deviations between the different runs. Comparing the TPR, again, our new approach has the highest overall accuracy, slightly outperforming the other approaches. Looking at the cumulative activation times of the nozzles, the nozzle time is quite similar for all approaches, which indicates a proper balance within the comparison.

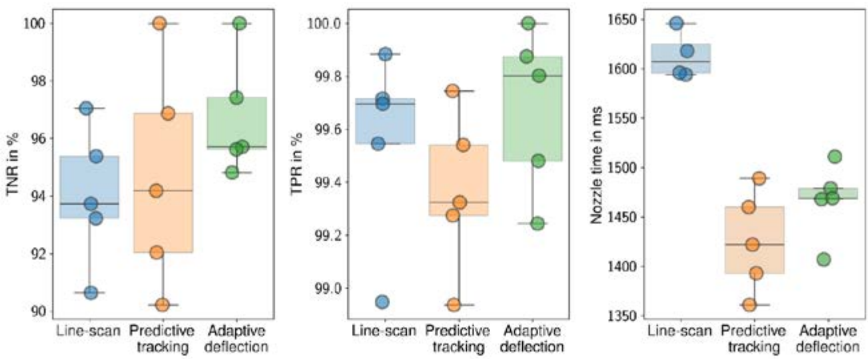

Fig. 5. Results of the sorting experiments for the three compared algorithms for optical sorting. Each point depicts the result of one of the five sorting trails. The box plots show the first, second, and third quartile of the results of the sorting trails with the whiskers extending to the most distant data point within the 1.5-fold interquartile range, starting from the upper or lower quartile, respectively.

6 Conclusion

We proposed a new method based on quantifying prediction uncertainty for determining the length of the deflection windows in optical sorting. Numerical simulations demonstrate that the approximations for the underlying distributions yield high precisions for the motion behavior of typical particles and are therefore suitable for application in optical sorters. Our sorting results show superior accuracies of the new method compared with line-scan-based prediction and predictive tracking, with an average TNR of approximately 96.7 %.

The proposed method therefore not only offers the possibility to further improve the sorting accuracy but also, and probably more importantly, to reduce the number of incorrectly deflected particles and the energy consumption by choosing the deflection window for each particle only as long as necessary. Future work may focus on this aspect, e.g., by incorporating a more accurate model of the particle–nozzle field contact and the conditions that must be satisfied for a particle to be ejected. A simple approach in this context may be to artificially reduce the size of a particle by a certain factor to account for that one may wish to target a potentially smaller range than given by the particle extent.

References

Bar-Shalom, Y., Li, X.-R., & Kirubarajan, T. (2001). Estimation with Applications to Tracking and Navigation. John Wiley & Sons, Inc.

Blake, I., & Lindsey, W. (1973). Level-crossing Problems for Random Processes. IEEE Transactions on Information Theory, 19(3), 295–315.

Ghahramani, Z., & Hinton, G. E. (1996). Parameter Estimation for Linear Dynamical Systems (CRG-TR-96-2). University of Toronto.

Gülcan, E., & Gülsoy, Ö. Y. (2018). Optical Sorting of Lignite and its Effects on Process Economics. International Journal of Coal Preparation and Utilization, 38(3), 107–126.

Maier, G. (2022). Bildfolgenbasierte Gewinnung und Nutzung partikelindividueller Bewegungsinformation in der optischen Schüttgutsortierung. KIT Scientific Publishing.

Maier, G., Pfaff, F., Pieper, C., Gruna, R., Noack, B., Kruggel-Emden, H., Längle, T., Hanebeck, U. D., Wirtz, S., Scherer, V., & Beyerer, J. (2021). Experimental Evaluation of a Novel Sensor-Based Sorting Approach Featuring Predictive Real-Time Multiobject Tracking. IEEE Transactions on Industrial Electronics, 68(2), 1548–1559.

Maier, G., Reith-Braun, M., Bauer, A., Gruna, R., Pfaff, F., Kruggel-Emden, H., Längle, T., Hanebeck, U. D., & Beyerer, J. (2023). Simulation Study and Experimental Validation of a Neural Network-based Predictive Tracking System for Sensor-based Sorting. Tm - Technisches Messen, 90(7–8), 489–499.

Nelson, A. T. (2000). Nonlinear Estimation and Modeling of Noisy Time Series by Dual Kalman Filtering Methods [PhD Thesis]. Oregon Graduate Institute of Science and Technology.

Nobile, A. G., Ricciardi, L. M., & Sacerdote, L. (1985). A Note on First-Passage Time and Some Related Problems. Journal of Applied Probability, 22(2), 346–359.

Pfaff, F. (2019). Multitarget Tracking Using Orientation Estimation for Optical Belt Sorting. KIT Scientific Publishing.

Pfaff, F., Baum, M., Noack, B., Hanebeck, U. D., Gruna, R., Längle, T., & Beyerer, J. (2015, September). TrackSort: Predictive Tracking for Sorting Uncooperative Bulk Materials. Proceedings of the 2015 IEEE International Conference on Multisensor Fusion and Integration for Intelligent Systems (MFI 2015).

Pfaff, F., Pieper, C., Maier, G., Noack, B., Gruna, R., Kruggel-Emden, H., Hanebeck, U. D., Wirtz, S., Scherer, V., Längle, T., & Beyerer, J. (2020). Predictive Tracking with Improved Motion Models for Optical Belt Sorting. At - Automatisierungstechnik, 68(4), 239–255.

Pollithy, D., Reith-Braun, M., Pfaff, F., & Hanebeck, U. D. (2020). Estimating Uncertainties of Recurrent Neural Networks in Application to Multitarget Tracking. 2020 IEEE International Conference on Multisensor Fusion and Integration for Intelligent Systems (MFI), 229–236.

Reith-Braun, M., Bauer, A., Staab, M., Pfaff, F., Maier, G., Gruna, R., Längle, T., Beyerer, J., Kruggel-Emden, H., & Hanebeck, U. D. (2023, July). GridSort: Image-based Optical Bulk Material Sorting Using Convolutional LSTMs. Proceedings of the 22nd IFAC World Congress (IFAC 2023).

Reith-Braun, M., Thumm, J., Pfaff, F., & Hanebeck, U. D. (2023, June). Approximate First-Passage Time Distributions for Gaussian Motion and Transpor-tation Models. Proceedings of the 26th International Conference on In-formation Fusion (Fusion 2023).

Stroud, J. R., & Bengtsson, T. (2007). Sequential State and Variance Estimation within the Ensemble Kalman Filter. Monthly Weather Review, 135(9), 3194–3208.

Thumm, J., Reith-Braun, M., Pfaff, F., Hanebeck, U. D., Flitter, M., Maier, G., Gruna, R., Längle, T., Bauer, A., & Kruggel-Emden, H. (2022). Mixture of Experts of Neural Networks and Kalman Filters for Optical Belt Sorting. IEEE Transactions on Industrial Informatics, 18(6), 3724–3733.

Udoudo, O. B. (2010). Modelling the Efficiency of an Automated Sensor-based Sorter. Univ. Exeter.

Zhang, L., Sidoti, D., Bienkowski, A., Pattipati, K. R., Bar-Shalom, Y., & Kleinman, D. L. (2016). On the Identification of Noise Covariances and Adaptive Kal-man Filtering: A New Look at a 50 Year-old Problem. 4, 31.

Potential of Deep Learning methods for image processing in sensor-based sorting: data generation, training strategies and model architectures

Felix Kronenwett[1]*, Georg Maier[1], Thomas Längle[1]

1 Fraunhofer IOSB, Institute of Optronics, System Technologies and Image Exploitation, Karlsruhe, Germany

* Corresponding Author: Fraunhoferstr. 1, 76131 Karlsruhe, felix.kronenwett@iosb.fraunhofer.de

Keywords: Sensor-based sorting, Deep Learning, synthetic data generation, instance segmentation, real-time image processing

Abstract

The main component of a sensor-based sorting system is an imaging sensor and the associated data processing unit for detecting and classifying bulk material objects. High occupancy densities and objects with similar appearance lead to increasing problems for conventional image processing algorithms in object and class separation. Therefore, in this article, specialized Deep Learning approaches were applied to two datasets for instance segmentation. Due to the need for a large amount of training data for such models, a method for synthetic training data generation has been developed. Subsequently, established model architectures as well as an own approach specialized for the problem characteristics is presented and compared regarding their detection performance. Finally, the models are evaluated in terms of their speed and therefore their potential use in a sorting system. Our approach more than halves the inference time of the fastest model while achieving the best detection performance.

1 Introduction

Sensor-based analysis of bulk materials has numerous areas of application, whether in the food industry or in the recycling of waste streams such as plastic, construction and demolition waste or glass sorting. Sensor-based sorting (SBS) systems typically use imaging sensors to characterize and sort bulk materials fully automatically and with high throughput. Individual objects must be recognized, object boundaries delimited and individual instances classified (Gundupalli et al., 2017). Extracted information about the material stream can then be used for subsequent sorting. In addition, knowledge of the material stream composition and properties enables adaptive parameterization of the downstream processing steps (Küppers, o. J.).

1.1 State of the art and challenges in SBS image analysis

The choice of sensors used in sensor-based sorting depends on the material properties on which the sorting decision is based. Color cameras are used for materials that can be distinguished based on their visual appearance. However, numerous materials, e.g., different types of plastic, cannot be distinguished by color characteristics, but only by their chemical molecular structure. The use of hyperspectral sensors in the near-infrared range is suitable for problems that require material-specific differentiation (Amigo et al., 2015).

Current state of the art methods for data analysis differ depending on the type of sensor used. However, they have in common that they are analyzed pixel by pixel. In the following, the use of color sensors is considered and a common processing chain is outlined.

Firstly, the image data is classified pixel by pixel (semantic segmentation) based on its three-dimensional feature vector (R-, G-, B-channel). These color features are learned, for instance, using a few training images that only show objects of one class. The classification decision is typically done using simple statistical methods. Object boundaries are differentiated using a Connected Component Analysis (CCA) or similar algorithms. Optionally, complex splitting algorithms can be used to separate contacting objects.

In the context of sensor-based sorting, conventional image processing methods are facing two major challenges. Firstly, the detection of object boundaries (single instances) through algorithms leads to a strongly decreasing detection performance with increasing occupancy density. Additionally, this process can be highly computationally intensive. Secondly, differentiating between distinct classes with similar color causes difficulties, despite having varying shapes or surface structures (see Figure 1). The use of Convolutional Neural Networks (CNNs) provides potential solutions to these challenges using information from neighboring pixels for image analysis. This additional contextual information makes it possible to also use shape and surface features for robust object detection and class differentiation (Gu et al., 2018).

Deep Learning has revolutionized the field of image processing, offering new possibilities for enhancing sensorial material detection and flow characterization. This can be used to improve accuracy and efficiency of sensor-based sorting systems and provide additional information on the composition of input material streams, thereby optimizing and controlling the entire sorting processes.

However, two major challenges exist for the practical implementation of these methods in sensor-based sorting systems (Krizhevsky et al., 2012). Firstly, these techniques require a significant amount of labeled training data for model training. Secondly, currently popular model architectures for instance segmentation such as Mask R-CNN (He et al., 2018), YOLACT (Bolya et al., 2019) and SOLOv2 (Wang et al., 2020), are not optimized for this specific problem domain, i.e., meeting real-time requirements as well as archiving high detection accuracy for a high number of small objects (Howard et al., 2017).

1.2 Contribution

In this contribution, we present strategies and solutions to overcome the presented challenges and make Deep Learning-based approaches applicable in sensor-based sorting. For this purpose, we acquire and analyze datasets for two exemplary sorting tasks. Our approach reduces data labeling requirements and computational demands, i.e., inference times. Hence, this will advance the industrial feasibility of these methods.

We provide a detailed analysis of Deep Learning usage for instance segmentation in sensor-based sorting systems. This analysis includes appropriate training strategies, specifically training data generation. The subsequent phase entails the selection of model architectures, considering the trade-off between real-time capability and achieved accuracy. The presented pipeline enables the generation of authentic synthetic training data. We then train and compare models for instance segmentation. Besides established top-down approaches, we consider a more suitable self-designed bottom-up approach. Further descriptions of both strategies can be found in chapter 3.2. The evaluation was carried out on real-recorded bulk-image Furthermore the models real-time capability for an explicit use in sensor-based sorting was analyzed.

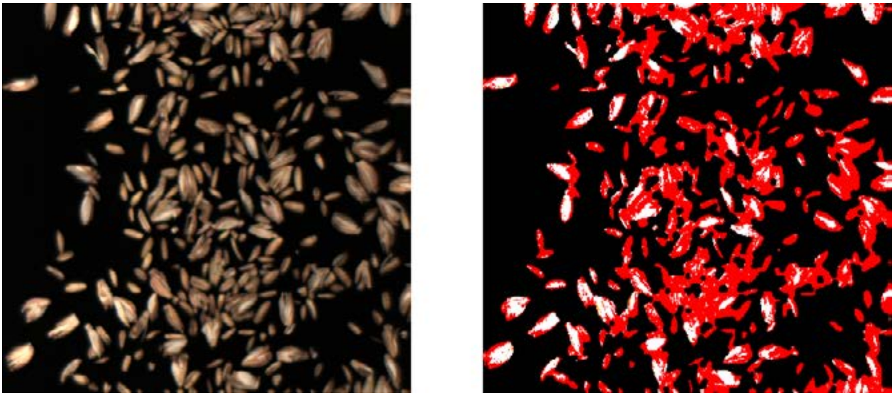

Fig. 1: Left: Original image of oats and husks, right: attribute image, calculated from pixel-by-pixel classification based on color features.

2 Methods

The following section describes the methods and datasets used. Methods for instance segmentation are considered and presented.

In general, segmentation in image processing refers to the task of summarizing the pixels of an image according to a homogeneity criterion, e.g., the affiliation of an object. Segmentation by pixel-by-pixel class assignment is also referred to as semantic segmentation. However, with this type of segmentation, no distinction is made between different instances of the same classes. With instance segmentation, on the other hand, individual instances are segmented. Each instance is also assigned a class. Unlike semantic segmentation, not every pixel has to be part of a mask.

Optimized ejection and a general characterization of a material stream requires additional information such as the number of objects, object size, etc. Since this information cannot be derived through semantic segmentation, instance segmentation is required.

2.1 Deep Learning Methods

In the following studies, three established Deep Learning methods for instance segmentation were selected, trained and applied to images acquired using a sensor-based sorting system. Top-down approaches, which first detect individual instances for which instance masks are then generated, have proven particularly successful in this context. They often consist of a backbone for feature extraction, as well as a neck and a head (Hafiz & Bhat, 2020). Fully convolutional architectures such as ResNet (He et al., 2015) are used as backbone architectures. The neck generates scaled feature maps that are used to segment objects of different sizes. The head detects individual objects on the generated feature maps and generates suitable masks. In more detail, the head often forms a Feature Pyramid Network (FPN), which generates feature maps for different scales of an image (Lin et al., 2017). The semantic meaning for FPNs is the same across all scaling levels.

Almost all top-down segmentation and detection models result in multiple detections of instances. The model then generates several bounding boxes or masks that overlap considerably, as they are actually intended for the same object. Hence, the excess masks must be suppressed. Top-down approaches therefore require non-maximum suppression (NMS) as a post-processing step. All masks or bounding boxes that have a certain overlap in terms of a threshold value with the detection that has the highest score are then searched for. These detections are then discarded as they are classified as multiple detections due to the strong overlap with a lower score. This procedure is repeated for the remaining masks.

2.2 Materials and Datasets

The methods and training strategies presented were evaluated and assessed using two different datasets. Both datasets differ in their properties and potential problems with object detection and mask generation.

The first dataset consists of approximately 4 mm to 6 mm sized fragments of brick and sand-lime brick. Both classes can be easily distinguished by simple color characteristics or differences in brightness. Due to the high variability in shape and size of the instances, the challenge here is to find the instance masks and separate adjacent instances. Particularly with high occupancy densities, the appearance of the images resembles a bulk.

The second dataset consists of oat grains and husks. The small object size results in images with a high object density. Both classes hardly differ in color tone and brightness but can be distinguished by their size and shape. The shape of the husk is highly variable and therefore useful for class differentiation, see Figure 2.

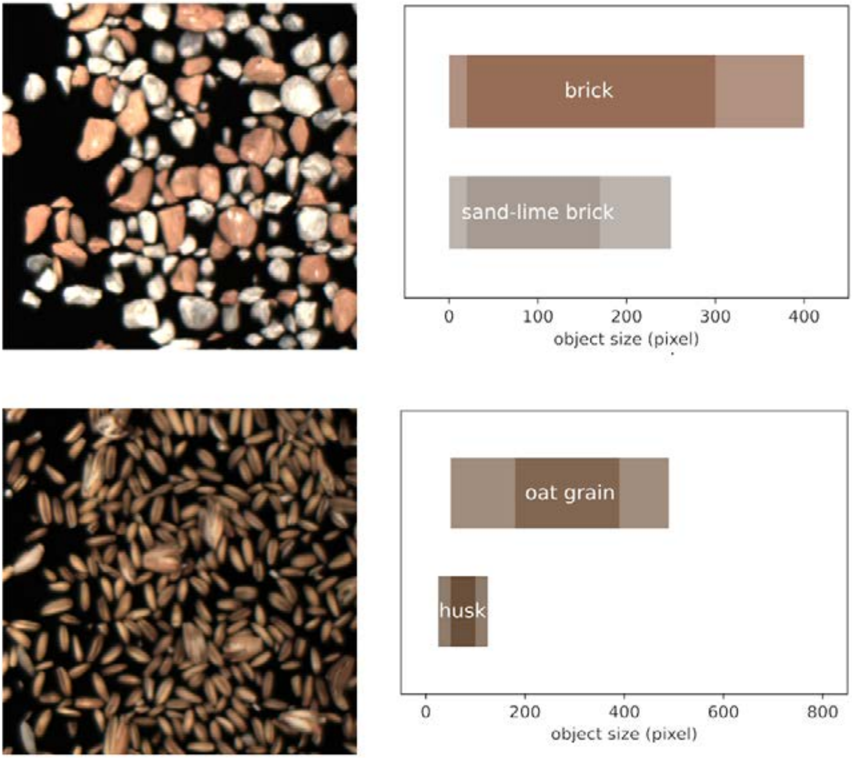

Fig. 2: Example image and class-dependent distribution of the size of the instances contained in the images for the brick and sand-lime brick data set (top) and the oats and husk data set (bottom). The color of the bars corresponds to the mean color of the objects within the respective class. The light areas indicate the variance in size.

3 Pipeline for Deep Learning-based image analysis in SBS

In the following, a pipeline is presented that is suitable for the training of Deep Learning models for the instance segmentation of bulk material images. It consists of the generation of synthetic training data and the selection of suitable models with subsequent training and evaluation.

3.1 Synthetic image generation

Deep Learning approaches require a large amount of labelled data for model training (Goodfellow et al., 2016)s. Manually labelling a single 256 x 256 training image of a bulk material scene with more than 100 objects may already take more than one hour. This is not feasible for obtaining several hundred training images. Therefore, an approach for the synthetic generation of labelled training data for instance segmentation of bulk material images was developed (see Figure 3).

Training data generation has several goals. Every single training image should be individual and unique to prevent the models from being adapted to given positioning patterns. In addition, the trained models should be made robust against disturbing influences such as variance in the background brightness within an image, varying illumination, or variances in the occupancy density, with the aim of achieving good generalization.

Segmentation on the synthetic training data may therefore be more difficult in certain respects than on the real data. For example, the arrangement of the instances in the training data may be more chaotic or have a higher maximum occupancy density. Models trained on such synthetic data might be more robust while dealing with perturbations in real-world images.

There are already approaches that have dealt with the synthesis of homogeneous object clusters (HOC). For example, in (Wu et al., 2018), an approach for the realistic placement of objects is proposed in which, similar to a GAN, a discriminator is trained to distinguish real from synthetic images. In (Toda et al., 2020) it is shown that with a simple approach, which includes the creation of a dataset by randomly placing grains of cereal on a background, a Mask R-CNN model can be trained.

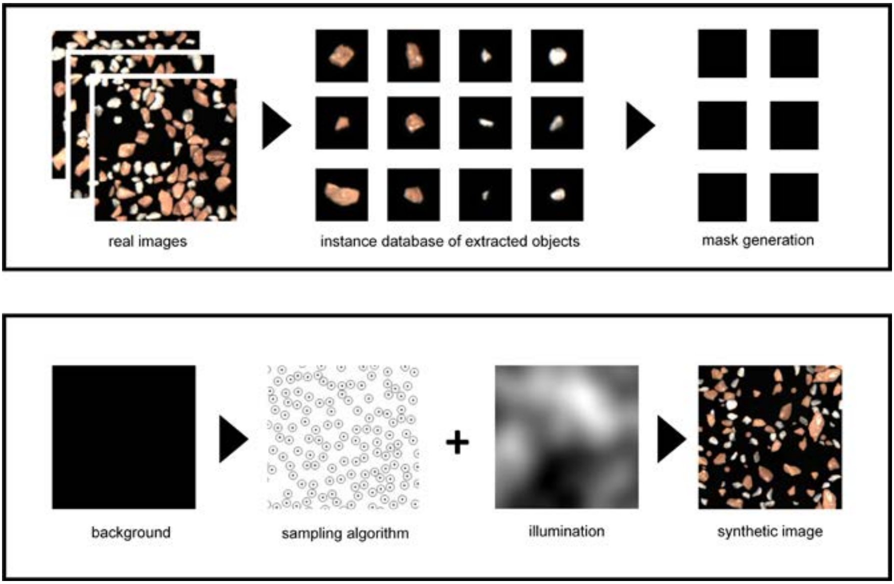

Fig. 3: Illustration of the procedure for synthetic training data generation, consisting of instance database generation from extracted objects and image generation.

3.1.1 Instance database creation

The instance database, from which the synthetic images are to be generated, consists of individual, detached instances. They form the basis for generating densely packed bulk material training images.

Recordings of a single class with a very low occupancy density are required for the creation. This allows individual, exposed instances to be extracted automatically using conventional image processing algorithms. Realistic insertion of individual instances, without the creation of hard or dark object edges, is necessary for usable training data. Object edges may not lie in the focal plane of the objects, resulting in a soft transition to the background. Therefore, simple masking and insertion is not possible and leads to the problems mentioned. Realistic images contain smooth transitions at object boundaries, which consist of a mixture of the object color of the object edge and the background color. This is modeled with so-called alpha blending, in which the resulting color p can be defined as a mixture of object $\mathrm{o}^{\mathrm{RGB}}$ and background $\mathrm{b}^{\mathrm{RGB}}$ (Porter & Duff, 1984):

$$p_{ij} = o_{ij}^{\alpha} \cdot o_{ij}^{RGB} + \left(1 - o_{ij}^{\alpha}\right) \cdot b_{ij}^{RGB}$$

This can be resolved to obtain the final object color. However, numerical instabilities occur at low alpha values o^{α}. Therefore, the alpha channel was estimated using an optimization problem. The final mask of the object is then generated by merging the estimated alpha mask and the hard mask when extracting the object instances. This process is very important to ensure that individual objects cannot be trivially distinguished from each other based on unrealistic object boundaries.

3.1.2 Image generation

An instance is now randomly drawn from the created instance database, depending on the desired percentage class distribution, and realistically positioned on a background. The positioning must be realistic, random, but still controllable in terms of occupancy density and maximum tolerated overlap (or even collision-free).

If objects are randomly dropped onto a flat surface that was previously divided into square elements of the same size, then the number of objects corresponds to that on a field of a Poisson distribution with a defined density (Jondral & Wiesler, 2002). This property can be achieved if the coordinates of an object to be placed are drawn from a normal distribution. However, this does not yet consider the area and thus the resulting overlap of objects, which makes the resulting images look unrealistic. Due to optimized material feeding on a conveyor belt, objects do not lie on top of each other but rather next to each other and only touch or overlap minimally.

To overcome these challenges, a problem specific adaption of the well know Poisson Disc Sampling algorithm (Bridson, 2007) is presented, which makes it possible to efficiently place arbitrarily oriented ellipses of different sizes without overlapping. In this way, each instance can be placed collision-free using its minimum enveloping ellipse. The degree of overlap can also be controlled by reducing the size of this ellipse. The conventional Poisson disc algorithm ensures that no two samples are too close to each other. Proximity is defined by the radius of the Poisson disc, which corresponds to half the distance between the two closest samples.

The following specific adjustments have been made:

- Collision free placement: extend Poisson Disk Sampling for ellipses of different sizes.
- Varying density: modify Poisson Disk Sampling for uniformly distributed samples.

- Disk radius is gamma distributed. The disk size of existing samples increases with each creation step.
- Two samples collide if the combined area of their disks is greater than the area of a circle whose radius is the distance between the two samples.

The object density can be defined by a parameter of the gamma distribution when randomly drawing the disk sizes. Resulting synthetic images from both datasets can be seen in Figure 4.

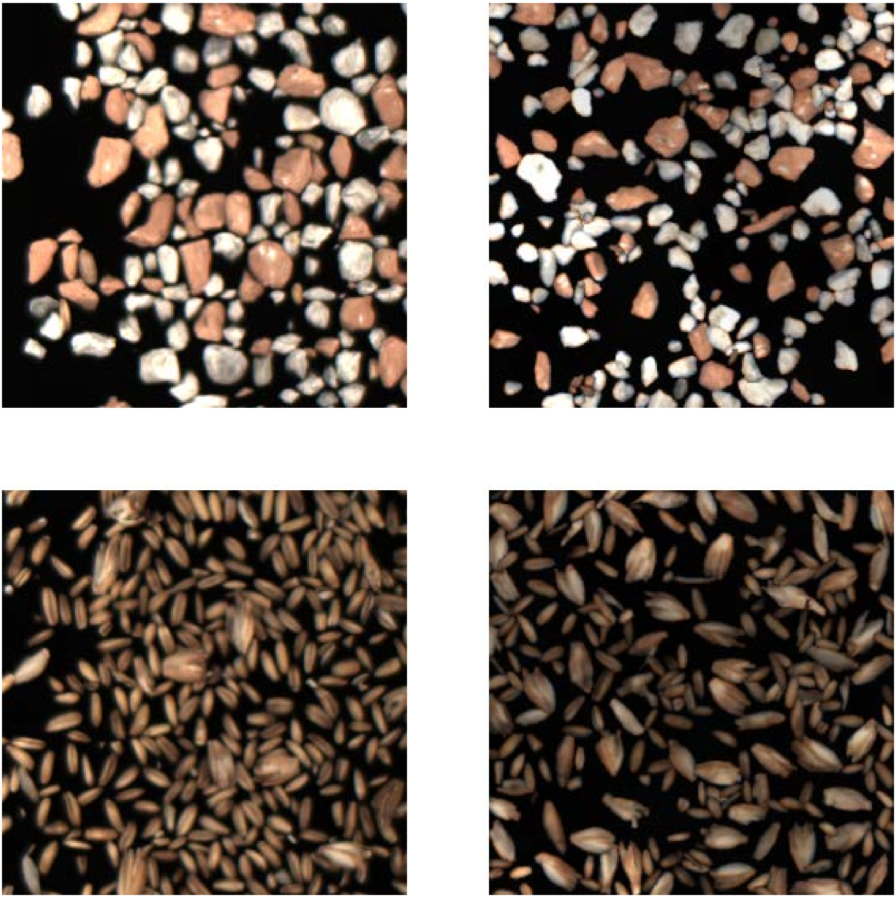

Fig. 4: Example images of the two datasets consisting of brick and sand-lime brick (top) and oats and husk (bottom), each with a real image (left) and a synthetically generated image (right).

3.2 Models for Instance Segmentation

Established top-down models for instance segmentation used as reference models in the investigation are Mask R-CNN (He et al., 2018), YOLACT (Bolya et al., 2019) and SOLOv2 (Wang et al., 2020).

However, the instance segmentation of bulk solids differs greatly from the tasks that motivated the development of the aforementioned models. These models have been developed for the use with specific large image datasets, which include many different object classes at different scales in everyday situations. Images of bulk materials are characterized by some simplifications, but also by aggravating differences, see Table 1.

Tab. 1: Differences between large image datasets and images of bulk material in terms of their image characteristics.

Large image datasets	Bulk material images
Few to many objects per image (wide range of number and size)	Very many small objects per image
Varying perspective	Consistent perspective
Lighting invariance	Uniform lighting
Different object scaling	Constant object scaling

The complexity of these model architectures is often high due to the necessary robustness against changing influences (Howard et al., 2017). In preliminary experiments we found that detecting a high number of small objects in bulk material images causes difficulties and is a disadvantage in terms of the suitability of these models. In addition to the three comparison architectures, a separate approach was tested. We developed it specifically for bulk images, i.e., the detection of a very high number of small objects with a short inference time.

A bottom-up approach was designed in which the pixels of the input image are projected into a vector space in which they can then be clustered into objects (De Brabandere et al., 2017). They generally have the disadvantage of poor mask accuracy with high variability of the expected large object shapes. Especially with a very high number of small objects, this disadvantage is greatly reduced and even becomes an advantage compared to top-down approaches. In addition, there is the advantage of a more efficient inference time with a high occupancy density.

The own bottom-up approach is based on a Fully Convolutional Neural Network (FCN) for semantic segmentation, which output is replaced by a custom head consisting of four outputs (see Figure 5). The first output provides a mask for pixel-by-pixel background segmentation. The second output provides an estimate of the relative position of the object center for each pixel that is part of an object. The third output provides the centers of the objects, i.e. the probability that each pixel is the center of an object, while the fourth output provides information about the class affiliation of the pixels or more precisely the object centers (see Figure 6).

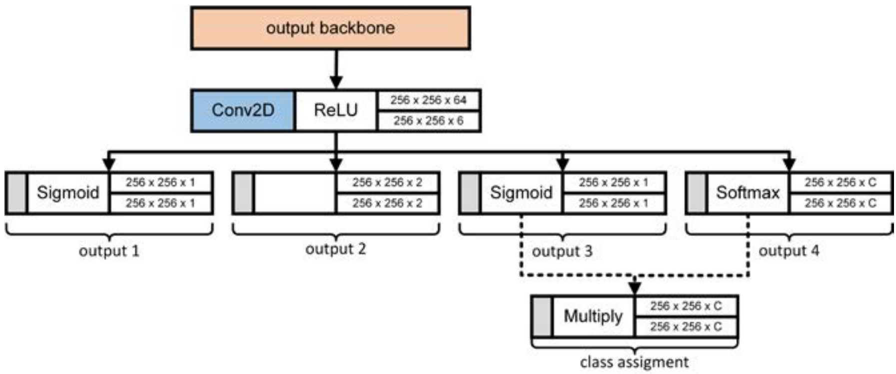

Fig. 5: Construction of the new head with the four outputs for the realization of an instance segmentation together with a fully convolutional backbone network.

The loss function in training is made up of the sum of the individual loss functions of the four outputs. According to the order of the outputs, the binary cross entropy, the mean squared error (MSE), the binary cross entropy and the focal loss were used as individual loss functions.

Merging all output data enables instance segmentation in a subsequent post-processing step. Firstly, the local maxima of the third output are searched for. Each maximum found, is regarded as an instance center. Each foreground pixel, defined by the mask of the first output, is assigned to an object. The relative pixel-by-pixel center estimation of the second output is used for differentiation of individual objects. Each foreground pixel is assigned to the object center whose center has the smallest Euclidean Distance to the relative object center point estimate. The class assignment is made by the estimated class of the fourth output at the location of the instance centers multiplied with output 3.

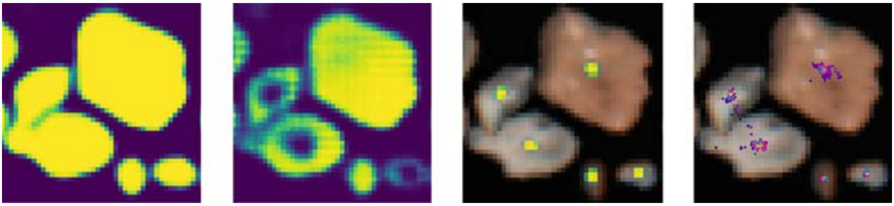

Fig. 6: Visualization of the four outputs (output 1-4 from left to right).

3.3 Training Strategies

All four models were trained with the same data. For the training, square images with a size of 256 x 256 pixels were generated. A mixture ratio of the two classes of 1:1 was used. Randomly, images of different occupancy densities between 25 and 80 % were generated with an average value of approx. 45 %. The maximum overlap of two instances of 8 pixels for the brick and sand-lime brick dataset and 4 pixels for the oats and husk dataset was selected. A total of 2000 synthetic training images were generated in each case.

For both data sets, real images were also acquired to test the models and annotated by hand. A total of 30 images per data set were labeled. We ensured that the occupancy densities in these images covered the same distribution and range as the training data.

4 Results

In the following, the results of the trained models are analyzed to determine their suitability for use in bulk goods detection. All models were trained on one of the two synthetic datasets and then evaluated on synthetic test data as well as manually labelled real test images regarding their achieved mean Average Precision (mAP) score.

The Average Precision (AP) is a measure of the detection or segmentation accuracy of detection or instance segmentation models. An object is considered correctly segmented for the AP calculation if the overlap of the predicted mask with a ground truth mask is sufficiently high. The intersection over union (IoU) is used as a measure for the overlap (UoU = Area of Overlap / Area of Union). Depending on IoU, the metric is stricter in terms of approved detections. The mAP is calculated by averaging over each class-depended Average Precision (AP) as defined for the COCO dataset (Lin et al., 2015).

4.1 Synthetic Data

The mAPs achieved are shown in Table 2 and Table 3. It can be seen that Mask R-CNN and our own approach achieve the best segmentation accuracy on both datasets. A closer look at the correlation between object size and segmentation accuracy (mAP) provides information about the suitability of the models for a given problem. This allows the performance of the models to be analyzed on different object sizes. All models have problems with the detection of small objects. Small inaccuracies in the estimated masks already have a relatively large negative impact on the metric compared with large objects. In addition, images with a high occupancy density have a larger number of small objects, as these fit and are located well in small gaps. This affects both the synthetic and the real images and causes a poorer metric in the object size-dependent analysis.

Further experiments were performed to investigate the mAP score at different occupancy densities. The mAP was calculated for each individual image of the synthetic sand-lime brick dataset and plotted against the occupancy density. As expected, the detection and mask accuracy decrease with increasing occupancy density. The scatter of the Mask R-CNN results is lower than for the other models. At very high occupancy densities, the own approach has an advantage over the other models, especially Mask R-CNN, which in turn has advantages at lower occupancy densities.

It should be noted that the mAP score of the entire dataset is calculated using the Precision Recall curve of all detections of all images and not by averaging the individual image-specific mAP scores achieved. Images with many objects have a greater influence on the metric and cause the advantage of the own approach over Mask R-CNN.

Tab. 2: Achieved mAP scores of the four different models on the synthetic brick and sand-lime brick dataset.

	Own approach	Mask R-CNN	YOLACT	SOLOv2
mAP [IoU=0.50:0.95]	0.674	0.655	0.305	0.440
mAP [IoU=0.50]	0.904	0.907	0.702	0.869
mAP [IoU=0.75]	0.793	0.769	0.216	0.413

Tab. 3: Achieved mAP scores of the four different models on the synthetic oats and husk dataset.

	Own approach	Mask R-CNN	YOLACT	SOLOv2
mAP [IoU=0.50:0.95]	0.722	0.716	0.343	0.493
mAP [IoU=0.50]	0.920	0.940	0.757	0.938
mAP [IoU=0.75]	0.855	0.863	0.273	0.460

4.2 Real Data

The results of the evaluation of the trained models on real images can be found in Table 4 and Table 5. In addition to the evaluation of the detection performance of the models, it enables an analysis of the transferability of the models trained on synthetic data to be applied to real images. The real images of the test dataset were manually annotated in a very time-consuming process.

As expected, the mAPs drop slightly for both datasets compared to the evaluation on synthetic test data for all models. Only SOLOv2 and YOLACT achieve comparable results on the sand-lime brick dataset. The evaluation shows that SOLOv2 has a better mAP than Mask RCNN on both datasets. A closer examination of the metrics shows a decrease in mask accuracy, while the detection capability remains the same. In general, our approach and SOLOv2 learn better, more generalized features on the synthetic training data. One of the reasons is the lower complexity and size of the models. YOLACT has a consistently low detection performance. Examination of the results reveals problems with the accuracy of the masks in very dense scenarios.

Tab. 4: Achieved mAP scores of the four different models on the real brick and sand-lime brick dataset.

	Own approach	Mask R-CNN	YOLACT	SOLOv2
mAP [IoU=0.50:0.95]	0.573	0.495	0.419	0.608
mAP [IoU=0.50]	0.935	0.940	0.848	0.941
mAP [IoU=0.75]	0.685	0.367	0.167	0.541

Tab. 5: Achieved mAP scores of the four different models on the real oats and husk dataset.

	Own approach	Mask R-CNN	YOLACT	SOLOv2
mAP [IoU=0.50:0.95]	0.387	0.361	0.153	0.408
mAP [IoU=0.50]	0.812	0.835	0.520	0.698
mAP [IoU=0.75]	0.349	0.251	0.102	0.317

4.3 Real time capability

Certain real-time conditions must be ensured for an application in a sensorbased sorting system. When using Deep Learning models for instance segmentation, this often becomes a critical factor, as many models were not designed for such applications. It must also be noted that the inference time, including post-processing of the data up to instance segmentation, depends on the number of detected objects.

In general, the inference time can be further optimized using suitable Frameworks such as TensorRT for Nvidia GPUs. In the following, this was dispensed with and primarily enables a comparison of the models with each other. Figure 7 plots the relationship between inference time and the mAP achieved by the models on the synthetic test datasets. The established models behave as expected, faster models such as YOLACT have a lower detection performance than large and slow models such as Mask R-CNN. The proprietary approach was developed for the instance segmentation of bulk material. It shows both the highest mAP value and the lowest runtime.

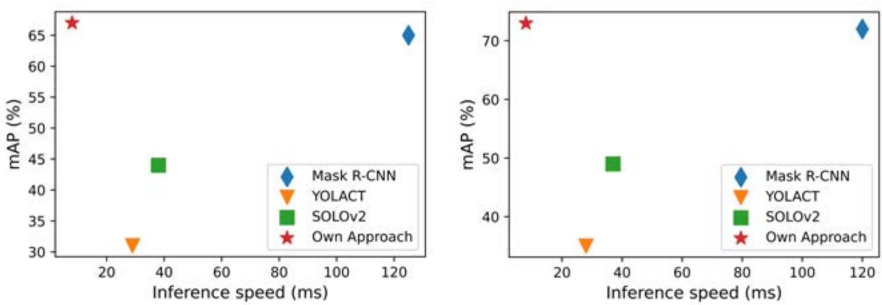

Fig. 7: Achieved mAP plotted over the achieved inference time, using a NVIDIA GeForce RTX 3080, of the different models on the brick and sand-lime dataset (left) and the oat and husk dataset (right).

5 Conclusion

The limitations of classical image processing algorithms for instance segmentation were demonstrated using two real bulk material datasets, consisting of bricks and sand-lime bricks as well as oats and husks. The results show that Deep Learning methods perform better with very high occupancy densities and material classes that do not differ in their color features. The presented training pipeline, consisting of the synthetic training data generation, is very well suited to avoid time-consuming, manual labeling. Generated images are realistic in their object arrangement and show sufficient stochastic fluctuations to learn robust models. The selection of models revealed the problem of established architectures, which sometimes do not perform well with the large number of small objects. Our approach has less than half the inference time compared to the fastest model and outperforms the detection performance and mask accuracy of the most accurate model. When using Deep Learning models, it is recommended using own architectures for instance segmentation, like the presented bottom-up approach, as these can satisfy real-time conditions for sensor-based sorting tasks.

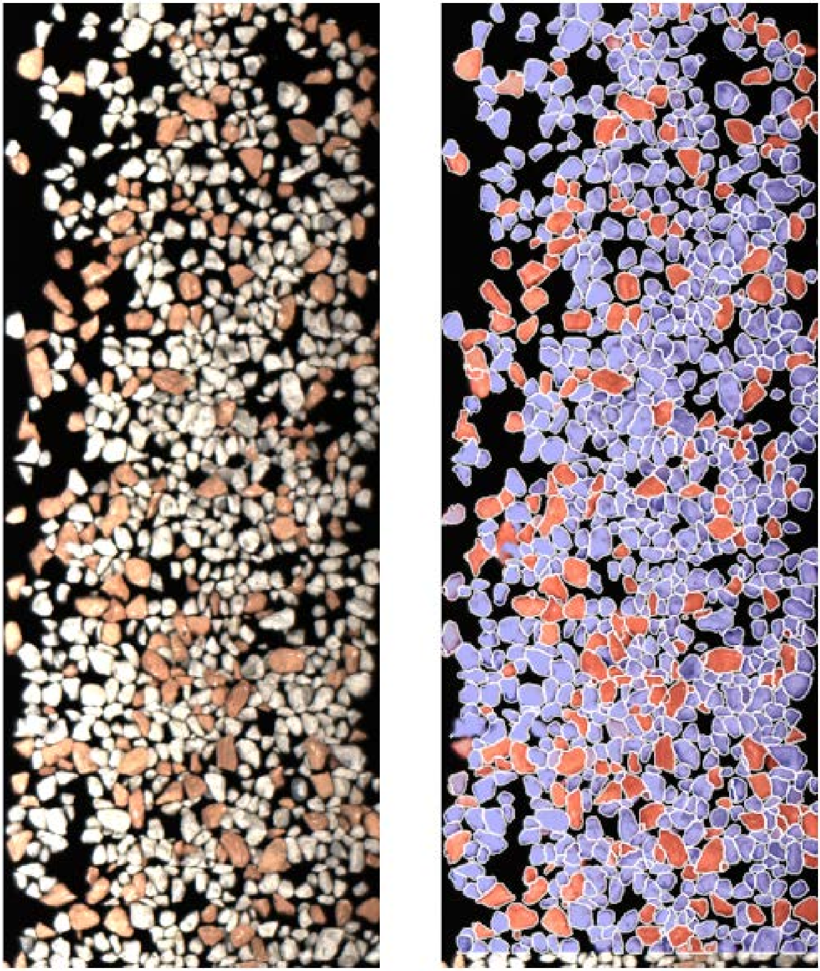

Fig. 8: Detection result of a Deep Learning based instance segmentation at high occupancy density of bricks (red masks) and sand-lime bricks (blue masks). The missing segmentation of the bottom lines is the result of the use of line scan sensors and the absence of padding in the model architecture used.

References

Amigo, J. M., Babamoradi, H., & Elcoroaristizabal, S. (2015). Hyperspectral image analysis. A tutorial. *Analytica Chimica Acta*, *896*, 34–51. https://doi.org/10.1016/j.aca.2015.09.030

Bolya, D., Zhou, C., Xiao, F., & Lee, Y. J. (2019). YOLACT: Real-time Instance Segmentation. *arXiv:1904.02689 [cs]*. http://arxiv.org/abs/1904.02689

Bridson, R. (2007). Fast Poisson disk sampling in arbitrary dimensions. *ACM SIGGRAPH 2007 Sketches*, 22. https://doi.org/10.1145/1278780.1278807

De Brabandere, B., Neven, D., & Van Gool, L. (2017). *Semantic Instance Segmentation with a Discriminative Loss Function* (arXiv:1708.02551). arXiv. https://doi.org/10.48550/arXiv.1708.02551

Goodfellow, I., Bengio, Y., & Courville, A. (2016). *Deep learning*. The MIT Press.

Gu, J., Wang, Z., Kuen, J., Ma, L., Shahroudy, A., Shuai, B., Liu, T., Wang, X., Wang, G., Cai, J., & Chen, T. (2018). Recent advances in convolutional neural networks. *Pattern Recognition*, *77*, 354–377. https://doi.org/10.1016/j.patcog.2017.10.013

Gundupalli, S. P., Hait, S., & Thakur, A. (2017). A review on automated sorting of source-separated municipal solid waste for recycling. *Waste Management*, *60*, 56–74. https://doi.org/10.1016/j.wasman.2016.09.015

Hafiz, A. M., & Bhat, G. M. (2020). A Survey on Instance Segmentation: State of the art. *International Journal of Multimedia Information Retrieval*, *9*(3), 171–189. https://doi.org/10.1007/s13735-020-00195-x

He, K., Gkioxari, G., Dollár, P., & Girshick, R. (2018). *Mask R-CNN* (arXiv:1703.06870). arXiv. https://doi.org/10.48550/arXiv.1703.06870

He, K., Zhang, X., Ren, S., & Sun, J. (2015, Dezember 10). *Deep Residual Learning for Image Recognition*. arXiv.Org. https://arxiv.org/abs/1512.03385v1

Howard, A. G., Zhu, M., Chen, B., Kalenichenko, D., Wang, W., Weyand, T., Andreetto, M., & Adam, H. (2017). *MobileNets: Efficient Convolutional Neural Networks for Mobile Vision Applications* (arXiv:1704.04861). arXiv. https://doi.org/10.48550/arXiv.1704.04861

Jondral, F., & Wiesler, A. (2002). *Wahrscheinlichkeitsrechnung und stochastische Prozesse: Grundlagen für Ingenieure und Naturwissenschaftler ; mit 45 Übungsaufgaben und Tabellen* (2., durchges. und aktualisierte Aufl). Teubner. https://doi.org/10.1007/978-3-663-01598-7

Krizhevsky, A., Sutskever, I., & Hinton, G. E. (2012). ImageNet Classification with Deep Convolutional Neural Networks. *Advances in Neural Information Processing Systems*, *25*. https://proceedings.neurips.cc/paper_files/paper/2012/hash/c399862d3b9d6b76c8436e924a68c45b-Abstract.html

Küppers, B. (o. J.). *Relevance and challenges of plant control in the pre-processing stage for enhanced sorting performance*.

Lin, T.-Y., Dollár, P., Girshick, R., He, K., Hariharan, B., & Belongie, S. (2017). *Feature Pyramid Networks for Object Detection* (arXiv:1612.03144). arXiv. https://doi.org/10.48550/arXiv.1612.03144

Lin, T.-Y., Maire, M., Belongie, S., Bourdev, L., Girshick, R., Hays, J., Perona, P., Ramanan, D., Zitnick, C. L., & Dollár, P. (2015). *Microsoft COCO: Common Objects in Context* (arXiv:1405.0312). arXiv. https://doi.org/10.48550/arXiv.1405.0312

Porter, T., & Duff, T. (1984). Compositing digital images. *ACM SIGGRAPH Computer Graphics*, *18*(3), 253–259. https://doi.org/10.1145/964965.808606

Toda, Y., Okura, F., Ito, J., Okada, S., Kinoshita, T., Tsuji, H., & Saisho, D. (2020). Training instance segmentation neural network with synthetic datasets for crop seed phenotyping. *Communications Biology*, *3*(1), Article 1. https://doi.org/10.1038/s42003-020-0905-5

Wang, X., Zhang, R., Kong, T., Li, L., & Shen, C. (2020). *SOLOv2: Dynamic and Fast Instance Segmentation* (arXiv:2003.10152). arXiv. https://doi.org/10.48550/arXiv.2003.10152

Latency evaluation of a CNN enhanced FPGA-based sorting system

Simon Wezstein[1,2]*, Oliver Gräff[2], Michael Stelzl[2], Michael Heizmann[1]

1 Karlsruhe Institute of Technology, Institute of Industrial Information Technology, Karlsruhe, Germany
2 MSTVision GmbH, Ginsheim-Gustavsburg, Germany

* Corresponding Author: Im Weiherfeld 10, 65462 Ginsheim-Gustavsburg, simon.wezstein@mstvision.de

Keywords: Latency, FPGA-based sorting, System optimization, Frame grabber, VisualApplets, Line scan, GPU real-time

Abstract

This contribution assesses the latency values of a field programmable gate array (FPGA) based sorting system, with a graphics processing unit (GPU) involved for convolutional neural network (CNN) inference. The system reaches a mean overall latency of 2.1 ms while the jitter is 4.0 ms for repeated single object experiments. The jitter originates from memory operations on the FPGA and dropouts in the PC processing pipeline. For multiple object experiments a currently unknown latency source is observed, increasing the maximum observed PC pipeline latency to 10.4 ms.

7 Introduction

The whole field of industrial image processing is talking about the usage and benefits of convolutional neural networks (CNNs) or other algorithms from the field of AI. Major benefits using CNNs are: The amount of required domain specific knowledge is reduced, because the user may annotate the classes, train the used model, and deploy the model directly to the machine – while he would need to know the influence of the parameters of a comparable rule-based system. Further, the complexity for the adaption of a classifier to a new product is reduced because the source code of the system does not need to be changed. The downside is – together with the need for meaningful training data – the high computational expense in the inference compared to an optimized rule-based system. This leads to limitations in data throughput. To compensate this, most applications rely on graphics processing units (GPUs), which are more suitable for most computational tasks in CNNs than Central Processing Units (CPUs). This leads to a latency bottleneck because data transfer and execution control on GPUs needs extra time.

The fully Field Programmable Gate Array (FPGA) integrated sorting approach by MSTVision GmbH achieves short image processing latencies (<1 ms) by running the whole rule-based sorting task on an FPGA. Low latencies keep the reaction time between line scan image acquisition and separation actuators low (Fig. 1), which results in less oversorting due to reduced accumulation of unexpected material movement like in-axis-shifts and tumbling (Pfaff et al., 2015). While the concept proved its capabilities in plastic granule sorting, customers asked for more capabilities in image processing and classification. The system has been extended with GPU based CNN inference for classification, which we showed on the Vision fair 2022. Regarding the previous, fully FPGA integrated system, the camera interface was changed from CameraLink to CoaXPress, too.

In this contribution we measure and describe the system latency after adding a GPU to the image processing pipeline. Like in our last contribution (Wezstein et al., 2022) for SBSC we aim for highly detailed measurements. We want to get comparable data to our last measurements, too. Since our contribution to SBSC in 2022, the shortcomings of actuator control were fixed, we assess that fix, too. The desired full system latency (image to actuator control) is 5 ms or less.

8 Setup and methods

A complete sorting system, processing multiple objects at a time and undefined material is not suitable for reproducible timing analysis. The experimental setup from (Wezstein et al., 2022) is re-used for the new measurements. In contrast to our previous measurements, the side camera, oscilloscope, valve controller and valve are not considered here and removed. In addition, GPU-only measurements are carried out. With the extra data captured, we can assess the PC-system's timing properties more appropriately.

Our prototype consists of an altered version of MSTVision GmbH's "High Speed Sorting" solution. The original system consists of one Basler AG frame grabber, whose FPGA is configured via VisualApplets, a line scan camera, an MSTVision Trigger Board and one or more of their Matrix 32 boards. Typically, a CameraLink interface and a matching monochrome line scan camera is used. (Stelzl, 2019) Our prototype uses a slightly different hardware configuration, see Tab. 1 for details. Instead of using the previously proven fast FPGA algorithms for object feature extraction and classification, the line scan data is merged into a 2D representation. A Blob analysis algorithm is used for object detection, where the objects are extracted and passed together with the Blob properties and the 2D representation to the host system's main memory. There may be multiple objects in one transfer, depending on the object count in the 2D representation. The data is preprocessed on the host and transferred to the GPU afterwards. After the CNN inference, the results are transferred back to the host system. The post processing algorithm determines the final classification result, which is then transferred back to the FPGA. The FPGA handles the object timing. After the set-up time, the object is rejected, if the inferred class should be rejected.

To achieve low latencies with a data loop through the host system including its GPU, a real-time environment is used. Real-time systems need to be a matching set of hardware and software, the used components are listed in Tab. 1 and Tab. 2. For communication and PC image processing the purposely developed MSTVision LowLatency Framework is used. All measurements use the same hard- and software configuration. The hardware components are used with optimized energy management parameters to lower the compute latencies.

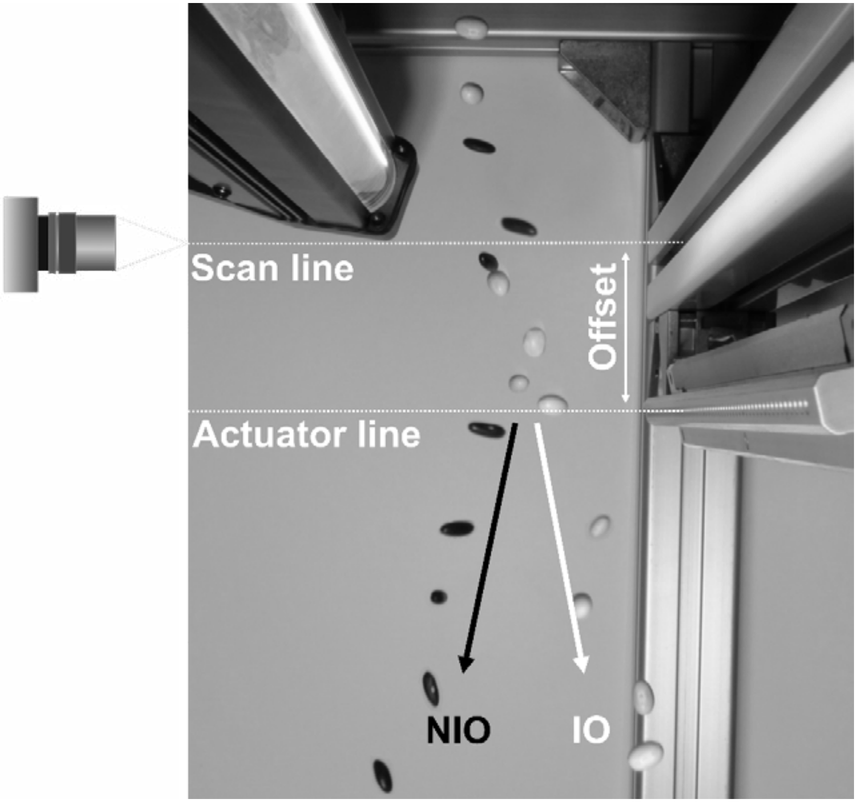

Fig. 1 Illustration of the effect of reducing the offset between scan line and actuator line in a sorting application. Overview of the system used for multiple object measurements.

Tab. 1: System hardware components.

Component	Model/Configuration
Frame grabber	Basler imaWorx CXP-12 Quad
Camera	Teledyne e2v Eliixa Plus EV71YC4MCP1605-BA0 (16384x1 pixels,100 kHz line frequency)
GPU	Nvidia Quadro RTX 4000
CPU	AMD EPYC 7551P
Mainboard	Supermicro H11SSL-I Rev. 2.0
RAM	8 channels of 8 GiB DDR4-ECC-Reg 2133 MHz

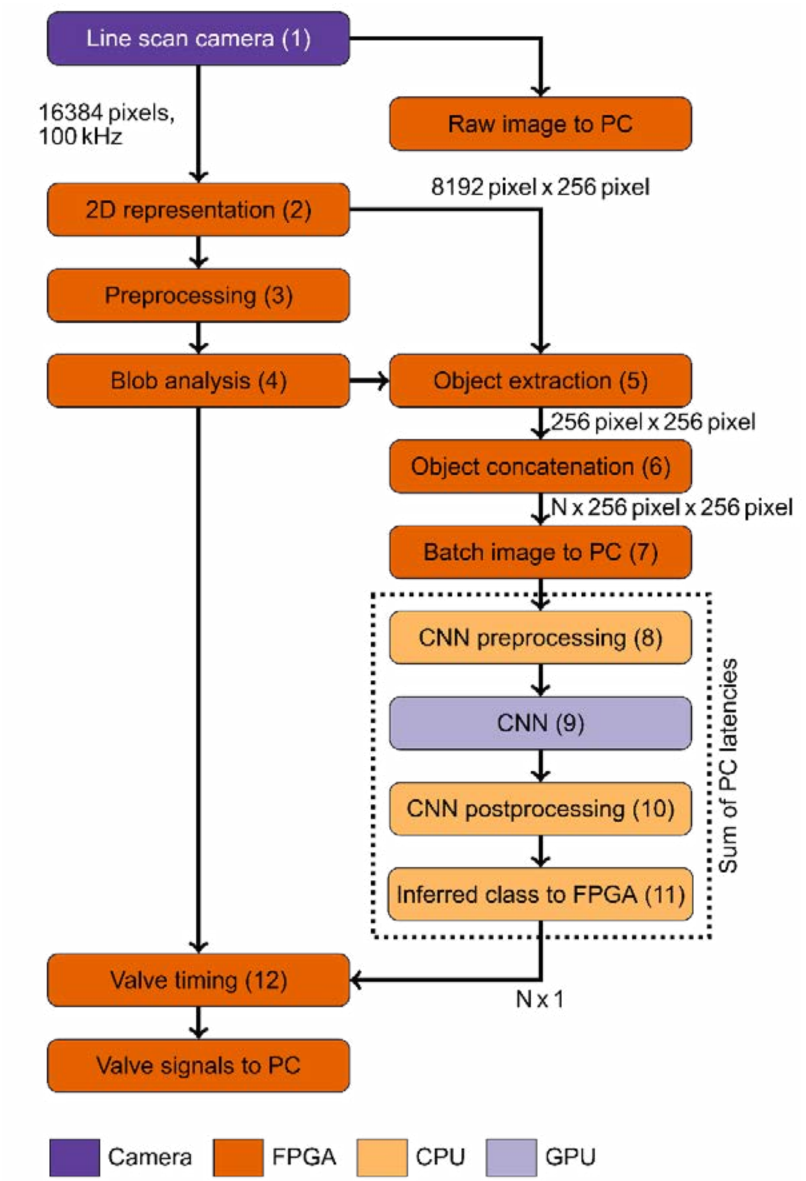

Fig. 2 System data flow model, all shown image dimensions are noted without our extra timing information, needed for the measurements.

Tab. 2: System software components.

Component	Model/Configuration
Operating system	Debian 11 with PREEMPT_RT 5.10
GPU driver	Nvidia 515.43.04
ONNXRuntime	rel-1.12.1 with modifications
CUDA	11.7
CUDNN	8.4.1
TensorRT	8.4.2.4

8.1 GPU only setup

A measurement series with the GPU on its own is used to determine the latency baseline for the whole system. There are three different measurements:

1. Measuring the compute time for a batch size of 1 with varying pause between subsequent calculations.
2. Measuring the compute time for a batch size of 1 with varying pause between subsequent calculations, but with latency optimizations in terms of GPU energy management.
3. Measuring the compute time for a varying batch size of 1 to 32 without unnecessary pausing between calculations. The optimizations of (2) are used, too.

In the Fig. 3 the measurement strategy is illustrated. For all measurements a single Nvidia Quadro RTX4000 GPU is used. The CNN is a grayscale modified version of the ShuffleNet v2 (Ma et al., 2018) provided in the ONNX format and loaded, optimized, and ran by Nvidia TensorRT. The measurements with varying batch sizes are carried out sequentially, every batch size for itself.

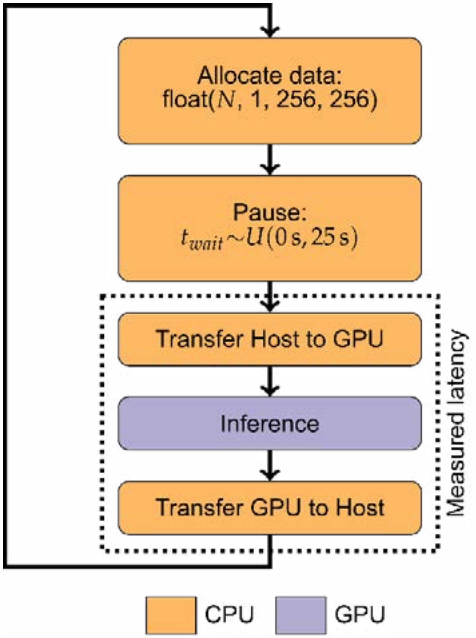

Fig. 3 Strategy for GPU only measurements. The Parameter N denotes the used batch size, the pause step is only used for the single batch measurements (see Sections 2.1.1 and 2.1.2). U denotes a uniform distribution.

8.2 Experimental setup for single objects

To create experimental data for single objects, plastic balls (diameter 6 mm, mass 0.12 g) are dropped with a dispenser. A single ball then falls through the scan line of the camera and is processed by our system. The line scan camera operates at a line frequency of 100 kHz and a line width of 16384 pixel in 8 Bit mode. The data is then binned to 8192 pixel width in the FPGA. The data rate for our sorting design is the same as in (Wezstein et al., 2022). The CNN is fed with extracted single object batches with a resolution of (256 x 256) pixel. The data is grayscale and because of single sized batches the resulting input dimension is 1x1x256x256. There is no rescaling of objects in the processing pipeline.

The collected timing information comprises:

- Camera trigger rising and falling edge,
- Camera line first and last pixel received,
- Object detection timestamp,
- Extracted image of the object with timing information,
- Latency of CNN inference (measured with CPU),
- Latency for uploading information (measured with CPU),
- Overall latency for “GPU-Loop” (measured with FPGA),
- Actuator data timestamps.

8.3 Experimental setup for multiple objects

To create experimental data for multiple objects falling simultaneously, our trade fair demonstration setup (Fig. 1) is used. The setup uses a vibrational feeder to feed the same plastic balls from the single setup. The inspection width is approximately 320 mm. The camera resolution and line frequency are the same as in the single setup. We don’t use any actuator; the setup is only used to generate all relevant timing data. The object data for the CNN comprises multiple batch sizes (N) and the resulting input dimension is Nx1x256x256. The image data and the measured latencies are written to an SSD array while the machine is running. The captured data comprises the same measurements as the single setup.

9 Results

In this chapter we explain and analyse the results of our measurements. The first section “GPU-Only Setup” covers baseline latencies for our CNN. With the expectations of these measurements, the measurements with single objects are evaluated. With the multi object measurements, we cover the latency effects for a higher system load.

9.1 GPU only setup

The following graphs show the results of the GPU measurements. The two measurements with varying pause times (Fig. 4, Fig. 5) show a clear latency jump after a pause of about 15 seconds. For the calculation of simple statistics, the data is divided into two parts: latencies for periods <= 14 seconds and latencies for periods >= 16 seconds. See Tab. 3 for a summary. We observed these latency jumps in previous measurements. Therefore, we started a thread at Nvidia's forums (Nvidia, 2023), but until today they didn't provide a detailed answer on that.

Our optimizations reduce the maximum latency of 25.3 ms to 5.5 ms. For values with pauses <= 14 s, the maximum latency reduces from 1.8 ms to 1.6 ms. For small pauses, the gain is only ca. 200 μs, but the coefficient of variation decreases from 8.7% to 2.0%.

The multi-batch size measurement, see Fig. 6, shows nearly linear latency increases for batch size increases. Batch size 1 is an exception. We don't know yet, why a value of 1 has 1.24 ms ± 1.2% while a value of 2 leads to 0.828 ms ± 0.39%, which means ca. 1.5 times more latency for calculating half the amount of data. We excluded it for the linear fit shown in the figure. We suspect PCIe transmission optimization of the system firmware or something similar in the GPU firmware to be the cause. Considering the intercept value of 395 μs, we estimate it to be the costs for controlling the data transfers and the control of the GPU by the host. The slope of 185 μs is considered as the costs for the inference and the raw data transfer.

Tab. 3: CNN processing timings for GPU-only, single batch measurements. All values except COV and Count in milliseconds, COV is the coefficient of variation and Count the sample count.

	Mean	COV	Min	Max	Count
Non-Optimized, Period <= 14 s	1.474	8.66%	1.352	1.796	7810
Non-Optimized, Period >= 16 s	15.12	23.0%	1.842	25.30	5022
Optimized, Period <= 14 s	1.297	2.04%	1.242	1.569	7509
Optimized, Period >= 16 s	1.823	12.2%	1.704	5.508	4823

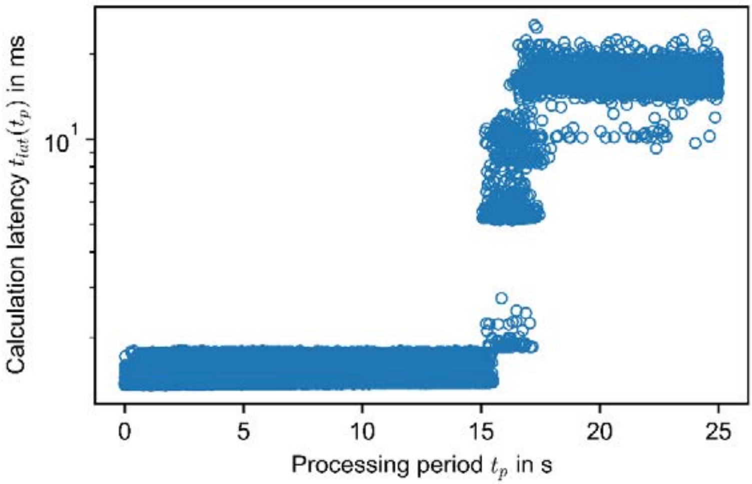

Fig. 4 Scatter plot of the non-optimized single batch latencies with varying period times between inferences.

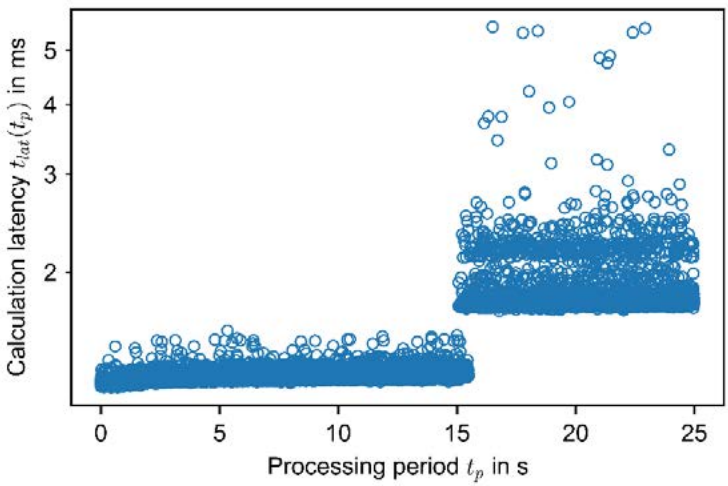

Fig. 5 Scatter plot of the optimized single batch latencies with varying pause times between inferences.

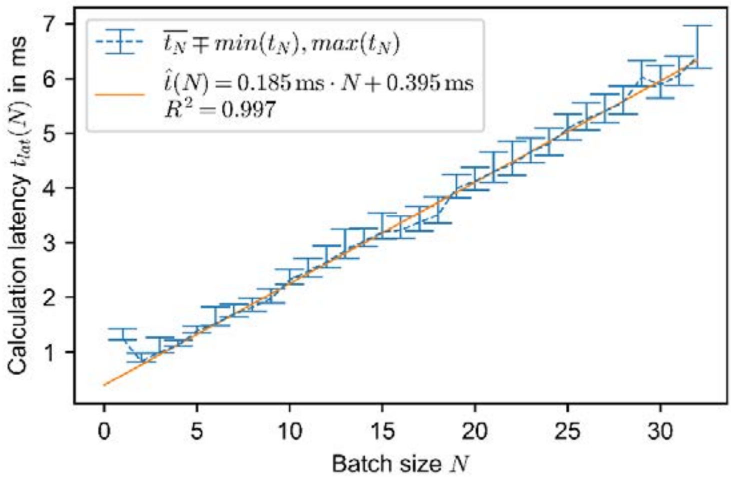

Fig. 6 Error bars of the multi-batch measurements. The linear fit is without .

9.2 Experimental setup for single objects

For the single experiment setup 1400 plastic balls were processed in 5 measurement series. For all timing values, the first object was removed from the series, because the first CNN inference was extremely long due to internal optimizations.

9.2.1 Image acquisition timings

The camera operates at 100 kHz line frequency and has a line width of 16384 pixels configured with 8 Bit depth. For triggering the CXP interface is used, the trigger signal and width are generated by the FPGA. The width controls the sensor integration time, and the frequency controls the line frequency. As the camera operates with 4 CXP links at 6 Gbit/s, we expect a theoretical maximum bandwidth of 3 GB/s. For a line of 16 KiB of data, the theoretical minimum transfer time is 5.46 µs. The expected transfer period is the same as the trigger: 10 µs. The “Trigger to full transfer” time describes the time from trigger start to receiving the last pixel of a line. It is the sum of trigger period, transfer delay and transfer period. The measured values (Tab. 4) are within expectation.

*Tab. 4: Camera timing, all values, except Count, in µs. The sample count is denoted as Count. *) Some standard deviations are smaller than one FPGA clock period (3.2 ns), therefore a continuous uniform distribution of one cycle period was used, leading to a standard deviation of 0.924 ns.*

	Expected	Mean	Std*	
Trig. period	10.0	10.0	0	9171718
Trig. width	4.0	4.0	0	9171958
Transfer delay	-	55.2	18.15e-3	9171958
Transfer time	5.46	7.41	4.58e-3	9171958
Transfer period	10.0	10.0	20.42e-3	9171718
Trigger to full transfer	66.6	66.6	18.44e-3	9171958

9.2.2 Object detection and extraction timings

A “first in first out” buffering like mechanism is used to form a 2D representation from the line scan data. The buffer’s height is 256 lines. Due to the nature of line accumulation, the expected latency for detection and extraction is approximately 256 lines multiplied by the line period of 10 µs.

The measurements (Tab. 5), except the extraction time, show a uniform distribution (Fig. 7) with an interval width of 2552 µs, which is near our expected, static latency. The root cause for this behaviour lies in the Blob analysis of VisualApplets: as soon as an object is scanned, the data is output and processed by our design (Basler AG ,2023). This jitter was initially not taken into account. The extraction time, with a value of 41.6 µs ± 0.7 µs for one object, is negligible in terms of latency and jitter.

Tab. 5: Object detection and extraction timings, all values in µs. The sample count is 1395 for each value.

	Expected	Mean	Std	Min	Max
Delay: Last pixel to detection	2560	1319.2	730.7	23.1	2574.7
Delay: Last pixel to extraction	2560	1326.5	730.8	28.5	2588.9
Extraction time	-	41.6	0.732	39.6	43.8

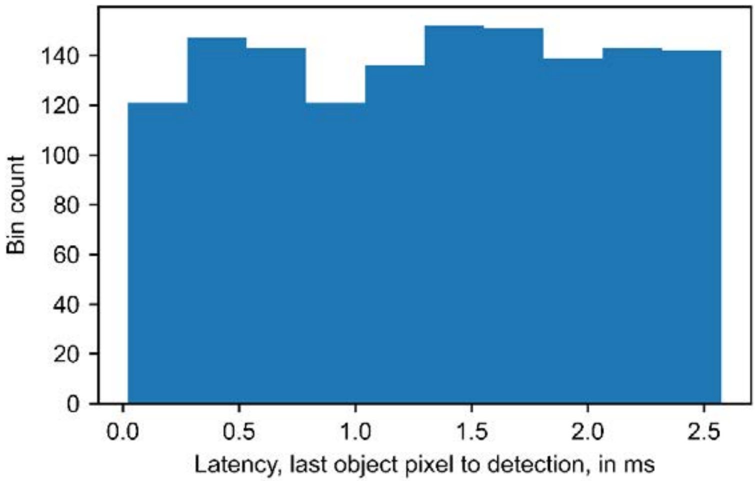

Fig. 7 Histogram of the latencies between last object pixel occurrence in the raw data stream and the detection, steps 1 to 4 in Fig. 2.

9.2.3 CNN processing timings

The expected latency for the CNN inference is ca. 1.3 ms, as measured in the GPU-only measurements. For preprocessing, postprocessing and data transfer, we expect lower latencies, because of the simple operations needed and highly optimized communication paths. The class response is communicated via PCI-Express port IO. Due to its directly CPU bound operation, we can measure it directly.

The measurement values, shown in Tab. 6, show higher values for CNN inference than expected. The root cause of this may lay in thread management as the used inference library creates its own thread pool. The high maximum values for the other operations may be thread blocking issues or additional latencies originating from the used non-uniform memory access (NUMA) architecture.

Tab. 6: CNN processing timings, all values in µs. The sample count is 1395 for each value.

	Expected	Mean	Std	Min	Max
Preprocessing	-	67.0	19.0	47.5	495.5
CNN Inference	1.3	1685.2	231.9	1434.0	3193.0
Postprocessing	-	10.7	10.7	7.2	33.9
Answer telegram	-	115.1	115.1	97.2	237.9

9.2.4 Actuator control timing

Actuators are controlled with a polling algorithm, running at a frequency of 3.125 kHz. The internal time base has a resolution of 0.1 ms. We set our system to a delay time of 10 ms. We expect the timing from object occurrence, step 1 in Fig. 2, to actuator control, step 12 in Fig. 2, to be a uniform distribution in the range of [10 ms, 10.32 ms].

Our measurements (Tab. 7) show a high standard deviation of 739.5 µs and a value span of 2862 µs for the delay time of the actuator control. To find the root cause, the delay between object detection and actuator control was measured, too. There the standard deviation is an order of magnitude lower (95.9 µs), and the value span is 391 µs, nearly as expected. We expect the sampling of the object occurrence time stamp as the root cause. It seems that the creation of the 2D representation passes its latency distribution (see Section 3.2.2) to the object detection, too. Initially we expected it just to add constant latency, which would not be a problem, as this can be calibrated. In Figs. 8a and 8b, the histograms of the two-value series are shown. They confirm the assumed uniform distribution.

Tab. 7: Actuator control timings, all values in µs. "U" denotes a continuous uniform distribution. The sample count is 1389 for each value.

	Expected	Mean	Std	Min	Max
Object to actuator	U(10 ms, 10.32 ms)	10.5e3	739.5	9.03e3	11.9e3
Detection to actuator	<10.0e3	9.17e3	95.9	8.97e3	9.36e3

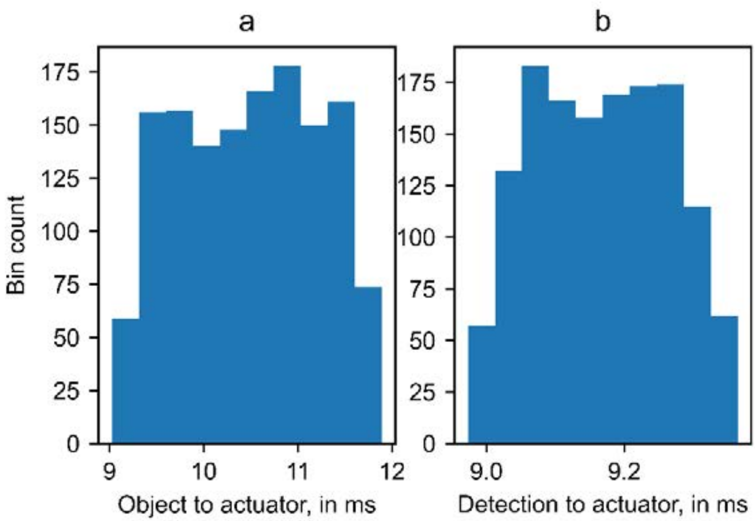

Fig. 8 Comparing the actuator timing value distributions, steps 1 to 12 in Fig. 2. Part a shows the delay time between the last object pixel acquired and the start of the actuator signal, part b shows the delay time from the object detection to the actuator signal.

9.2.5 Full round-trip timings

A full round-trip is the complete time needed for one object to get processed by the system, measured between the last object pixel acquired and the end of the reply telegram of the PC. In addition, we measure the time for the system to process one extracted object and the time for the PC operations to complete. The difference between these values suggests that the latencies are caused by direct memory access (DMA) and thread communication.

All measurements (Tab. 8) show high standard deviations. The histogram for the measurement “Sum of PC latencies”, Fig. 9, shows a distribution typical for real time dropouts, while the histogram for the full round trip (Fig. 10) looks more like a uniform distribution. The problem found in Section 3.2.2 dominates the jitter of our system, limiting it to a minimal practical useable delay setpoint of 6 ms. The second highest impact for system performance is the high value span (1.95 ms) of the PC operations.

Tab. 8: Full round-trip timings, all values in μs. The sample count is 1395 for each value.

	Expected	Mean	Std	Min	Max
Object extraction to answer	ca. 2e3	2063.8	269.1	1771.7	3851.2
Sum of PC latencies	<2e3	1878.1	248.1	1601.1	3551.5
Full round trip	ca. 3.3e3	3431.9	791.4	1877.4	5895.7

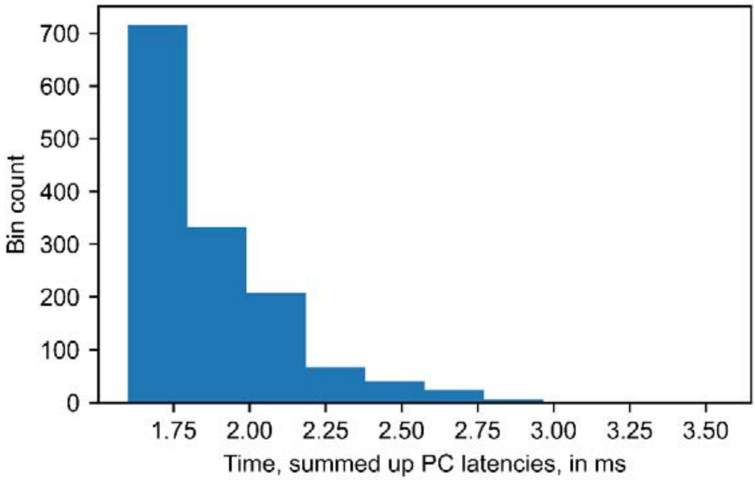

Fig. 9 Histogram of the latencies of the PC based operations, steps 8 to 11 in Fig. 2. The sample count is 1395.

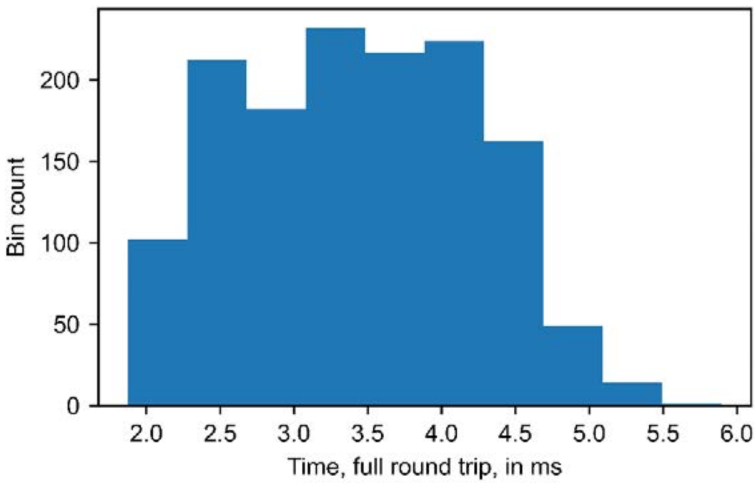

Fig. 10 Histogram of the full round-trip latencies, steps 1 to 11/12 in Fig. 2. The sample count is 1395.

9.3 Experimental setup for multiple objects

For the experimental measurements of multiple objects 259621 object batches were processed. The batch size varies between 1 and 17. The period time, which is the time between the last encountered batch on the PC and the current batch is used to filter the data. Only data in the 99% quantile of the period time is considered. To get an acceptable number of samples, our data set is reduced to batch sizes between 1 and 10. The sample count for the batch sizes are: 1; 182631, 2; 50934, 3; 13907, 4; 4941, 5; 2279, 6; 1225, 7; 575, 8; 300, 9; 128, 10; 57." → "1) 182631; 2) 50934; 3) 13907; 4) 4941; 5) 2279; 6) 1225; 7) 575; 8) 300; 9) 128; 10) 57.

The object extraction measurements (Fig.11) show a nearly linear increase of the latency when the batch size is increased, as we expected it. We can't explain the cause of the outliers, it may lie in the memory management of the FPGA. The sum of the PC latencies (Fig. 12) increases with the batch size. Considering the median values of the box plot, the increase seems to be mostly linear. There are high latency outliers, too. They are higher than the measured maximum latency, measured in Section 3.2.5. This may originate from the higher batch frequency in the more realistic scenario tested here. To investigate this, Fig. 13 shows a 2D histogram of the latencies between object extraction and the answer of the inferred class. It's the overall latency for the host actions measured in the FPGA. The histogram shows a jump in latency, for the shortest displayed histogram bin (2.1 ms to 3.5 ms) with an outlier of 10.4 ms. For longer period times, the outliers are not as high, but too high for the targeted 5 ms overall latency. In Fig. 14 the difference between the values shown in Fig. 13 and Fig. 12 (only batch size 1) is shown. We expected a nearly constant value for this, as measured in Section 3.2.5, of around 200 µs to 300 µs. This is the case for lower frequencies. For higher frequencies, the value explodes. It seems that most of the frequency-based latency increase originates from the communication between the modules, which we didn't measure. There are multiple threads communicating with others, the first approach should therefore be the optimization of thread priorities and scheduling, as already stated in Section 3.2.3.

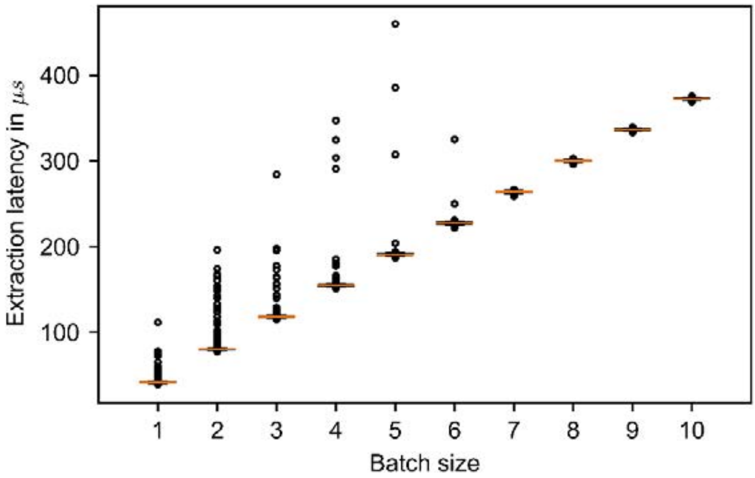

Fig. 11 Latencies for the extraction of objects from the 2D representation, step 5 in Fig. 2.

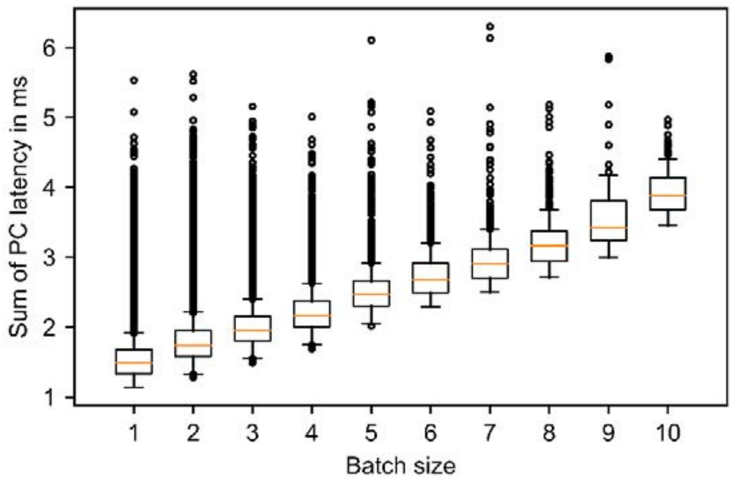

Fig. 12 All measured latencies of the host system combined, step 8 to 11 in Fig. 2.

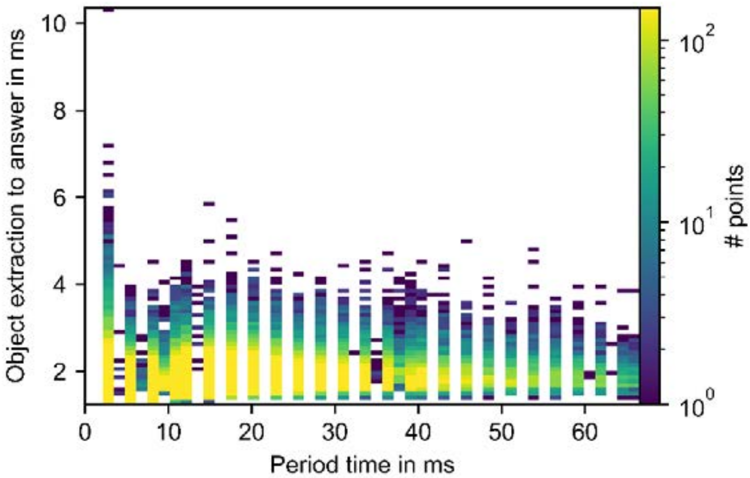

Fig. 13 2D histogram of the round-trip latency depending on period time in multi object measurements. Only data with a batch size of 1 is considered. The latency is measured between object extraction and the answer from the host, step 5 to 11/12 in Fig. 2.

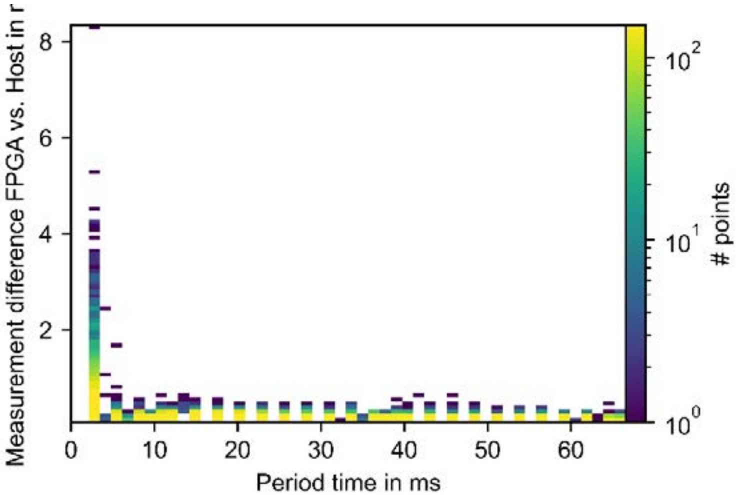

Fig. 14 Histogram of the differences between FPGA and PC latency measurements depending on period time in multi object measurements. Only data with a batch size of 1 is considered.

10 Conclusion

With our measurements, we gained access to interesting and helpful timing insights. While the GPU inference has relatively stable timings (1297 µs ± 2.04%) when run alone, the inference (step 9 in Fig. 2) has high timing variance and a higher mean latency (1685 µs ± 13.8%) when used with our software framework. The other PC processing operations have high jitter values, too. Changing the camera interface to CoaXPress while doubling the data throughput has no practical negative impacts, the transfer delay rises from 27.5 µs ± 7 ns to 55.2 µs ±.18 ns while the transfer time reduces from 9.64 µs ± 4 ns to 7.41 µs ± 5 ns. Acquisition latencies and jitters increased, but they are still far from being a problem in our application.

Our main jitter contributor is the creation of the 2D representation of the line scan data (step 2 in Fig. 2). Its measured jitter is 2552 µs, which is 64% of our complete system jitter of 4018 µs. Our second important jitter contributor is the PC processing pipeline (step 8 to 11 in Fig. 2) with 1950 µs. The mean latency from object extraction to class answer (step 5 to 11/12 in Fig. 2) is 2064 µs, a value considered as good from our point of view.

The measurements show that it is possible to reach low latencies which are usable for sorting of objects in free fall. The problems with the actuator control are fixed by higher poll rates.

For the multi object experiments, we observe a nearly linear increase in object extraction and PC latencies, but extreme outliers for the PC latencies. It seems, that for higher frequencies, a currently unknown source of latencies increases latency. We suspect non optimal thread priority settings. This needs to be investigated further.

In our future work, we seek to minimize the jitter in the PC processing path. Possibly thread scheduler optimizations can reduce the latency and jitter there. The FPGA design needs to be improved in memory management, eliminating its extreme jitter. Together with improved time stamp generation, the system reaches good timing stability and the targeted 5 ms overall latency.

References

Pfaff, Florian, Baum, Marcus, Noack, Benjamin, Hanebeck, Uwe D., Gruna, Robin, Längle, Thomas, & Beyerer, Jürgen (2015). TrackSort: Predictive tracking for sorting uncooperative bulk materials. In 2015 IEEE International Conference on Multisensor Fusion and Integration for Intelligent Systems (MFI) (pp. 7-12).

Ma, Ningning, Zhang, Xiangyu, Zheng, Hai-Tao, & Sun, Jian (2018). ShuffleNet V2: Practical Guidelines for Efficient CNN Architecture Design. In V. Ferrari, M. Hebert, C. Sminchisescu, & Y. Weiss (Eds.), *Computer Vision -- ECCV 2018* (pp. 122–138). Cham: Springer International Publishing.

Stelzl, M. (2019). *Minimale Responsezeit. Materialsortierung mit FPGA-Framegrabber und Trigger Boards*. Downloads Sorting | MSTVision. Retrieved December 12, 2023, from https://mstvision.de/downloads-sorting/.

Wezstein, S.; Stelzl, M.; Heizmann M. (2022). Latency evaluation of an FPGA-based sorting system. In K. Greiff, H. Wotruba, A. Feil, N. Kroell, X. Chen, D. Gürsel, V. Merz (Eds.), *Sensor-based sorting & control 2022* (9th ed., pp. 145-159). Shaker Verlag. DOI 10.2370/9783844085457

NVIDIA Corporation (2023). *Strange CNN inference latency behavior with CUDA and TensorRT - Deep Learning (Training & Inference) / TensorRT - NVIDIA Developer Forums* | Nvidia. Retrieved December 12, 2023, from https://forums.developer.nvidia.com/t/strange-cnn-inference-latency-behavior-with-cuda-and-tensorrt/237501

Basler AG (2023). *VisualApplets 3 Operator Reference Operator Blob_Analysis_2D* | Basler. Retrieved December 12, 2023, from https://docs.baslerweb.com/visualapplets/files/manuals/content/Blob.Blob_Analysis_2D.html.

Fusion between Event-Based and Line-Scan Camera for Sensor Based Sorting

Paul Bäcker[1]*, Nick Terzer[1], Georg Maier[1], Uwe D. Hanebeck[2], Thomas Längle[1], Jürgen Beyerer[1,3]

1 Fraunhofer IOSB, Institute of Optronics, System Technologies and Image Exploitation, Karlsruhe, Germany
2 Intelligent Sensor-Actuator-Systems Laboratory, Karlsruhe Institute of Technology (KIT), Karlsruhe, Germany
3 Vision and Fusion Laboratory, Karlsruhe Institute of Technology (KIT), Karlsruhe, Germany

* Corresponding Author: Fraunhoferstr. 1 76131 Karlsruhe, paul.baecker@iosb.fraunhofer.de

Keywords: Event-based Vision, Multi Target Tracking, Sensor-based Sorting, Real-time, Sensor Fusion

Abstract

In sensor-based sorting systems, there is usually a time delay between the detection and separation of the material stream. This delay is required for the sensor data to be processed, i.e., to identify the objects that should be ejected. In this blind phase, the material stream continues to move.

In most current systems, homogeneous movement for all objects is assumed, and actuation is timed accordingly. However, in many cases, this assumption does not hold true, for example, when unknown, foreign materials are present that have varying density and shapes, leading to inaccurate activation of the separation actuators and in turn lower sorting quality. Minimizing the blind phase by reducing the distance between the sensor and the actor is limited by the processing time of the detection process and may lead to interference between actuation and sensing. In this work, we address these issues by using an event-based camera placed between the sensor and actuator stages to track objects during the blind phase with minimal latency and small temporal increments between tracking steps. In our

proposed setup, the event-based camera is used exclusively for tracking, while an RGB line-scan camera is used for classification. We propose and evaluate several approaches to combine the information of the two cameras. We benchmark our approach against the traditional method of using a fixed temporal offset by comparing simulated valve activation. Our method shows a drastic improvement in accuracy for our example application, improving the percentage of correctly deflected objects to 99.2% compared to 78.57% without tracking.

1 Introduction

Sensor-based sorting is a process that separates a material stream into two or more fractions based on data acquired by one or multiple sensors. It involves a series of steps, including material transport, sensor examination, and single particle separation. A typical sensor-based sorting system that uses a line-scan camera as a sensor and a pneumatic valve array for separation is shown in Figure 1. We refer to the fraction of the material which is to be deflected as residue and the fraction that should pass as product.

The applications of sensor-based sorting are extensive and continue to expand. It is widely used in recycling facilities to sort various types of waste materials. For example, construction waste is sorted to recover valuable metals, clay brick, and concrete. Furthermore, household waste is sorted to recover polymers such as polyethylene (PE), which is commonly found in packaging. By efficiently separating recyclable materials from the waste stream, sensor-based sorting contributes to higher recycling rates and reduces the environmental impact of waste disposal. In addition, sensor-based sorting finds applications in industries such as mining, food processing, and pharmaceuticals. In mining operations, it is used to separate valuable ores from gangue or waste materials, leading to increased resource efficiency. In the food processing industry, sensor-based sorting helps to remove impurities and foreign bodies from food products, thus ensuring safe and high-quality food production. In the pharmaceutical industry, it can be used for quality control and the separation of different pharmaceutical ingredients.

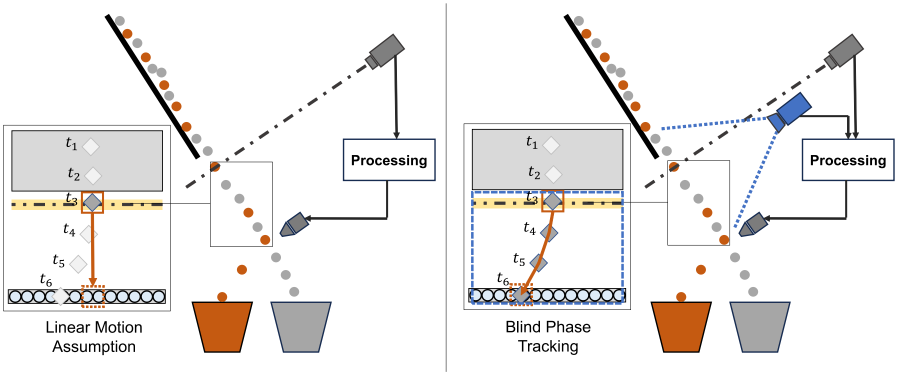

Fig. 1: Left: widely used sorting system with chute and single line-scan camera. Right: Proposed system with additional event-based camera for tracking.

For many of these applications, the high purity of the sorted fractions is crucial. Especially recycling applications further require a high throughput, as the material is often of low value. These two goals are usually conflicting (Gülcan & Gülsoy, 2017). There are two main causes for sorting errors. The first constitutes misclassification of objects. For example, a foreign object may be classified as product and is therefore not removed. These errors can be mitigated by gathering more data or employing more complex and refined classifiers. The second cause is the physical separation process of the material. A particle may have been classified correctly as residue, but is not deflected correctly. One reason for these errors is the necessary temporal delay between sensor examination and separation, as sensor data needs to be processed to calculate the separation actuation. This area is depicted in Figure 1 and is typically called the blind phase. To activate the actors, an assumption for the movement of the object during the blind phase is used. However, the actual particle movement remains unknown and may deviate significantly from the motion assumption, especially for unknown foreign objects and low-density objects that can be diverted by air turbulence near the pneumatic valve arrays. This unknown particle movement can result in incorrect activation of the pneumatic valve arrays.

To address this issue, we propose the use of event-based tracking, which combines a line-scan sensor for classification with an event-based sensor for tracking. We propose three methods for sensor fusion and evaluate them in terms of accuracy and computational cost. Furthermore, we benchmark these results against baseline methods.

2 Related Work

Significant research has been conducted on object tracking using frame-based area-scan cameras for sensor-based sorting (Maier et al., 2016, 2021). This approach has shown promising results in improving sorting accuracy, particularly for challenging scenarios such as spherical objects or material transport using a chute. However, this approach still has limitations, including temporal latency due to frame-based object detection, as well as limitations imposed by frame rate and motion blur, especially for high object velocities. Currently, RGB frame-based cameras are used for classification and tracking, limiting classification to color, shape and texture features and lacking hyperspectral data that can be captured using specialized line-scan cameras. Hyperspectral data is however crucial for material specific sorting such as different types of polymers. In our approach we propose a combination of an event-based camera and a line-scan camera, enabling hyperspectral image acquisition.

In recent years, significant advances have been made in the development of event-based cameras (Lichtsteiner et al., 2008) These cameras differ from frame-based cameras by capturing changes in the scene rather than capturing frames at fixed time intervals. Due to their remarkable properties, such as low latency, high dynamic range, and low power consumption, event-based cameras have garnered considerable attention in fields such as autonomous driving, drones, and tracking tasks (Gallego et al., 2022).

In the context of sensor-based sorting, an event-based camera for tracking and classification tasks has been proposed (Beck et al., 2021). However, the authors focus was mainly on classification based on texture features and motion, and only single-object tracking was considered.

Various methods have been proposed for event-based tracking. Some methods employ event-by-event approaches (Delbruck & Lang, 2013; Drazen et al., 2011) while others utilize the tracking of event-clusters (Barranco et al., 2018). Single-event methods provide excellent temporal resolution, while cluster-based methods offer benefits in terms of computational cost.

Fusion of event-based sensors with frame-based cameras has been extensively explored for both temporal (Pan et al., 2022; Scheerlinck et al., 2019) and spatial (Jing et al., 2021) super resolution. Furthermore, a stereo setup of frame and event-based cameras has been proposed for 3D vision (Wang et al., 2021; Zuo et al., 2021). However, to our knowledge, the combination of line-scan and event-based cameras has not yet been investigated.

3 Experimental Setup

For this work, a sensor-based sorting setup was conceptualized and built. The task of separating clay brick from limestone was selected as an example sorting task. The required sensors were implemented and synchronized. The data was then analyzed offline.

3.1 System Setup

The experimental setup used in this work is shown in Figure 2. The sorting system consists of several components:

- **Material Feeding:** The material is fed into the system using a vibrational feeder. The feeder has adjustable settings to control the throughput of the material.
- **Material Transportation:** The material is transported through a chute. The chute was chosen over a conveyor belt to create more variation in the trajectories of the objects. Furthermore, a chute is often preferred in the industry due to its lower maintenance requirements and easier material handling. The chute's width is 14 cm.
- **Sensor Examination:** Immediately after discharge from the chute, the material undergoes a sensor examination using both a line-scan and an event-based camera. The line-scan camera used is Jai 3-CMOS SW-4000T-10GE, which provides detailed color information. The event-based camera used is DAVIS 346 with a resolution of 346 x 260 pixels. The line-scan camera and the event-based camera are positioned roughly parallel to each other to avoid the parallax effect. The event-based camera captures the field of view from the chute to the funnels.
- **Valve Array:** The valve array is responsible for deflecting the material either into the funnel marked in red or allowing it to continue into the funnel marked in green. In this work, the deflection of the material is not implemented in the hardware setup.

The two cameras are synchronized using the trigger output of the line-scan camera. For every captured line, the line-scan camera sends a trigger to the event-based camera. The timestamp of this trigger is saved in the event data, allowing each captured image line to be referenced within the event stream.

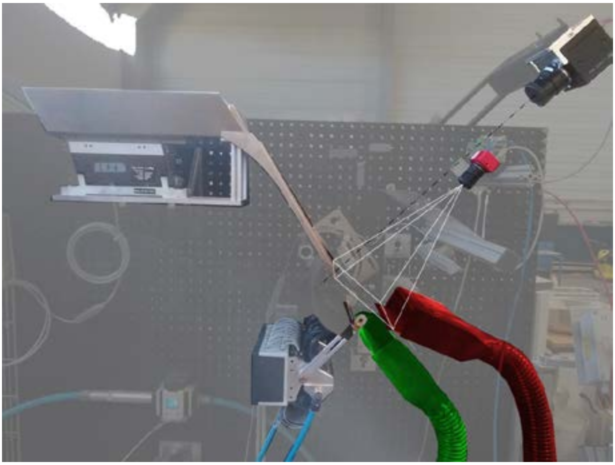

Fig. 2: Experimental hardware setup.

3.2 Sorting Task

The material used in the sorting experiment consists of two fractions: Limestone and clay brick (as shown in Figure 3). The material composition is approximately one-third clay brick and two-thirds limestone. Our method focuses solely on improving the material separation step, not the classification task. Hence, a task with an easy material distinction based on color was deliberately chosen. It can therefore be assumed that sorting errors occur only due to errors in tracking or matching between line-scan and event-based cameras.

Fig. 3: Sorting material containing limestone and clay brick.

4 Methods

Our goal is to use the line-scan camera with its high spatial resolution for the characterization (classification) of the material and the event-based camera with its high temporal resolution at low data rates for the tracking task is enhanced, leading to better physical separation. When the system, based on the data of the line-scan camera, classifies an object as residue, the event-based camera comes into play for tracking. This camera tracks objects detected by the line-scan camera all the way to the pneumatic valve array. It determines how the object should be deflected by activating the appropriate valve at the precise time. This way, we are able to accurately identify and deflect objects in our system, ensuring efficient control and redirection.

4.1 Classification

The classification process begins by accumulating 48 acquired lines from the line-scan camera into an accumulated image. This accumulation is done in order to perform classification on full objects at once. However, to mitigate issues that arise when an object is located on the borders of the image, the previous image is appended to the current image. This accumulation process is illustrated in Figure 4.

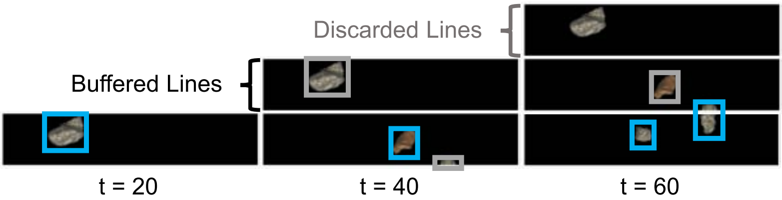

Fig. 4: Image accumulation process.

The classification steps are further detailed in Figure 5. The process involves background segmentation, connected component analysis, masking, and color classification.

The classification itself is done by applying a simple thresholding technique to the relative red value in the RGB color space according to

$$\text{class} := \frac{c_r}{c_g + c_b} > \text{thr}$$

with c_r, c_g, c_b being the sum over all pixels inside the bounding box for the respective color channels. The threshold thr has been determined experimentally.

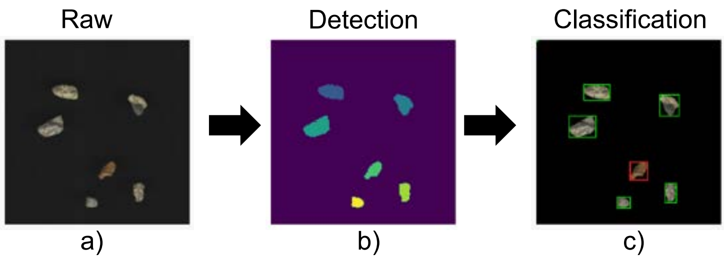

Fig. 5: Classification steps. a) camera image; b) background segmentation & connected component analysis; c) masking & classification

4.2 Tracking

In our work, we build upon the cluster-based tracking approach proposed in (Barranco et al., 2018). This approach employs the mean-shift clustering algorithm combined with a Kalman filter to enable multi-object tracking in an event stream. The algorithm operates by considering events over time as a set of points and grouping close events to clusters with preliminary mean values. Using a multivariate Gaussian Kernel for weighting the distances to all mean values, neighboring clusters are merged iteratively, thus representing separate recorded objects.

Processing each event separately during clustering and prioritizing events with recent timestamps using a weight function allows for an accurate detection of object positions. Every time step, the Kalman filter is then used to estimate the object position at the next time step, initializing the next cluster by assigning it the events within a region around this position. A constant-velocity-model, updating only the positions, allows for an efficient estimation, thus enabling the use of a short time interval for each tracking step.

We have chosen the cluster-based approach over single-event tracking methods for several reasons. Although using event clusters introduces slightly larger time-windows between tracking steps, which can make correspondence between frames difficult, we can leverage known motion assumptions in our specific use-case to mitigate this effect. Moreover, fewer tracking steps contribute to improved overall speed.

Furthermore, we have expanded upon the approach proposed in (Barranco et al., 2018) by introducing additional modifications. For instance, when events are situated within the regions of two objects, they are assigned lower weights to minimize the risk of merging two separate objects.

To facilitate comparison, we also incorporated two baseline methods. The first method involves no tracking or event-based camera and relies solely on the line-scan camera and motion assumptions to activate the valves. The second method tracks the objects for a certain duration, but then predicts valve activation well in advance, highlighting the advantage of tracking objects until they are near the pneumatic valve array.

4.3 Sensor Fusion Methods

Merging the classification results from the line-scan camera with the event-based camera poses a significant challenge in our system. This problem can be considered as a correspondence problem, as illustrated in Figure 6. While the line-scan camera and event-based camera are aligned through calibration using a linear transformation, the time difference between object classification and event detection introduces challenges. As time passes, the object moves, resulting in the corresponding event cluster being located at a different position. This challenge becomes more difficult as the time for classification increases and more objects are involved.

To address this correspondence problem, we have developed three approaches, each with its own characteristics and advantages. Figure 7 provides a visual representation of the differences between these methods.

4.3.1 Linear Assignment

This approach assumes linear movement during classification time. The position of the object detected at a specific time is extrapolated to the current time. Tracking is then initialized with events within a certain radius (also detected using the line-scan camera) around this extrapolated position. However, this approach still faces challenges similar to the original correspondence problem.

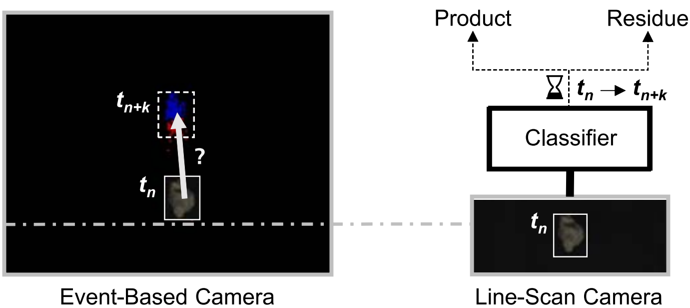

Fig. 6: Illustration of the correspondence problem. Left: Event-based camera view. The shown events are at time t_{n+k} which is the time when the classification result is available. Right: Line-scan image at time t_n, which is used for classification.

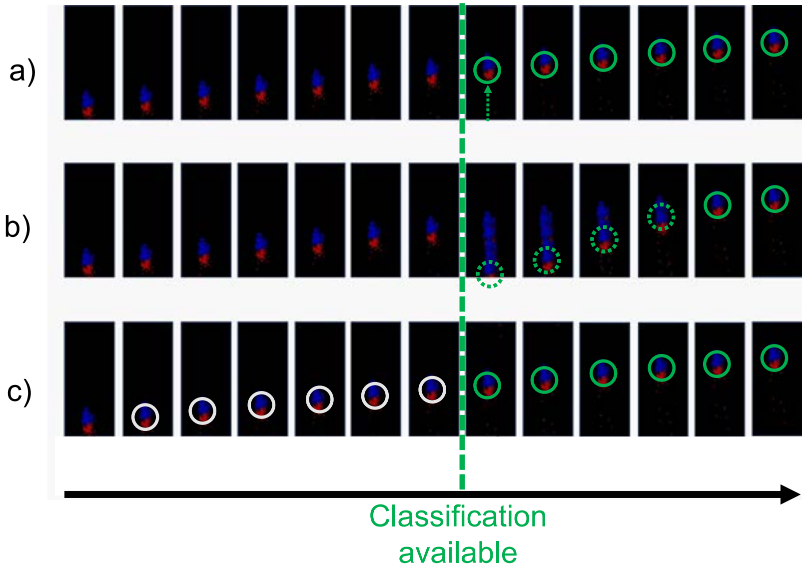

Fig. 7: Three variants for solving the correspondence problem between line- scanning sensor and event-based tracking. a) Linear Assignment; b) Backtracking; c) Event Clustering.

4.3.2 Event Clustering

In this method, new objects are identified using mean-shift clustering in the event stream prior to each tracking step. Initially, these objects are unclassified. The classification is performed separately using the line-scan camera. The trajectories of the unclassified objects are stored, and once a classification becomes available, it is assigned to the next unclassified object based on Euclidean distance and time of detection. By incorporating system knowledge, such as considering only unassigned events and searching for new objects only at the drop-off edge, the clustering process can be simplified and accelerated.

4.3.3 Backtracking

Tracking is initiated when an object is detected, providing information on its position, radius, and detection time. Old events are buffered for a specific duration and the tracking is initialized with the events in the buffer at the time of detection. The tracking therefore starts in the past and needs to be significantly faster than real-time to catch up before the objects reach the pneumatic valve array. This can be achieved by focusing the tracking only on the objects that have to be deflected.

We refer to the phase of catching up to the current object position as backtracking phase. In contrast to the method *Event Clustering*, tracking is only initialized when an object is detected. All events outside these detected objects are implicitly ignored. A drawback of this approach is the handling of collisions during the backtracking phase. Since tracking is asynchronous for each object, neighboring objects cannot be accounted for. Therefore, the method of assigning lower weights in overlapping zones, as presented in Section 4.2, cannot be applied.

5 Results and Analysis

The evaluation of our approach is performed offline using the captured event stream from the event-based camera and the images of the line-scan camera. This approach allows for repeatability and easier prototyping since the algorithms do not have to run in real-time initially. The tracking methods used in the evaluation calculate virtual valve activation. For validation, ground truth trajectories have to be acquired in order to test the proposed tracking methods against them. For acquiring the ground-truth, we used a high-frequency frame reconstruction based on the event data on which we performed a frame-based tracking method. All methods were implemented and tested using a pseudo real-time simulation. This simulation allows testing the methods in real-time conditions based on the captured data. This has the benefit of repeatability and the option of slowing down time for development purposes. The methods were compared in terms of accuracy and computational cost.

5.1 Ground Truth Generation

Acquiring ground truth trajectories for all objects is a prerequisite for this evaluation method. Since the real object trajectories are unknown, we used an alternative method to acquire them. Specifically, we employed a conventional tracking approach based on high frequency frame reconstruction from the event stream. In addition, the estimated trajectories were manually refined to ensure precision. For ground truth generation, we initially tested : the described “recurrent, fully convolutional network” architecture from (Rebecq et al., 2019), However, in our controlled scene, we found that this model was outperformed by a rule-based reconstruction method, employed in the dv-vision toolbox (*DV · Dynamic Vision System*, o. J.), where a more detailed fine-tuning of parameters to match our controlled scene was possible.

For each object, we determined the position and timestamp of the crossing point with the pneumatic valve array line using the ground-truth trajectories. We defined an object as deflected if an air nozzle with its center within the object's radius was activated at the exact timestamp. This activation is illustrated in Figure 8. The object is counted as deflected if at the time it reaches the center of the nozzle array either valve *b* or *c* are opened, since the centers of the air nozzles are within the radius of the object. Activation of valve *a* would not suffice for a deflection. All methods initially calculate the valve activation based on the predicted crossing point with the valve array. The duration of valve activation was set to 7.2 ms for all methods, with the valve opening 3.6 ms before the estimated crossing point and closing 3.6 ms after the crossing point.

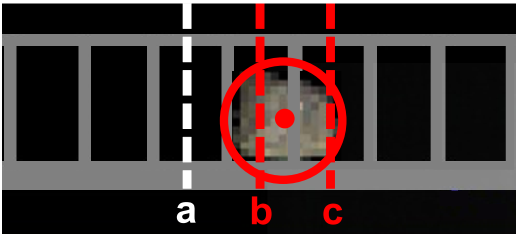

Fig. 8: Virtual valve activation.

5.2 Accuracy of Valve activation

We compared the methods at two different throughputs, specifically 10 g/s and 20 g/s. For each throughput, approximately 60 s of data was captured, resulting in roughly 1300 objects for low throughput and 2800 objects for high throughput. We have defined the clay brick, which constitutes about one third of the total material, as residue. Table 1 presents a comparison of the false positive and false negative rates for the different methods and throughputs, including the baseline (BL) methods that used no or limited tracking.

The results demonstrate that the tracking methods significantly outperforms the method that relied solely on a line-scan camera. For the line-scan camera, due to the lower accuracy, a method with an extended temporal and spatial activation window was implemented. This improves false negative rate F_N but also results in higher false positive rate F_P rates. In a physical system, this larger window would further require more compressed air and therefore increase operating costs. Furthermore, the methods that aim to track objects as far as possible exhibited better performance compared to the predictive tracking. This finding suggests that the trajectories of objects still undergo changes close to the nozzle array.

As expected, all methods experience a decrease in performance with higher throughput. However, it is worth noting that all methods suffer by similar relative amounts. The reasons for the lower performance can be attributed to a higher number of collisions, as well as more challenging correspondence problems. Overall, the method employing *Event Clustering* performs best. However, for this analysis, the real-time constraints were relaxed, which benefits this method as it is the computationally most expensive.

5.3 Computational Cost

A very important aspect for the suitability of the different methods is the real-time capability. Figure 9 shows a boxplot of the computation times for a single tracking step. The methods were implemented on an off-the-shelf notebook with 8 GB RAM and AMD Ryzen 3 5300U-Processor. The target tracking step size is 1.8 ms.

Tab. 1: Error-rates for different methods at high and low throughput.
Tracking methods outperform the baseline.

Method	**Throughput**	F_N	F_P
BL Line only	10 g/s	38.02 %	2.41 %
BL Line only, ext. act.	10 g/s	21.43 %	3.61 %
BL Extrapolation	10 g/s	10.00 %	**1.20 %**
Linear Assignment	10 g/s	2.00 %	1.38 %
Event Clustering	10 g/s	**0.76 %**	1.34 %
Backtracking	10 g/s	1.22 %	1.60 %
BL Line only	20 g/s	48.56 %	3.06 %
BL Line only, ext. act.	20 g/s	28.42 %	7.22 %
BL Extrapolation	20 g/s	11.11 %	4.62 %
Linear Assignment	20 g/s	2.58 %	**3.65 %**
Event Clustering	20 g/s	**1.58 %**	4.23 %
Backtracking	20 g/s	1.74 %	4.18 %

Since the computational effort required for the tracking depends on the number of objects and event rate in the scene, the computation times vary strongly. Several algorithms have been implemented, such as increasing the step size, ignoring events, or terminating the tracking in advance, to ensure real-time capability even with temporarily high loads. The methods of *Linear Assignment* and *Backtracking* point have shown to be significantly faster than the *Event Clustering* approach. The reason for this is that they do not need to perform object detection based on the event stream as they utilize the line-scan camera. Therefore, the costly clustering algorithm does not have to be performed. Especially for larger sorting systems with higher throughput, the factor of computational cost is increasingly crucial.

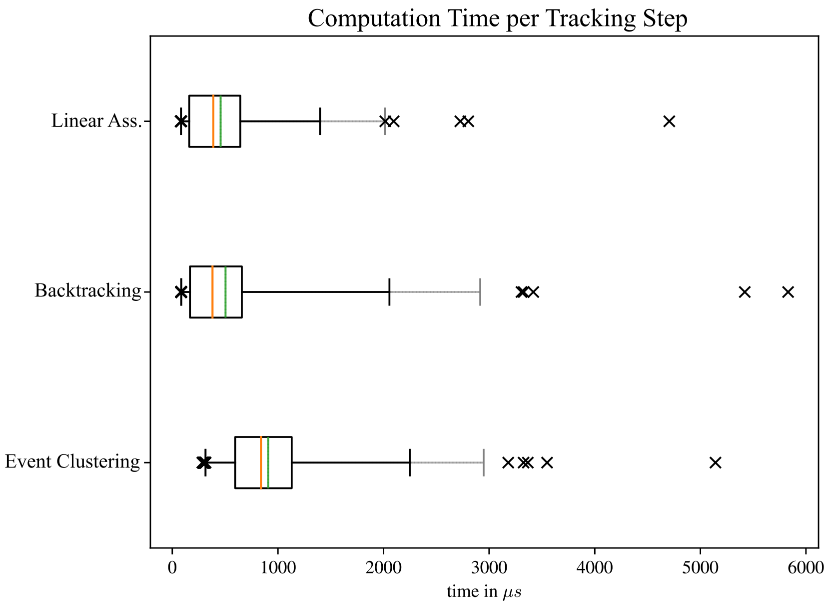

Fig. 9: Boxplot comparison of the three methods. Shown are median (orange), mean (dotted green), as well as 25-75% (gray box), 1-99% (black whisker) and 0.1-99.9% (gray whisker) quantiles.

6 Conclusion and Future Work

In this work, we proposed combining a line-scan and an event-based camera for sensor-based sorting. We believe that these two sensors complement each other ideally. The event-based camera gives high temporal resolution at the cost of a lack of overall intensity information, making it ideal for tracking tasks, but very limited in classification of objects. The line-scan camera excels at capturing intensity information both in spatial, as (in the case of hyperspectral cameras) in spectral domains. These cameras are therefore especially suitable for classification tasks, as they can distinguish between materials based on appearance. We implemented and evaluated three different methods for combining the two camera systems. The following key findings emerged. All tracking methods significantly improved accuracy compared to baselines. *Event Clustering* exhibited the highest accuracy, but was the slowest method. The *Linear Assignment* method performed worst in terms of accuracy, as it still relies on the assumption of linear object movement. The *Backtracking* method performed slightly worse than the *Event Clustering* approach. This is due to faulty correspondence/assignment and the discarding of collisions during backtracking steps. Both of these error types are largely due to the inlier estimation attributing all events inside a radius to an object. Therefore, objects that are close together may merge to a single object in some cases.

These errors could be mitigated by employing more precise inlier estimation using object boundaries. For the *Event Clustering* method, errors were also attributed to incorrect object identification/initialization due to the clustering approach, which is sensitive to fine-tuned parameters such as expected object size. In addition to these specific errors, there were general challenges observed. Some objects were lost during tracking, suggesting the need for smaller time intervals. Collisions between objects remained difficult to handle effectively.

It is worth mentioning that the overall high error rates are primarily due to intentionally long blind phases and maximum object movement in the experimental setup. However, in many cases, such as herb-sorting, great effort is taken to create object movement, which is as uniform as possible. Using tracking approaches, these cost intensive measures could be discarded, since object movement is allowed to be non-uniform. Further, the event-based camera allows for much higher object speeds and therefore throughput than a frame-based camera.

Moving forward, we aim to test the methods on different materials, such as polymer flakes or herbs, as they could potentially yield even more significant improvements for these materials. We also plan to use a hyperspectral line-scan camera to enable material specific sorting along with tracking. Future development efforts will include implementing a fully working real-time sorting system using these methods. This would not only facilitate better comparability with existing approaches but also serve as a practical application of the research findings.

References

Barranco, F., Fermuller, C., & Ros, E. (2018). Real-Time Clustering and Multi-Target Tracking Using Event-Based Sensors. *2018 IEEE/RSJ International Conference on Intelligent Robots and Systems (IROS)*, 5764–5769. https://doi.org/10.1109/IROS.2018.8593380

Beck, M., Maier, G., Flitter, M., Gruna, R., Längle, T., Heizmann, M., & Beyerer, J. (2021). *An Extended Modular Processing Pipeline for Event-Based Vision in Automatic Visual Inspection*. https://publica.fraunhofer.de/handle/publica/269656

Delbruck, T., & Lang, M. (2013). Robotic goalie with 3 ms reaction time at 4% CPU load using event-based dynamic vision sensor. *Frontiers in Neuroscience*, *7*. https://www.frontiersin.org/articles/10.3389/fnins.2013.00223

Drazen, D., Lichtsteiner, P., Häfliger, P., Delbruck, T., & Jensen, A. (2011). Toward real-time particle tracking using an event-based dynamic vision sensor. *Experiments in Fluids*, *51*, 1465–1469. https://doi.org/10.1007/s00348-011-1207-y

DV · Dynamic Vision System. Accessed 11/29/2023, https://inivation.gitlab.io/dv/dv-docs//dv/dv-docs/

Gallego, G., Delbruck, T., Orchard, G., Bartolozzi, C., Taba, B., Censi, A., Leutenegger, S., Davison, A., Conradt, J., Daniilidis, K., & Scaramuzza, D. (2022). Event-based Vision: A Survey. *IEEE Transactions on Pattern Analysis and Machine Intelligence*, *44*(1), 154–180. https://doi.org/10.1109/TPAMI.2020.3008413

Gülcan, E., & Gülsoy, Ö. Y. (2017). Performance evaluation of optical sorting in mineral processing – A case study with quartz, magnesite, hematite, lignite, copper and gold ores. *International Journal of Mineral Processing*, *169*, 129–141. https://doi.org/10.1016/j.minpro.2017.11.007

Jing, Y., Yang, Y., Wang, X., Song, M., & Tao, D. (2021). *Turning Frequency to Resolution: Video Super-Resolution via Event Cameras*. 7772–7781. https://openaccess.thecvf.com/content/CVPR2021/html/Jing_Turning_Frequency_to_Resolution_Video_Super-Resolution_via_Event_Cameras_CVPR_2021_paper.html

Lichtsteiner, P., Posch, C., & Delbruck, T. (2008). A 128$\times$ 128 120 dB 15 µs Latency Asynchronous Temporal Contrast Vision Sensor. *IEEE Journal of Solid-State Circuits*, *43*(2), 566–576. https://doi.org/10.1109/JSSC.2007.914337

Maier, G., Pfaff, F., Pieper, C., Gruna, R., Noack, B., Kruggel-Emden, H., Längle, T., Hanebeck, U. D., Wirtz, S., Scherer, V., & Beyerer, J. (2016). Fast multitarget tracking via strategy switching for sensor-based sorting. *2016 IEEE International Conference on Multisensor Fusion and Integration for Intelligent Systems (MFI)*, 505–510. https://doi.org/10.1109/MFI.2016.7849538

Maier, G., Pfaff, F., Pieper, C., Gruna, R., Noack, B., Kruggel-Emden, H., Längle, T., Hanebeck, U. D., Wirtz, S., Scherer, V., & Beyerer, J. (2021). Experimental Evaluation of a Novel Sensor-Based Sorting Approach Featuring Predictive Real-Time Multiobject Tracking. *IEEE Transactions on Industrial Electronics*, *68*(2), 1548–1559. https://doi.org/10.1109/TIE.2020.2970643

Pan, L., Hartley, R., Scheerlinck, C., Liu, M., Yu, X., & Dai, Y. (2022). High Frame Rate Video Reconstruction Based on an Event Camera. *IEEE Transactions on Pattern Analysis and Machine Intelligence*, *44*(5), 2519–2533. https://doi.org/10.1109/TPAMI.2020.3036667

Rebecq, H., Ranftl, R., Koltun, V., & Scaramuzza, D. (2019). *High Speed and High Dynamic Range Video with an Event Camera* (arXiv:1906.07165). arXiv. https://doi.org/10.48550/arXiv.1906.07165

Scheerlinck, C., Barnes, N., & Mahony, R. (2019). Continuous-Time Intensity Estimation Using Event Cameras. In C. V. Jawahar, H. Li, G. Mori, & K. Schindler (Hrsg.), *Computer Vision – ACCV 2018* (S. 308–324). Springer International Publishing. https://doi.org/10.1007/978-3-030-20873-8_20

Wang, Z., Pan, L., Ng, Y., Zhuang, Z., & Mahony, R. (2021). Stereo Hybrid Event-Frame (SHEF) Cameras for 3D Perception. *2021 IEEE/RSJ International Conference on Intelligent Robots and Systems (IROS)*, 9758–9764. https://doi.org/10.1109/IROS51168.2021.9636312

Zuo, Y.-F., Cui, L., Peng, X., Xu, Y., Gao, S., Wang, X., & Kneip, L. (2021). Accurate depth estimation from a hybrid event-RGB stereo setup. *2021 IEEE/RSJ International Conference on Intelligent Robots and Systems (IROS)*, 6833–6840. https://doi.org/10.1109/IROS51168.2021.9635834

Limitations in detection of textiles with NIR technology

Annika Ludes[1*], Bastian Küppers[1], Amrei Becker[2]

1 STADLER Anlagenbau GmbH, Altshausen, Germany
2 Institut für Textiltechnik of RWTH Aachen University, Aachen, Germany

* Corresponding Author: Max-Planck-Straße 21, 88361 Altshausen, Gemany. E-mail: annika.ludes@w-stadler.de

Keywords: Textiles, Challenges, NIR, CO/PET, False Color Analysis

Abstract

The recycling industry is preparing for 2025: it will become mandatory to separately collect textiles taking the first step towards a closed loop recycling system. With this new material flow the recycling-industry will face new challenges. Indicative tests show that quantitative textile-analysis regarding material composition is feasible based on NIR-technology. However, depending on the properties of the textiles (e.g., material composition or structure) and how they are presented to an optical sensor, textile detection can be affected significantly. Thereby constraints in future sorting and analysis tasks can be predicted. Spectral analysis of CO/PET-Textiles were conducted and analyzed regarding the effect of textile characteristics on false color analysis.

1 Introduction – Development of textile recycling industry

Nowadays textile recycling is a niche market, as most textiles (73 wt%) are landfilled or incinerated worldwide (Ellen MacArthur Foundation, 2017). The European Union aims at changing this. Heading towards a circular economy for textiles, the European Commission wants to enforce separate collection, sorting, re-use, and recycling. Part of this approach is harmonization of extended producer responsibility (EPR) schemes for textiles in all EU member states. This will be tackled through a targeted amendment of the Waste Framework Directive in the EU (European Commission, 2023). Furthermore, a stop of textile export outside the EU is planned, resulting in additional 1.5 Mio. Mg/a of textiles to be treated in the EU (European Environment Agency, 2023).

Of 12 kg textiles produced per capita in the EU, only 22 wt% (of post-consumer textile waste) is collected separately (European Commission, 2023). The existing collection systems across Europe leading to collection-rates which differ from 11 wt% (Italy) to 75 wt% (Germany) (Watson et. Al, 2018). However, while collection can be a key bottleneck to circular economy, also (pre-)sorting and the actual recycling process are of significant relevance.

As neither broad collection schemes are fully implemented (bvse, 2020) nor standardized/ established recycling processes exist, the development of textile (pre-)sorting processes poses a significant challenge. Additionally, textiles entail issues for sensor technology, that is established and shows most potential for sorting and analysis application in textile sorting: Near-infrared (NIR) spectroscopy. This area of tension will be discussed by means of an exemplary task – distinction of cotton- and PET-rich textiles.

2 Relevance of external factors on NIR-based textile recognition

The afore mentioned challenges for the development of textile (pre-)sorting plants are related to:

- Unknown input composition, as no harmonized collection schemes exist as well as there is not enough information about the material(-mixtures) the collected goods are composed of and

- Unknown pre-product requirements due to non-standardized/established recycling processes.

Variability and partly extremely complex structure of textiles due to just partly implemented and ongoing development of EPR (Office of the European Union, 2022)

2.1 Textile structure

Textiles are made of fibers, which can be endless, so-called filaments, or a defined length, so called staple fibers. Different materials can be combined in textile structures on multiple levels – on yarn, fabric and textile level:

Yarn level - Staple fiber and filament yarns can contain several fiber types or materials. Often, different staple fiber types are combined in the spinning of staple fibers, for example cotton and PET. Furthermore, filaments can be combined on in a texturing or twisting process, for example elastane and PET, or during fabric production.

Fabric level – Manufacturing semi-finished and finished products of flat textiles is mainly carried out by joining. The main joining methods are knitting, weaving, crocheting, or felting. In order to achieve certain mate-rial properties (e.g., patterns or wearing comfort), yarns made of different materials are sometimes combined with each other within one fabric. Depending on how, for example, warp and weft yarns in woven fabrics are distributed.

Textile level – For some textiles several fabrics are combined. There are also combinations possible with non-textile materials including imprints, rivets, zippers, buttons, etc.

2.2 Input composition

The composition of any material stream determines the limitations and the required endeavor for any pre-processing/-sorting. Accordingly, any uncertainties regarding the collection schemes and their potential constituents may inhibit the development of sound sorting processes. Especially if NIR inactive constituents are present in the input material, sorting technology, solely based on this technology might not be feasible. But also, the shares of various material Types (PET, cotton, viscose, polyamide [PA], etc.) must be known to allow for dimensioning of processing as well as sorting machinery.

On the other hand, collection schemes might be customizable to a certain extent, allowing for the elimination of prohibited materials (to be defined) in the material stream to the greatest possible extent. This way technological blind spots of pre-sorting plants could be circumvented. However, it has to be questioned whether the public is able to make such distinctions between desirable and prohibited materials.

In addition to the aforementioned factors a fundamental problem in data on textile composition persists: Lab results contradict the material composition of textiles, specified on their labels. Often those differences amount to low single digit percentages but also range up to 20% or more. To cope with such uncertainties extensive chemical analyses is necessary to correctly assess textile compositions, creating a dependable data basis.

2.3 Pre-product requirements

Just like knowledge regarding the input composition is necessary, data on product requirements is essential. This, however, can be a multidimensional issue.

The simplest quality requirements could define the average content of an exemplary PET-textile bale - on garment level. It might specify that such a bale must consist of at least 90 wt% of textiles, that are each composed of at least 95% of PET yarn. Additional specifications could exist like:

- 2 wt% out of the 10 wt% of other (than specified above) garments, may contain cotton contents > 50 %
- Textiles with PA content > 10% must not exceed 0.5 wt% share of any PET-textile bale
- Textiles that contain metals (rivets, buttons, e.g.) cannot exceed share of 3 wt% of any PET-textile bale

A different quality definition of exemplary PET-textile bales might be on chemical level, specifying such bales by the average PET-content, which might be min. 90 wt%. This could mean, that singular garments with much higher cotton contents could be found in this bale, as long as the average PET-share of 90 wt% is not undercut.

However, also for such a case additional requirements might be formulated, resulting in thresholds for shares of certain material types on chemical or garment level, similar to the examples given for quality requirements on garment level.

3 Potential and limitations of NIR technology for textile sorting

NIR sensors can distinct material types based on their spectral fingerprint, as long as those material types are made of NIR-active molecules (Kroell et al., 2022). With regard to textiles potential applications might be the distinction of PET, cotton, viscose, PA, PE, etc. to separate those material types (see Fig. 1).

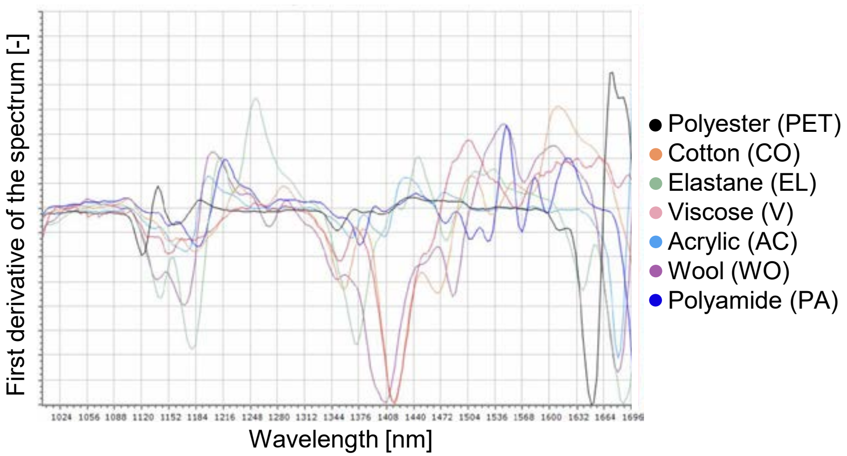

Fig. 1: NIR-spectra of different materials used for textile production (Becker et al. 2023)

Also, analysis of those product fractions might be an application. However, depending on the type of product specification quantitative analysis might be a necessity, especially when quality is defined on chemical level (cf. Section 1.1.3). Exemplary, quantitative analysis of PET-cotton mixtures on spectral level is displayed in Fig. 2.

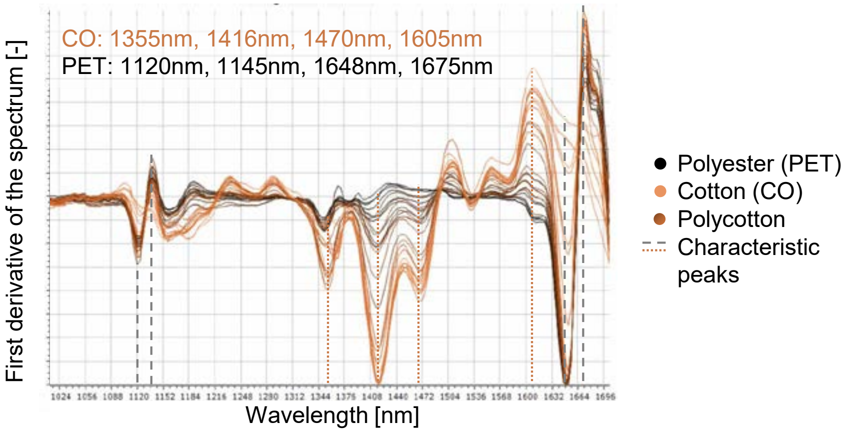

Fig. 2: NIR-spectra of different PET-cotton mixtures (Becker et al. 2023)

Wavelength ranges, typical for cotton and PET (around 1420 nm and 1650 nm accordingly) are predominantly used to quantitatively assess each object pixel with regard to its Cotton/PET content. Systematic shifts in the respective wavelength ranges allow for quantitatively assessing the chemical composition (PET & Cotton shares) per pixel. Exemplary result can be shown quantitatively as a heatmap-diagram, as can be seen in Fig. 3.

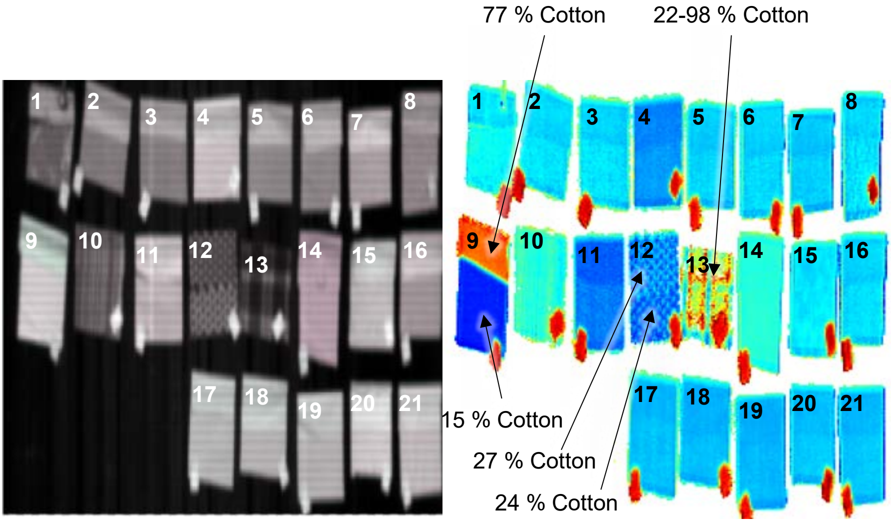

Fig. 3: Raw data image (left) visualized in grey-scale image and heatmap-diagram (right) - red =high cotton-share, blue = high PET-share; red spots are paper labels on each textile which are flipped on the upper half

Fig. 3 displays 21 sample textiles, analyzed with an EVK HELIOS EQ32 sensor. The processing of the raw data was done with SQALAR-software and the built in QCI-function (Quantitative Chemical Imaging). According to the labels of each textile all the above shown fabrics are supposed to contain 35% cotton and 65% PET. However, cotton-shares vary between 46% and 17% according to chemical analysis, proving the shortcoming of labels for teaching purposes. Indicative tests (based on NIR-analysis) have shown an average deviation of approx. 3% regarding cotton/PET-shares in comparison to chemical analyses of the respective textiles.

Despite the variation in PET/cotton contents, three challenges can be re-traced in Fig. 3 with the marked textiles:

1. Depending on the structure of any textile the quantitative analysis with a surface technology like NIR-sensors is restricted regarding the representativity of the generated data. The textile on the left displays 15% or 77% cotton share according to the NIR sensor, depending on which side is visible.

2. Large-meshed textiles constitute problematic fabrics as many meshes reveal the background, resulting in edge effects all over the textile. Despite a systematic under/over representation of a material type this can result in increased fluctuations regarding the measured composition in one textile (see Fig. 3 (12)).
3. Woven patterns are characterized by revealing certain threads more than others locally. This can result in high compositional fluctuations within one fabric (see Fig. 3 (13)).

In addition to the fluctuations mentioned above that occur within one fabric, the combination of fabrics with various chemical compositions within one garment can result in wrong classification of a whole garment, depending on the presentation of the respective item.

To which extend the potential of NIR-technology will be utilized in textile sorting and how its limitation will influence sorting, depends on the up- and downstream processes. For example, if a mean composition is needed per bale, it might not be necessary to present each single textile to the scanner from all sides. But if there will be strict requirements on article-basis (e.g., each article must contain a specific mixture or there are critical thresholds not to be exceeded) the presentation at the sensor will be more complex and costly.

Additionally, the success of the sorting process also depends on how accurately each article is recognized. Otherwise, it must be expected that statistically some articles will be sorted incorrectly if the entire textile cannot be considered during detection.

How much effort is put into recognition therefore depends on unknown framework conditions. These must either be defined first or determined iteratively across the industry. In addition, the cost-benefit factor and the energy balance of the processes should be considered.

4 Conclusion

The upcoming obligation to collect textiles separately in 2025 entails many novelties, challenges and potential. The amount of textiles to be dealt with will rise - not only due to the changed collection system, but also due to changes in stricter export-laws and recycling policies. The increasing volume requires automated sorting solutions. NIR technology is an established and promising sensor technology that is already used in textile sorting.

Challenges exist at the different levels of garments (on yarn, fabric, and textile level) and can therefore be discussed at these levels. The challenges include: the input composition, the measurement methods of product qualities after (pre-)sorting and the quality requirements for the (pre-)product fractions (e.g., on the part of the recycling processes).

Information on the aforementioned framework conditions is necessary to specify the sorting process using NIR technology more precisely. As these variables are partly interdependent, iterative steps will be necessary.

From a technical point of view, a lot is possible in terms of process engineering, detection, and data processing. The analysis is possible both qualitatively (relevant raw materials are NIR-active and distinguishable) and quantitatively (proportions can be differentiated within a median absolute deviation of ±4,6%). The technical feasibility is influenced by the presentation on the sensor and the nature of the textile.

References

Ellen MacArthur Foundation. (2017). *A new textiles economy: Redesigning fashion's future.* https://emf.thirdlight.com/file/24/uiwtaHvud8YIG_uiSTauTIJH74/A%20New%20Textiles%20Economy%3A%20Redesigning%20fashion%E2%80%99s%20future.pdf

Kroell, N., Chen, X., Greiff, K., Feil, A. (2022), Optical sensors and machine learning algorithms in sensor-based material flow characterization for mechanical recycling processes: A systematic literature review, https://doi.org/10.1016/j.wasman.2022.05.015

European Commission. (2023). Circular economy for textiles: taking responsibility to reduce, reuse and recycle textile waste and boosting markets for used textiles. https://ec.europa.eu/commission/presscorner/detail/en/ip_23_3635

Office of the European Union. (2022*) Extended Producer Responsibility for textiles*. https://ec.europa.eu/commission/presscorner/detail/en/fs_23_3636

European Environment Agency. (2023, February) *EU exports of used textiles in Europe's circular economy.* https://www.eea.europa.eu/publications/eu-exports-of-used-textiles

bvse (2020) *Bedarf, Konsum, Wiederverwendung und Verwertung von Bekleidung und Textilien in Deutschland*. https://www.bvse.de/dateien2020/1-Bilder/03-Themen_Ereignisse/06-Textil/2020/studie2020/bvse%20Alttextilstudie%202020.pdf

Watson, D., Aare, A.K., Trzepacz, S., Petersen, C. D. (2018), *Used Textile Collection in European Cities.* European Clothing Action Plan. http://www.ecap.eu.com/wp-content/uploads/2018/07/ECAP-Textile-collection-in-European-cities_full-report_with-summary.pdf

Becker, A., Datko, A., Kroell, N., Küppers, B., Greiff, K., Greis, T. (2023) Near-Infrared-Based Sortability of Polyester-Containing Textile Waste http://dx.doi.org/10.2139/ssrn.4581448

Sensor based sorting solutions for reuse and recycling in textile and apparel industry

Gesine Köppe[1*], Amon Krichel[2], Sebastian Geldhäuser[2], Anna Pehrsson[3], Florian Pohlmeyer[4], Kai Müller[4], Julien Breton[5], Felix Merkord[2], Thomas Gries[4], Mesut Cetin[2]

1 ITA Academy GmbH, Digital Manufacturing, Aachen, Germany

2 ITA Augsburg gGmbH, Recycling Technologies, Augsburg, Germany

3 TEXAID Textilverwertungs-AG, Recycling Solutions, Steinhausen, Switzerland

4 Institut für Textiltechnik der RWTH Aachen University, Aachen, Germany

5 SAS CETIA, Recycling Solutions, Bidart, France

* Corresponding Author: Vaalser Straße 460, g.koeppe@ita-academy.de

Keywords: Recycling, Reuse, Sorting, NIR, Artificial Intelligence, Robotics, Automation

Abstract

Europe has a textile waste problem. In numbers: 7-7.5 million tons of textile waste are produced in 2020. Up to 9 million tons are expected until 2023. At a certain point in the lifecycle, textile products become non-reusable waste – therefore, fiber to fiber recycling is critical to turn waste into value. The value chain for textile recycling is not yet fully developed. Therefore, only 30-35 % of the discarded textile waste is collected. In the EU, about 15-20 % of the collected textile waste is sorted at scale by mid and larger-sized sorting facilities. (McKinsey & Company, 2022)

The project “Transform Textile Waste into Feedstock” (TTWiF), led and initiated by TEXAID Textilverwertungs-AG, Steinhausen (CH) within the EURATEX ReHubs Initiative and well renown clothing brands, sorters, recyclers, industry partners aimed to understand the state of art of sorting technologies, aiming for highly automated sorting solutions for fiber-to-fiber recycling. TEXAID aims to establish scalable sorting facilities across Europe, the first one with a capacity of 50,000 tons by the

end of 2024. The technology assessment (TA) for the project has been entrusted to ITA Academy GmbH, Aachen in cooperation with ITA Augsburg gGmbH, Institut für Textiltechnik of RWTH Aachen University and SAS CETIA, Bidart, France. The interdisciplinary technology assessment team focused on examining the current state-of-the-art of processes and technologies for three main scenarios in the topics of (Semi-) automated sorting for reuse and recycling and automated pre-processing for recycling. Facing the aim of achieving sorting capabilities aligned with the principles of automation, sensorics, robotics and artificial intelligence, several technologies in transportation, preparation, feeding, detection, and logistics were scouted, tested and evaluated. Within the research phase, more than 160 requirements for technologies and feasibilities were collected and evaluated in cooperation with an international consortium of recyclers, manufacturers, and brands. To ensure a feedstock supply for circularity, according to the waste hierarchy, the technology assessment was designed to fill the gap in current sorting solutions for reuse, to evaluate and to train algorithms for AI-based pattern recognition and non-destructive handling of garments. In parallel, sorting categories for recycling scenarios were developed to elaborate a training scenario for Near Infrared Spectroscopy (NIR), Fourier Transform Infrared Spectroscopy (FTIR) and other sensors. Within the collaborative project, current challenges in developing innovative processes with new technologies were demonstrated. A central result of the study is a lack of market-ready technologies to close the loop in textile recycling. Sensor technologies for the recognition of material composition doesn't meet the current needs of recyclers. Also, data science and digitalization will play an important role in scaling sorting solutions for the textile and apparel industry.

1 Introduction

Textile consumption in Europe contributes the fourth largest part worldwide to environmental pollution, following food production, housing, and mobility. This industry also puts significant pressure on raw material usage and greenhouse gas emissions, making it one of the top three sources. (European Environment Agency, 2019) Reacting on this enormous impact, in September 2023 all over the world students participated in the 13th Global Climate Strike against global warming, climate change and wasting of resources (Deutsche Welle, 2023).

The problem of textile waste in Europe is significant. Currently, 7-7.5 million tons of gross textile waste are generated (McKinsey & Company, 2022). According to the authors at a certain point, textile products become non-reusable waste, and it becomes necessary to recycle them into usable materials. Fiber-to-fiber recycling is critical, as it can help turn waste into value. However, the value chain for textile recycling is not yet fully developed. Only 30 - 35 % of the discarded textile waste is collected. Out of the collected waste, 15 - 20 % is sorted at scale by mid and larger-sized sorting facilities in the European Union, as McKinsey (2022) noted. Currently, less than 1 % of apparel and home textiles are recycled.

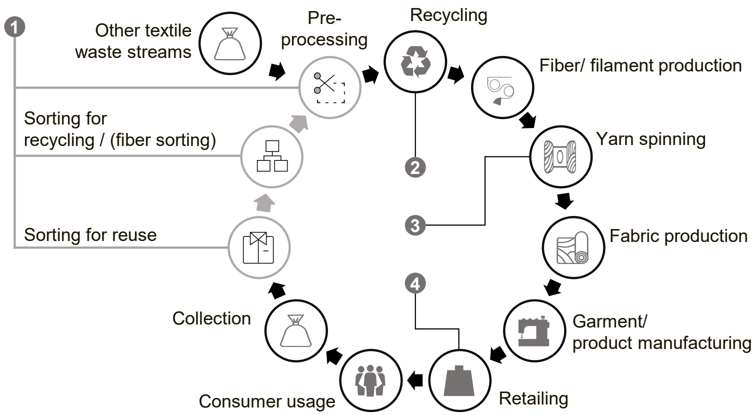

1 **Feedstock:** Transform textile waste into feedstock

2 **Mechanical recycling:** Increase the adoption of mechanically recycled fibers in the value chain

3 **Thermo-mechanical recycling:** Expand capacity and solve technical challenges for thermo-mechanical textile recycling

4 **Capsule collections:** Create capsule collection(s) with post-consumer recycled products

Fig 1: Four major gaps in the value chain. Identified by ReHubs Initiative by Euratex (EURATEX, 2022)

By 2025, all European Union member states are obliged to collect textile waste separately according to the European Union Law (Directorate-General for Environment, 2022). This will increase the quantity of collected textile waste substantially. However, the quality of the collected items may decrease since the textiles that are currently being incinerated will also be collected. As a result, a higher percentage of the collected textile waste will need to be recycled. To create a circular textile loop, the recycled material will have to be sorted by many parameters such as composition and material type. Currently, the sorting process is primarily manual and not automated. To meet future demands on the amount of waste that needs to be collected and sorted, as well as the demand for recycling feedstock, it is necessary to match liability and create cost efficiency.

2 Aim of the project

The aim of the “Transform Textile Waste into Feedstock” (TTWiF) project, led by TEXAID Textilverwertungs-AG, Steinhausen, Switzerland and initiated within the ReHubs Initiative by EURATEX, was to understand the state of art in sorting of textiles for reuse and recycling in Europe and how this could be scaled to meet future demands. The technology assessment (TA) aims to identify state of the art technologies which are suitable to be implemented within a waste sorting facility. Within the TA, the consortium was able to provide an overview and blueprint plan of the best available techniques, systems and technologies on how the sorting process would be built up best. Also, it was shown how different technologies will be able to be integrated and connected. Three major segments have been identified for which an in-depth TA is necessary:

1. (Semi-)Automated sorting for reuse
2. Automated sorting of recycling qualities
3. Automated pre-processing for recycling

Within the TA, the technologies of each subfield are evaluated on:

- **Technology Readiness Level** (TRL): The degree of development the technology has reached, from concept to commercialization.
- **Scalability**: The ability for the technology to be scaled up or down as needed.
- **Availability**: The extent to which the technology is accessible and readily available.
- **Speed**: How quickly the technology can perform its intended function.

- **Size**: The physical dimensions of the technology.
- **Upgradability and modularity**: The degree to which the technology can be easily disassembled and reassembled for maintenance or upgrades.
- **Integrability**: The capacity of the technology to be integrated with other technologies or systems.
- **Environmental and economic performance**: The impact the technology has on the environment and the economic feasibility.

2.1 (Semi-)Automated sorting for reuse

Sorting mixed clothes, shoes, and accessories for reuse and recycling is a labor-intensive task that is typically performed manually through several sorting steps. The goal of the process is to separate waste and sort items into specific product and quality categories. To improve efficiency and accuracy, it is planned to involve implementing automated handling and transportation technologies and sensor-based parameter detection. The system must recognize specific attributes such as product type, garment condition, size, brand, style, main material, color, textile construction, and trims. The system should also be capable of scanning garments with Digital Product Passports (DPP) as well as those without an information tag.

2.2 Automated sorting of recycling qualities

Currently, sorting of recycling qualities is carried out manually, relying merely on the look and feel of the material to determine its condition. However, this method cannot guarantee the accuracy of the material composition of a batch going for recycling. The process becomes even more complicated when the garment consists of a mixture of different fibers or is multilayered with various materials used. To enable fiber-to-fiber recycling, product and quality categories must be further sorted by fiber composition. Therefore, it is vital that the system sorts the products based on the complexity of the garment, scanning both the outside and inside, front and back of a garment and preferably recognizing trims.

2.3 Automated pre-processing for recycling

To achieve successful fiber-to-fiber sorting, the recycling qualities of the products need to undergo pre-processing. This involves removing impurities like trims, buttons and other components that might disrupt the recycling process. Trims can be cut off manually or by semi-automatic cutting tools. However, complex garments with multiple layers and trims pose a challenge and are usually sorted into downcycling or incineration fractions. To address this challenge, different vision and leading-edge technologies will have to be used to remove trims automatically.

3 Solution Approach

The TA has been segmented into three parts reuse and recycling, sorting of qualities and pre-processing for recycling. The reuse decision revolves around extending the lifespan of textiles by selling them as second-hand ware. After the end of their useful life, the recycling decision focuses on finding the most useful application of materials. In the context of pre-processing for recycling, additional process steps such as cutting, or the removal of contaminants are intended to provide a high-quality feedstock for various recycling technologies. These segments are designed to be established independently as standalone steps and distinct topics, while also integrating each other for a cohesive process. The initial layer of the TA provides a comprehensive overview, interconnecting various competencies and technologies, emphasizing integrability between the segments. To effectively sort garments, a promising approach was defined, that maintains a holistic perspective, prevents duplicative efforts, and maximizes synergies among competences and technologies. The following steps outline the recommended approach:

- Establish **general requirements** and **sorting criteria for recycling** technologies. Evaluate physical measurement principles and identify suitable technologies from diverse sectors, considering multiple sources.
- Compile a list of best-available technologies in the market, adaptable to various process steps. Research extensively, conducting **technology assessments** based on criteria like detection rate, removal efficiency, waste generation, speed, investment and cost.

- Conduct **comprehensive tests** for most promising technologies to elaborate technology readiness level, relevant key performance indicators (KPIs) and feasibility for detection and sorting.
- Employ a **decision matrix** for technology and supplier evaluation, incorporating prioritization and risk analysis. Test selected technologies for output quality, detection rate, removal efficiency, waste generation, speed, investment and cost.
- Develop a comprehensive **plan for a demo plant**, covering capacity, equipment sizing, storage, etc.
- Conduct a **gap analysis** between the current state and desired outcomes, identifying areas for improvement and optimization in the recycling process.

4 Key Findings

To achieve the capabilities in automatic sorting for reuse and recycling, several technologies in transportation, preparation, feeding, detection, sorting, and logistics were analyzed. For the observation, current state of the art machines, processes and software solutions were investigated, tested, and evaluated aligning and incorporating automation, robotics, sensor technology and artificial intelligence.

4.1 Requirements

In the research phase of the project, over 160 technology and feasibility requirements were gathered and evaluated through collaboration with an international consortium comprising recyclers, manufacturers, tech startups and brands. General prerequisites included autonomous operation and non-damaging effects on garments. For material characterization, historical sensor and machine data must be stored centrally for traceability. Recycling demands consideration of product and quality categories, particularly focusing on fiber composition for successful fiber-to-fiber recycling. Sorting complexity involves detailed scanning of external and internal garment aspects, ensuring a maximum 5 % tolerance level for accurate sorting. The system should ideally recognize trims and facilitate color sorting, with the goal of automating over 90 % of the recycling process. Additionally, the system should be designed for extendibility, allowing for future upgrades or adaptations to accommodate evolving recycling technologies and standards.

4.2 Definition of recycling categories

A comprehensive survey was conducted involving various companies across the textile recycling process chain. The objective was to gather insights into source materials, processing methods, and sector-specific requirements to support both open and closed loop recycling practices. The survey covered existing and prospective recycling technologies, focusing on establishing a circular economy in the textile industry. The analysis included mechanical, chemical, and thermo-chemical recycling processes to identify relevant recycling categories. Key performance indicators were derived from the findings, emphasizing their significance in automated textile sorting, and subsequently ranked through pairwise comparison.

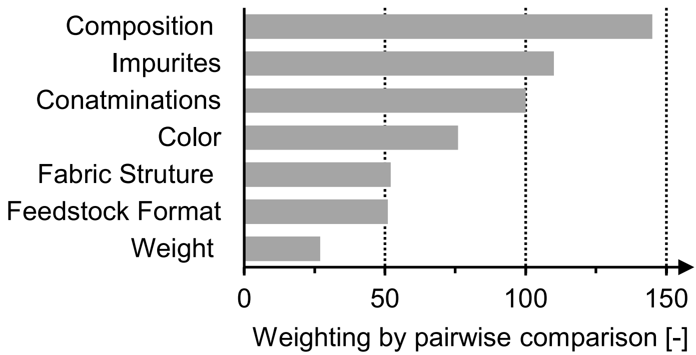

Fig 2: Ranking of the importance of measurement criteria for recycling solutions

4.3 Technology assessment and selection

To ensure a reliable feedstock supply for circularity, as defined per waste hierarchy (UNEP, 2011), the TA was designed. The assessment aimed to address the current shortcomings in sorting solutions for reuse and to evaluate and train AI-based algorithms for pattern recognition and non-destructive handling of garments. In addition, sorting categories for recycling scenarios were developed and a training program was created for sensors like NIR, FTIR and others.

4.3.1 Pattern recognition for reuse solutions

A project internal taskforce for artificial intelligence (AI) solutions conducted a workshop for acquisition of requirements and definition of the recognition and classification process. While acquiring the requirements, the taskforce conducted a pairwise comparison to rank the performance metrics.

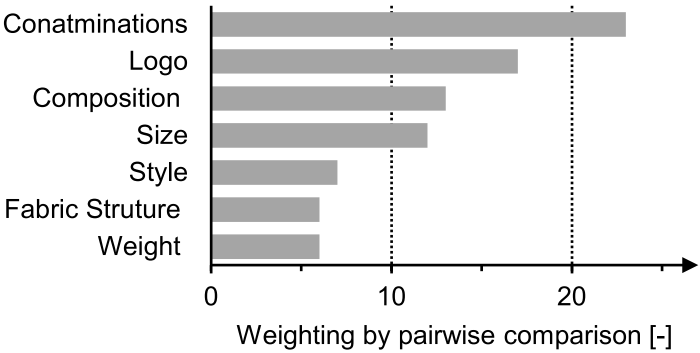

Fig 3: Ranking of Importance of detection criteria for reuse solutions

Four AI technologies which can identify garments regarding their attributes (e.g.: color, size, fabric structure) were identified and evaluated:

- Software for garment recognition
- Software for garment recognition & tagging
- Software for AI training & deployment platform
- Software for garment size measuring

The technologies were evaluated regarding their identification precision, speed as well as their integration requirements. As the project advanced, the search for technologies capable of meeting the project's prerequisites commenced. These technologies could include individual solutions or complete industrial systems. Following this, a comprehensive assessment of these technologies was conducted to gauge their suitability for the specific application. This assessment involved a thorough review of scientific papers, patents, and existing industrial solutions.

4.3.2 Handling, reuse-sorting and logistics solutions

During the evaluation process, various technologies like a tray sorter, separation robots and garment-on-hanger (GOH) sortation systems were inspected and examined for feasibility, and implementation concepts were discussed with providers. The tray sorter was found to be the best suitable option for large volume operations, due to performance speed, flexibility, and modularity. The system consists of a network of trays that transport items to designated destinations. These trays move along a conveyor system, and the items are sorted based on predetermined criteria, such as destination or parameters. The efficiency of tray sorters lies in their ability to handle a high volume of items rapidly, reducing manual labor and increasing accuracy (Lenkeit, 2023). They come with a high TRL and are commonly used in e-commerce, retail, and postal services where fast and precise sorting is crucial. However, tray sorters may face limitations in handling flexible, irregularly shaped items or items with varying dimensions.

However, the system is not yet applied to textile and specifically garment handling. The feasibility study with various garments has shown four major risks to be solved:

- **Damage to garments**: Soft and flexible garments, may be more prone to damage when subjected to the mechanisms of a tray sorter. The rigid structure of trays and potential drop points could cause wrinkles, creases, or tears in the fabric.
- **Inefficient sorting**: Tray sorters are optimized for handling items with defined shapes and dimensions. Soft garments may not stack neatly or consistently on trays, leading to sorting errors and inefficiencies.
- **Reduced accuracy**: The sorting process relies on precise item positioning and orientation. Soft garments may not maintain a consistent form on the trays, leading to misalignment and errors in the sorting process.
- **Maintenance challenges**: Soft fabrics may be more likely to get caught or tangled in the machinery, leading to increased maintenance requirements and potential downtime.

Further automation systems like automated folding systems and GOH transportation systems are already sufficiently implemented in textile manufacturing scenarios, due to smaller variety and recurring fabric sizes, surfaces, and weight. But in the sorting scenario with tremendous product variations, the existing technologies are coming to their limits. In further tests and expert interviews, the feasibility could not be proven. To ensure an optimal feedstock for reuse of garments, a manual separation step is necessary to pre-sort into the sections “recycling” and “reuse” and the subcategory “feedstock format”. The pre-sorted garments are then transported through a conveyor belt equipped with an AI-based camera system for detection of further parameters like style, size, color, and brand.

4.3.3 Sorting for recycling solutions

For each of the described measurement criterions (see Fig 2), technical solutions were developed. In the case of each identified solution, the underlying physical principles were initially documented and categorized. Subsequently, the solutions were assigned to the specific measurement tasks, further classified as individual sensors, measurement systems, or industrial sorting solutions. Measurement systems could be further subdivided into handheld sensors, laboratory equipment, and industrial systems. In accordance with the requirements for an automated sorting system with high market readiness, only industrial individual solutions and complete sorting solutions were considered. Within the scope of the project, systems from six providers were subsequently put to the test. For the testing process, three different batches were utilized (Fig 4). The first batch drew upon the material database from Refashion/Eco TLC, France offering insights into the accuracy of material composition recognition. This batch (“Batch 0”) comprised 409 samples with known compositions determined through laboratory analyses. In addition, there was a second batch (“Batch 1”) composed of whole garments, representing a cross-section of the raw materials generated during textile collection. The third batch (“Batch 2”) consisted of cut textiles containing various contaminants and impurities.

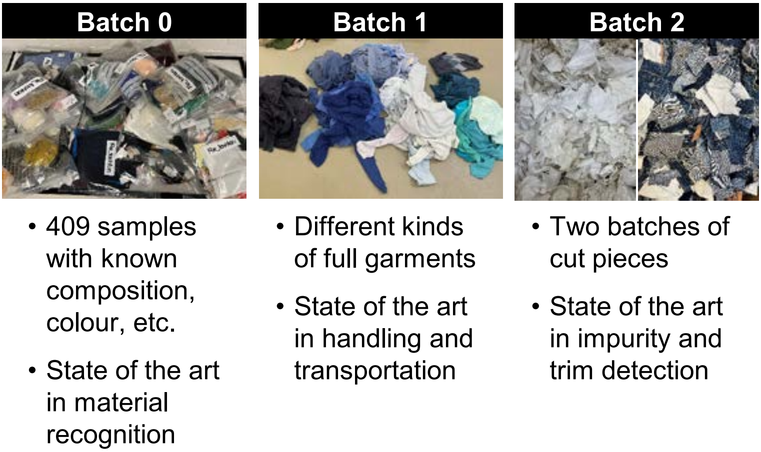

Fig 4: Overview: Garments used of the technology assessment

Depending on the type of technology to be tested and the capacity available at the provider's testing centers, one or more batches were subjected to evaluation using these systems. Systems capable of capturing and sorting entire garments were tested with "Batch 0" and "Batch 1".

The testing process encompassed a qualitative assessment of material recognition and the system's ability to handle a diverse range of clothing items. The systems under consideration typically comprise a conveyor belt with an inspection unit positioned above it. They incorporate various technologies such as near-infrared sensors, cameras, and metal detectors. Located behind these units is a rejection mechanism, typically operated using compressed air.

The results from the system tests reveal that the requirements for material composition recognition are not entirely met. Initial qualitative pretests had already indicated that significant deviations, particularly in the case of material mixtures, are present. This is not an issue specific to a single provider but rather a widespread challenge due to the relatively recent application of near-infrared (NIR) technology to mixed textiles. On the other hand, there are no significant concerns with color recognition. As per current knowledge, the employed color cameras can meet the requirements for sorting in recycling applications. Notably, the systems do not have the capability to capture the other five performance metrics.

Due to the significant number of unmeasured performance metrics, including impurities, contamination, feedstock format, fabric structure, and weight, a two-step sorting stage is necessary for precise sorting, as required for fiber-to-fiber recycling.

- Step: Multicategory sorting
- Step: Binary sorting

Based on the decision for a two-step sorting procedure, each process was designed individually.

5 Conclusion

The critical challenge identified in this study is the difficulty in developing a process for textile waste sorting due to the rare and varied process steps, each at different Technology Readiness Levels (TRLs). The complexity increases with the unexplored nature of textile waste sorting and the use of technologies not originally designed for textiles. Textile waste, unlike other waste streams, lacks standardization, especially in terms of sorting for reuse. The test results in the reuse section have shown, that current industry solutions are not matching the degree of precision in detection of style and shape and variety in labelling as garment type and e.g. sex. Semi-automated sorting for reuse is at a premature TRL, making full automation challenging, with skilled operators remaining crucial. For automated sorting for recycling, research indicates that current sensors lack the maturity to precisely meet recyclers' feedstock requirements. While current sensors lack the maturity to precisely meet recycler's feedstock requirements (Du, et al., 2022) (Zhou, et al., 2019) challenges arise in quantification and real-world application for post-consumer textiles. The identified technology gaps encompass the necessity for advancements in databanks supporting the technologies, as well as improvements in scanning accuracy and precision.

Pre-processing is highly specific and varies based on use cases and specific recyclers, making standardized solutions difficult. A proposed solution involves a two-step sorting process for recycling to address quality control and pre-processing challenges. Overall, the diverse requirements across different use cases, value chains, and stakeholders contribute to the complexity of sorting and preprocessing for reuse and recycling. The study also highlights a lack of datasets, both technologically and in terms of the need for digitalization, hindering the unlocking of potential data in sorting processes in the future.

6 Outlook

The collaborative project has revealed current challenges in developing an innovative process with new technologies due to the unexplored field of textile recycling. Developing a new process with new technologies comes with its own set of challenges. One of the biggest issues is dealing with different technology readiness levels (TRLs) within the reuse, pre-processing, and recycling stages. Sensor technologies for recognizing material compositions currently don’t meet the needs of textile recyclers. Additionally, requirements vary significantly for different use cases, value chains, and stakeholders. Medium-term, skilled operators will play a crucial role in textile waste sorting, and data will be essential for digitalizing and scaling sorting solutions for the textile and apparel industry.

References

Deutsche Welle. (2023, 09 15). *Weltweiter Streiktag für das Klima*. Retrieved from Weltweiter Streiktag für das Klima: https://www.dw.com/de/weltweiter-streiktag-f%C3%BCr-das-klima/a-66827146

Directorate-General for Environment, E. C. (2022). *Call for Evidence: Revision of the Waste Framework Directive*. Von Call for Evidence: Revision of the Waste Framework Directive: https://environment.ec.europa.eu/news/waste-framework-directive-revision-2022-02-14_en abgerufen

Du, W., Zheng, J., Li, W., Liu, Z., Wang, H., & Han, X. (2022). Efficient Recognition and Automatic Sorting Technology of Waste Textiles Based on Online Near infrared Spectroscopy and Convolutional Neural Network. *Resources, Conservation and Recycling, 180*. doi:https://doi.org/10.1016/j.resconrec.2022.106157

EURATEX. (2022). *ReHubs - A joint initiative for industrial upcycling.* EURATEX, Sustainable Businesses.

European Environment Agency. (2019). *Private consumption: Textiles EU's fourth largest cause of environmental pressures after food, housing, transport*. Retrieved from Private consumption: Textiles EU's fourth largest cause of environmental pressures after food, housing, transport: https://www.eea.europa.eu/highlights/private-consumption-textiles-eus-fourth-1

Lenkeit, M. (2023, 08 24). Feasibility trials for tray sorters at Vanderlande B.V. (K. Müller, Interviewer)

McKinsey & Company. (2022). *Scaling textile recycling in Europe - turning waste into value.* McKinsey Apparel, Fashion & Luxury Group.

UNEP. (2011). *Waste - Investing in energy and resource efficiency.* United Nations Environment Programme.

Zhou, J., Yu, L., Ding, Q., Wang, R., & , . (2019). TEXTILE FIBER IDENTIFICATION USING NEAR-INFRARED SPECTROSCOPY AND PATTERN RECOGNITION. *AUTEX Research Journal, 019, no. 2*, 201. doi:https://doi.org/10.1515/aut-2018-0055

Sensor-based sorting for plastic-rich shredder residues on industrial scale

Dagmar Arends[1]*, Martin Schlummer[1], Laura Strobl[1],
Jutta Schoberer[2], Alfred Schmidt[3]

1 Fraunhofer Institute IVV, Process development Polymer Recycling, Freising, Germany

2 Audi AG, Ingolstadt, Germany

3 Unisensor Sensorsysteme GmbH, Karlsruhe, Germany

* Corresponding Author: Fraunhofer IVV, Giggenhauser Str. 35, 85354 Freising, Germany, dagmar.arends@ivv.fraunhofer.de

Keywords: WEEE, ELV, laser spectroscopy, XRT, plastics

Abstract

WEEE devices and end-of-life vehicles contain large shares of metals and plastics. Many WEEE devices and all ELV undergo manual treatment and are then treated in shredder plants with the focus on high metal recovery rates. Most plastics end up in plastic-rich shredder residues, showing elevated bromine contents for WEEE residues and elevated chlorine contents for ELV residues. Laser spectroscopy and XRT sorting have been combined to sort PC/ABS and bromine-free ABS and PS from WEEE plastics with purities of 98% and more in a dry process chain. Trials with shredder residues from one automotive OEM demonstrated that laser spectroscopy is also a powerful tool to enrich polyolefins, polyamides as well as PC/ABS in separate sorting fractions, regardless of color and soot content, and of mineral or fiber shares. Combinations with other sorting technologies can further enhance regrind qualities and even produce highly purified recompounds, freed from inert and soluble contaminations to supply closed-loop feedstock.

1 Introduction

Electrical and electronic products as well as passenger vehicles are firmly established in everyday life. At the end of their useful service life these products, so-called waste electrical and electronic equipment (WEEE) and end-of-life vehicles (ELV), must be recycled. Large amounts of WEEE and ELV plastics escape recycling via sorting residues that cannot be recovered by state-of-the-art waste sorting.

The European Strategy for Plastics in a Circular Economy sets the target of recycling more than half of plastic waste generated in Europe. Discussions on recycled contents, plastics tax, recycling rates and waste coverage have been going on in the revision of the Waste Framework Directive (WFD) and the revision of the Ecodesign Directive. They reveal the need to increase existing recycling capacities and to further develop and implement waste collection systems and treatment concepts to recycle more plastics from WEEE and ELV wastes. In addition, they clearly indicate the demand for high mechanical quality as well as legal compliance of recycled polymers, both being key for a successful implementation of a circular economy for plastics.

With regard to plastic-rich WEEE streams, bromine-contaminated, plastic-rich sorting fractions are produced in primary treatment plants, either as dismantling fractions or as post-shredder fractions. According to the state-of-the-art, acrylonitrile butadiene styrene (ABS), polystyrene (PS) and polyolefins with a density of $\rho < 1.1$ g/cm^3 can be recovered via two-stage density separation and tribo-electrostatic sorting. Other high-quality engineering plastics - in particular PC and PC/ABS as well as bromine-rich ABS and PS grades - accumulate in the density fraction $\rho > 1.1$ g/cm^3 and are not recycled. (Arends et al., 2022)

ELVs are handed over to shredder plants after pre-treatment in dismantling centers. In shredder plants plastics end up in the shredder light fraction (SLF) and in residues of the shredder heavy fraction (SHF) and can be enriched in rigid plastics fractions by state-of-the-art post-shredder treatment. These shredder residues contain high shares of thermoplastics as well as rubbers, residual foams, textiles and metals. State-of-the-art post-shredder sorting of ELV plastics can comprise the enrichment of target plastics in density fractions $\rho < 1.1$ g/cm^3. Since plastic-rich shredder residues from ELV contain polyolefins with and without mineral fillers and fibers, fiber-free and fiber-reinforced polyamides as well as ABS, PC and blends thereof, most ELV plastics cannot be recovered by state-of-the-art sorting yet. (Schlummer & Merkert, 2023)

In the scope of the finalized WEEEsense project (BMBF FKZ 033RK063) a sensor based sorting chain was developed and tested to sort ABS, PS and PC/ABS regrinds with high purities for reuse in the EEE industry. Specific flame retardant analysis was performed in the frame of the KUREA project (UBA FKZ 3719343090) for WEEEsense output fractions of one sorting trial.

Trials with automotive shredder residues aimed at sorting polyolefins, polyamides as well as PC, ABS and PC/ABS, regardless of soot content, and mineral or fiber shares.

2 Materials and Methods

2.1 Materials WEEE

Five groups of WEEE devices were pre-sorted and treated in a German dismantling facility: 1. TV casings, 2. Laser printers, 3. Inkjet printers, 4. Small household appliances and 5. Consumer electronic devices. Metals were separated after shredding by state-of-the-art metal separation. Fine grains were removed in a sieving step to provide plastic-rich residues with particle sizes > 10 mm. Plastics from laser and inkjet printers were merged as were those from small domestic devices (SDA) and small consumer electronics (ICT). Spectroscopic sorting trials were performed with input amounts of 79 kg to 246 kg.

3 Materials ELV

ELV shredder residues from one automotive original equipment manufacturer (OEM) were produced in German shredder plants. Rigid plastics were enriched post-shredder by state-of-the-art sieving, wind-sifting, metal and cable separation. Spectroscopic sorting trials were performed with input amounts of 70 kg to 260 kg of plastic-rich, rigid shredder residues. Each input contained the target plastics PP, PE, PA6, PA6.6, PC, PC/ABS and ABS.

3.1 Methods

Based on the thermoplastic polymer contents of the input fractions three target polymer fractions were defined for WEEE sorting, i.e. 1. PS, 2. ABS and 3. PC + PC/ABS and three target fractions were defined for ELV sorting, in particular 1. Polyolefins (PO), 2. Polyamides (PA) and 3. PC + ABS + PC/ABS (PCABS).

Spectroscopic WEEE sorting was performed according to Fig. 1 with industrial sorting equipment.

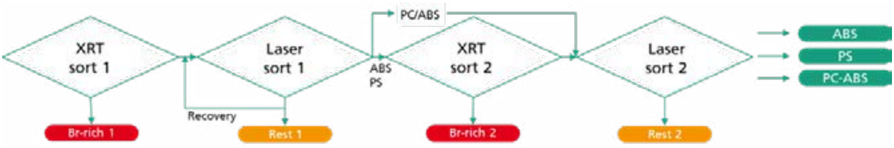

Fig. 1: Sorting chain of the WEEEsense project

For X-ray transmission (XRT) sorting the X-TRACT (Tomra Sorting GmbH, Germany) was used. ELV trials did not comprise XRT sorting.

Separation by plastic types was performed for all inputs, from WEEE and ELV, by laser spectroscopy. According to the particle size, the Powersort 360 (Unisensor Sensorsysteme GmbH, Karlsruhe, Germany) and the Powersort 200 (Unisensor Sensorsysteme GmbH, Karlsruhe Germany) were used. Target plastics were enriched and purified by multiple laser spectroscopic sorting.

Fourier transform infrared (FTIR) screening was performed throughout the process chain with the FTIR-ATR Nicolet iS 5 (Thermo Fisher Scientific Inc., Waltham, USA) and ALPHA (Bruker Corporation, Billerca, USA) to determine target polymer contents of ejects and drops.

Energy dispersive x-ray fluorescence (EDXRF) analyses were performed with a Spectro XEPOS (Spectro Analytical Instruments GmbH, Kleve, Germany) to determine bromine and phosphorous contents of input and output fractions.

Specific brominated flame retardant analysis was performed via gas chromatography (GC) with a GC-2010 Plus AF using an electron capture detector (ECD) (Shimadzu, Japan) with a 15 m DB-5 column. The GC-ECD method used was an in-house method for the determination of a range of flame retardants. An external calibration was used for the quantification.

Qualitative and quantitative determination of phosphorous flame retardants was carried out after chromatographic separation with the high pressure liquid chromatography system HPLC Waters Alliance 2695 by using the low-resolution mass spectrometer Waters Quattro Ultima Platinum (Waters Corporation, Milford, USA) in a heated gas stream in positive electrospray mode. Quantification was performed using external standard solutions.

4 Results

4.1 Results WEEEsense

Fig. 2 shows the output fractions of the sorting chain tested. 42% of the plastics from TV flat screens, 51% of SDA & ICT plastics and 63% of plastics from printers were enriched in target fractions. Target polymers were sorted into recovery fractions from sorting rejects, they accounted for 15% to 20%. The bromine-rich fraction accounted for 15% for TV flat screens, 9% for SDA & ICT and 3% for printers.

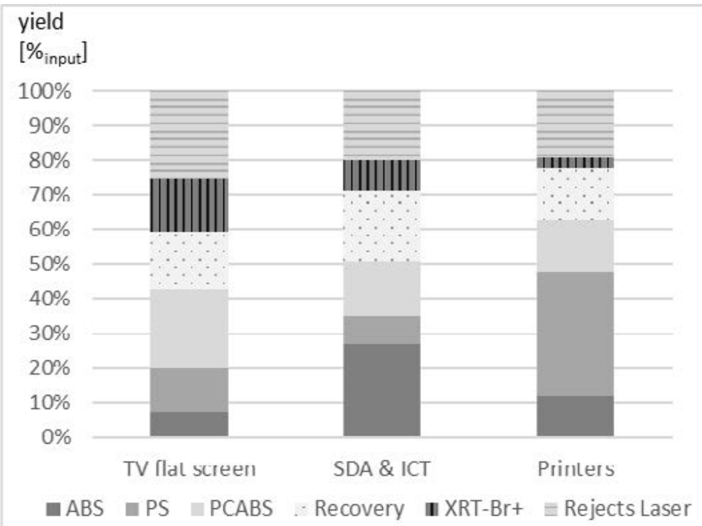

Fig. 2: WEEEsense output fractions

The target fractions showed purities > 98% for all but one target fraction that only exhibited a purity of 95%. The recovery fractions contained > 90% target polymers.

Mechanical testing of ABS and PS recompounds, including melt flow rate, impact strength and E-modulus, met specifications of feed-stocks for the printer production. The PC/ABS needed further laser spectroscopic sorting to reduce residual polyoxymethylene (POM) contents and showed good mechanical properties afterward.

Phosphorous enriched in PC/ABS target fractions with approximately 3.000 ppm and is mainly caused by the presence of triphenyl phosphate (TPP). Bromine levels were below 2.000 ppm for all target fractions, and below 1.000 ppm for most of them. Bromine concentrations determined in bromine-rich XRT fractions were between 23.000 ppm and 71.000 ppm. Specific flame-retardant analysis of SDA & ICT output fractions showed that BDE-209, subject to the restriction on hazardous substances (RoHS) and the regulation on persistent organic pollutants (POPs regulation), and DecaBDEthane contents were close to or below the limit of detection in all SDA & ICT target fractions. They enriched in the bromine-rich XRT fractions, first and foremost Tetrabromobisphenol A (TBBPA) but also Decabromodiphenyl ester 209 (BDE-209) and decabromodiphenyl ethane (DecaBDEthane). (Potrykus & Schlummer, 2022)

4.2 Discussion WEEE

ABS, PS and PC/ABS from different WEEE input streams were sorted in a dry process chain, comprising XRT and laser spectroscopic sorting. The target fractions show high purities and low bromine levels. As TPP is a commonly used flame retardant for PC/ABS, it enriches in the PC/ABS sorting fraction. Mechanical test results, not presented in this paper, show good properties of the recompounds even without adding virgin material.

Sorting residues can be reduced by enriching target plastics from sorting rejects. The recovery fractions show high contents of target plastics and can be reinserted into the sorting chain. With regard to SDA & ICT, yields can also be increased by considering polyolefins that were out of the scope of the WEEEsense project.

Bromine levels were below 1.000 ppm for most target fractions. Contents of regulated brominated flame retardants were close to the limit of detection in all target fractions. With the combination of XRT and laser spectroscopy, they can be enriched in separate bromine-rich PS and bromine-rich ABS fractions. Elimination of brominated flame retardants can be performed in dissolution-based plastic recycling to supply purified ABS and PS (Strobl et al., 2021).

4.3 Results ELV

Sorting trials were performed for four different input fractions to enrich the target plastics into three sorting fractions PO, PA and PC/ABS. Target plastics were enriched in a first step and purified by a second laser spectroscopic cleaning step. Tab. 1 shows the average yield for the target polymers with reference to the input content of each polymer. PO yields amounted to 74%, PA yields to 80% and PC/ABS yields to 87%, indicating a percentage rise of purities (Fig. 4 right) to 79% for PO, to 67% for PA and to 86% for PC/ABS.

Tab. 1: Average target polymer yields with reference to input content and purities of target fractions after enrichment

	PO	PA	PC/ABS
yield	74 %	80 %	87 %
purity	79 %	67 %	86 %

26% of polyolefins, 20% of polyamides and 15% of PC/ABS could not be sorted into target fractions and were lost in sorting rejects of the trials instead. Target polymers were sorted from one of the sorting rejects with yields and purities comparable to the ones shown in Tab. 1.

To further increase the target polymer contents, another laser spectroscopic cleaning step was performed for a PO fraction with an input purity of 66%, a PA fraction with an input purity of 71% and a PC/ABS fraction with an input purity of 91%. Tab. 2 shows the yields with reference to the input content of laser spectroscopic cleaning. PO yields of 82%, PA yields of 89% and PC/ABS yields of 92% were determined. This cleaning step increased the purities (Tab. 2) to above 85% for PO and PA and to 94% for PC/ABS.

Tab. 2: Target polymer yields with reference to input content and purities of target fractions after further purification

	PO	PA	PC/ABS
yield	82 %	89 %	92 %
purity	87 %	85 %	94 %

4.4 Discussion ELV

The sorting trials show that high shares of polyolefins, polyamides, PC, ABS and PC/ABS were enriched in sorting fractions with purities of almost 90% for PO and PA and even 94% for PC/ABS. However, each sorting step entails yield losses. Yield losses are lower for inputs with higher target polymer content. Valuable amounts of target polymers that reach reject fractions can be enriched by sorting recovery fractions aiming at the target polymers from sorting residues to reinsert them into the sorting chain.

Residual contaminations are too high for direct recompounding to high quality recycled polymers and thus, sorted target fractions require additional purification technologies before recompounding. These should address the reduction of residual rubbers and other foreign polymers, the reduction of fiber and mineral contents, the discharge of residual chlorinated particles, the separation of residual foreign polymers and also the separation of PA6 and PA6.6 from the PA sorting fraction.

However, advanced sorting chains can produce feedstock for physical, dissolution based recycling processes, also known as solvent-based purification, to recover highly pure rPP, rPC/ABS, rPA6 and rPA6.6 grades from shredder residues as has been demonstrated by the CreaSolv® Process in earlier projects (Schlummer et al., 2022; Strobl et al., 2021; Kohlmeyer, 2023).

5 Perspective

The sorting trials performed with XRT and laser spectroscopy open up ways to include more technical thermoplastics and fiber reinforced or filled polypropylene into existing recycling concepts. Combining these sensor-based technologies with density-based and tribo-electrostatic or solvent-based recycling can further increase regrind qualities and closed-loop recycling rates.

References

Arends, D., Schlummer, M., Faltermayr, B. Jehle, B., Gossmann, O., Kochler, P., Fey, D., Lautenschläger, D., Schmidt, A., Hoffmann, A. (2022). WEEEsense – hochwertige Polymercompounds aus Elektroaltgeräten. Technische Informationsbibliothek (TIB) / Leibniz-Informationszentrum Technik und Naturwissenschaften und Universitätsbibliothek.

Kohlmeyer, R. (2023, June 28-29). Recycling WEEE Plastics – advanced separation techniques and mandatory recycling targets [conference presentation]. E-Waste World 2023, Frankfurt, Germany.

Potrykus, A., Schlummer M. (2022, May 30 – June 3). Stärkung des Recyclings Technischer Kunststoffe aus Elektroaltgeräten und Altfahrzeugen – KUREA (vorläufige Ergebnisse) [conference presentation]. IFAT 2022, Munich, Germany

Schlummer, M., Merkert, L. (2023, June 21-22). Recycling of Plastics from Automotive Shredder Residues [conference presentation]. PIAE 2023, Mannheim, Germany.

Schlummer, M., Schoberer, J., Merkert, L. (2022). Eine Lösung für Kunststoffe aus Automobilen. Kunststoffe 11/22.

Strobl, L., Diefenhardt, T., Schlummer, M., Leege, T., Wagner, S. (2021). Recycling Potential for Non-Valorized Plastic Fractions from Electrical and Electronic Waste. Recycling, 6(33). https://doi.org/10.3390/recycling6020033

Analysis of Process Parameters in Sensor-Based Sorting using Automated Material Flow Characterization

Chanchan Li[1]*, Menglai Yuan[1], Malte Vogelgesang[1], Alice do Carmo Precci Lopes[1,2], Emanuel Ionescu[1]

[1] Fraunhofer IWKS, Digitalization of Resources, Alzenau, Germany

[2] Technical University of Darmstadt, Institute IWAR, Material Flow Management and Resource Economy, Darmstadt, Germany

* Corresponding Author: Brentanostr. 2a, 63755 Alzenau, chanchan.li@iwks.fraunhofer.de

Keywords: Sensor-Based Sorting, Material Flow Characterization, Plastic Waste, Computer Vision, Artificial Intelligence (AI), Mathematical Modelling

Abstract

Solid wastes contain various and valuable materials. Due to their differing properties, individual treatment processes are needed for their recovery. After liberating the materials from one another, sorting is necessary to channel them into their respective treatment pathways. Sensor-based sorting offers flexible, customized solutions for various sorting problems. Sensor-based sorting machines can be equipped with different types of sensors for the specific sorting tasks. The quality of the sorting process depends not only on the sensors used, but also on the individual characteristics of the material flows and on various other factors related to the design and configuration of the sorting machine.

The present study aimed at (1) developing artificial intelligence (AI)-based and non-AI-based digital methods to automatically analyze input and output streams of a sorting plant; and (2) understanding the correlation between specific process parameters of a sensor-based sorter and the sorting quality (e.g., purity and yield) of plastic waste. Four process parameters including the air pressure for the pneumatic

ejection, the material size, the position of the separating vertex and the occupation density of the conveyor belt were investigated. Experiments were conducted by varying single factor to evaluate the relationship between the process parameters and the sorting results. The sorting process was automatically analyzed with tools of computer vision and machine learning. During the sorting experiments, the material flow characteristics of the input and output stream were monitored using camera. Based on these data and the respective process settings, the relationship between process parameters and sorting quality (i.e., purity, yield) was analyzed.

This paper shows the possibility of digital methods to monitor sorting processes with the goal of automated evaluation of experiments. The experimental results reveal that the purity and yield of ejected material is influenced by the size of the material. The occupation density on the conveyor belt shows a negative impact on the purity of the eject fraction, meaning that a higher occupation density lead to a lower purity of the eject fraction.

1 Introduction

Solid waste management is a critical global challenge due to the large volume and diversity of materials in solid waste streams. In 2021, the global plastics production was 390.7 million tons (Plastics Europe, 2022). In Germany, the plastic waste production for the same year was of 21.1 million tons (Plastics Europe DE, 2022). Material recovery from waste is essential for contributing to the reduction of natural resources demand. However, still more than half of the plastic waste in Germany in 2021 was incinerated rather than recycled (Umweltbundesamt, 2022). The incineration of plastics increases the greenhouse gas emissions for two reasons: (1) the combustion of carbon-based material and (2) the production of virgin material, which leads to negative environmental impacts. Thus, incineration as a way of treatment of plastic waste goes against the goal of achieving climate neutrality by 2045 in Germany. The first step of managing household wastes is a source-separated collection. The collected recyclable waste is transported to a transshipment point, before being transported to a sorting facility. In the sorting facility, the waste is mechanically separated into different fractions (e.g., polypropylene [PP], polyethylene terephthalate [PET], high-density polyethylene [HDPE]), ferrous metals and non-ferrous metals). Each fraction is then transported to a recycling facility to produce recyclates (Umweltbundesamt, 2021).

An effective recycling of waste streams requires specialized treatment processes according to the different types of waste. A key aspect of this recovery process is the sorting of materials, which involves separating them based on their unique properties (Küppers et al., 2020). In recent years, sensor-based sorting has emerged as a promising and flexible solution for addressing the complexities of solid waste sorting (Feil et al., 2019; Kroell et al., 2022).

The design and configuration of sorting machines and the characteristics of material flows have a significant impact on the overall performance of the sorting process. Therefore, a comprehensive understanding of these factors is crucial for optimizing the performance of sensor-based sorting systems in waste management. Several research papers have been dedicated to investigating the impact of physical characteristics, such as sample thickness, labeling and surface roughness of materials on the performance of sorting processes (Küppers et al., 2019; Masoumi et al., 2012; Zhang et al., 2022). Recently, with the digital transformation, artificial intelligence (AI) has emerged as a promising tool for optimizing waste treatment processes.

This study aims to (1) develop AI-based and non-AI-based digital methods to automatically analyze input and output streams of a sorting plant, including the material's physical characteristics, material flow of the conveyor belt and digital assessment of the sorting result; and (2) understanding the relationship between specific process parameters in the sorting of plastic waste and the sorting quality (e.g., purity and yield) of the target fractions.

2 State of the art

In Germany, the collected recyclable waste from households is preprocessed in centralized sorting plants. These sorting plants use sifting, screening, magnetic separation, eddy-current separation, ballistic separation and other processes to separate the incoming waste stream into marketable fractions. Subsequently, the recyclable waste is sorted using near-infrared (NIR) spectroscopy into different types of plastics such as PP, polystyrene (PS), PET, polyethylene (PE). The sorted plastic is then pressed into bales for transport to the processing company (Knappe et al., 2021). Sink-float density separation is also widely employed for plastics sorting due to its simplicity in design and low operating costs (Karmana et al., 1997). However, this method does not allow the separation of material streams of similar density, such as PP and PE (Umweltbundesamt, 2021). As they have distinct near-infrared spectra, NIR-based sorters are primarily used in plastic sorting (Gundupalli et al., 2017).

According to a study by (Gabriel & Maulana, 2018), the printing and coloring of plastics can have a negative effect on NIR sorting, especially in terms of light transmission level. (Küppers et al., 2019) discussed the influences and consequences of mechanical delabelling on PET recycling. The overall shape of the spectrum remains the same for different plastic thicknesses and the peak points are fixed, with the absolute reflectance values increasing with thickness (Masoumi et al., 2012). Increased surface roughness improves the classification of both, spectrally similar and transparent plastics. However, the influence of surface moisture on the yield of plastics is usually very low and depends on the spectral differences between the different plastics (Küppers et al., 2019). Experimental studies made by (Küppers et al., 2020) have shown that the material composition of sorting machines has no influence on the yield (amount of eject material discharged into the target fraction), while the yield decreases exponentially with increasing occupation density/throughput rate. (Maisel et al., 2020) showed the effectiveness of plastics sorting can be increased if the particle size is within a standardized range and the different sorting technologies require different particle size ranges for efficient separation. But this work focuses more in the pre-treatment operation instead of the sorting process.

Digitalization and automated processes have already been state of the art in many industry sectors for some years and were mainly used to reduce the need for physical work, making the processes more efficient (Sarc et al., 2019). The continuous development of machine learning technology, especially the use of deep learning methods to classify waste, opens new research possibilities. Zhang et al. (2022) conducted in his study a deep learning, multi-label waste classification model of multiple waste. (Maier et al., 2021) developed an image processing approach in multi-object tracking in sensor-based sorting to achieve a more precise control over physical particle separation. However, those works focused either on one factor or on the development of machine learning methods instead of sorting process. (Friedrich et al., 2023) created regression models for finding out the optimal operation point on the sensor-based sorting based on the 3D plastic samples composition and the throughput rate. Kroell (Kroell et al., 2022; Kroell et al., 2024) developed an automatic assessment of sorting processes and digital twins to optimize sorting plants. To monitor the results of the sorted material, the authors developed a NIR based model. However, installing an extra NIR module for monitoring is expensive. In our present paper, we propose and discuss the application of a low-cost alternative, namely a web-camera, to monitored the sorting results.

3 Material and Methods

3.1 Sorting Machine

The experiments were carried out on a customized, modular sorting machine at the Fraunhofer Research Institution for Materials Recycling and Resource Strategies IWKS, located in Germany (Fig. 1a). The sorting machine consists of several modules on pilot scale that can be configured and operated independently to simulate industrial sorting procedures. The zig-zag air separator and the flip-flow screen allow for classification based on particle weight and size, whereas magnetic and eddy-current separators separate metals. The most versatile module is the sensor-based sorting machine Varisort Compact (Sesotec), which was the focus of the present work.

a)

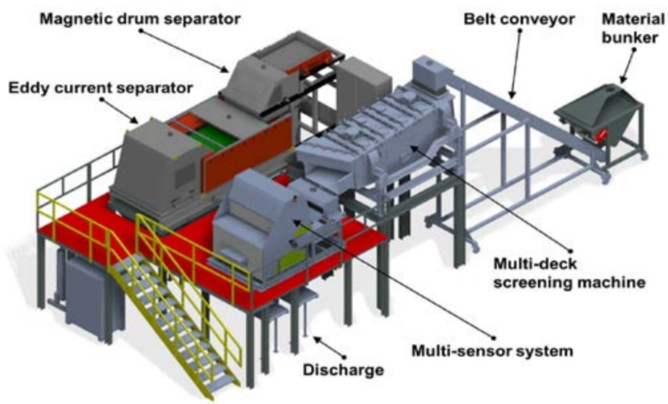

b)

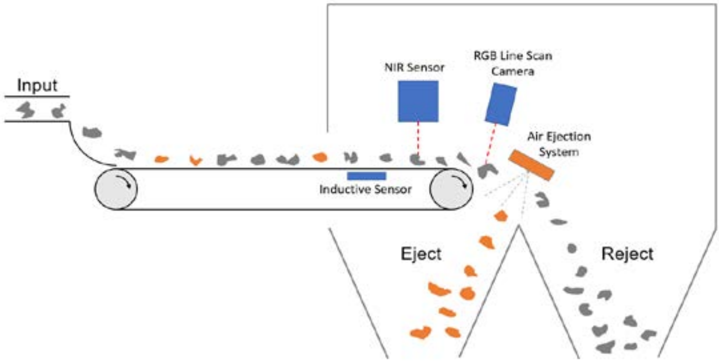

Fig. 1. (a) Waste sorting system at Fraunhofer IWKS; and (b) schematic drawing of the working principle and sensor arrangement of the multi-sensor system. NIR = near infrared.

Fig. 1(b) shows the schematic drawing of the working principle and sensor arrangement of the multi-sensor system. The multi-sensor system includes an inductively working electromagnetic sensor to detect conductive materials, such as metals; an NIR sensor in the range of 1325 nm to 1900 nm to classify polymers, such as plastics, or cellulose in paper and wood: and two line-scan cameras to capture RGB color images of the materials.

A conveyor belt accelerates the objects to be sorted by the multi-sensor system. The conveyor belt is 1,024 mm wide, 2,538 mm long, black and can reach a maximum transport speed of 2.5 m/s. The objects to be sorted pass the sensors and they are released from the conveyor belt at its end, leaving in a horizontal trajectory. Compressed air, which can be adjusted from 0 to 5 bars, is used to eject particles meeting defined sorting criteria from the rest of the stream. The pass and eject fractions then fall into separate chutes and onto additional output conveyor belts. Additionally, for this work, two webcams were installed above the output chutes to enable an automated evaluation of the sorting results.

3.2 Material

Samples of lightweight packaging waste were provided by a sorting facility, which sorts separately collected recyclable packaging waste in Germany. HDPE and PP are common plastic types in packaging (Plastics Europe DE, 2022). As was stated above, these polymers have similar densities and cannot be sorted by sink-float density separation. However, they have different characteristics in the NIR spectral range and can be sorted by NIR spectroscopy. To visually evaluate the results of the sorting trials, the different types of polymers were made distinguishable through their color as follows: blue for HDPE and white for PP (Fig. 2. *Samples used in the experiments. HDPE (blue) and PP (white) in the three different particle sizes.*). Since the material used for the trials originated from real collected waste streams, the colors of the materials were not uniform, especially in the case of the blue PP materials, which ranged from dark blue to light blue.

Considering the design of the sorting machine and its proposed operating window for sorting particles between 5 mm and 50 mm, the materials were prepared in three groups concerning their particle size: large (30 mm to 50 mm), medium (10 mm to 30 mm) and small (5 mm to 10 mm), see Fig. 2. The materials were divided into three samples, namely, samples 1, 2, 3 representing large, medium and small sizes, respectively. Each sample contained 250 g of PP (white) and 250 g of HDPE (blue). Material in a sample is considered uniform in size.

30 mm – 50 mm　　10 mm – 30 mm　　5 mm – 10 mm

Fig. 2. Samples used in the experiments. HDPE (blue) and PP (white) in the three different particle sizes.

3.3 Methods

This research focuses on the sensor-based sorting machine. Considering the state of the art and the features of the sorter, four parameters of the sensor-based sorter were investigated, namely the air pressure for pneumatic ejection, the material sizes and the position of the separating vertex and the occupation density on the conveyor belt. Further, the influence of these parameters on the sorting results was evaluated. Thus, experiments were combined with digital tools and modelling approaches to find the relationships between these parameters and the resulting purity and yield of the process. In the following experiments, the sorting procedure was carried out based on the NIR spectroscopy.

3.3.1 Experimental procedure

Various series of experiments were carried out and each experiment was repeated three times. In each experiment, one of the samples, consisting of HDPE flakes (blue) and PP flakes (white) of a specific particle size range was fed through the sensor-based sorting machine. The machine was set up for an NIR detection of HDPE, which was then targeted by the pneumatic ejection. The fixed speed of the conveyor belt is 1.78 m/s as per direct measurement. The experiments can be divided as follows:

1. Air pressure (1-5 bar) for pneumatic ejection and particle size (large: 30 mm – 50 mm, medium: 10 mm – 30 mm and small: 5 mm – 10 mm).
2. Horizontal and vertical position of the separating vertex.
3. Occupation density and overlapping particles for the input streams on the conveyor belt.

To evaluate the influence of those parameters on the sorting results, purity and yield of the target material were monitored using cameras and digital scales.

3.3.2 Assessment of the influencing parameters

Air pressure for pneumatic ejection in the sorter was adjusted manually from 1 to 5 bar. To evaluate the influence of the **particle size**, experiments were conducted in all three sample groups.

A mathematically-based model was constructed to further explore the impact of the **position of the separating vertex**. In this model, the trajectory of the material between leaving the conveyor belt and the upper edge of the separating vertex was analyzed. When an object is accelerated through the conveyor belt of a sorting machine and leaves it in horizontal motion, the dropping process is simplified and described as equation (1):

$$F_D = \frac{1}{2} \cdot \rho \cdot v^2 \cdot C_d \cdot A \tag{1}$$

- F_D: the resistance force;
- ρ: density of the medium, in this case is air, 1.225 kg/m^3;
- v: the speed of the medium in relation to the object;
- A: the reference area, in this case is the particle size;
- C_d: the resistance coefficient.

The resistance coefficient is closely related to the shape of the object. And in this experiment, the material is cut into pieces and laid flat on the conveyor belt. Therefore, a relatively large value of 1.28 is selected.

In this model, the last point of touch with the conveyor belt is seen as the origin of the coordinates. The top point of the separating vertex is represented by the red dot in Fig. 3. The separating vertex can be moved along the y-axis through an offset of a metal plate and rotated along the x-axis through flexing the plate structure.

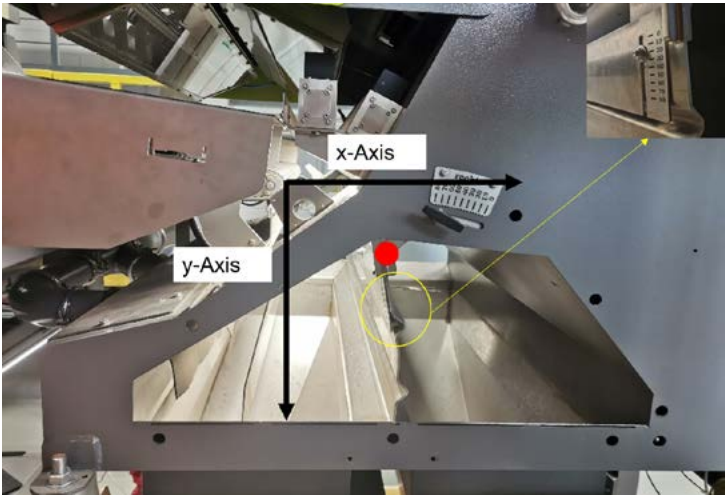

Fig. 3. The position of the separating vertex of the sorter: the red dot is the upper edge of the separating vertex, and the area of the yellow circle shows the areas area for adjusting along the y-axis, with a clearer view shown in the upper right of the image.

The two related factors **occupation density** and **overlap** represent the most complex factors. Occupation density is the proportion of the conveyor belt area that is covered with material, whereas overlap is the ratio of object area covered by another object. To analyze these two factors, data from the RGB cameras in the sorter were combined with image processing. To calculate the occupation density, a Python script was written to count the covered pixels of the image. The image always possesses a black background due to the camera position. To reduce image noise, a threshold value of 10 was used. The image was then transformed into a binary image, in which objects were represented by a white value of 255.

The machine learning model YOLO (You Only Look Once) (Redmon et al., 2016) was fine-tuned with a customized dataset to detect the overlap of the input stream. The customized dataset includes around 200 images, which were collected from the RGB camera. Resizing of the images was used to reduce the quality of the image from the line scan camera to simulate the quality of the webcams.

Although overlap in the input material stream can be identified by machine learning model, the direct calculation of the overlapping area and multilayer overlap is still not possible, since the images from the RGB cameras cannot see through the objects and measure the covered area of the object beneath. Therefore, the Singling Ratio (SR) approach, presented by (Kroell et al., 2022), was used. The SR describes the percentage of covered area that is singled, i.e. that contains only one particle (Kroell et al., 2022). However, the SR does not consider the multilayer overlap that often occurs in small or nearly 2D material. Thus, in this study, considering the similar density in the sample material and its 2D shape, the monolayer rate (MR) was defined as the single object ratio in the input stream and was calculated according to Equation (2):

$$MR = \frac{A_{single} \times thickness \times density}{m_{input}} \tag{2}$$

A_{single} represents the detected single Area (A_{single}) and m_{input} represent the mass of the input steams.

3.3.3 Assessment of the sorting result

To evaluate the sorting results, a color-based model with the support of two common webcams was built. The webcams monitored the conveyer belt of the eject and reject fractions. Utilizing the different colors of the sample materials, computer vision was used to calculate the area of pixels for each material. To ensure the optimized value of the threshold, this model provides a user-customizable window to adjust the maximum and minimum value of hue, saturation and value respectively, adjusting the result dynamically. The purity and yield of the targeted materials were then estimated. The following are the definitions of purity and yield. In this study, the target material of HDPE was set as the eject fraction, and the sorting result was described as eject purity (EP_m) and eject yield EY_m:

$$EP_m = A_{recy} \times \text{thickness} \times \text{density}/m_{eject} \tag{3}$$

$$EY_m = A_{recy} \times \text{thickness} \times \text{density}/m_{target} \tag{4}$$

A_{recy} is the area of the target material in eject fraction; m_{eject} is the mass of the eject fraction; m_{target} is the weight of the target material.

All programming work was done in the Python programming language, since many of the required frameworks are provided in Python. Fig.4 presents an overview of the varied parameters and the methods used to assess them.

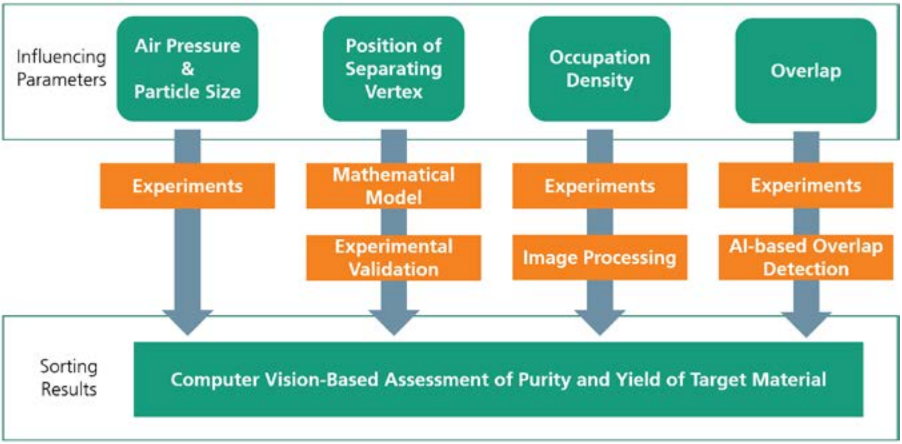

Fig. 4. Structure of the methods used for the assessment of the influences of different parameters on the sorting result.

4 Results

4.1 Results of Digital Methods

The original image of the input streams on the conveyor belt is shown in the Fig.5 left. The noise-reduced and binarized image is shown in the right image of Fig.5 and the white part represents the occupied area by the materials. The occupation density of the image shown is 7.5%.

Fig. 5. Binary image processing of the input stream in the conveyor belt: left is the original image; right is the binary image.

After 300 iterations, the mAP (mean Average Precision)_0.5 of the fine-tuned YOLO model reached 0.83 and the average precision in the class of SR was around 0.90. The error was mainly caused by multilayer overlap of several objects. Fig. 6 shows the overlap detection results in three sample groups.

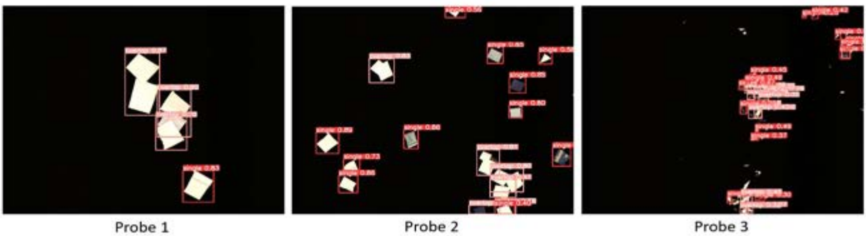

Fig. 6. Result of overlap detection in three sample groups: left to right: Samples 1-3.

Fig.7 presents an example of image processing applied to images of the output fractions. The left image is the original captured by the webcams, the middle and right images are the extracted blue and white areas, respectively. The result shows that HDPE (blue) and PP (white) could be mostly separated correctly.

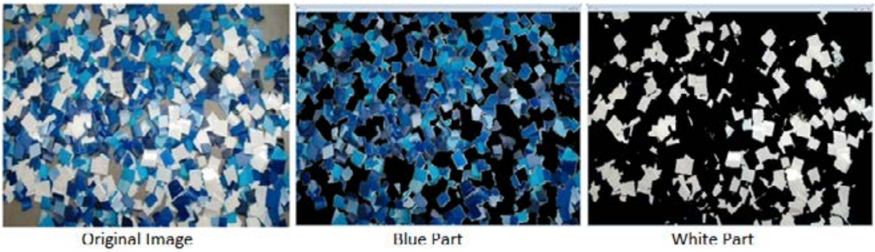

Fig. 7. Image processing on the output fractions: left is the original webcam image, middle is the extracted blue area and right is the extracted white area.

4.2 Preliminary Results

4.2.1 Compressed air and material size

Fig.8 shows the results of the air pressure preliminary tests. The x-axis represents the value of the compressed air pressure at the valves. The differences in purity and yield varied for different particle sizes with increasing air pressure. The decrease in sample 1 (large particles size) is the most obvious, which attained the best purity, 90%, at 2 bar of compressed air pressure and a reduction to 83% at 4 bar. In comparison, the reduction of purity in sample 2 and sample 3 is less when pressure increases. The reason may be that the objects hit the chute's wall and are reflected into the wrong chute. Although the reaction of purity and yield to changes in the air pressure were not consistent across the groups, the trend was similar. In general, high purity and yield were attained at compressed air pressure levels between 1 and 2 bar.

Furthermore, the results indicate that eject purity of medium-sized sample 2 is the best and small-sized sample 3 gets the worst eject purity and eject yield independent of the air pressure.

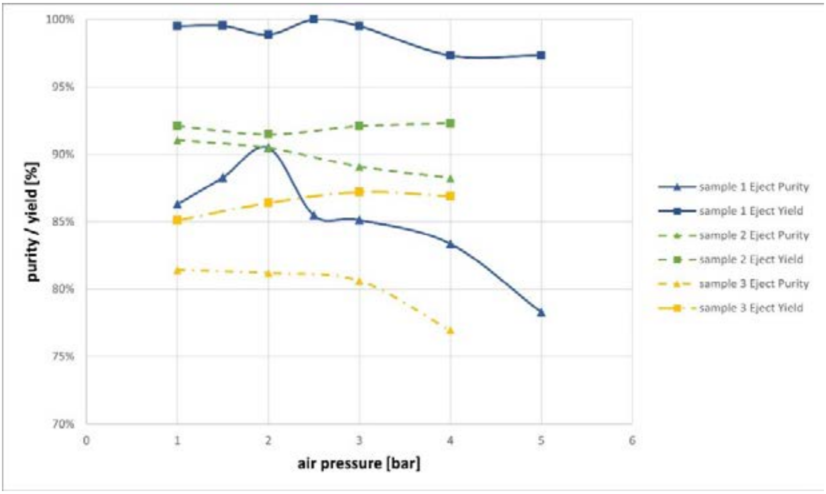

Fig. 8. Influence of air pressure on sorting performance in three particle size groups: (sample 1: 30 mm - 50 mm, sample 2: 10 mm - 30 mm and sample 3: 5 mm - 10 mm).

4.2.2 Separating vertex

The adjustment area of vertex positions in the sorter based on the statistical model were converted into x and y coordinates and they are depicted in Fig. 9 as blue dots. The coordinate information is shown in Fig 3. The black curve represents a resistance-free (i. e. without drag) motion curve of a particle. Since no object can pass over the black curve with its initial speed, even without air-induced drag, the positions of the vertex above the black curve are not relevant. The blue curve shows the theoretical trajectory of the motion for most of the samples. The small red dots are experimental values and are located below and adjacent to the blue curve. Since the vertex should be adjusted to closely below the trajectory of the particles, the optimal position of the separating vertex of used samples is shown as an orange star in Fig. 9.

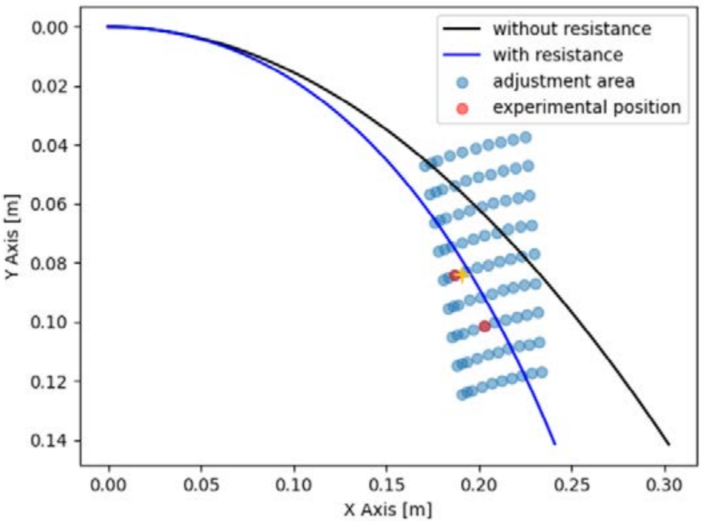

Fig.9. The trajectory of the material from conveyor belt to the separating vertex. The yellow star shows the optimized position.

4.2.3 Occupation density

Fig. 10 shows the occupation density on the x-axis and the reject purity on the y-axis. The dots show the measured data in experiments. Based on the experimental results, the probable regression curves are depicted as well. For each set of test samples, the eject purity decreased with increasing occupation density from above 85% to around 65%, while the occupation increased from below 1% to about 8%.

To prove the trend of decreasing eject purity with increasing occupation density, more experiments were conducted in example 2. The experiments showed that the eject purity is around 56% while the occupancy density reached 35%. The results confirmed the regression curve in Fig. 10.

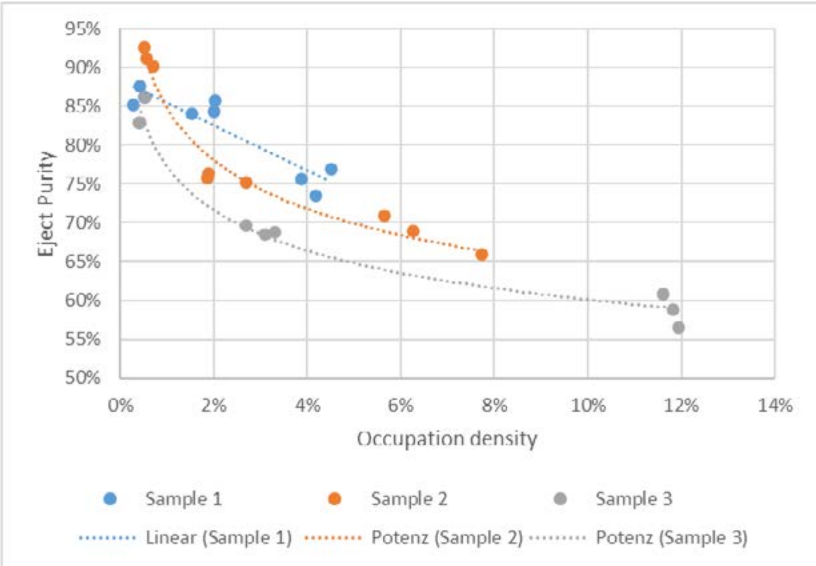

Fig. 10. Experimental results of the eject purity for different occupation densities.

Table 1 presents the experimental results of singling ratio with occupation density and eject purity for sample 2 (particle size 10 mm – 30 mm). As the occupation density increased, the monolayer rate decreased and the eject purity became worse. Such trend is consistent with the research of (Kroell et al., 2022), which also analyzed the occupation density and SR on the sorting performance.

Tab. 1. Results of singling ratio with occupation density and eject purity in sample 2 (10 mm - 30 mm).

Occupation density	Monolayer rate	Eject purity
0.5%	84.4%	92.5%
0.6%	74.0%	91.2%
0.7%	83.2%	90.2%
1.8%	79.2%	75.7%
1.9%	84.6%	76.3%
2.7%	74.8%	75.1%
5.7%	78.2%	70.9%

Occupation density	Monolayer rate	Eject purity
6.3%	77.2%	68.9%
7.7%	71.8%	65.9%

5 Conclusions and Outlook

Based on the literature review and the properties of the sensor-based sorting machine, four influencing factors for a sensor-based sorting were identified. They included the air pressure for the pneumatic ejection, the material size, the position of the separating vertex and the occupation density of the conveyor belt. An AI-based method for overlap detection, a statistical model for the position of separating vertex, and non-AI-based methods for detection of occupation density and the analysis of purity and yield of the output fractions were developed. Those methods were implemented to analyze the material flow in the conveyor belt and assist in the assessment of the sorting results. Various experiments were conducted in a pilot-scale sorting machine. This paper shows the possibility of using machine learning and image processing methods to analyze sorting processes.

The experimental results showed that the material size has a significant influence on the purity and yield of the targeted fraction. The sorting machine presented the best sorting result with a pressure of 2 bar independent of the material size. The position of separating vertex could be modeled with statistical model, which guided the adjustment of the sorter. The occupation density and overlap were highly correlated. Both parameters had a large influence on the eject purity. An increase of occupation density decreased the eject purity.

The experimental results were based on one specific sorting machine at pilot scale. Further experiments are necessary at full scale plants. The investigation of the occupation density was performed in a relatively small area, less than 35% of the sorting machine’s belt width. Further research with higher occupation densities and using other material types should also be considered.

References

Feil, A., Coskun, E., Bosling, M., Kaufeld, S., & Pretz, T. (2019). Improve-ment of the recycling of plastics in lightweight packaging treat-ment plants by a process control concept. Waste Management & Research : The Journal of the International Solid Wastes and Public Cleansing Association, ISWA, 37(2), 120–126. https://doi.org/10.1177/0734242X19826372

Friedrich, K., Kuhn, N., Pomberger, R [Roland], & Koinig, G. (2023). Feasi-bility Study for Finding Mathematical Approaches to Describe the Optimal Operation Point of Sensor-Based Sorting Machines for Plastic Waste. Polymers, 15(21), 4266. https://doi.org/10.3390/polym15214266

Gabriel, D. S., & Maulana, J. (2018). Impact of Plastic Labelling, Coloring and Printing on Material Value Conservation in the Products of Secondary Recycling. Key Engineering Materials, 773, 384–389. https://doi.org/10.4028/www.scientific.net/KEM.773.384

Gundupalli, S. P., Hait, S., & Thakur, A. (2017). A review on automated sorting of source-separated municipal solid waste for recycling. Waste Management (New York, N.Y.), 60, 56–74. https://doi.org/10.1016/j.wasman.2016.09.015

Ihsanullah, I., Alam, G., Jamal, A., & Shaik, F. (2022). Recent advances in applications of artificial intelligence in solid waste management: A review. Chemosphere, 309(Pt 1), 136631.

Karmana, E., Eiler, B., Mainiero, D., Bedner, M., & Enick, R. (1997). The microsortation of high loadings of post-consumer mixed polyole-fins using liquid carbon dioxide in a slightly agitated, batch appa-ratus. Resources, Conservation and Recycling, 20(3), 143–152. https://doi.org/10.1016/S0921-3449(97)00009-8

Knappe, F., Reinhardt, J., & Kauertz, B. (2021). Technische Potenzialanaly-se zur Steigerung des Kunststoffrecyclings und des Rezyklateinsat-zes.

Kroell, N., Chen, X., Greiff, K., & Feil, A. (2022). Optical sensors and ma-chine learning algorithms in sensor-based material flow charac-terization for mechanical recycling processes: A systematic litera-ture review. Waste Management (New York, N.Y.), 149, 259–290. https://doi.org/10.1016/j.wasman.2022.05.015

Kroell, N., Dietl, T., Maghmoumi, A., Chen, X., Küppers, B., Feil, A. H., & Greiff, K. (2022). Assessment of sensor-based sorting perfor-mance for lightweight packaging waste through sensor-based ma-terial flow monitoring: Concept and preliminary results. Sensor-Based Sorting & Control.

Kroell, N., Maghmoumi, A., Dietl, T., Chen, X., Küppers, B., Scherling, T., Feil, A., & Greiff, K. (2024). Towards digital twins of waste sorting plants: Developing data-driven process models of industrial-scale sensor-based sorting units by combining machine learning with near-infrared-based process monitoring. Resources, Conservation and Recycling, 200, 107257. https://doi.org/10.1016/j.resconrec.2023.107257

Küppers, B., Chen, X., Seidler, I., Friedrich, K., Raulf, K., Pretz, T., Feil, A., Pomberger, R [Roland], & Vollprecht, D. (2019). Influences and consequences of mechanical delabelling on PET recycling. Detritus, Volume 06 - June 2019(0), 1. https://doi.org/10.31025/2611-4135/2019.13816

Küppers, B., Schloegl, S., Oreski, G., Pomberger, R [Roland], & Voll-precht, D. (2019). Influence of surface roughness and surface moisture of plastics on sensor-based sorting in the near infrared range. Waste Management & Research : The Journal of the Inter-national Solid Wastes and Public Cleansing Association, ISWA, 37(8), 843–850. https://doi.org/10.1177/0734242X19855433

Küppers, B., Seidler, I., Koinig, G. R., Pomberger, R [Roland], & Voll-precht, D. (2020). Influence of throughput rate and input compo-sition on sensor-based sorting efficiency. Detritus(9), 59–67. https://doi.org/10.31025/2611-4135/2020.13906

Maier, G., Pfaff, F., Pieper, C., Gruna, R., Noack, B., Kruggel-Emden, H., Langle, T., Hanebeck, U. D., Wirtz, S., Scherer, V., & Beyerer, J. (2021). Experimental Evaluation of a Novel Sensor-Based Sorting Approach Featuring Predictive Real-Time Multiobject Tracking. IEEE Transactions on Industrial Electronics, 68(2), 1548–1559. https://doi.org/10.1109/TIE.2020.2970643

Maisel, F., Chancerel, P., Dimitrova, G., Emmerich, J., Nissen, N. F., & Schneider-Ramelow, M. (2020). Preparing WEEE plastics for recy-cling – How optimal particle sizes in pre-processing can improve the separation efficiency of high quality plastics. Resources, Con-servation and Recycling, 154, 104619. https://doi.org/10.1016/j.resconrec.2019.104619

Masoumi, H., Safavi, S. M., & Khani, Z. (2012). Identification and classifica-tion of plastic resins using near infrared reflectance spectroscopy, 6(5). https://www.researchgate.net/profile/hamed-ma-soumi/publication/285330830_identification_and_classification_of_plastic_resins_using_near_infrared_reflectance_spectroscopy

Plastics Europe (2022). Plastics-the Facts 2022. https://plasticseurope.org/knowledge-hub/plastics-the-facts-2022/

Plastics Europe DE (2022). Material flow diagram for plastics in Germany 2021: Facts and figures on the life cycle of plastics. https://plasticseurope.org/de/knowledge-hub/stoffstrombild-kunststoffe-in-deutschland-2021/

Redmon, J., Divvala, S., Girshick, R., & Farhadi, A. (2016). You Only Look Once:Unified, Real-Time Object Detection. https://arxiv.org/pdf/1506.02640.pdf

Sarc, R., Curtis, A., Kandlbauer, L., Khodier, K., Lorber, K. E., & Pomber-ger, R [R.] (2019). Digitalisation and intelligent robotics in value chain of circular economy oriented waste management - A review. Waste Management (New York, N.Y.), 95. https://doi.org/10.1016/j.wasman.2019.06.035

Umweltbundesamt. (2022). Generation and recycling of packaging waste in Germany in the year 2020. https://www.umweltbundesamt.de/publikationen/aufkommen-verwertung-von-verpackungsabfaellen-in-16

Umweltbundesamt. (2021). Plastic waste. https://www.umweltbundesamt.de/daten/ressourcen-abfall/verwertung-entsorgung-ausgewaehlter-abfallarten/kunststoffabfaelle#kunststoffe-produktion-verwendung-und-verwertung

Zhang, Q., Yang, Q., Zhang, X., Wei, W., Bao, Q., Su, J., & Liu, X. (2022). A multi-label waste detection model based on transfer learning. Re-sources, Conservation and Recycling, 181, 106235. https://doi.org/10.1016/j.resconrec.2022.106235

Rethinking Comminution Circuit Optimisation Beyond Mineral Processing Equipment

Tobias Vraetz[1]*, Bjorn Dierx[1]

[1] Weir Minerals, Venlo, The Netherlands

* Corresponding Author: Egtenrayseweg 9, 5928 PH Venlo, The Netherlands, tobias.vraetz@mail.weir

Keywords: High Pressure Grinding Rolls, Digitalization, Sustainability, Digital Twin, Redefined flowsheet

1 Introduction

The mining industry is generally regarded as a slow adaptor when it comes to digital technologies; however, many sector experts also recognize that it could radically reshape their day-to-day operations.

A significant opportunity to reduce energy and emissions sits within comminution, which is the process that turns big rocks into small particles. This process is responsible for at least one-third of an average mine's energy use and CO_2 emissions and globally consumes around 3% of the world's electrical power (Allen, 2021).

Apart from rethinking flowsheets and replacing traditional circuits with more energy efficient alternatives, such as high pressure grinding rolls (HPGR) and vertical stirred mills, there's more to be explored in efforts to reduce the circuit's footprint. One of the most recently discussed developments in the field of automation, optimisation and digitalization is the concept of digital twins (DT). While some industries have been early adopters of digital twin technology, the mining and minerals processing industry is still largely defining its scope, framework and dedicated outcomes.

Key to implementing digital twins is the mining industry's ongoing sustainability agenda, as well as equipment and process optimisation with regards to availability, performance and quality, which is commonly and industry-wide defined as operational equipment efficiency (OEE).

2 HPGR-based comminution circuits

There is a common industry consensus that HPGRs are firmly cemented in making comminution processes more efficient, while delivering high equipment availability. With lowest energy consumption and no water or grinding media required, typical operating costs for HPGR-based circuits are over 20% lower compared to conventional semi-autogenous-ball mill-crusher (SABC) circuits, while also reducing comminution CO_2 emissions by 30%. (Lovatt et al, 2023)

Greenfield mines are increasingly located in remote regions, while the ore bodies are becoming less homogenous and more complex to process. Under these challenging conditions, Weir Minerals has, instead, opted to minimise operational complexity. The design fundamentals that underpin its Enduron® HPGR provide greater flexibility and, ultimately, more operational certainty and equipment availability.

However, to provide increased control of the HPGR's health and operational performance, a combination of physical and soft sensors connected to an online monitoring platform provides remote operators with the intelligence to make impactful decisions and assure adequate supply of performance consumables. The introduction of AI-based algorithms, combined with a comprehensive operational database, provides automatic recommendations to the operator, allowing them to weigh up the need to meet their production targets, while not overstretching the machine before scheduled maintenance shutdowns.

3 Weir Minerals' Digital Platform

Weir Minerals' digital offering, includes an intelligence platform with cutting edge applications and tools, including DTs, which can align to individual business goals. Alongside performance, health and sustainable operational objectives, Weir Minerals is strongly focused on working with its customers to become a leader in reaching its zero emissions objectives. Operators can achieve true end-to-end integration with their overall mining process by leveraging recommendations from their intelligence platform (Figure 1).

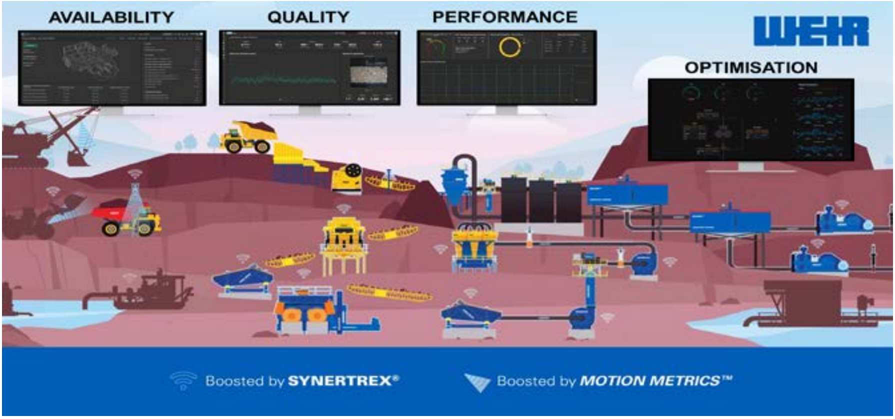

Fig. 1. Weir Minerals' redefined flowsheet, schematically including digital technologies for optimisation of availability, performance and quality (OEE).

Connected equipment – in this case HPGRs – form the foundation of gathering insights about the equipment and the related processes. Weir Minerals' recently released digital platform for HPGR equipment underpins further optimisation approaches on both an equipment and process level. This then provides insights and support to the customers, allowing them to make decisions based on their priorities with regard to achieving their individual business goals (for example, but not limited to availability, performance, quality and sustainability).

Figure 2 visualizes a digital platform example of a large, multi-staged HPGR configuration.

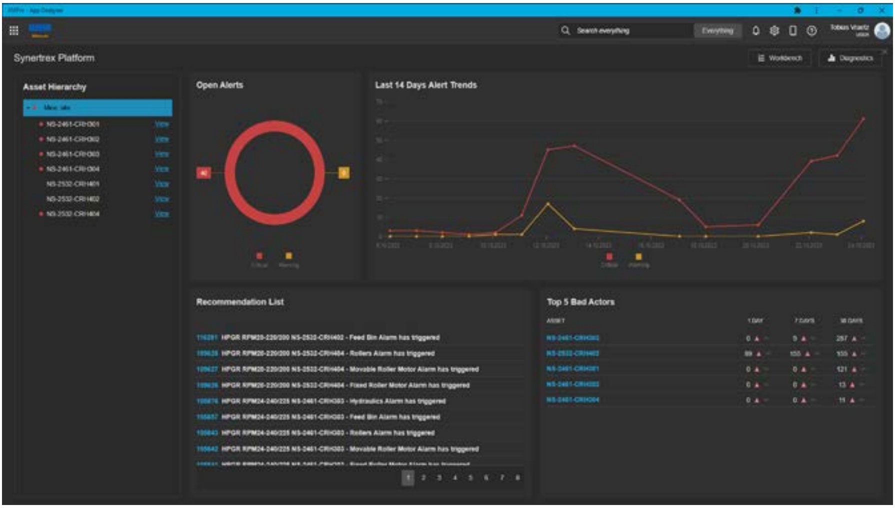

Fig. 2. Weir Minerals' digital intelligence platform: Landing Page (site level)

The landing page of the application provides an overview of critical warnings and alarms, enabling the operator to manually benchmark equipment. Furthermore, a summary of critical alarms and bad actors (on the equipment level) are shown, which enables Weir Minerals as an OEM to proactively support customers to optimize the equipment by checking each equipment's status, recommending the adjustments of setpoints and other operational parameters. For example, if alarms are being raised on a piece of equipment's hydraulic system, over an extended period of time (days/weeks/months), the customer can be proactively approached to check the equipment in order to address the underlying issues and, ultimately, ensure a safe, continuous and efficient operation.

The equipment page (Figure 3) visualizes the current status of one particular piece of equipment, which includes the status of the HPGR, as well as actual real-time data (right hand side).

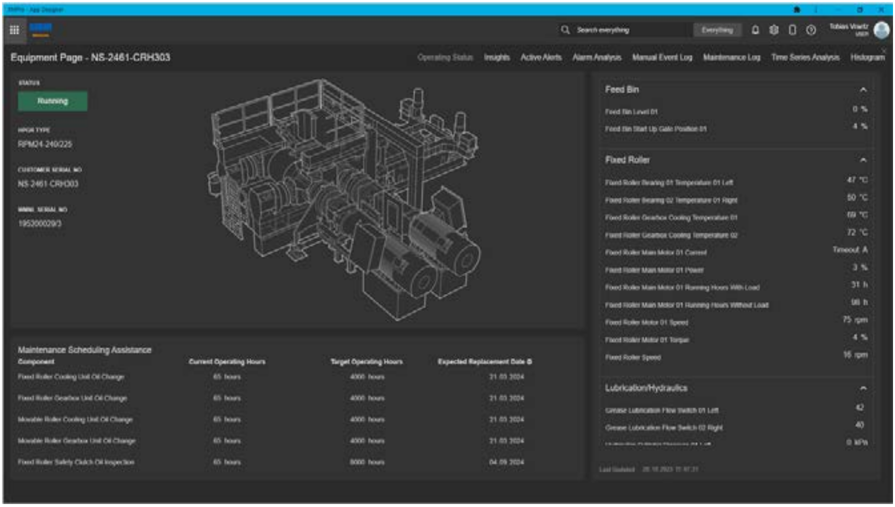

Fig. 3. Weir Minerals' digital intelligence platform: Equipment Page

All live data is frequently being updated; thus, it provides remote service engineers or monitoring room engineers with a clear picture of what is happening on site. This puts the Weir Minerals' monitoring room engineers into a position where they can access the information that normally only customers will see on site.

Within the equipment section the user also benefits from a maintenance scheduling assistant. With this assistant the user of the intelligence platform receives dynamic updates on when the optimal time the next maintenance activities should be scheduled.

Another useful piece of functionality is the user's ability to analyse time series data (Figure 4). This functionality can include multiple data streams.

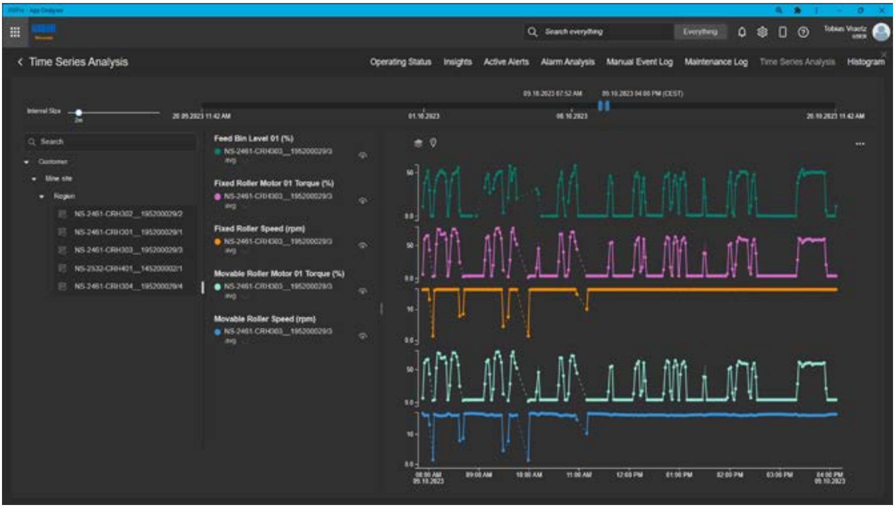

Fig. 4. Weir Minerals' digital intelligence platform: One example of the analysis capabilities (Time Series Analysis) to benchmark machines on mine sites.

This can include multiple attributes and time series data from one machine, like shown in the above example, or it can contain data streams from multiple pieces of equipment.

From an (end-user) operator perspective, this enables benchmarking of various pieces of equipment. For Weir Minerals as an equipment manufacturer, this enables it to compare various machines in different operations, categories and regions.

In the example shown in Figure 4, the feed bin level, speed and torque of both HPGR rollers are shown. Furthermore, the application in current release has functionality to track maintenance and events, histogram functionality, as well as alarm analysis, which supports operators and Weir Minerals to identify "pain points". This leads to further potential improvement and proactively makes recommendations to the operator to deliver improved circuit efficiency, while also allowing them to manage the asset effectively in the lead up to the next scheduled maintenance shut down.

While not yet completely implemented in the current release, the integration of particle size distribution (PSD) cameras will be made available in the near future. As the comminution and recovery circuit are interdependent, both over and under grinding can have a profound impact on mineral recoveries. Whereas, historically, recirculating loads and power consumption were used to estimate grind size performance, having optical sensors integrated in the overarching monitoring platform as a tangible control lever offers operators more accurate input on the overall circuit performance.

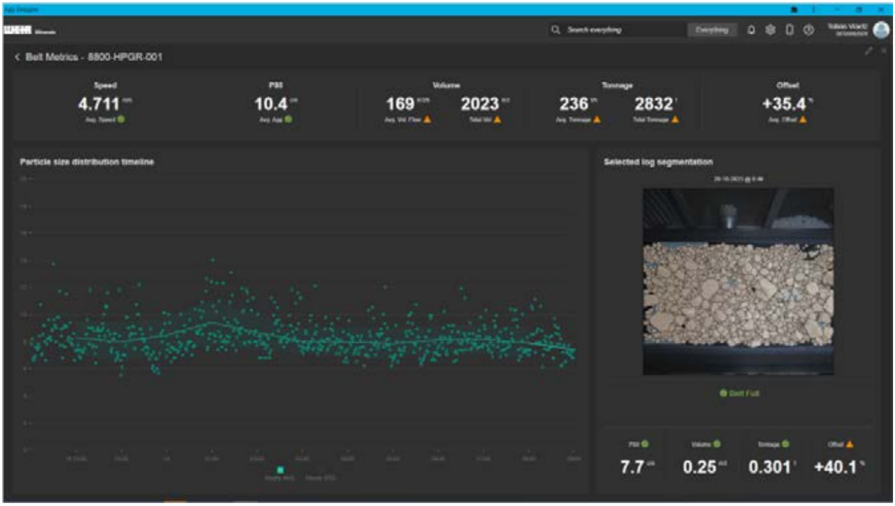

Fig. 5. Weir Minerals' digital intelligence platform: Integration of PSD information for process optimisation.

Figure 5 visualizes the camera system recording the PSD over time, as well as additional process parameters, like volume, belt speed and P80. The combination of internal HPGR parameters with additional process parameters, like PSD, paves the way to further optimisation in the future control of HPGRs with regard to performance and quality (as two pillars of the OEE definition).

The objective is to be proactive in the use of user data and customer feedback. The designs and user journeys outlined above are under constant review to ensure that the users can easily find their desired functionality, gain insights, and navigate the platform.

4 Conclusion and Outlook

Mining is a series of inter-related processes, often beginning with blasting/excavation, then transporting the material, crushing, grinding and milling it to produce a final product. But equipment and processes are typically analysed in isolation, rather than being evaluated holistically; downstream effects are not considered in upstream equipment and vice versa. For example, the HPGR's overall performance influences its up- and downstream processes; therefore, it needs to work intelligently with other equipment in the flowsheet to maximize OEE. This holistic view of process optimisation provides an opportunity to significantly reduce the environmental impact of mining.

Weir Minerals' digital platform builds the foundation for future process optimisation. The platform provides insights to every operator and provides them with the tools to make considered decisions based on tangibles, rather than assumptions. This facilitates increased availability, performance and product quality, while also decreasing the overall environmental footprint. Besides that, Weir Minerals is actively developing technologies to increase the amount of insights and to substantiate the automated decision-making for process optimisation.

The examples highlighted in this paper are hard sensor systems (e.g. automated tyre wear monitoring and automated cheek plate wear monitoring system). Additionally, Weir Minerals' digital team is collaborating with universities (like the Advanced Mining Technology Center in Chile) to develop soft sensing capabilities. This will enable access to information for process optimisation based on operational parameters without directly measuring the dedicated attribute with hard sensors.

References

Ivka Lovatt, Michael Becker, Brian Putland, Radford & J. Robinson., (2023) Trade-off realities in HPGR vs SAG milling - A Practical Comparison of Tropicana and Gruyere Comminution Circuits, SAG 2023, Vancouver, Canada

Marc Allen., (2021) Mining energy consumption 2021, A high-level study into mining energy use for the key mineral commodities of the future

From Hyperspectral Edge Computing to Offline Algorithm Based Feedback-loops. An Update.

Matthias Kerschhaggl*[1]

[1] EVK DI Kerschhaggl GmbH, Raaba, AUSTRIA

* Corresponding Author: matthias.kerschhaggl@evk.biz

Keywords: hyperspectral data processing, sorting classifiers, training and inference, data and information

Abstract

In this update on the previously presented topic, „From Hyperspectral Edge Computing to Offline Algorithm-Based Feedback-Loops,“ we delve deeper into the ever-evolving landscape of hyperspectral systems and their transformative applications in data-driven decision-making. Building upon the foundations laid out in the original presentation two years ago, we explore recent insights and developments in this field.

The core premise of hyperspectral systems remains intact: the fusion of edge computing technology with hyperspectral and other multimodal data streams, enabling rapid data reduction in order to extract key data for informed decision-making, particularly needed in industrial contexts like sorting. However, our understanding of this field has matured, and new developments are shaping its evolution. To fully exploit the potential of a broad bandwidth hyperspectral data stream, the development of sophisticated classification and regression algorithms is essential. These algorithms form the basis for extracting crucial insights and maximizing the value of the data.

This presentation will showcase the latest outcomes derived from a closed hyperspectral data processing loop, from the acquisition of industrial data, to machine learning-based algorithm training, to in-line and real-time extraction of key features.

Enhancing the Sortability of Packaging Films in Near Infrared

Gerald Koinig[1]*, Nikolai Kuhn[1], Thomas Fink[1], Alexia Tischberger-Aldrian[1]

1 Montanuniversität Leoben, Chair of Waste Processing Technology and Waste Management, Leoben, Austria

* Corresponding Author: Franz Josef Straße 18, 8700, Leoben, Austria, gerald.koinig@unileoben.ac.at

Keywords: Waste Management, Near Infrared Spectroscopy, Machine Learning, Packaging Film Waste

Abstract

Enhancing the recyclability of plastic packaging film waste (PPFW) is necessary to increase Austria's recycling rate, considering its substantial contribution of 150,000 tons to the annual 300,000 tons of plastic packaging waste. Currently, PPFW are thermally recovered due to challenges in distinguishing mechanically recyclable monomaterial films from multimaterial films. This study employs machine learning models utilizing spectral fingerprints recorded in transflection to classify PPFW inline into monolayer and multilayer films. Hardware adaptations, which include the implementation of a copper reflector to increase spectral quality and enable measurement in transflection, are shown to increase spectral quality. Further, feature selection methods are used to identify important spectral ranges, optimizing the model's efficiency by reducing complexity and prediction time with minimal loss in accuracy. The resulting models demonstrate an 85% prediction accuracy on unseen specimens recorded in line with minimal prediction latency, showcasing the feasibility of inline applicability for sorting aggregates with minimal hardware adaptations to enable measurements in transflection.

1 Introduction

Waste management facilities for sorting Plastic Packaging Waste are faced with frequently changing inhomogeneous input material. One of these input fractions, which are currently mainly ejected during preliminary input treatments with ballistic separators or screens and then thermally recovered, are plastic film packaging. Plastic film packaging amounts to roughly 46% of the plastic packaging waste that is annually put into circulation in Austria (Van Eygen et al., 2018). Therefore, the settings of waste sorters/sorting units need to be adapted to allow for the separation and subsequent recycling of this fraction. Including these fractions in the circular economy of polymers, could be beneficial for reducing abiotic resource consumption and CO_2 emissions caused by the production of virgin polymers (Koinig et al., 2022b). One reason for the lack of recycled plastic packaging films is the complexity they present in Near Infrared (NIR) sorting (Chen et al., 2020). The characteristics which make them ideal for packaging goods, like thin thickness, low weight, and the possibility to combine different polymers to cover a vast array of packaging requirements leads to suboptimal performance during sorting operations (Tartakowski, 2010).

This work shows an approach to adapt an industrial scale NIR sorting rig employing transflection to optimize yield, and purity. For this, different reflective background surfaces were evaluated for their respective effect on spectral quality. The evaluated reflectors included copper, aluminum, and gold. These materials were chosen for their reflective properties in the relevant NIR wavelength range (Cui, 2011).

The proposed changes in the NIR sorting aggregate counteract this impediment and allow for the characterization and ejection of multilayer films. This enables the creation of monolayer and multilayer fractions. The clean monolayer fraction could then be used in mechanical recycling while the multilayer fraction can be used as feedstock for chemical recycling methods.

2 Methods and Materials

This section describes the used NIR sorting aggregate and its adaptation to allow for image acquisition in transflection. Further, the principle behind transflection and its effect on spectral quality is explained. Additionally, the used machine learning model to classify these enhanced spectra is described. Because the inline use of these models requires short inference latency, the method to reduce the number of input features to decrease inference latency is explained.

2.1 Film Packaging Specimen

The film specimen used in this trial were collected from the lightweight packaging waste (LWP) collection system in Austria, called the “Yellow Bag”. No prior washing or pretreatment of the specimen was performed. In total 633 films were used in these trials for model creation and subsequent testing for its prediction accuracy. The specimens’ materials included monolayer films made from polyethylene (PE), polypropylene (PP) and polyethylene terephthalate (PET). The multilayer specimen combined these polymers and in addition polyamide (PA) and compatibilizers and other barrier layers to ensure gas or vapor impermeability. The films were separated into a training set used in the creation of the classifier and a second, independent testing set for in line validation on the sensor-based sorting aggregate of the created model on unseen specimen. The specimen were conventional post-consumer packaging films. The material composition of the specimen was analyzed prior using Fourier-transform infrared spectroscopy (FTIR) measurements employing a Spectrum Two FTIR spectrometer (Perkin Elmer) with a Zn/Se crystal with diamond tip. The spectral range of the spectrometer is 650 cm^{-1} to 4,000 cm^{-1}.

2.2 Sensor-Based Sorting Aggregate

The sensor-based sorting (SBS) aggregate used in this study is a chute sorter. This aggregate allows access to the data stream created by the NIR smart camera. The NIR camera is an EVK G2 Hyperspectral Imaging camera, which allows for spectral acquisition in a spectral range from 900 nm to 1,700 nm in a resolution of 312 pixels over the working width of 50 cm and 220 spectral points over the stated spectral range. This camera is a line sensor working in brush-broom acquisition yielding between 450 and 500 lines per second. Figure 1 shows the SBS aggregate used in this work and a functional schematic of its working principle. Alongside the

NIR camera an additional camera working with visible light (VIS) is included in the experimental setup. This camera enables the sorting using colors.

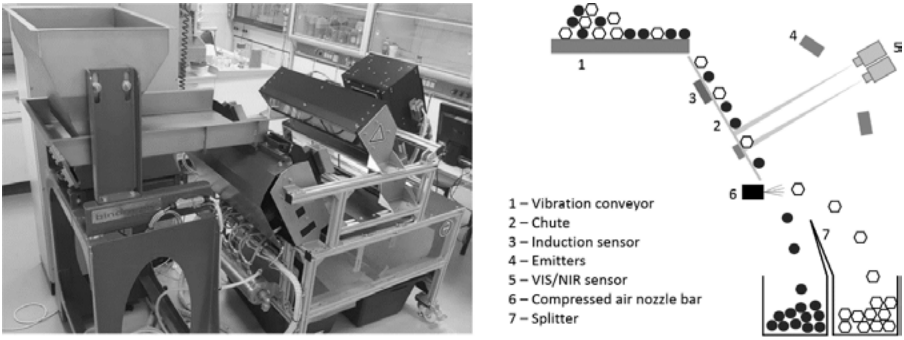

Fig. 1: Sensor based sorting aggregate used in this work and a functional schematic of its working principle

2.3 Recordings in Transflection

Preliminary research has shown that the spectral quality of film packaging is inadequate for classification in NIR when recorded in reflection. This issue may be solved by changing the measurement geometry to transflection (Chen et al., 2020; Koinig et al., 2022a). Therefore, a reflector, which allows for a second pass through of the radiation and minimizes the amount of radiation lost to transmission, has been implemented. The reflector is made of copper as this material evidently yields high reflectiveness in the NIR spectral range while exhibiting no spectral fingerprint of its own (Koinig et al., 2022a). Furthermore, copper is resilient to corrosion and relatively cheap when compared to other materials with better reflective characteristics like gold (Cui, 2011). To compare the increase in spectral quality, reference measurements have been conducted. This allowed for a comparison between the spectra yielded by reflection measurements and transflection measurements. As references glass, commonly used in chute sorters, and black polymers, commonly used for conveyor belts, were implemented. The increase in spectral quality is essential for further classification of the film specimen, as it allows for the characterization of multilayer films. Figure 2 shows the principle of transflection measurement of film packaging. It demonstrates that the reflector allows for a second pass through the specimen, increasing the interaction between the film specimen and the radiation Thereby, the amount of information yielded by the spectra is increased while simultaneously reducing the loss of intensity to transmission. The spectral acquisition in this work was performed using EVK Helios Optimizer Version 3.4.2017.1.

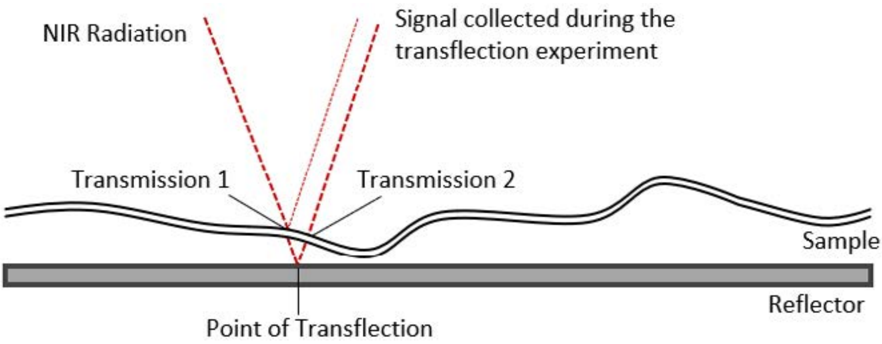

Fig. 2: Functional schematic showing the principle of transflection measurement

2.4 Machine Learning Classification

The increased spectral quality can further be used as the basis for creating machine learning models which are capable of distinguishing monolayer from multilayer films, irrespective of the actual material composition. This is to counteract the necessity for creating large spectral databases to cover the vast number of possible combinations of layer composition. All computations necessary for this work were performed in MATLAB, Version 9.13.0.2105380 (R2022b) Update 2 on a workstation equipped with moderate hardware. This workstation does not have a dedicated graphics card, so all computations were performed on the CPU. The CPU of this workstation is an Intel Core i5-4570 clocked at 3.20 GHz. No parallel computing was performed. These hardware limitations proved a great boon in the course of this work as they enabled to show the feasibility of inline application using the created model on limited hardware.

2.4.1 Feature Selection with MRMR and PCA

Prior to the creation of a classification model, principal component analysis (PCA) was applied to the recorded spectra to gauge the predictive value of the spectral data. This PCA was performed gauge when there was sufficient information present in the data to feasibly distinguish between monolayer and multilayer films. The PCA results were analyzed based on the resulting Pareto distribution of the explained variance in the data by the individual principal components (PCs).

After this initial assessment, further analysis of the resulting loading plots of the first three PCs were conducted. This was done to gauge the predictive value of individual spectral ranges for the classification task at hand.

To increase the fidelity in this feature ranking, feature selection for classification using the minimum redundancy maximum relevance (MRMR) algorithm was performed. The MRMR algorithm is a feature selection technique that identifies the most informative features by maximizing their relevance to the target variable while minimizing redundancy among selected features (Ding et Peng, 2005). Initially developed for genetics, it proved of high value when ranking spectral feature for the task at hand (Koinig et al., 2023). The results of these two feature selection methods were combined to determine the number of features necessary for classification and to subsequently reduce the inference latency for each classification to make inline use of the classification model feasible.

2.4.2 Creation of Machine Learning Classifier

Various classifiers were created and compared for their inference latency and prediction accuracy. Of these, a decision tree and a shallow neural network have been selected for further analysis regarding these metrics (Koinig et al., 2022c). After this comparison the shallow neural network has been selected for the appropriate classification model. The architecture of the neural network consisted of the fully connected layers with a layer size of 10. After parameter optimization, a rectified linear unit (ReLU) was chosen as fully connected layer activation function. The output layer activation function was by default performed with Softmax. To gauge the resulting accuracy with a reduced number of input parameters, the training and testing step has been repeated with each number of input parameters. The input layer size coincided with the number of input parameters chosen in the feature selection. The inference latency for each of these steps and the resulting accuracy on an unseen testing set has been recorded for further evaluation. A split of 80%

training data and 20% testing data was performed when creating these models following current standards shown to be good practice when creating a training and testing set and yielded good results in existing trials when performing classification on film packaging specimen (Nguyen et al., 2021; Koinig et al., 2023). To limit overfitting, a k-fold cross validation was performed with 5 folds. The training set consisted of 326 specimens. Table 1 shows the main polymer composition and number of training specimens.

Tab. 1. Main polymer composition and number of training specimen

Material	PE	PP	PET	PE-PP	PE-PP-PA	PP-PA	PP-PET	PE-PA	PE-PET
nObjects	14	9	3	73	3	6	17	92	109

2.5 Inline Classification with Trained Classifier

The inline testing of the prediction accuracy with the trained classifier was performed with live data acquired from the NIR sensor via the Gigecam Interface. The live data was pre-processed using a normalization with z-Score and a numerical differentiation using gradient and normalization functions integrated in MATLAB. The data was then further processed to eliminate background pixels using a thresholding method which classifies all pixels under a given intensity as background. The remaining pixels were then classified using the trained neural network. The spectra were recorded with the specimen in motion. This approach was chosen to mimic the condition that would be prevalent when sorting on an industrial scale. This allows to gauge the robustness of the model to changes in the spectral acquisition resulting from changing environmental condition which cannot be reproduced when statically sorting prerecorded spectral images.

3 Results

This chapter describes the results obtained during the experimental phase of this work. Details are given on the achieved improvements in spectral quality and the resulting classification accuracy and inference latency of the machine learning classifier with reduced input parameters after feature selection. Further, the ranking of the individual features is given resulting from the PCA and MRMR feature selection.

3.1 Improved Spectral Quality

Figure 3 shows the changes in spectral quality of a PE film specimen. The spectra of the recorded PE film in transflection specimen have increased fidelity in the relevant spectral regions at 1,100 nm and 1,300 nm. Here the characteristic peaks and troughs have increased resolution and the relative height to rest of the spectrum. Furthermore, the spectral variability has decreased. This is shown by the first standard deviation of the specimen´s spectra. In addition, sinusoidal interference that stem from the interaction of the NIR radiation wavelength and the material thickness (Jeszenszky et al., 2004) could be decreased. This substantial increase in spectral quality is the basis for the creation of a robust classification model. With the gain in information content, minute differences in the spectra become more pronounced and the spectra are less susceptible to noise.

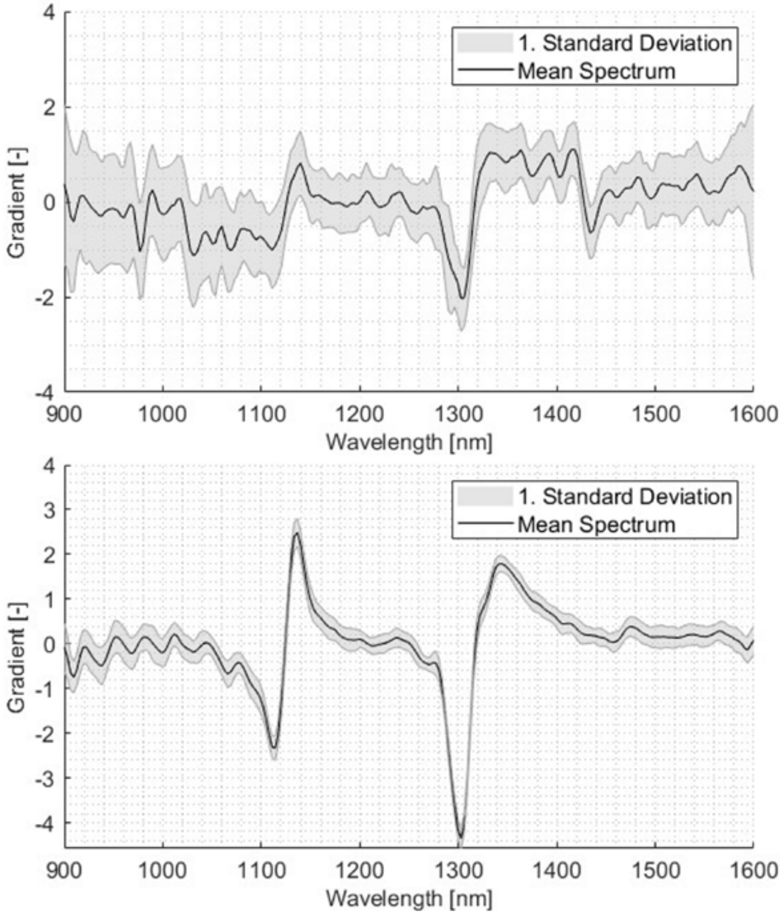

Fig. 3: Comparison of spectral quality of a PE film specimen when recorded in reflection (top) and transflection (bottom)

3.2 Definition of Spectral Features with Minimum Redundancy and Maximum Relevance with MRMR and PCA

Comparisons of monolayer and multilayer film spectra using PCA show a distinct difference in the spectra of these classes which can allow for classification using this increased level of abstraction. With the changed measuring setup, these overlaying spectral differences are revealed. The PCA conducted on the spectral data showed that approximately 70% of the variance in the data set can be explained by the first three PCs. Figure 4 shows the resulting PCA loading plots and the MRMR feature scores. The loading plots show high absolute weights for the spectral regions between 1,178 nm and 1,300 nm and further for the spectral region of 1,365 nm – 1,428 nm. These spectral regions represent the most abundant polyolefins in film packaging. Because through and peak heights correlate with the thickness of the material at hand, the heights of the throughs and peaks in this region is lower in multilayer films than in monolayer films. This results in the comparatively lower thickness of the polyolefins in a multilayer film. The MRMR score supports this finding and further yields high scores in higher spectral ranges. In addition to the important regions mentioned above, high feature scores were attributed to the spectral ranges at 1,490 nm, 1,552 nm, and 1,615 nm. These results show that the thickness differences in polymer films can be used to distinguish monolayer films from multilayer films. In addition, wavelengths in higher regions contain further information. This information may be independent from the material composition itself but caused by optical effects due to the transition of the NIR radiation from one layer to another layer with different optical densities and the presence of compatilizers to allow for the lamination of different polymer films. Regarding the model creation these results allow for a reduction of features in accordance with their ranked prediction values. This enabled the reduction of features to be evaluated for each classification which in turn reduced inference latency.

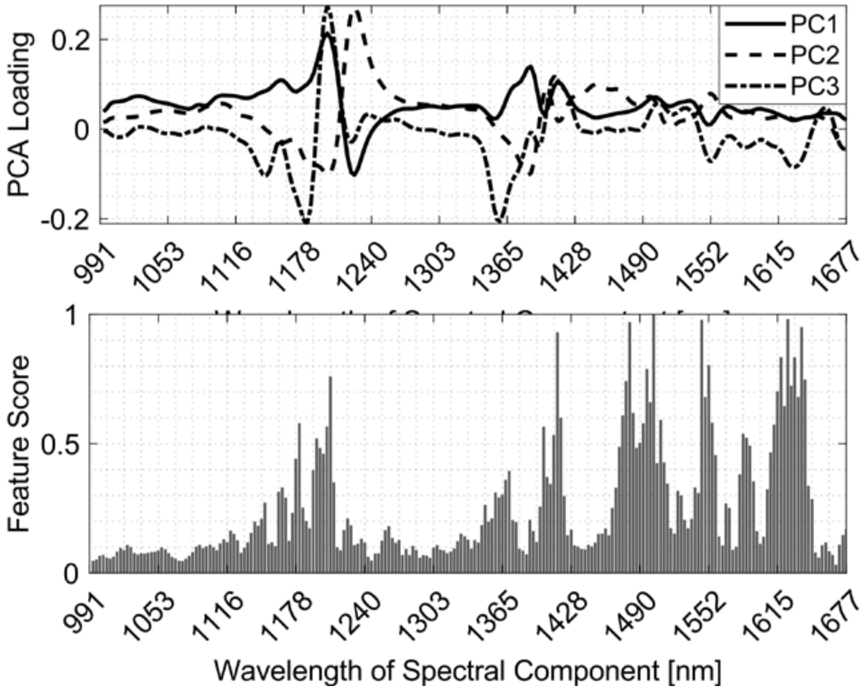

Fig. 4: Results of spectral ranking using PCA loading plots and the MRMR algorithm and the thus calculated feature scores

3.3 Reduction in inference latency

According to the ranking of features, the classifier has been trained repeatedly with an increased number of features. The resulting inference time of a test set consisting of 3,000 spectra and the resulting prediction accuracy have been recorded. Figure 5 shows the resulting inference latency and prediction accuracy of the neural network classifier. The prediction accuracy rises strongly with the increasing number of predictors. The cutoff point was derived from the gradient of the accuracy. The point at which the gain in prediction accuracy was minimal in comparison to the incurred time cost was calculated. This method yielded an optimal number of predictors of 83, which was then used to train the classification model for later inline trials. The resulting prediction accuracy of the training data could be maximized while the prediction latency could be reduced by about two thirds enabling the model to be deployed inline at the NIR sorting aggregate.

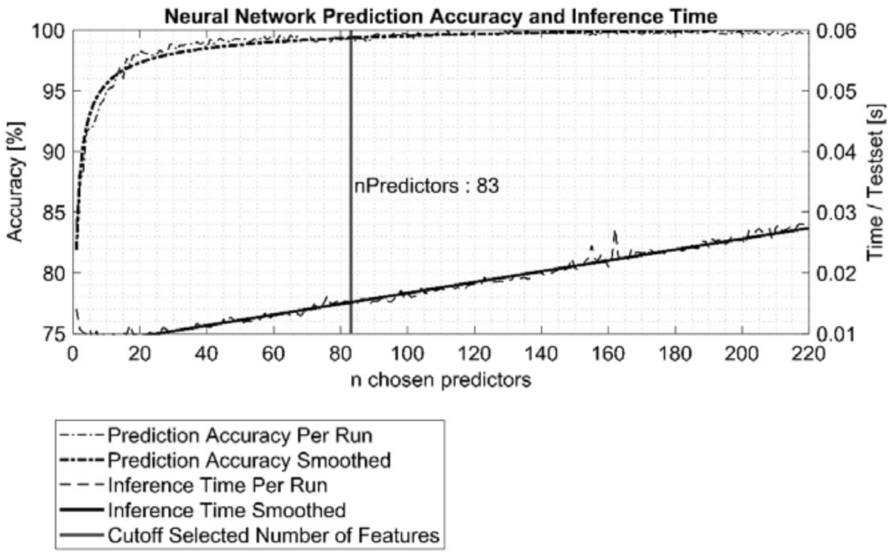

Fig. 5: Resulting inference latency and prediction accuracy of the neural network classifier with increasing number of predictors and derived cutoff point at optimal value according to the gradient of the prediction accuracy

3.4 Inline Prediction Accuracy of Trained Classifier

The inline classification trials showed that the model copes rather well with new data acquired from the sensor. This is shown by the confusion plot in Figure 6. With a prediction accuracy of 85% of all classified spectra the model performed reasonably well. One issue was the high misclassification rate of multilayer as monolayer. To clarify this, the classification results have been analyzed for each material class. The film specimens were grouped according to their main polymer composition and the achieved prediction accuracy was then calculated anew. This showed that only 22% of PEPP films were classified correctly. The second class which caused problems was the PPPA fraction, which was correctly classified in 33% of all specimens. These materials reduced the overall prediction accuracy and need to be further examined to increase the prediction of the 2D fraction.

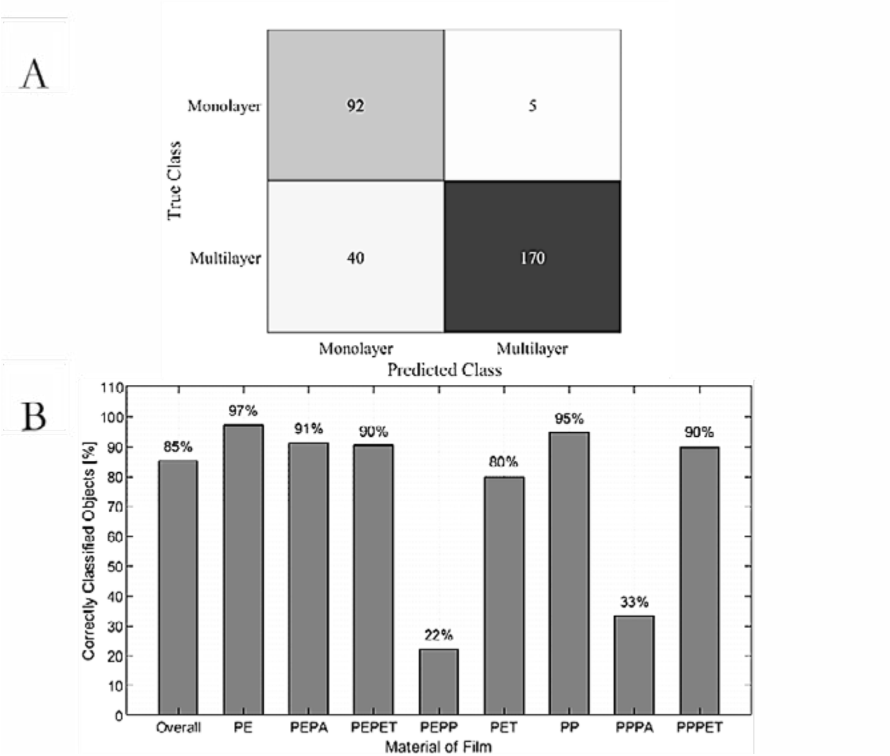

Fig. 6: Confusion Matrix showing the classification errors of the model for the two classes monolayer and multilayer and a bar chart showing the results in regard to the main composition of the film specimen

4 Discussion

This chapter aims at further discussing relevant issues that arose during the presented work. These issues include the application of transflection measurements on a belt sorter and the low prediction accuracy of PEPP and PPPA films.

4.1 Application of Transflectance on Belt Sorters

As the implementation of a reflector for transflectance measurements on a chute sorter is comparatively easy and has been shown to increase spectral quality, this approach should further be applied to belt sorters, as these sorters are far more common in the field of waste management. To answer this question, multiple solutions have been proposed/assessed during this work. One would entail the implementation of a copper reflector band over the belt. This would be a simple implementation but greatly depends on the circumstances and type of the belt sorter in question. A more commonly applicable solution could be the usage of belts, which are inherently reflective in the NIR spectrum. This could include belts made from metals as which could enable transflection measurement. Another solution would be conventional polymer bands made from materials that allow for some reflectivity of the NIR radiation. One example are non-carbon black colored conveyor belts as these allow for some reflection. These questions have not yet been answered but are subject to current research.

4.2 Low Prediction Accuracy of PEPP and PPPA films

PEPP films are an example of a challenging multilayer composition. These polymers are easily distinguishable in spectral images of 3D materials (Wu et al., 2020). However, the low spectral quality of film specimen in comparison to 3D materials obscures the differences between these materials especially when one of the two components is present in low thickness. However, the implementation of a second sorting model, which is primarily trained to classify PEPP films from a monolayer fraction has shown promise to increase the classification rate of PEPP films. PA leads to complications in the extrusion phase due to its incompatibility and comparatively high melting point, necessitating compatibilizers to achieve useable mechanical properties (Czarnecka-Komorowska et al., 2021). Excluding this fraction with NIR is difficult however due to the low thickness of PA layers in multilayer films. As the expression of characteristic peaks is correlated with the materials thickness, the minor component is near invisible in the NIR spectrum (Masoumi et al., 2012). This issue could be resolved by implementing Fast Fourier Transformation spectral enhancement. By evaluating the Fourier Components of the spectrum, the Fourier components contributing noise can be eliminated and the spectrum can be reconstructed from the relevant Fourier components only (Koinig et al., 2022c). At the moment this process is rather cumbersome and involves high levels of human input to determine the relevant Fourier components for reconstruction. Thus, automation is necessary prior to inline application.

5 Conclusion

The results of this work showed that the spectral quality of film packaging can be increased with minimal adaptation of existing hardware on chute sorters and that existing methods of feature selection and machine learning are capable of sorting monolayer from multilayer films with comparatively low computing power. This work further opened two research questions regarding the implementation of transflection measurements on belt sorters and the issues regarding the classification of PPPA films. The presented work showed the possibility of including the film fraction in the recycling loop. This would enable the use of a fraction which is hitherto primarily thermally recovered. The inclusion of film packaging as an input fraction for mechanical and chemical recycling would increase the recycling rate of LWP waste, improve the circular economy of polymers and create a feedstock for chemical recycling processes that are currently under development.

References

Chen, X., Kroell, N., Feil, A., & Pretz, T. (2020). Determination of the composition of multilayer plastic packaging with NIR spec-troscopy. In Detritus (Issue 13, pp. 62–66). Eurowaste SRL. https://doi.org/10.31025/2611-4135/2020.14027

Cui, Y.X., 2011. Study and Development of near-Infrared Reflective and Absorptive Materials for Energy Saving Application. Carlton University, Ottawa, Ontario. ISBN: 978-0-494-87749-4. Doctoral thesis.

Czarnecka-Komorowska, D., Nowak-Grzebyta, J., Gawdzińska, K., Mysiukiewicz, O., & Tomasik, M. (2021). Polyethylene/Polyamide Blends Made of Waste with Compatibilizer: Processing, Morphology, Rheological and Thermo-Mechanical Behavior. In Polymers (Vol. 13, Issue 14, p. 2385). MDPI AG. https://doi.org/10.3390/polym13142385

Ding, C., & Peng, H. (2005). Minimum redundancy feature selection from microarray gene expression data. In Journal of Bioinformatics and Computational Biology (Vol. 03, Issue 02, pp. 185–205). World Scientific Pub Co Pte Lt. https://doi.org/10.1142/s0219720005001004

Jeszenszky, É., Kocsányi, L., & Richter, P. (2004). Eliminating the Interference Pattern in Near-Infrared Spectra Used for Identi-fication of Thin Plastic Foils. In Applied Spectroscopy (Vol. 58, Issue 6, pp. 693–697). SAGE Publications. https://doi.org/10.1366/000370204872953

Koinig, G., Friedrich, K., Rutrecht, B., Oreski, G., Barretta, C., & Vollprecht, D. (2022a). Influence of reflective materials, emitter intensity and foil thickness on the variability of near-infrared spectra of 2D plastic packaging materials. In Waste Management (Vol. 144, pp. 543–551). Elsevier BV. https://doi.org/10.1016/j.wasman.2021.12.019

Koinig, G., Grath, E., Barretta, C., Friedrich, K., Vollprecht, D., & Oreski, G. (2022b). Lifecycle Assessment for Recycling Processes of Monolayer and Multilayer Films: A Comparison. In Polymers (Vol. 14, Issue 17, p. 3620). MDPI AG. https://doi.org/10.3390/polym14173620

Koinig, G., Kuhn, N., Barretta, C., Friedrich, K., & Vollprecht, D. (2022c). Evaluation of Improvements in the Separation of Monolayer and Multilayer Films via Measurements in Transflection and Application of Machine Learning Approaches. In Polymers (Vol. 14, Issue 19, p. 3926). MDPI AG. https://doi.org/10.3390/polym14193926

Koinig, G., Kuhn, N., Fink, T., Grath, E., & Tischberger-Aldrian, A. (2023). Inline classification of polymer films using Machine learning methods. In Waste Management (Vol. 174, pp. 290–299). Elsevier BV. https://doi.org/10.1016/j.wasman.2023.11.028

Masoumi, H., Safavi, S. M., & Khani, Z. (2012). Identification And Classification Of Plastic Resins Using Near Infrared Reflectance Spectroscopy. Zenodo. https://doi.org/10.5281/ZENODO.1076916

Narukawa, Y., Pasi, G., & Viviani, M. (2004). Modeling Decisions for Artificial Intelligence. Lecture Notes in Computer Science. Available online at: https://link.springer.com/content/pdf/bfm:978-3-540-27774-3/1 (accessed 10 Mai 2023)

Nguyen, Q. H., Ly, H.-B., Ho, L. S., Al-Ansari, N., Van Le, H., Tran, V. Q., … Pham, B. T. (2021). Influence of data splitting on performance of machine learning models in prediction of shear strength of soil. Mathematical Problems in Engineering, 2021, 1–15. doi:10.1155/2021/4832864

Tartakowski, Z. (2010). Recycling of packaging multilayer films: New materials for technical products. In Resources, Conservation and Recycling (Vol. 55, Issue 2, pp. 167–170). Elsevier BV. https://doi.org/10.1016/j.resconrec.2010.09.004

Van Eygen, E., Laner, D., & Fellner, J. (2018). Circular economy of plastic packaging: Current practice and perspectives in Austria. Waste Management (New York, N.Y.), 72, 55–64. doi:10.1016/j.wasman.2017.11.040

Wu, X., Li, J., Yao, L., & Xu, Z. (2020). Auto-sorting commonly recovered plastics from waste household appliances and electronics using near-infrared spectroscopy. In Journal of Cleaner Production (Vol. 246, p. 118732). Elsevier BV. https://doi.org/10.1016/j.jclepro.2019.118732

Classification of black plastic using active thermography

Kevin Schmitz[1*], Nina Shpakova[1], Andreas Keller[1], Udo Netzelmann[1]

1 Fraunhofer Institute for Nondestructive Testing IZFP, Saarbrücken, Germany

* Corresponding Author: Campus E3.1, 66123 Saarbrücken, E-Mail: kevin.schmitz@izfp.fraunhofer.de

Keywords: machine learning, recycling, sorting black plastic, thermography, waste management

Abstract

Sustainability is undoubtedly one of the most important goals in modern society and has a major impact on economic and political decisions. One of the strategies towards sustainability is the European Green Deal. A key policy initiative that determines the regulatory landscape supporting the European Green Deal is the Circular Economy Action Plan (CEAP) (EC, 2020), whose objective is to reduce the EU's consumption footprint and double its circular material use rate in the coming decade, while boosting economic growth. Specific actions were launched in several areas, including electronics and ICT[1], packaging, plastics and textiles. An important segment of a circular economy, especially in waste management, is the sorting and recycling of materials. To raise levels of high-quality recycling, improvements are needed in waste collection and sorting.

The sensor systems currently available on the market for sorting plastics in waste management largely rely on near-infrared (NIR) and short-wave infrared (SWIR). However, the sorting of black plastics, including those manufactured in the automotive field, remains problematic with these systems. The task of sorting these black plastics from the shredder light fraction poses a demanding challenge to sorters.

1 Information and communications technology

As part of the Fraunhofer lighthouse project »Waste 4 Future« (W4F), which deals with the holistic improvement of plastic recycling, an active thermography system for distinguishing different plastic materials was developed. In this context, three black materials from the shredder light fraction were investigated on a running conveyor belt. The sample set consisted of ten defined samples each of the material polypropylene glass fiber (PP-GF) as well as two polyamide glass fiber materials, namely PA6-GF and PA66-GF. The samples were heated up by using an infrared heater. An infrared camera mounted at a fixed distance above the conveyor belt was able to record the cooling curve of the samples over time. Due to their different heat conduction properties, different materials should have different heating, as well as cooling characteristics. By analyzing the cooling curves, it was possible to identify characteristic patterns in different materials. Feature extraction enabled the quantification of the observations, which were then processed by machine learning algorithms. Using three samples per material as validation data, a pixel-wise f1-score above 97% was achieved. When using majority decision per sample, every sample could be classified without any misclassifications.

The knowledge gained from active thermography opens up promising perspectives for integration with the current state-of-the-art sensor technologies. Thermography systems can contribute to the further development of sorting systems and play a crucial role in improving the recycling process, especially with regard to black plastics. This approach can contribute to enabling more precise sorting and thereby more efficient recycling of plastics.

1 Introduction

Global warming and the increasing depletion of resources are major challenges society is facing today and in the future. In this context, the pursuit of sustainability has become an undeniable priority and acts as a central goal for responsible development. Both political and economic decisions are significantly influenced by the efforts to achieve these goals. To accelerate the transformation of the European Union towards climate neutrality and resource efficiency, the “European Green Deal” was launched at the beginning of 2020. One important initiative of this sustainability strategy is the Circular Economy Action Plan (CEAP) (EC, 2020). The CEAP focuses on reducing the environmental footprint within the EU and proposes various measures in different areas. A central aspect of this plan is the sustainable circular economy, which aims to minimize the consumption of resources and extend the life cycle of products. The recycling of materials in particular plays a key role in this, which means that the recycling process is not only seen as a waste management strategy, but also as an essential part of realizing the goals of the CEAP. In this context, CEAP aims to double the use of recycled materials over the next ten years. This ambitious measure is intended to intensify the use of recycled raw materials in production and thus make a significant contribution to conserving resources and reducing emissions. Doubling the use of recycled material emphasizes the ongoing shift towards a sustainable economy and highlights the need to strengthen the recycling process as a central element in the circular economy.

Sorting is undoubtedly a crucial segment of an effective recycling process. The precise and clean separation of recyclable materials plays a key role in the process of increasing their usage. Accurate sorting not only enables more efficient reuse of materials, but also contributes significantly to improving the quality of recycled products. By ensuring separation by type, impurities can be minimized, which ultimately leads to higher quality and more versatile recycled materials. This focus on precision in sorting is therefore key to making the circular economy effective and sustainable.

The sorting of plastics has seen significant technological advances in recent years (Gundupalli et al., 2017). The focus here is on near-infrared (NIR) and short-wave infrared (SWIR) based techniques (Chen et al., 2020; Sensors Unlimited). These technologies enable fast and precise identification of plastic types by analyzing the absorption in the respective wavelengths. However, the sorting of black plastics remains particularly challenging, as they are more difficult to recognize in the near-infrared range (Masoumi et al., 2012; Rozenstein et al., 2017). Fundamental research regarding the usage of terahertz waves to separate multiple black plastics is currently being conducted and could prove beneficial in the future (Brandt et al., 2016). Lastly, tracer-based sorting (TBS) is already employed by some plastics manufacturers (Polysecure GmbH), wherein plastic additives or fluorescent markers are added to a compound, resulting in a separation by type and area of application of the plastic (e.g. food packaging) (Olscher et al., 2022). Despite all the progress, challenges remain, particularly due to different additives (Jehanno et al., 2022), multilayer packaging (Schmidt et al., 2022) and the ever-increasing amount of plastics that are being used (Stegmann et al., 2022). The development of technologies that address these challenges is crucial to increasing recycling efficiency and ensuring the sustainable utilization of plastic waste.

There exists a wide variety of analytical methods to characterize and classify polymers, e.g. thermogravimetric analysis (TGA) or differential scanning calorimetry (DSC) (Menczel & Prime, 2009). However, the use of infrared thermography to classify polymers is an underdeveloped field of research, but with possibly promising results (Aujeszky et al., 2017).

In the Fraunhofer lighthouse project »Waste 4 Future« (W4F) seven Fraunhofer institutes are working together to achieve a holistic improvement in the recycling process. The efficient utilization of carbon contained in plastics should result in high-quality output materials. Using an evaluation model and innovative sorting technology, the project aims to efficiently recycle plastics in a circular economy and reduce thermal utilization. Economic aspects and regulatory requirements are also taken into account in order to develop a sustainable business model. One part of the innovative sorting technology is a new approach using active thermography, which is explained in more detail below and the insights gained are described.

2 Active thermography

Other than in NIR spectroscopy around room temperature, infrared thermography in the thermal infrared range (about 2 to 15 µm wavelength) relies on the thermal emission of infrared radiation according to Planck's law. Besides the temperature of the object, its emissivity is a decisive factor. The reflectivity plays a minor role, in contrast to NIR spectroscopy. Polymers appearing black in the visible absorb visible and NIR light very well and convert the light energy efficiently into heat and then into thermal radiation. Active thermography uses short-time intentional heating of the sample beyond its initial temperature, e. g. by a strong optical light source. Sample surface heating increases the infrared emission and leads to a heat flow from the surface into the depth of the object. The resulting increase in transient surface temperature is influenced by its thermal conductivity, its density, and its specific heat capacity. In addition, most polymers are usually semi-transparent in the thermal infrared. Their thermal radiation comes both from the surface and from the volume. A short time after optical heating, the radiation from the surface-near region is dominant and more dependent on the spectral properties in the thermal infrared than at later times (Jones Roger W. & McClelland John F., 1989), it is therefore useful to record the time dependence of the infrared radiation.

By combining the effects of thermal diffusion, optical absorption, and emission of thermal radiation, a differentiation between different polymer materials should be possible. In order to accurately capture the effects described, the infrared sensor FLIR A35 was chosen. The operational characteristics of this camera, including the spectral range, were deemed sufficient to effectively fulfil the requirements. An overview of the technical specifications of the FLIR A35 camera can be found in Table 1.

Tab. 1: Thermal camera specifications

Camera type	Focal Plane Array, uncooled VOX-microbolometer
Framerate	60 fps
Resolution	320 x 256 px
Spectral	7.5-13 µm
Distance camera-sample	62 cm
Thermal sensitivity NEDT	50 mK
Field of View	48 ° x 39 °

3 Design of Experiment

The implementation of a proper design of the experiment is crucial in researching new measurement techniques. A proper and well-thought experimental design ensures that the objective of the experiment is achieved with high accuracy and efficiency. Measuring quantities is always an integral collection of data across many factors. Therefore, it is important to systematically control the variables, minimize the biases, and enhance the statistical validity of the measurement. A disciplined approach increases the reproducibility of results and ensures an identification of causal relationships, instead of correlations.

To ensure a stable measurement setup, the configuration was carefully planned and mechanically secured, preventing any alterations in distances throughout the project. A conveyor belt is moving the samples at a constant speed. This is a critical aspect, enabling the construction of a cooling curve for each pixel from a sequence of frames. The samples are transported to an infrared heater, actively introducing heat. Subsequently, the samples are transported further and enter the recording range of the infrared camera. By maintaining a fixed position and belt speed, uniform cooling times for the samples across all measurements are ensured. This standardized approach enhances the reliability and precision of the experimental outcomes. A schematic of the measurement setup is shown in the figure Fig. 1.

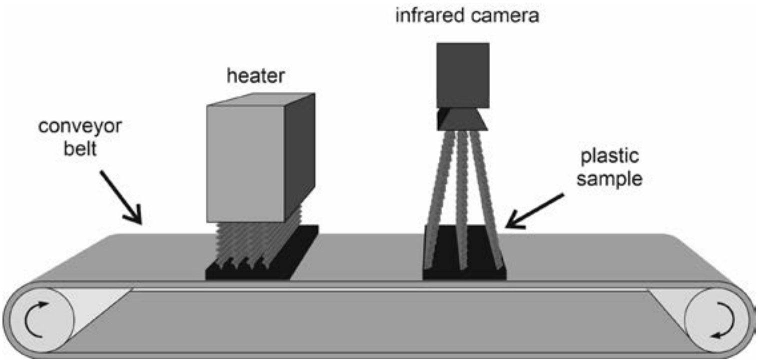

Fig. 1: Measurement setup schematic

With the setup being defined, it is essential to identify the most dominant influences that affect the whole measurement procedure. Once the influences relevant to this measurement have been identified, they must be classified. A list of influences including their categorization is shown in Fig. 2. Influencing factors are displayed in three different categories. The “star” marks the relevant information that is categorized as a measurement effect, which is the aim of the measurement. The wrench symbolizes influences that are marked as parameters, which means that they can be actively controlled by the measurement setup. The “warning sign” influences are non-predictable, not measurable or changing influences, and in real world applications especially not controllable, which can affect the measurement. In real-world applications, factors such as the sample geometry, ambient temperatures, and containments play significant roles but cannot be controlled by the sorting facilities. When analyzing the data, it can always happen that unknown influences exist, that may exhibit correlation over time. Factors like the self-heating of sensors or alterations in boundary conditions can influence the data over time. Additionally, the inherent inaccuracies in sensors contribute to what is commonly known as sensor scattering.

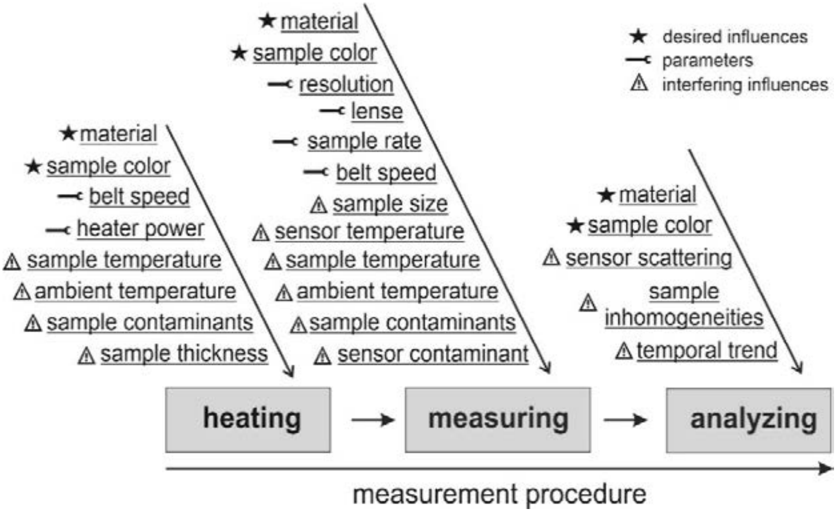

Fig. 2: Categorized major influences that affect the measurement

In the initial phase, it is crucial to optimize the parameters and set them to their best possible values, so that subsequent adjustments are no longer necessary. This initial optimization step effectively mitigates some of the influences. All interfering influences are kept constant, to attempt to maintain consistency along all the measurements. The first series of measurements therefore is made on clean samples with fixed dimensions, as well as controlled sensor-, sample- and ambient temperature.

The selection of samples must be chosen wisely to ensure a comprehensive representation of the desired influences (illustrated as “star” factors). This is essential to account for inhomogeneities and sensor scattering. These factors are difficult to control by other means and must therefore be included in the training process. The three polymers examined in this work are black due to the addition of carbon black to the batch and filled with 30 % glass fiber. The samples consist of a polyamide 66 (PA66-GF) (TECHNYL A216 V30 BLACK 21N by DOMO Chemicals, Leuna, Germany), a polyamide 6 (PA6-GF) (DOMAMID 6G30 BK, also by DOMO Chemicals) and a polypropylene (PP-GF) (Scolefin 53 G13-9 by Ravago Group, Arendonk, Belgium). All polymers were injection molded in the facility of Fraunhofer Institute for Structural Durability and System Reliability LBF. The geometrical shape is composed of a square with a side length 80 mm and a thickness of 3 mm and a triangle with the longest side of 90 mm. The triangular part is only used for numbering and touching the samples, whilst the square part is the actual analyzed area. This prevents measurement errors introduced by heat transfer through contact with the hand or by measuring the numbering of a sample instead of their cooling curve. An example of a sample can be seen in Fig. 3

Fig. 3: PA6-GF sample no.874

To ensure a minimum in variance between the samples, the injection molding process was kept running for a while before ten samples of a given material were produced in series. The thermal conductivity λ of the three analyzed polymers are shown in Table 2, taken from the matweb website (matweb).

Tab. 2: Thermal conductivity of the three analyzed polymers

Material	Thermal conductivity λ[W/mK]
PA66-GF	0.24-0.25
PA6-GF	0.25
PP-GF	0.27-0.331

Finally, in order to suppress the possible influence of temporal dependencies, a randomized sample sequence is selected. This approach eliminates dependencies in the data and contributes to a more robust and unbiased analysis.

4 Data analysis

Data analysis plays a central role in the measurement process, as it establishes a correlation between the measured data and the material properties. An essential process is preprocessing, which aims to amplify the desired effect while minimizing interfering influences. After pre-processing, the actual analysis is carried out using various machine learning (ML) techniques to identify patterns and correlate the data to its respective material.

4.1 Feature extraction

The conveyor belt is moving the samples at a consistent speed, and the camera takes frames with a constant frame rate that enables a precise calculation of the pixel shift, i.e. the distance traversed by the samples between the consecutive camera frames. As parts of the sample move out of the camera view, cooling curves are constructed for each pixel along the sample line by line, using a corresponding stack of the previously taken camera frames. The number of camera frames taken for each piece of the sample, i.e. the cooling curve resolution, depends on the conveyor belt speed and the camera frame rate. Greater resolution improves result precision, yet, finding a tradeoff is necessary for maximizing both the performance and the quality of the result. Since in most cases, the pixel shift is a non-integer number, linear interpolation was utilized while creating the cooling curves to enhance the accuracy of the results.

A polynomial fitting technique was employed to approximate the logarithmic temporal evolution of pixels, enabling the synthesis of data based on the resulting coefficients, as suggested by Shepard et al. (Shepard et al., 2001). The synthetic data, as shown in Fig. 4, reproduces the authentic thermal characteristics of the signal, effectively mitigating high-frequency noise components. Signal processing, e.g. the Fast Fourier Transform (FFT), performed on the synthetic data does not introduce additional noise, thus enhancing the efficiency of further data analysis. Another advantage is the reconstruction of the complete temporal evolution of a pixel using only the derived coefficients. This reduces storage demands and makes the overall computational process more efficient, therefore playing an important role for time critical on-the-fly sorting of plastics. In addition, the use of synthetic data allows us to mitigate some other artifacts, such as camera reflections, observed in a circular region directly beneath the camera. The uncooled camera heats up during use, reaching temperatures of about 40 °C. This heat (infrared radiation) is then reflected on the surface of a sample and, depending on the incident angle, sent back into the lens of the camera. These artifacts are prominent as an erroneous elevation roughly in the middle of the cooling curve, i.e. in the region where the samples are halfway along the camera view, as illustrated in Fig. 4.

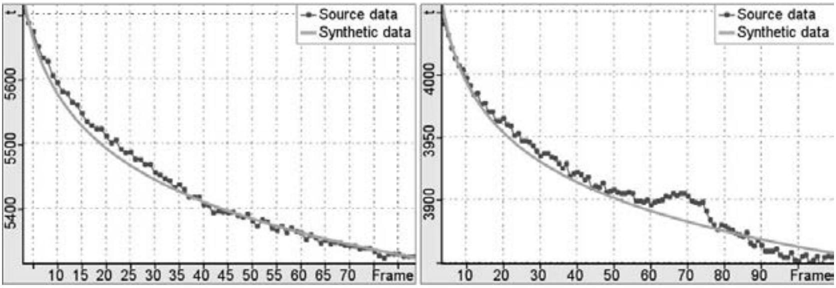

Fig. 4: Cooling curve source data and synthetic data; left: without artifacts, right: camera reflection artifact at frames ~60-75; a subset of the total of 136 frames

The FFT was applied to the cooling curves, as suggested by Maldague & Marinetti (Maldague & Marinetti, 1996) and widely adopted in related studies. The phase shift and amplitude information extracted via FFT helps to distinguish materials based on their thermal response (as shown in Fig. 5 and Fig. 6), avoiding the complexity of directly examining and comparing the cooling curves.

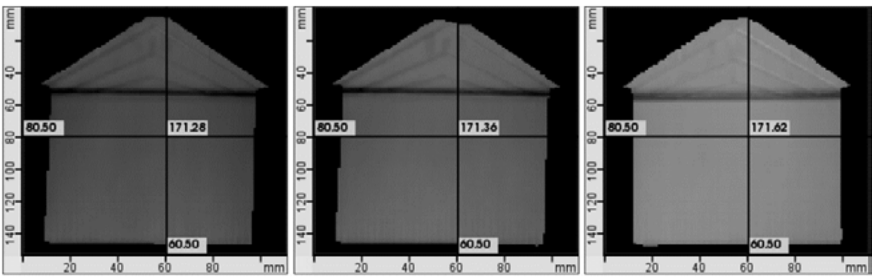

Fig. 5: FFT phase images (first frequency bin after DC) for PA66-GF, PA6-GF and PP-GF samples

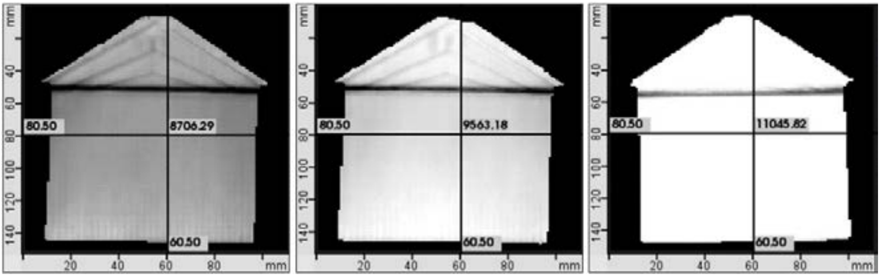

Fig. 6: FFT amplitude images (first frequency bin after DC) for PA66-GF, PA6-GF, and PP-GF samples

Different features and parameters were evaluated, considering their influence on the machine learning model's effectiveness. A comparison of FFT results obtained using source and synthetic data proves the effectiveness of the chosen approach. Through a series of extensive tests involving polynomials and derivatives of different orders, their outcomes were systematically compared, identifying the most effective parameters for further analysis. In addition to FFT-related features, it has proved useful to calculate the relative temperature drops by putting different target frames in relation to the initial frame, where an example for different materials is shown in Fig. 7. The following features were identified as the most significant and were selected as the input for the machine learning model:

- FFT amplitude (first 10 frequency bins after DC)
- FFT phase (first 10 frequency bins after DC)
- relative temperature drop for target frames 10, 20, 50, 80 and 90
- two polynomial coefficients (first-order polynomial in the logarithmic domain)

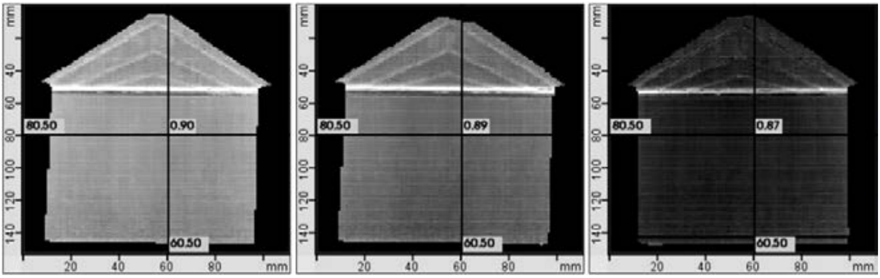

Fig. 7: Relative temperature drop for PA66-GF, PA6-GF and PP-GF samples, target frame 80

Data inspection

The analysis of the data initially begins with a univariate perspective. In this particular case, where the potential influences are largely suppressed, a univariate approach already can be effective in solving the classification problem. By looking at individual variables in isolation, this method enables a comprehensive understanding of the contribution of each factor and provides valuable initial insights. With these insights, a foundation is established for more complex analyses and a deeper understanding of the underlying patterns. Fig. 8 shows the value of one feature (first amplitude of the FFT) for each material. This approach would already allow a partial classification. However, in order to obtain a more accurate and stable prediction, all available features should be taken into account.

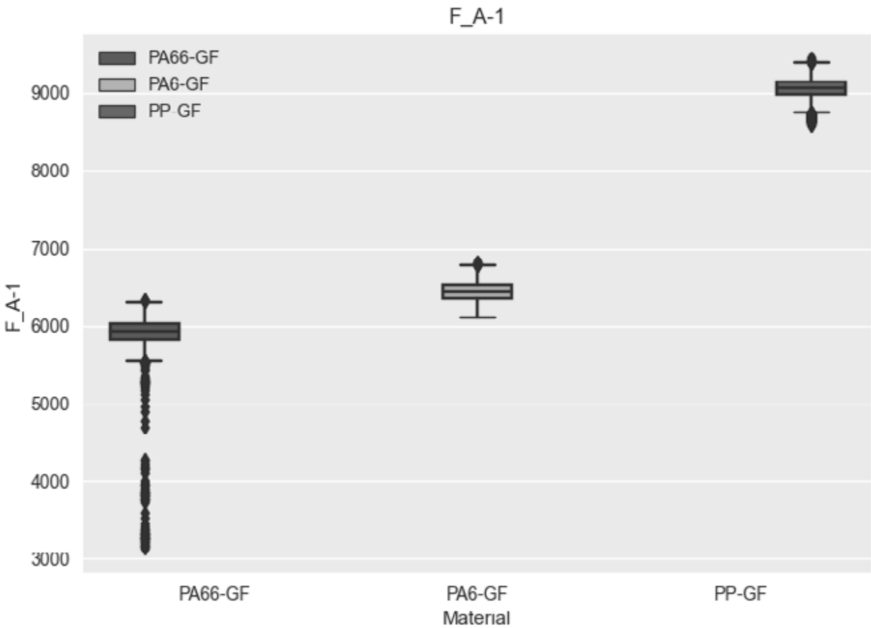

Fig. 8: First amplitude feature A-1 extracted from all samples

To inspect the multidimensional space of the dataset, different machine learning methods are applied using Python (version 3.8.10) and the Scikit-learn library (version 1.2.2) (Pedregosa et al., 2011). A multivariate technique that can be used is the Principal Component Analysis (PCA) (Jolliffe, 1986). PCA is generally used for dimensionality reduction. However, by analyzing the newly generated components, this algorithm can be applied to identify the most influential factors in the data set. This capability enables the identification of previously unseen or unknown influencing factors when designing the experiment. As the PCA is unsupervised, it is not trained to differentiate between classes. However, observing the differentiation of different classes in the newly generated principal components demonstrates the ability of this measurement setup to achieve material separation. Fig. 9 illustrates the first and second principal components, visually distinguishing the classes with different shapes. In the figure shown, only every 60th point is displayed for visibility reasons. Except for outliers in the top right, the difference between PP-GF and both PA-GF's is the highest influence in the dataset.

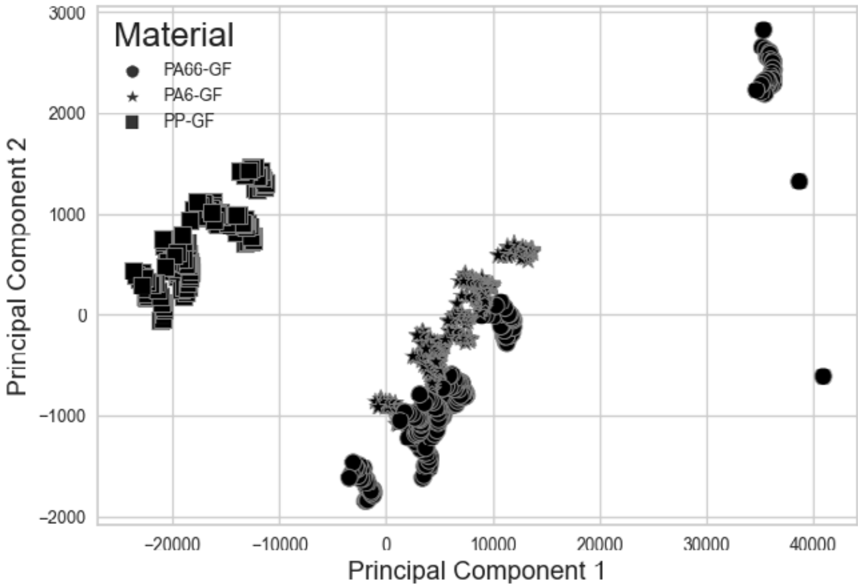

Fig. 9: Dataset plotted over two principal components (every 60th point for visibility)

4.2 Classification model

To create a machine learning model capable of distinguishing between three black plastic materials, the dataset is divided into training and validation sets. The validation set includes three complete samples that have been selected manually for each material. A pipeline is created containing a standard scaler followed by a linear discriminant analysis (LDA) (Fisher, 1936), which is a supervised method of multivariate statistics. During the training phase, the model is taught with the training dataset. Using the validation data, a transformation of the higher dimensional dataset is projected onto two new axes, called canonical variables (Fig. 10). In comparison to the unsupervised method (PCA) before, this projection with a supervised method improves the separation of the different materials. In this illustration, the classes are represented by different symbols. The distinction between PP-GF and the two PA materials is very clearly recognizable. Even PA6-GF and PA66-GF are mostly separable but have a slight overlap.

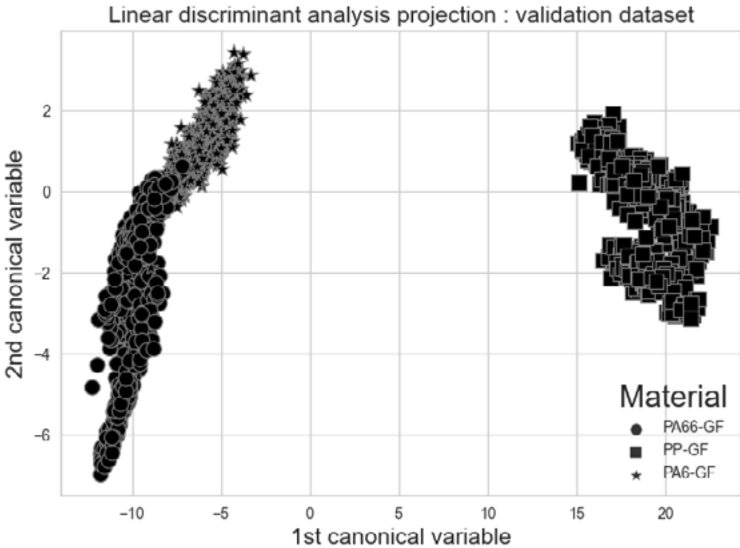

Fig. 10: Projection of the validation dataset in two new canonical variables

To measure the accuracy of the predicted results, a commonly used score is the f1-score. The f1-score combines precision and recall, its calculation is described in Fig. 11 (Fawcett, 2006).

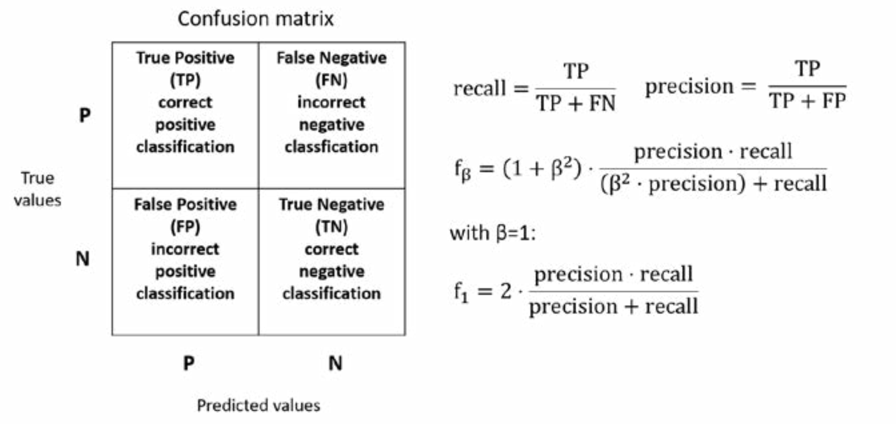

Fig. 11: Calculation of the f1-score

As shown in Fig. 12, an averaged f1-score of 0.985 could be achieved. Challenges in the prediction accuracy can be observed only between the materials PA6-GF and PA66-GF, which have very similar physical and chemical properties. However, the discrimination between PA6-GF/PA66-GF and PP-GF can be performed with perfect precision, achieving 100% accuracy.

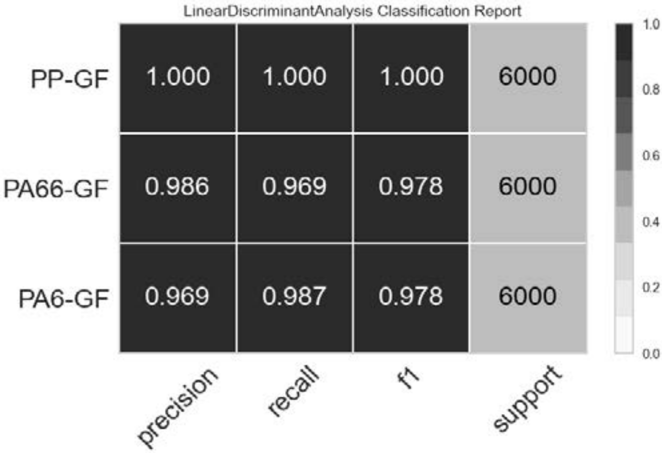

Fig. 12: Classification report of the validation dataset

Since pixel-wise sorting is infeasible, a strategic approach is to make a majority decision for each sample. Fig. 13 shows the confusion matrices in which the pixel-wise predictions (left) and the results obtained from majority decision per sample (right) are compared. The use of the majority decision method has led to an accurate classification of each sample.

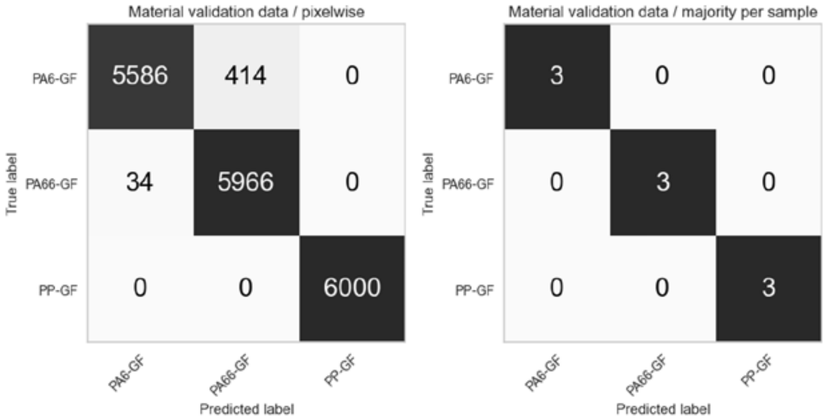

Fig. 13: Confusion matrices; left: pixel-wise, right: majority per sample

5 Conclusion and outlook

In this paper, an attempt has been made to classify black plastic materials (PA6-GF, PA66-GF, PP-GF) using active thermography. A setup has been developed that enables stable and defined measurements. All influencing factors were identified and classified, with the goal of reducing unknown and unwanted influences. Through iteratively improved pre-processing techniques, a machine learning model was created that demonstrated the capability to correctly classify all validation samples. In doing so, it has been shown that the current state of the art in sorting plastics can be improved through the application of this technology.

The next steps involve using this laboratory setup and the knowledge gained to add more and more of the real-world influencing factors, which were previously excluded (most importantly: different ambient temperatures, and different sample geometries). A calibration and temperature correction for the acquired signals can be trained and performed, increasing the stability of the data. In addition, the camera can be substituted to allow an increase of the belt speed through a higher frame rate. A camera with a higher resolution can also improve the quality and precision of the analysis, which is important for smaller sample sizes in the future. Another challenge is to reduce the self-reflection effects of the camera. This can be done, e.g. by placing the camera at an angle instead of vertically. In this case, the recorded images must be rectified using a corresponding geometric transformation. Also ongoing is the fusion of active thermography in the »Waste 4 Future« project into a demonstrator including other modalities, creating a multimodal sorter for plastic materials. As shown in this paper, the active thermography approach is capable of increasing the accuracy of classification on black plastics.

References

Aujeszky, T., Korres, G., & Eid, M. (2017). Thermography-based material classification using machine learning. In *2017 IEEE International Symposium on Haptic, Audio and Visual Environments and Games (HAVE)*.

Brandt, C., Kieninger, M., Negara, C., Gruna, R., Längle, T., Küter, A., & Nüßler, D. (2016). *Sorting of black plastics using statistical pattern recognition on terahertz frequency domain data*. https://publica.fraunhofer.de/handle/publica/391776

Chen, X., Kroell, N., Feil, A., & Pretz, T. (2020). Determination of the composition of multilayer plastic packaging with NIR spectroscopy. *Detritus*, *13*, 62–66. https://doi.org/10.31025/2611-4135/2020.14027

EC. (2020). *Circular Economy action plan.* Euopean Comission. https://environment.ec.europa.eu/strategy/circular-economy-action-plan_en

Fawcett, T. (2006). An introduction to ROC analysis. *Pattern Recognition Letters*, *27*(8), 861–874. https://doi.org/10.1016/j.patrec.2005.10.010.

Fisher, R. A. (1936). The use of multiple measurements in taxonomic problems. *Annals of Eugenics*, *7*(2), 179–188. https://doi.org/10.1111/j.1469-1809.1936.tb02137.x

Gundupalli, S. P., Hait, S., & Thakur, A. (2017). A review on automated sorting of source-separated municipal solid waste for recycling. *Waste Management*, *60*, 56–74. https://doi.org/10.1016/j.wasman.2016.09.015

Jehanno, C., Alty, J. W., Roosen, M., Meester, S. de, Dove, A. P., Chen, E. Y.-X., Leibfarth, F. A., & Sardon, H. (2022). Critical advances and future opportunities in upcycling commodity polymers. *Nature*, *603*(7903), 803–814. https://doi.org/10.1038/s41586-021-04350-0

Jolliffe, I. T. (1986). *Principal Component Analysis*. Springer Science. https://doi.org/10.1007/b98835

Jones Roger W., & McClelland John F. (1989). Transient infrared emission spectroscopy. *Analytical Chemistry*, *61*(7), 650–656. https://doi.org/10.1021/ac00182a003

Maldague, X., & Marinetti, S. (1996). Pulse phase infrared thermography. *Journal of Applied Physics*(79), 2694–2698. https://doi.org/10.1063/1.362662

Masoumi, H., Safavi, S. M., & Khani, Z. (2012). Identification and classification of plastic resins using near infrared reflectance. *International Journal of Mechanical Sciences*, *6*, 213–220.

matweb. https://www.matweb.com/index.aspx

Menczel, J. D., & Prime, R. B. (2009). *Thermal Analysis of Polymers: Fundamentals and Applications*. John Wiley & Sons, Inc. https://doi.org/10.1002/9780470423837

Olscher, C., Jandric, A., Zafiu, C., & Part, F. (2022). Evaluation of Marker Materials and Spectroscopic Methods for Tracer-Based Sorting of Plastic Wastes. *Polymers*, *14*, 3074. https://doi.org/10.3390/polym14153074

Pedregosa, F., Varoquaux, G., Gramfort, A., Michel, V., Thirion, B., Grisel, O., Blondel, M., Prettenhofer, P., Weiss, R., Dubourg, V., Vanderplas, J., Passos, A., Cournapeau, D., Brucher, M., Perrot, M., & Duchesnay, E. (2011). Scikit-learn: Machine Learning in Python. *Journal of Machine Learning Research*, *12*, 2825–2830.

Polysecure GmbH. *Polysecure*. https://www.polysecure.eu/en/sort-reliably/tracer-based-sorting

Rozenstein, O., Puckrin, E., & Adamowski, J. (2017). Development of a new approach based on midwave infrared spectroscopy for post-consumer black plastic waste sorting in the recycling industry. *Waste Management*, *68*, 38–44. https://doi.org/10.1016/j.wasman.2017.07.023

Schmidt, J., Grau, L., Auer, M., Maletz, R., & Woidasky, J. (2022). Multilayer Packaging in a Circular Economy. *Polymers*, *14*(9). https://doi.org/10.3390/polym14091825

Sensors Unlimited. https://www.sensorsinc.com/applications/machine-vision/plastic-sorting

Shepard, S. M., Ahmed, T., Rubadeux, B. A., Wang, D., & Lhota, J. R. (2001). Synthetic processing of pulsed thermographic data for inspection of turbine components. *Insight: Non-Destructive Testing and Condition Monitoring*, *43*, 587–589.

Stegmann, P., Daioglou, V., Londo, M., van Vuuren, D. P., & Junginger, M. (2022). Plastic futures and their CO2 emissions. *Nature*, *612*(7939), 272–276. https://doi.org/10.1038/s41586-022-05422-5

W4F. *Waste 4 Future.* Fraunhofer-Gesellschaft. https://www.waste4future.fraunhofer.de/en.html

Recent developments in hyperspectral imaging technology for sensor-based sorting applications

Tobias Kreklow[1]*, Michel Reifenrath[1]

1 HAIP Solutions GmbH, Hannover, Germany

* Corresponding Author: Escherstraße 23, 30159 Hannover, Germany
kreklow.tobias@haip-solutions.com

Keywords: sensor-based sorting, plastic recycling, NIR, imaging spectroscopy, NIR sorting illumination,

Abstract

Spectral imaging or Near-infrared (NIR) imaging spectroscopy has developed over the past years into an established technology for sensor-based sorting applications, for example by sorting different types of plastic based on their different molecular composition to retrieve recyclable materials from waste (Bilitewski & Härdtle, 2013). By using spectral imaging it is possible to make the chemical, color and geometric properties of an object visible, which enables identification of materials or material properties in sensor-based sorting applications (Kulcke et al., 2003).

Indium gallium arsenide (InGaAs) sensors, which are particularly sensitive in the shortwave infrared (SWIR) range, are usually used as sensors for hyperspectral imaging (HSI) cameras. Standard InGaAs sensors can be used from 900 nm to 1700 nm. Two important criteria for qualitative optical sorting with high throughput are spatial and spectral resolution. Spectral resolution refers to how many wavelength bands are available for the material identification. Spatial resolution refers to the number of available pixels. With high spatial resolution, the radiation information from significantly more points on the conveyor belt is used for identification than

with a low spatial resolution (Fleischhacker, 2011; Kroell et al., 2022; Maier et al., 2024; Schlögl, 2021).

In the last three years, new further developed sensor technologies have evolved and created the foundation for a third generation of imaging spectrometers. HAIP Solutions has introduced the BlackIndustry SWIR 1.7 (900-1730 nm) camera series in summer 2023 providing a never-before-seen spatial resolution of 1280 spatial pixels in a hyperspectral camera for the SWIR range. With higher spatial resolution it is now possible to detect even very small particle sizes, for example in pastic flake sorting or foreign object detection within the food industry. Next to the higher spatial resolution is also the increased sensitivity in the 1600-1750 nm region in combination with so called Fast Midwave IR emitter illumination of high importance with the new camera generation.

Still until today, radiation emitted by halogen lamps is the standard illumination to be used in all NIR-sorting applications (Gundupalli et al., 2017). After conducting trials and building lab-based prototypes, we propose the use of a new type of illumination for NIR-sorting with better fitting peak response at 1500 nm for SWIR range (900-1700 nm) in comparison to halogen at 1100 nm (see Fig. 1). By increased sensitivity in the third absorption band of polymers, it will now be possible to separate plastic waste more accurate.

Previously extended shortwave infrared (exSWIR) range HSI cameras (1000-2500 nm) had to be used for the detection of absorption features occurring at the edges of standard SWIR HSI cameras. exSWIR camera however are more costly than conventional SWIR HSI cameras, making them less attractive for integration into NIR-based sorting machines.

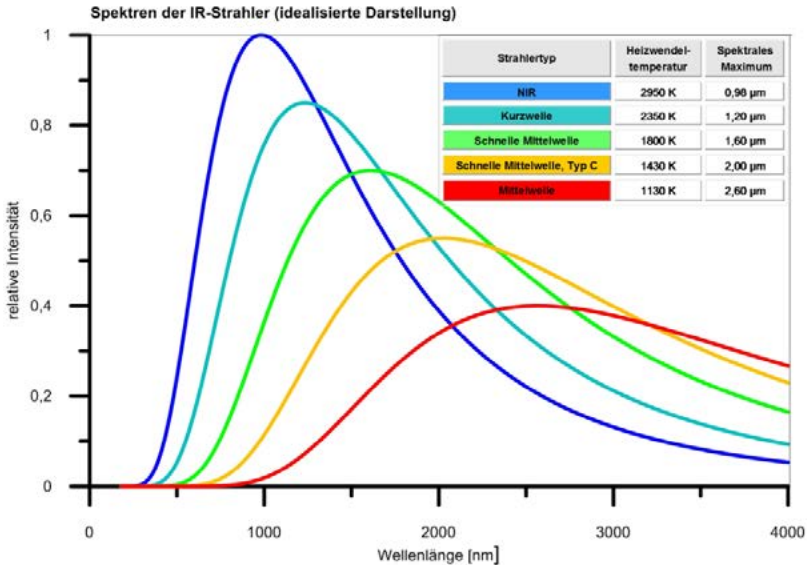

Fig. 1. Spectral energy distribution (Optron GmbH, 2024)

Integration of spectral imaging cameras in sensor-based sorting has developed rapidly in recent years and has found many applications in waste processing and recycling, mining as well as food industry. It is to be expected that further technological developments will continue to decrease prices and make hyperspectral cameras economically more attractive. Increased spatial resolution makes it possible to use less cameras to monitor the same conveyor belt width as previously needed.

A newly proposed illumination solution for combined use with SWIR range HSI cameras, can create better intensity values in the upper wavelengths from 1600-1750 nm, which could potentially lead to better separation of polymers without the need extended SWIR range sensors.

References

Bilitewski, B. & Härdtle, G. (2013). *Abfallwirtschaft* – Handbuch für Praxis und Lehre. *Springer Berlin Heidelberg, 955*. https://doi.org/10.1007/978-3-540-79531-5

Fleischhacker, S. (2011). Stoffliche Verwertung von Abfällen-Einsatz der Nahinfrarot-Sortiertechnik im Bereich von Gewerbeabfällen. 123.

Gundupalli, SP., Hait, S., Thakur A. (2017). *A review on automated sorting of source-separated municipal solid waste for recycling*. Waste management (New York, N.Y.) 60: 1–18.

Kroell, N. (2022). Optical sensors and machine learning algorithms in sensor-based material flow characterization for mechanical recycling processes: A systematic literature review. https://doi.org/10.1016/j.wasman.2022.05.015

Kulcke, A., Gurschler, C., Spöck, G., Leitner, R., Kraft, M. (2003). *On-line classification of synthetic polymers using near infrared spectral imaging*, Journal of Near Infrared Spectroscopy, 11 (1), pp. 71–81, https://doi.org/10.1255/jnirs.355.

Maier, G., Gruna, R., Längle,T., Beyerer,J. (2024). *A survey of the state of the art in sensor-based sorting technology and research*. *IEEE Access*, doi: 10.1109/ACCESS.2024.3350987.

Optron GmbH (2024), *Infrarottechnik* (https://optron.de/infrarot-systeme/technik/infrarottechnik/?lang=930)

Schlögl, S. (2021). Stand der Technik von Kunststoffsortieranlagen und Potentiale durch sensorische Stoffstromüberwachung. 102.

Classification of post-consumer plastic waste using CMOS-based near-infrared sensors

Zhihong Dou[1*], Huashu Deng[1], Nils Kroell[1], Alexander Feil[1], Kathrin Greiff[1]

1 RWTH Aachen University, Chair of Anthropogenic Material Cycles, Aachen, Germany

* Corresponding Author: Wüllnerstr. 2, 52062 Aachen, Germany; zhihong.dou@ants.rwth-aachen.de

Keywords: post-consumer plastic, near-infrared, decision tree, random forest, sensor-based sorting, waste management

Abstract

Over the past 20 years, the research on the topic of sensor-based sorting has flourished. In the area of recycling post-consumer plastic waste, sensor-based sorting has become an essential step in the mechanical recycling process due to its several advantages including a higher level of automation, and improved accuracy. Thanks to the booming of artificial intelligence and machine learning methods, the analysis of the hyperspectral data generated by the optical sensors can be processed automatically and precisely.

Near-infrared (NIR) sensors are adopted as the state-of-the-art technology in classifying post-consumer plastics due to their high technical maturity, which has been proven to be robust to the disturbing factors in real waste flows and reached a 99% classification accuracy (Kroell et al., 2022). Conventional NIR sensors usually operate in a wavelength range of 1000 nm to 1700 nm, in which different polymers can be distinguished by their characteristic absorption spectra. Due to the increasing demand for process monitoring and quality control in the recycling plants, a larger number of sensors are to be installed. The high unit price of NIR sensors leads to higher investment costs in case of scale effect, which makes the application situation

rather unattractive. Therefore, in this paper, the feasibility of cost-effective CMOS-based NIR for the classification of post-consumer plastics is explored for the first time, which operates in the NIR band from 750 nm to 1050 nm. The optical sensor used is the HAIP BlackIndustry NIR Camera provided by HAIP Solution GmbH.

As part of an experiment, post-consumer plastic wastes of different material properties (colors and shapes) that were collected from the preconditioning stage in a sorting plant were used and consisted of four common plastic types: high-density polyethylene (HDPE), polypropylene (PP), polystyrene (PS), and polyethylene terephthalate (PET). This allows us to cover the influence of different colors, shapes, and applications on the spectra, making the results more widely applicable. They were then placed on a running conveyor belt of the NIR-Measurement-Stand, and spectral information was saved and analyzed by the decision tree and random forest model.

The results show that CMOS-based NIR sensor which operates in the above-mentioned limited wavelength range cannot compete with the performance of conventional NIR technology in practical applications for post-consumer plastic waste recycling. However, the research shows how far the potential and feasibility of CMOS-based NIR sensors in the sorting are and provides a good starting point for further research, such as incorporating more advanced deep learning models, as well as exploring the application of CMOS-based NIR sensors in more homogeneous waste, e.g. post-industrial waste classification.

1 Introduction

Plastic is one of the most important and most frequently used materials and is widely used in almost all industries (Andrady & Neal, 2009). Since 1950, the global production of plastic has experienced unprecedented growth and has increased 230-fold to date. This has led to a significant increase in plastic waste, which has risen from 156 million tons in 2000 to 353 million tons in 2019. In 2019 however, only 9 wt% of plastic waste was recycled and 19 wt% was used to generate energy (OCDE, 2022). Plastics are not biodegradable due to fossil hydrocarbons like ethylene and propylene and consequently accumulate in landfills and natural environments instead of decomposing (Geyer et al, 2017; Barnes et al., 2009). The almost pollution of the natural environment by plastic waste is becoming an increasing concern.

Near-infrared (NIR) spectroscopy is a modern technology for sensor-based characterization of plastic waste. The principle of NIR is to classify materials based on their characteristic spectra (Siesler et al., 2002). These spectra contain information about the chemical composition and physical state of the material (Linnemann, 2008). Today, the use of NIR sensor-based sorting (SBS) to classify common plastics is a state-of-the-art technology (Maier et al., 2024). While NIR technology offers high accuracy in the identification of plastic materials, it requires significant investment costs. Sensor-based sorting using NIR sensors is already a widely adopted application. However, for newer applications like quality control and process monitoring, a significant number of sensors need to be installed, making it economically unattractive due to the high costs involved (Kroell et al., 2022). To tackle this challenge, this paper delves into the potential of inexpensive CMOS-based NIR sensors and their ability to be used in the process, by filling the research gap of exploring the feasibility of sorting post-consumer plastic waste by CMOS-based NIR spectroscopy in the wavelength range from 850 nm to 1050 nm.

2 State-of-the-art research

Based on the common terminology in the sensor-based-sorting industry, the wavelength range from 750 nm to 1050 nm is usually referred to as part of the visual to near-infrared range (VNIR), which is from 400 nm to 1000 nm (Maier et al., 2024). VNIR technology is currently used in many areas to classify materials. For example, it is used in agriculture to analyze wheat leaves when exposed to salt (Mokhtari et al., 2014). In mineralogy, it is used to analyze olivine samples (Carli et al., 2018). VNIR technology is also used in the food industry to classify chicken meat samples (Chung & Yoon, 2021). In the field of plastic classification, it is currently more common to use it on satellites, airplanes, drones, unmanned aerial vehicles, and handheld devices to monitor plastic waste that is easily submerged or floating in the oceans (Moshtaghi et al., 2021).

In the area of plastics from post-industrial and post-consumer material streams, conventional NIR technology is generally adopted. Given the fact that some common functional groups in plastic products already exhibit characteristic absorption peaks in the spectral range from 850 nm to 1050 nm (Stuart, 2008), the investigation of the potential and feasibility of CMOS-based NIR spectroscopy for the sorting of post-consumer plastics is of great research value. The purpose of this paper is to explore whether it is technically feasible to classify post-consumer plastic wastes using

CMOS-based NIR sensors, how accurately can CMOS-based NIR sensors classify post-consumer plastic wastes, and whether there is an opportunity for CMOS-based NIR sensors to replace conventinal NIR sensors in the recycling industry.

3 Materials and methods

3.1 Input materials

In this paper, we only focus on classifying the plastic types of the samples into which the samples are pre-categorized as HDPE, PP, PS, and PET. The packages include different applications of food and non-food, shapes of bottles, trays, and others, and colors and grey tones from transparent, and semi-transparent to opaque, red, blue, yellow, white, etc. Dark colors like dark grey are not considered because the CMOS-based NIR sensor cannot capture sufficient reflectance intensity on them according to our pre-experiments. As far as possible, the selection was considered to ensure that each packaging color and application type was evenly represented across the plastic types. Caps and sleeves made from a different material than the bottle are still retained, to best present the original material flows in the sorting plant. The total number of samples of each plastic type is listed below. The quantity of each type of plastic bottle will be balanced according to the number of pixels in the data processing step.

Tab.1: Number of each type of plastic bottle in the experiment

Plastic type	HDPE	PET	PP	PS
Number of packaging	153	149	191	195

3.2 Experiment setup

The setup of the test bench is shown in Fig. 1. The samples are manually placed on a conveyor belt and pass underneath it in sequence. Two 400 W halogen lamps on the same side provide adequate lighting intensity for the CMOS-based NIR sensor. The scanning software automatically saves the scanned information as hyperspectral images in .h5 format files every two seconds.

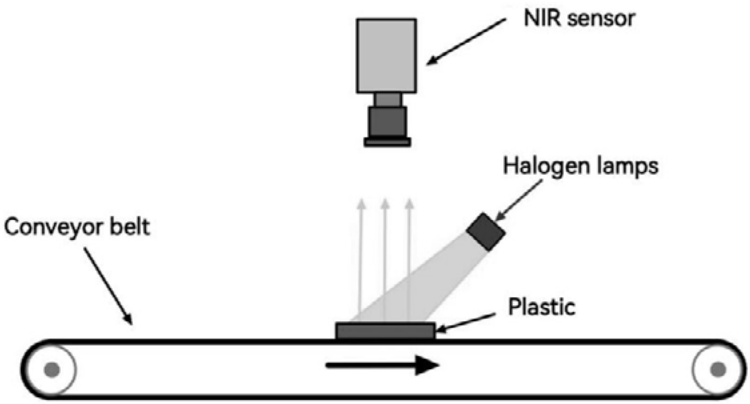

Fig.1: Experiment setup

3.3 Data preprocessing

Due to variations in light sources at different daytimes and uneven spatial distribution of illumination, the first step is to perform black and white balance on the hyperspectral images. Before each recording experiment, five images are recorded for black balance and white balance by masking the lens and photographing a white ceramic plate, respectively. We average the 5 images along the conveyor belt direction and end up with an array of one row in the conveyor belt direction, which are named dark field images and white field images. Using the averaged one-dimensional black-and-white balanced correction array, each pixel point at the corresponding position of the sample images is corrected according to the following formula:

$$\text{Corrected image}=\frac{(\text{raw image} - \text{dark field image})}{(\text{white field image} - \text{dark field image})} \qquad (1)$$

After this, the area of the image containing the sample was manually intercepted via a self-developed Python script. This was done by dragging the mouse along the edge of the sample area in an opened window which visualizes the h5 image in a single channel, which is shown in Fig. 2.

Fig.2: Schematic of sample selection by dragging the mouse

After recording, each plastic type has a different number of samples and a different number of pixels in the region of interest (ROI). To reduce the risk of overfitting a particular plastic type during the training of the machine learning model, the plastic type with the smallest number of pixels, which is PS in this paper, should be used as the baseline, and a final dataset with an equal total number of pixels for each plastic type should be obtained by randomly discarding pixel points of the other plastic types. Afterward, since the absorption peaks of common functional groups in plastics are above 850 nm, we discarded the spectral information up to 850 nm.

The data were derived once to make the characteristic peaks more visible and to facilitate comparison with related studies in the field. After obtaining the first derivative, the data were smoothed through a rolling window to smooth out the effect of possible outliers at certain wavelengths in the spectra and to clearly show the characteristic reflectance peaks.

3.4 Machine learning model

In this paper, a decision tree model (Grajski et al., 1986) and a random forest model (Breiman, 2001) are used for classifying the spectrum from the pixels of each sample to the correct plastic type.

3.4.1 Description of the models

The decision tree model is widely used in the field of classification problems, its basic principle is that firstly, the data set is divided into a test set and a training set, the test set is only used to test the model, and the training set is only used to train the model, then the input training set is partitioned into multiple subsets by setting nodes. Then it is determined whether all these subsets are the same class of plastics, if not, then proceed to repeat the node setup for these subsets to perform recursive partitioning.

The basic principle of random forest is to first construct multiple independent decision trees, then each tree independently predicts the classification of the same input sample, the prediction result of each tree is equivalent to one vote, for a given sample, and the algorithm aggregates the votes of all the decision trees, and then selects the category with the most votes as the final prediction result. Random forest combines the predictions of multiple decision trees to improve the accuracy and stability of the overall model while reducing the risk of overfitting.

3.4.2 Model tuning

Then 5-fold cross-validation is used to reduce the risk of overfitting, the dependence of the final model, and parameter selection on the division of the training and test sets and making full use of the data for the training of the model. Because the spectra of the pixels in the neighborhoods within the same sample are very homogeneous, the dataset is grouped by samples before shuffling, so that the neighbored pixels in the same sample will not be divided into both the train and test dataset.

Afterward, GridSearchCV was used to try different parameter combinations on the machine-learning model. The best-performing parameter combination is finally selected in conjunction with five-fold cross-validation, and the optimal model is generated.

4 Results

The spectra from the CMOS-based NIR sensor of the 4 plastic types are visualized in Fig. 3. PS, PP and HDPE show distinct peaks, whereas PET, represented by the grey curve, has no identifiable peaks in its spectrum in this wavelength range.

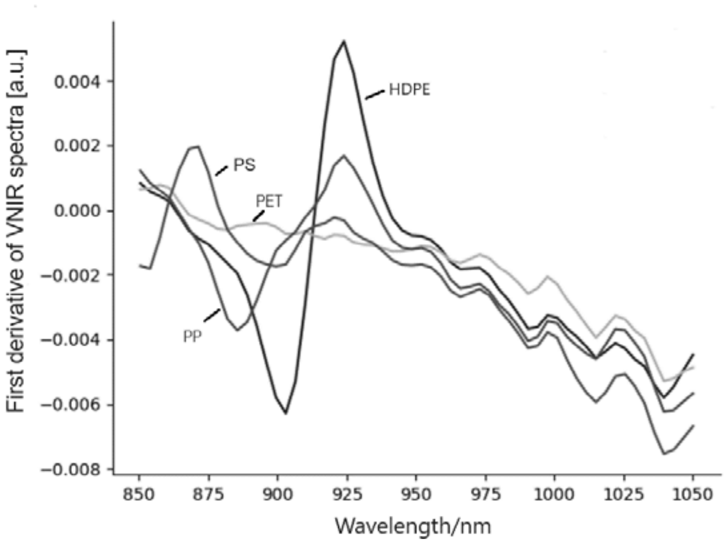

Fig. 3: Averaged spectra of HDPE, PET, PP, and PS samples from the experiment

Fig.4 shows the correctly classified number of pixels of each plastic type. Random forest realized a better classification performance than decision tree for all the plastic types. Both models produced more misclassifications when distinguishing between PS and PET. HDPE demonstrates the highest classification accuracy and false negative rates in both models. According to the decision tree model, the F1-scores for HDPE, PP and PS are of 89%, 83%, and 75%, respectively. For PET, the F1-score was only 69%. However, the random forest model performed even better, achieving F1-scores of 95%, 89%, and 81% for HDPE, PP, and PS, respectively, and a better result for PET, which was 77%.

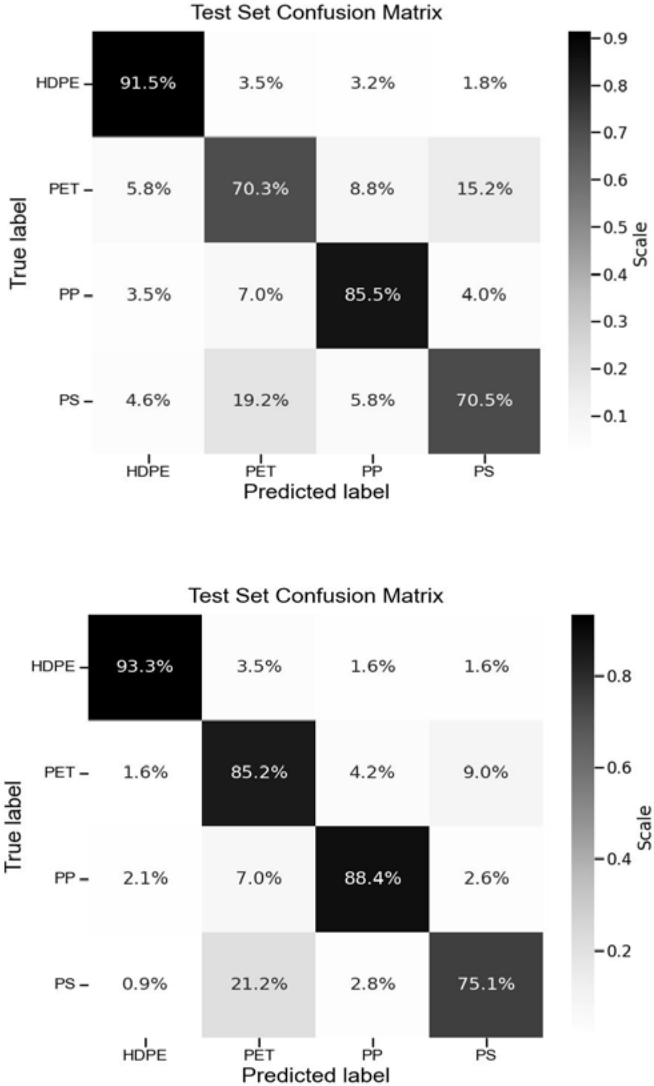

Fig. 4: Confusion matrix of the classification of HDPE, PET, PP, and PS from decision tree (upper) and random forest (lower)

Fig. 5 shows the boxplots of the distribution of the percentage of correctly classified pixels in each sample in the test set. If we set the classification logic in a way that when over 70% of the pixels in a sample are categorized as a particular plastic type, the sample will be classified as that plastic type (Chen et al., 2021). Following this logic, we can achieve the correct classification at the particle level by decision tree, which is as follows: HDPE 89%, PET 55%, PP 86%, and PS 60%. When using random forest, the correct classification is: HDPE 87%, PET 94%, PP 77%, and PS: 73%.

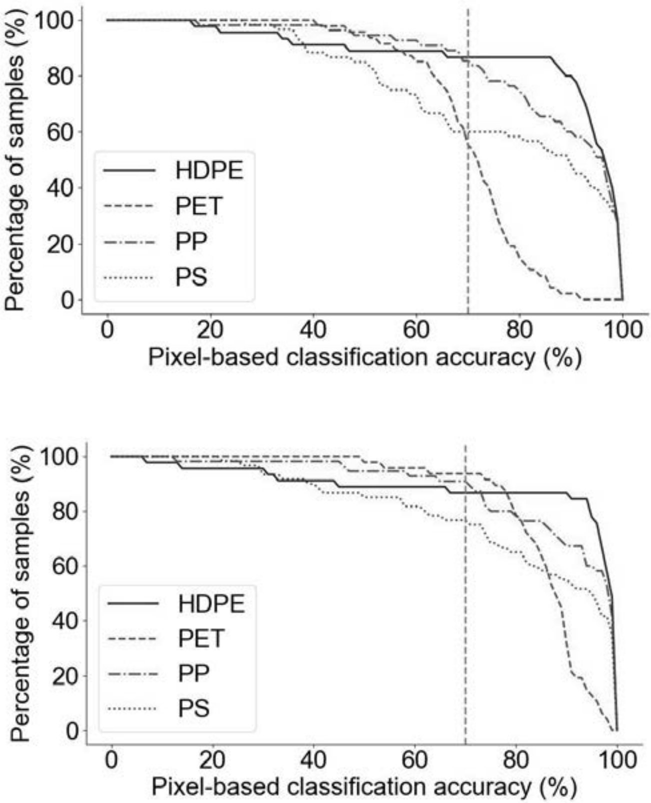

Fig. 5: Cumulative accuracy curves of the percentage of correctly classified pixels in each single plastic sample for each plastic type PS from decision tree (upper) and random forest (lower)

5 Conclusion and outlook

Our investigations show that HDPE has the best utilization potential in the classification by using the CMOS-based NIR sensor. PET has no recognizable peaks in the spectrum and interferes with the classification of other plastic types, especially PS. For this experiment, due to the influence of bottle caps, and sleeves, as well as the contamination and the brightness of the bottle on the exposure, we explored the confidence level of the CMOS-based NIR sensor for particle-level classification at 70% threshold. The results show that CMOS-based NIR sensors cannot completely replace conventional NIR technology both in the laboratory and industrial scale. However, for the classification of specific plastics such as HDPE and PP, CMOS-based NIR shows potential for application alone or in sensor fusion in combination with, e.g., conventional NIR sensor.

In future research, the ability of CMOS-based NIR sensors to classify specific plastic types such as HDPE and PP on the industrial scale could be further validated, which can also be done by combining sensor fusion or by conducting experiments in real sorting plants. Besides, it is also meaningful to explore the application of deep learning techniques such as convolutional neural network (CNN) for classification by using CMOS-based NIR sensors. In addition to post-consumer plastic wastes with complex properties, the potential application of CMOS-based NIR sensors to classify more homogeneous waste streams like post-industrial plastic flakes deserves to be further explored.

6 Acknowledgment

We are thankful to the company HAIP Solutions GmbH, especially Tobias Kreklow, for lending and installing the CMOS-based NIR Camera, which made the trial possible. The responsibility for the content of this publication lies with the authors.

References

Andrady, A. L., & Neal, M. A. (2009). Applications and Societal Benefits of Plastics. Philosophical Transactions of the Royal Society B: Biological Sciences, 364(1526). https://doi.org/10.1098/rstb.2008.0304

Barnes, D. K. A., Galgani, F., Thompson, R. C., & Barlaz, M. (2009). Accumulation and Fragmentation of Plastic Debris in Global Environments. Philosophical Transactions of the Royal Society B: Biological Sciences, 364(1526), 1985–1998. https://doi.org/10.1098/rstb.2008.0205

Breiman, L. (2001). Random forests. Machine learning, 45, 5-32.

Carli, C., Pratesi, G., V. Moggi-Cecchi, Zambon, F., F. Capaccioni, & Santoro, S. (2018). Northwest Africa 6232: Visible–near infrared reflectance spectra variability of an olivine diogenite. Meteoritics & Planetary Science, 53(10), 2228–2242. https://doi.org/10.1111/maps.13056

Chen, X., Kroell, N., Wickel, J., & Feil, A. (2021). Determining the composition of post-consumer flexible multilayer plastic packaging with near-infrared spectroscopy. Waste Management, 123, 33–41. https://doi.org/10.1016/j.wasman.2021.01.015

Chung, S., & Yoon, S.-C. (2021). Detection of Foreign Materials on Broiler Breast Meat Using a Fusion of Visible Near-Infrared and Short-Wave Infrared Hyperspectral Imaging. Applied Sciences, 11(24), 11987. https://doi.org/10.3390/app112411987

de cooperation et de developpement economiques, O. (2022). Global plastics outlook: economic drivers, environmental impacts and policy options. OECD publishing.

Geyer, R., Jambeck, J. R., & Law, K. L. (2017). Production, use, and fate of all plastics ever made. Science Advances, 3(7). https://doi.org/10.1126/sciadv.1700782

Grajski, K. A., Breiman, L., Di Prisco, G. V., & Freeman, W. J. (1986). Classification of EEG Spatial Patterns with a Tree-Structured Methodology: CART. IEEE Transactions on Biomedical Engineering, BME-33(12), 1076–1086. https://doi.org/10.1109/tbme.1986.325684

Kroell, N., Chen, X., Greiff, K., & Feil, A. (2022). Optical sensors and machine learning algorithms in sensor-based material flow characterization for mechanical recycling processes: A systematic literature review. Waste Management, 149, 259–290. https://doi.org/10.1016/j.wasman.2022.05.015

Linnemann, B. (2008). Einsatz spektroskopischer Verfahren für die Eigenschaftsbestimmung von Polyethylenterephthalat-Multifilamenten.

Maier, G., Gruna, R., Längle, T., & Beyerer, J. (2024). A survey of the state of the art in sensor-based sorting technology and research. IEEE Access, 1. https://doi.org/10.1109/access.2024.3350987

Mokhtari, M. H., Sodae, H. R., Hakimzadeh, M. A., & Tarighat, F. (2014). Application of visible and near-infrared spectrophotometry for detecting salinity effects on wheat leaves (Triticumasativum L.). Agricultural Engineering International: CIGR Journal, 16(4), 35-42.

Moshtaghi, M., Knaeps, E., Sterckx, S., Garaba, S., & Meire, D. (2021). Spectral reflectance of marine macroplastics in the VNIR and SWIR measured in a controlled environment. Scientific Reports, 11(1). https://doi.org/10.1038/s41598-021-84867-6

Siesler, H. W., Ozaki, Y., Kawata, S., & H. Michael Heise. (2008). Near-Infrared Spectroscopy. John Wiley & Sons.

Stuart, B. H. (2008). Infrared spectroscopy: fundamentals and applications. Wiley.

Universal LIBS Sensor for Efficient Use of Variable Feedstock in Metal Making Processes

Cord Fricke-Begemann[1*], Rüdiger Fleige[1], Markus Dargel[2]

1 Fraunhofer institute for laser technology ILT, Aachen, Germany

2 Laser analytical systems & automation GmbH, Aachen, Germany

* Corresponding Author: Cord Fricke-Begemann, Fraunhofer ILT, Steinbachstr. 15, 52074 Aachen; E-mail: cord.fricke-begemann@ilt.fraunhofer.de

Keywords: Metals, scrap, LIBS, continuous analysis, inline measurement

Abstract

Metal recycling strongly reduces the CO_2 emissions and raw material consumption in comparison to primary production. To improve the useability of variable scrap feedstock, there is a need for fast inspection of the material batches being delivered to the processing plants.

For this purpose, an optical sensor system was developed using the method of laser-induced breakdown spectroscopy (LIBS). In three different industrial plants for production of aluminium, lead, and steel, the universal sensor system was tested. Individual application schemes have been worked out to retrofit the sensor into the material flow schemes of each of the plants. The LIBS system itself is equipped with a 3-dimensional optical scanner to enable measurement positions being freely distributed within a distinct volume. Nevertheless, the presentation of the material to the sensor is a key issue to obtain a representative result.

For the material transport by belt conveyors, a good coverage of fine-grained material is achieved by a guided distribution of measurement points based on laser line section monitoring of the surface. When being applied to aluminium chips, the

average composition is determined but also individual outliers are detected, which present single pieces of significantly deviating origin. In the case of lead recycling, a large variety of metallic and non-metallic materials is used for which the major elements of interest such as lead, antimony, calcium, and tin are determined.

For a steel plant installation, an inspection of the individual truck loads must be performed prior to unloading the trucks at the target location. For this use case, an applicator was designed to access the truck load from above for the LIBS measurements. In all use cases, the immediate knowledge of the material composition supports the plant operators and material mix optimizing tools enable cost-, material- and energy-efficient plant operation.

1 Introduction

Metals are suitable for recycling without quality loss, in principle, if contaminations could be completely avoided, and with a high degree of energy saving which can amount to 95% in comparison to primary production from ores in the case of aluminium (IAI 2020). To increase the secondary production is thus intended in order to reduce the consumption of natural resources and carbon emissions. On the other hand, a perfect match of the input material composition to the required product quality would be required to achieve a complete circular production which is not feasible in practice. The feedstock material available to the recycling plants today is inhomogeneous and of widely unknown composition as many sources of metal scrap are not suitable for individual collection of alloys or single piece sorting by composition.

The definition of trade categories is often rather broad, e.g., for steel as old scrap, new scrap, shredded, turnings, high-residual, and incineration scrap according to the European Steel Scrap Specifications. In relation to chemical composition only desired upper limits of some contaminants are defined, e.g., below 0.4 m.-% Cu for old scrap type E1 (BDSV, 1995), and it can often not be validated if they are obeyed.

However, metal recycling plants are aiming to include scrap feedstock of low quality into their feedstock, which is of better availability and at lower prices. The desired increase of both secondary raw material share and production quality requires a good knowledge of the used feedstock.

To optimize the scrap mixture for the furnace process in terms of costs and production quality based on the material on stock is a task that is even more complicated if the composition of the feedstock is not well defined. Since not all feedstock is suitable for single piece sorting or available as pure pre-defined fractions, batches of mixed or undefined materials are used in the production. Thus, there is a large need to analyze the incoming metal scrap batches at the time of delivery and thereby assign the material to the right storage fraction and provide the compositional data to the scrap control system of the plant. Currently, no sensor is available to perform this task by inline measurements.

2 LIBS sensor system

To approach the task of scrap feedstock chemical analysis, a system was designed based on laser-induced breakdown spectroscopy (LIBS, Fig. 1), which has been used for metal analysis and sensor-based scrap sorting before (Noll *et al.*, 2018). The LIBS method uses a pulsed laser to ablate and excite sample material to induce emissions of its constituting elements for spectroscopic analysis. A universal sensor was developed for retrofitting of various existing metal recycling plants, which all have their individual feedstock handling processes and material requirements.

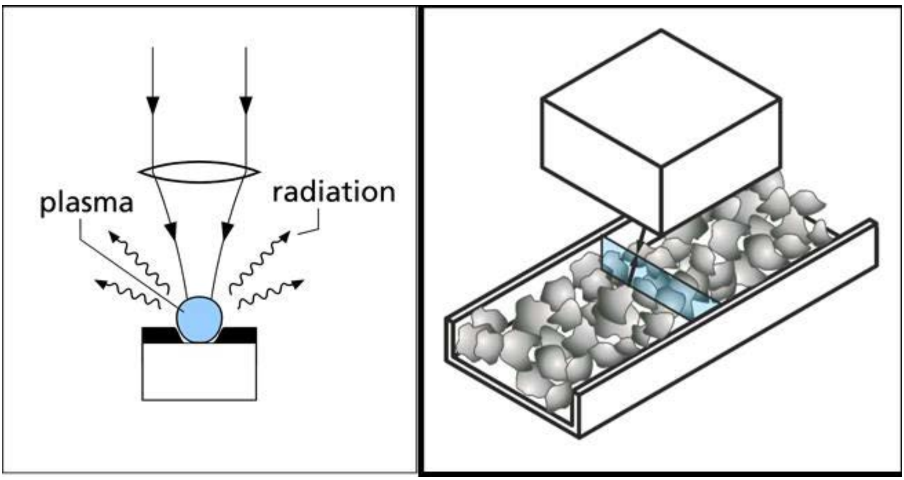

Fig. 1: Scheme of LIBS measurement process (left) and LIBS scanning of a material layer (right).

The concept includes a laser optical system that is placed overhead the material to be inspected. The downward pointing laser beam is directed via a laser scanner to the material surface in three dimensions. As shown in Fig.1 (right) a scanning in lateral direction allows to access any piece of a continuous material stream. A movement of the laser focal spot in vertical direction is used to adapt the LIBS measurement process to the local material surface height. As indicated in Fig.1 (left, bold black) a surface contamination is often present on the surface, which is not of representative composition. Therefore, a laser ablation process is included into the LIBS measurement process which allows a local cleaning of each individual measurement spot within milliseconds before the analytical laser-induced plasma is created.

3 Application cases

The LIBS sensor system has been tested on-site in three industrial recycling plants, adapted to the existing feedstock handling.

3.1 Aluminium recycling plant

The aluminium plant involved is specialized on the recycling of aluminium chips from manufacturing processes, being obtained from a wide range of providers. Since manufacturers of aluminium components are machining a variety of different alloys, also the composition of the residual chips is changing. Within the plant, the delivered batches are pretreated and partly transported on conveyor belts. As the material on the belt is presented as a shallow layer to the LIBS sensor, a direct optical access is possible to most pieces and the scanner allows a representative sampling. The system during operation is shown in Fig. 2.

Fig. 2: LIBS measurements of aluminium chips transported on the conveyor belt.

The LIBS system and data evaluation are calibrated using measurements of certified reference samples, leading to a high reliability of the results. For example, Fig.3 shows the observed variation of manganese content of five batches of processed aluminium chips (V-A to V-E) in the sub-percent range.

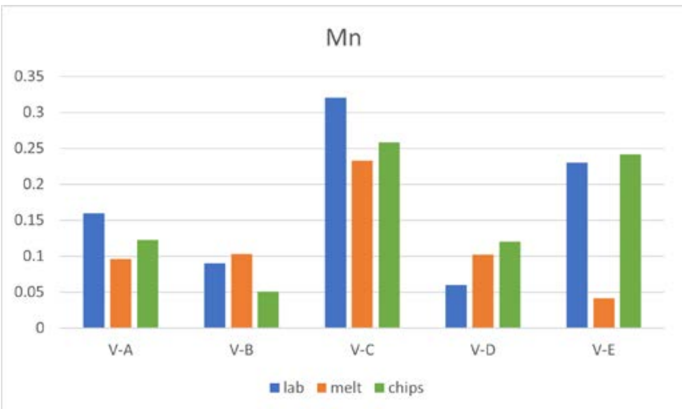

Fig. 3: LIBS inline analysis for Mn content in weight-% of aluminium chips (green) in comparison to laboratory analyses (blue) and melt sample analysis (orange).

The results from the LIBS measurements carried out inline on the moving belt are in good agreement with the lab analyses according to a standardized sampling procedure which is used for reference but is time consuming and its representativeness strongly depends on the amount and distribution of sampling spots over the material batch. Within one minute more than 1000 LIBS measurements at individual locations are executed, which provide a good statistical average at the temporal resolution required for the material control.

3.2 Steel recycling plant

In steel plants, the scrap feedstock is often not transported internally by means which would make it easily accessible. The scrap is delivered by trucks directly to the scrapyard where they are unloaded at the assigned feedstock fraction. It is therefore desired to inspect the truck load on arrival before unloading. This will enable an assignment of the feedstock fraction for unloading according to the composition of the delivered material. A concept was developed for scanning the material on a truck which is guided through a gantry, see Fig. 4.

Fig. 4: Schematic drawing of a LIBS system (blue) mounted on a gantry for inspection of truck delivered scrap batches.

An additional wide scanning range for the LIBS measurements is realized which allows to inspect individual truck delivery within a time of a few minutes which is acceptable as delay before unloading.

Fig. 5: Scanning LIBS measurements carried out on a batch of steel scrap.

As visible in the example of Fig. 5, the old type steel scrap is not a continuous layer of material but exhibits a complex surface geometry. The scanning LIBS concept based on included 3D surface geometry inspection allows to focus the laser to the individual scrap pieces not only on the very top, but also through gaps between other parts within a given height range of 20 – 30 cm.

Considering the rust covered scrap pieces, it is obvious that accurate measurements are only possible after the previous laser cleaning of the measurement spots. The measurement results can directly be validated for single scrap pieces. However, it still has to be considered that the LIBS measurements can incorporate only scrap pieces which are optically accessible from the top. The representativeness of such measurements cannot be validated based on individual batches but it has to be monitored in relation to production data over a longer time period.

3.3 Lead recycling plant

As a third use case, the LIBS sensor was tested in a lead recycling plant. Here, again, delivered material batches are put on a belt conveyor, where it can be accessed for LIBS measurements during the continuous movement. Whereas the general set-up is comparable to that shown for aluminium above, additional challenges are posed by this use case. Fig. 6 shows examples of the material. Although it is delivered as bulk freight, the material exhibits large agglomerates and can be dusty. Because lead containing material is of significant risk to health and environment, it can only be handled in dedicated facilities with protective measures.

Fig. 6: Left: LIBS measurements on dusty lead feedstock (drosses). The scattering of the light section laser is visible in red over the full width of the belt. The path of the LIBS laser is visible as a white vertical line in the front. Right: metallics from lead acid battery recycling.

The optical 3D geometry measurements have proven to work reliably, providing target data permanently inspite of the dust generation, and also the LIBS measurements when right positioning is achieved. Whereas the LIBS sensor has been calibrated using certified lead metal alloy samples, the variety of compositions in the feedstock is much larger. In addition to metallic lead, lead in various chemical compounds occurs as well as lead-containing non-metallic materials, as for example in Fig. 6 (right).

An extension of the LIBS data evaluation to such materials was worked out based on the alloy calibration. The abundance of lead as main material is determined, which ranges from above 90 wt.-% in metallic scrap down to about 10 wt.-% in slag. In addition, a wide range of other metal elements is determined as shown in Fig. 7 for a range of material batches (numbered on the x-axis). Each batch consists of several tons of recycling material. In addition to lead, other most abundant elements are antimony, tin, iron, calcium, and silicon.

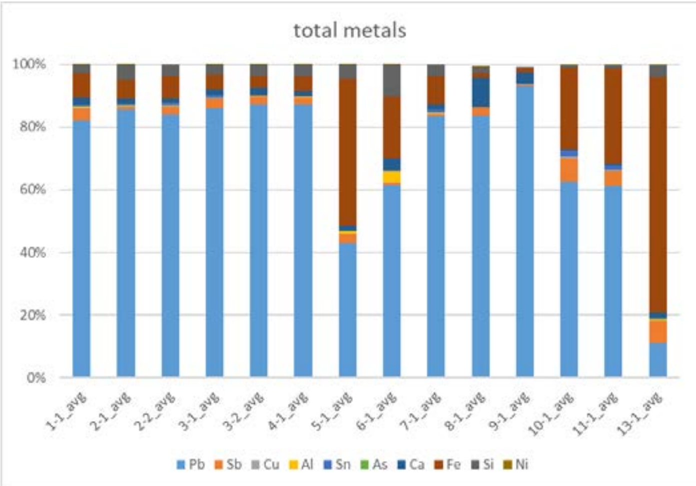

Fig. 7: Results of inline LIBS measurements of lead recycling feedstock batches.

Whereas these results are useful for feeding and controlling the metallurgical recycling process, is has to be noted that it is only semi-quantitative at this stage. As shown in the graph, the sum of all metal elements is defined as 100% here, whereas the light elements which are present in the compounds of oxides, sulphates, carbonates, and plastics are not quantified. At the time of the trials, no method for deriving reference data over the wide range of materials was available.

4 Summary and Conclusions

A system for scanning LIBS measurements of the variety of material feedstock in metal recycling plants has been developed. It was successfully installed for trial campaigns in industrial plants for aluminium, steel, lead production. Although specific challenges are found in each individual application case, the universal LIBS sensor concept was shown to be applicable in each of the cases. Beyond the analysis of single metal pieces, where LIBS is successfully applied for many years now, the analysis of complex metal containing materials has been demonstrated.

5 Acknowledgements

The project is funded in the European Union’s Horizon 2020 research and innovation programme under grant agreement No 869882.

References

Aluminium recycling factsheet, International aluminium institute (IAI), October 2020; https://international-aluminium.org/resource/aluminium-recycling-fact-sheet/

European Steel Scrap Specifications, Bund deutscher Stahlrecyclings- und Entsorgungsunternehmen e.V. (BDSV), 1995; https://www.bdsv.org/fileadmin/service/gesetze_und_regelwerke/sortenliste_en.pdf

Noll, R., C. Fricke-Begemann, S. Connemann, C. Meinhardt, V. Sturm, LIBS analyses for industrial applications – an overview of developments from 2014 to 2018, Journal of Analytical Atomic Spectrometry, 2018 (6), DOI: 10.1039/C8JA00076J

Fostering the Circularity of Critical Raw Materials: LIBS for the in-line identification of Li-ion battery cathodes

Iratxe Uria-Tellaetxe*[1], Paule España[1], Íñigo Cacho[1],
Ainara Pocheville[1], Sixto Arnaiz[1]

[1] GAIKER Technology Centre, Basque Research and Technology Alliance (BRTA), Department of Recycling and Circular Economy, Zamudio, Spain

* Corresponding Author: Parque Tecnológico de Bizkaia, Edificio 202, 48170, Zamudio, Spain, uria@gaiker.es

Keywords: LIBS, Li-ion batteries, critical raw materials, recycling, automated identification, Machine Learning

Abstract

In current battery recycling processes different cathode types and anode materials are thoroughly mixed, hindering the subsequent extraction of the Critical Raw Materials (CRM) they content. However, the prior separation and concentration of materials would enhance the efficiency of this process and enable compliance with recovery targets. In this study, multi-elemental quantitative analysis by laser induced breakdown spectroscopy (LIBS) in combination with Machine Learning techniques is proposed to improve this separation. On the basis of these technologies a classification model was developed following an iterative procedure. When validated to in-line classify Lithium-ion battery (LIB) cathodes according to their electrochemistry a success rate higher than 90% was obtained, demonstrating the potential of this methodology to foster the recycling of LIB from e-waste as a consistent alternative supply of CRM.

1 Introduction

Lithium-ion batteries (LIB) vary in size, design and electrochemistry, but essentially, all cells contain an anode layer, a cathode layer, and a separator film inserted between them, tightly packed, and submerged in Li electrolyte, all together sheltered by an outer case (Thompson et al., 2020). The cathode active material is mostly composed of lithium metal oxides, where the metallic element is usually Co, Ni, Mn, Al, different combinations of them, Fe, P or Ti (Saldaña et al., 2019). On the other hand, spherical graphite is generally used as anode material. The imbalance between raw material supply and demand in battery manufacturing over the past years has led to the inclusion of most of these substances in the fifth Critical Raw Materials (CRM) list of the European Union (Proposal for Regulation 2023/0079/COD). Due to the sharp growth in CRM usage in electric/electronic devices, electric vehicle (EV) included, and the limited access of Europe to these materials (Charles et al., 2020), LIB recycling has been prioritised in the European legislation and policies, after second life applications, as a way of ensuring the secure and sustainable supply of materials for a successful mobility transition towards a carbon-neutral future (European Commission, 2021).

In line with the above, the global demand for LIB is expected to rise by about 10 times this decade, reaching to 2,600 GWh in 2030 (World Economic Forum, 2019), mostly driven by the stand-out position of the mobility applications. Together with these figures, the amount of LIB waste generated every year is sharply increasing and it is expected to exceed 1 million tonnes by 2025 (Chakraborty & Saha, 2022). To address the secure and sustainable access to secondary raw materials through recycling, LIB treatment throughput should be increased (Karali & Shah, 2022).

However, the recycling technologies have not been developed at the same pace. The diversity in LIB composition, the lack of standardization in their design and the risks associated to their storage and handling poses important challenges for efficient recycling (Toro et al., 2023). Current waste battery collection systems produce mixed upcoming streams and sorting processes prior to recycling are necessary. Although different battery classification systems (vision, induction, X-rays) can recognize battery types (alkaline, zinc-carbon, NiMH, NiCd, Li-ion), they do not distinguish the specific electrochemistry of LIB, and manual process still dominates the market (Zheng et al., 2023). Regarding material extraction, hydrometallurgy is nowadays the main used technology for LIB recycling due to the higher recovery rates that can obtain, although pyrometallurgy is also applied

(Neumann et al., 2022). Hydrometallurgical processes use specific combinations of chemical reactions which performance is highly dependent on the input material quality (Weigl, 2022). As a result, previous thorough pre-treatment operations are required for active materials preconcentration, habitually including intensive shredding and separation stages in which all battery materials are deeply blended (Sommerville et al., 2021). Therefore, an additional earlier cathode sorting step to classify them according to their chemistry could lead to an increase in the efficiency and recovery rates of the LIB recycling processes (Thompson et al., 2021; Zheng et al., 2023).

To this regard, the significant development of photonic technologies in recent years, together with the improvements in data analysis, have made it possible to address challenges in real-time classification of complex mixed materials (Araujo-Andrade et al., 2021). The presence of carbonaceous substances in electrodes makes some advanced sensors, such as Raman or NIR, struggle in detecting chemical patterns. In contrast, LIBS technique can virtually detect all chemical elements (Rifai et al., 2020). As a result of this and other many advantages (Yang et al. 2023), LIBS technique has been broadly investigated over the last years in a wide range of applications (Jean-Noël et al., 2020; Kabir et al., 2022). Applied to battery technology, LIBS has shown good performance in real-time cathode quality control applications. Kappeler et al. (2022) used nanosecond LIBS and univariate calibration for depth-resolved concentration measurement, and Pamu et al. (2021) determined the composition by applying calibration-free quantitative LIBS.

However, in contrast with other traditional techniques such as chromatography, due to matrix effect and nonlinear laser-substance interactions univariate calibration methods show low performance in laser ablation (Song et al., 2022). Alternatively, Machine Learning techniques are widely used to model the relationship between spectra and measured elemental concentration (Chen et al., 2020; Zhang et al., 2018). Partial least squares regression (PLSR) is a standard linear multivariate method, highly interpretable and low complexity, that can efficiently handle high-collinearity, high-dimensionality, and limited sample number, which is common in spectral data studies. Because of these features, it is commonly used in spectral data analysis, such as LIBS and Raman spectroscopy (Han et al., 2021), and its performance has been demonstrated to be comparable or even better to more complex nonlinear models in several studies (Guo et al., 2019).

In this work, the application of LIBS analysis together with PLSR multivariate calibration to the real-time classification of LIB cathode was explored. 27 waste LIB from varied origins and chemistries were selected to train, test and validate the classification model. Cathode samples were extracted and analysed by ICP-OES to get reference concentration dataset. The classification model was developed in an iterative procedure including data pre-processing. The accuracy, precision and linearity of the calculated concentration values were compared in order to evaluate the goodness of the model prediction. The models that showed the best figures of merit were implemented in a sorting prototype to further validate them in a real-time application. The results demonstrated how the combination of LIBS spectra and Machine Learning algorithms could be successfully applied to the classification of cathodes early in the recycling process, as a way of improving the overall efficiency of waste LIB treatment.

2 Materials and methods

2.1 Sample preparation

A total of 27 end-of-life LIB (Fig. 1), of 5 different electrochemistries (10 LCO, 5 NMC, 1 NCO, 1 NCA and 2 LFP), including different combinations (2 LCO-NMC, 1 LCO-NCA, 4 NMC-NCA and 1 LMO-NMC), were selected. Also varied origins were considered, 2 battery cells from electric vehicle packs and 25 cells from electric-electronic portable devices, such as mobile phones, tablets, laptops or walkie talkies. In order to get cathode samples, first batteries were manually opened, electrolyte was evaporated, cathode sheets were separately extracted (Fig. 2) and, finally, pieces of about 40x70 mm were taken, one from each LIB, under strict safety measures.

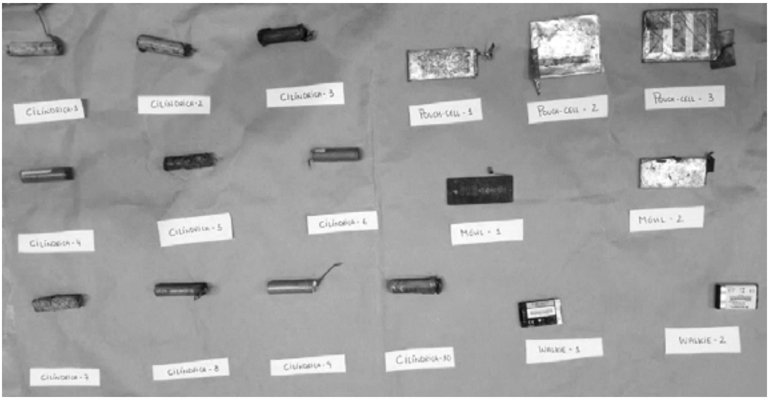

Fig. 1. Example of waste LIB used to develop the classification method

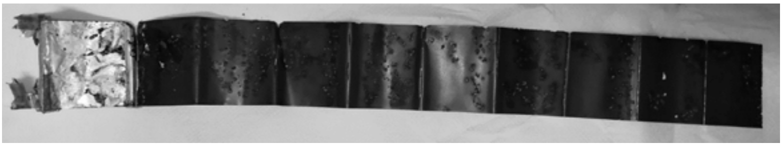

Fig. 2. Cathode from a mobile phone prismatic cell unrolled

ICP-OES (Perkin-Elmer Optima 2100 DV) with previous microwave-assisted acid digestion was applied as a reference technique for sample elemental analysis. All metals contained in cathode active materials were determined but aluminium, since current collector sheet material contaminated digested samples.

2.2 LIBS analysis

Cathode samples were analysed using a state-of-the-art LIBS system (FiberLIBS inline by Secopta Analytics GmbH), coupled with a Czerny Turner spectrometer (230.295 - 501.264 nm, CCD detector), a 1064 nm DPSS passive Q-switched laser (3 mJ pulse energy, < 1.5 ns pulse duration) and complementary standard components (mirror optics, optical fibre and external controller). The analyser is also provided with a dedicated software that includes several application modules that allow to (1) set the operational parameters and acquire spectra, (2) review and pre-process spectra, (3) develop classification models based on PLSR multivariate analysis, and (4) apply models in real-time operation to predict the class of the target materials according to their elemental composition.

The LIBS system was installed into an automated classification prototype, which directed the samples to the laser beam at 0,2 m/s. This system consisted of a conveyor belt with adjustable speed, a structure for supporting the laser head at a fixed focus distance, and a protective cover, preventing the exposure of operators to hazardous radiation. Measures were taken at 100 Hz, the maximum sampling frequency, and 2 ms integration time was used. For each measurement 10 spectra were averaged, after removing first 2 and last 2 spectra to avoid edge irregularities. Given the sample cathode dimensions, for 25 of them 3 measurements were obtained, while for the remaining 2 samples only 2 valid measurements were retained due to cathode peeling. This made a total of 79 subsamples available to build the classification method.

As can be seen in Fig. 3, overall, quite good quality spectra were obtained, characterized by well-defined peaks and low signal-to-noise ratio. Nevertheless, a drift in the baseline is observed, particularly intense in the last part of the individual spectrum, together with sample-to-sample baseline intensity differences.

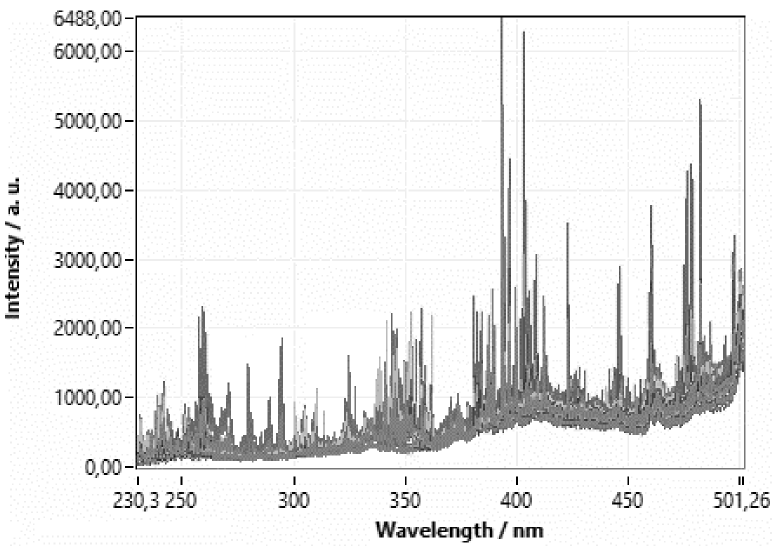

Fig. 3. Raw spectrum of the 27 samples measured using LIBS system

2.3 Classification model development

The development of the LIB cathode classification model involved iterative process characterized by sequential stages of data pre-processing, model training, deployment, and refinement.

2.3.1 Data pre-processing

First obtained spectral data base was split into training and testing sets in a 1:1 ratio (37:37). Samples were selected so that in both sets the composition of target elements covered the complete measured range. Then, raw spectra were corrected by using habitual mathematical transformations, such as normalization, baseline correction, noise filtering, and data reducing, to eliminate the multiplicative effects and reduce superfluous information introduced to the model. Best classification results were obtained by applying the Standard Normal Variate (SNV) normalization and the Piecewise Linear Approximation (PLA) baseline correction to remove multiplicative non-linear interferences and scaling problems. To apply SNV each spectrum is centred by subtracting the mean and then scaled by dividing it by its standard deviation, so that each spectrum has a mean of 0 and a standard deviation of 1. For the PLA a 20 nm window width and centred nodes were implemented for segmentation (Pedrycz et al., 2004).

Regarding dimension reduction, wavelength ranges containing the characteristic lines of the elements included in the calibration were screened, together with those in which major differences were observed (Fig. 3). As a result, the following bands were eventually removed from the analysis: 392-398, 324-328, 765-770.5, 330-363, 402-404 and 488-501 nm.

2.3.2 Classification model training

Partial least squares regression (PLSR) is a multivariate linear regression method which extracts the latent factors from the factor matrix (spectral data) that account for most of the variation in the response matrix (reference chemical composition). It is implemented by simultaneously decomposing both matrixes to exclude redundant information and find an optimized calibration model (Se et al., 2019). As a result, a linear regression is obtained as calibration function for the quantitative analysis.

The PLSR model was trained with 40 spectra subsamples and Co, Ni, Mn and Fe data, and then validated using another 37 independent subsamples. Cross-validation was parallelly implemented as an estimate of the performance of the model. The leave-one-out configuration was chosen considering the size of the dataset studied. In this approach a k-fold cross-validation is performed in which the *k* is the number of samples in the set. The optimum number of factors is that for which the Root Mean Square Error (RMSE) and the Standard Error (SE) of the cross-validation reach a global minimum, or a local minimum with less factors when low and noisy regression vector values are attained (Olivieri, 2015).

2.3.3 Classification model validation

To evaluate the prediction performance and the accuracy of each classification model the coefficient of determination (R^2), the Standard Error (SE), the Root Mean Square Error (RMSE) and the bias of the calibration, the prediction and the cross-validation were used as figures of merit. Models with highest R^2 and lowest errors were further validated by in-line applying them in the sorting prototype to the test samples.

3 Results and discussion

ICP analysis results showed that the LCO batteries contained 49-54 % Co; the NMC 9-11 % Co, 15-29 % Ni and higher variable quantities of Mn, 2-13 %; the LFP were composed of about 29-27 % Fe and 12-15 % P; the Ni content in NCA was 50 %, in contrast with 5 % Co; while the NCO had significantly high Co content, 31 %, and 21 % of Ni. The cathodes with different mixtures of active materials showed intermediate concentrations between both types of electrochemistries.

Model performance indicators are summarised in Tab. 1. The goodness of the quantification differs from one element to another. Highest linearity and lowest error figures are attained for Fe quantitation. The linearity is also significant for Co and Ni, contrasting with the low values showed by Mn. This element exhibited also high RMSE and SE, indicating wide scattering of the predictions, while attaining reasonably accurate results. In contrast, estimates for Co and Ni reveal lower accuracy and precision. Nevertheless, due to the magnitude of the differences in composition between the cathode classes quantification performance was good enough to achieve high purity sorting, as it will be shown later in this chapter.

Tab. 1: Figure of merit of the optimum PLSR model

		CALIBRATION			VALIDATION			
Element	**Factor**	**R^2**	**RMSE**	**SE**	**R^2**	**RMSE**	**SE**	**Bias**
Co	8	0.984	2.641	2.677	0.826	9.253	8.965	2.713
Fe	9	0.998	0.338	0.342	0.942	1.316	1.260	0.430
Mn	4	0.906	3.128	3.170	0.479	4.419	4.376	0.938
Ni	10	0.999	0.383	0.389	0.809	4.945	3.845	3.172

*T*o accomplish the classification based on the predicted quantities it is necessary to set the concentration ranges that define each class. To estimate this ranges stochiometric data on lithium metal oxides most habitually applied to battery cathodes (e.g., NMC 532, NCA $LiNi_{0,85}Co_{0,15}Al_{0,04}O_2$) were considered (Greenwood et al., 2021), together with analysed values, since cathode active material is composed also of variable quantities of organic binder and conductive carbon additive(s), such as graphite and/or black carbon (Hu et al., 2021). In Tab. 2 elemental concentration ranges deployed to classified LIB cathodes are gathered.

Tab. 2: Elemental composition ranges used for cathode class determination (w%)

Element	LCO	NMC	LFP	LMO	NCA
Co	> 45	> 9	≤ 0.5	≤ 0.5	> 10
Fe	≤ 2	≤ 2	> 2	≤ 2	≤ 2
Mn	≤ 0.5	> 1.5	≤ 0.5	> 0.5	≤ 0.5
Ni	≤ 0.5	> 0.5	≤ 0.5	≤ 0.5	> 0.5

Regarding classification performance, when the model was implemented in the real-time validation, 12 samples out of the 13 in the test dataset were correctly sorted (Tab. 3). This makes a success rate of 92,3%, if rating as good, for mixed chemistries, when the model properly identified one of the classes. If non mixed compositions are only considered, 8 out of 9 samples were successfully sorted, slightly reducing the classification rate down to 88,9%, which is still high. Still, the previous assumption is reasonable since extraction processes are mostly affected by elemental composition and other current macro spatial techniques for elemental analysis are neither able or struggle to determine the stoichiometry of cathodic blends (Sita et al., 2021). The only cathode that was wrongly classified was a LCO sample that was regarded as a NCA because of low Co prediction. In this study these two cathode classes were differentiated based only on Co composition, but if Al accurate data had been available for the reference samples this would have aided in distinguishing between LCO and NCA high Co content cathodes.

Tab. 3: Results for the real-time validation of the classification model

Sample No	Reference class	Predicted class
01	LCO	LCO
02	LCO-NCA	NCA
03	LCO-NMC	NMC
04	LFP	LFP
05	LMO	LMO
06	NMC	NMC
07	NMC-NCA	NMC
08	LCO	NCA
09	LCO	LCO
10	LCO-NMC	NMC
11	LCO	LCO
12	NMC	NMC
13	LCO	LCO

4 Conclusions

Due to the widespread use of LIB in e-mobility and consumer electronics, increasingly high amounts of spent batteries are being discarded. These waste streams contain relevant quantities of CRM, that, if efficiently recycled, could guarantee a secure and sustainable supply of these materials to be incorporated again in the battery value chain and assure a carbon-neutral Europe in the future. Regarding current recycling processes, a better material classification in the first steps of LIB pre-treatment could increase CRM recovery efficiency.

In this study the joint implementation of LIBS and Machine Learning is proposed to develop a real-time classification method that can sort cathode sheets before they are further ground, to avoid intensively blending different chemistries, with each other and with the anode and other battery materials. Despite the many advantages of this spectroscopic technique for multi-elemental analysis, the quality of LIBS data is usually affected by matrix and multiplicative effects. To solve this issue multivariate calibration based on PLSR is applied. Here an iterative procedure was stablished to develop an optimized quantification model, including tailored data pre-processing. Once an optimum classification model was trained and tested, it was validated in real-time application with test samples. In this trial a success rate of 92,3% was achieved, considering mixed cathodes positively identified by one of their constituents. Just one LOC sample was wrongly identified as NCA. In this point, including Al in the calibration method could improve the differentiation of high Co cathode classes.

According to the results obtained in this study it can be concluded that applied to an industrial process, LIBS technology together with Machine Learning techniques can potentially improve the separation and concentration of CRM, eventually increasing the overall efficiency of their recovery from end-of-life LIB.

5 Acknowledgments

This work was partially supported by the Basque Government through the Elkartek research and innovation program (Grant agreement no. KK-2019-00097).

References

Araujo-Andrade, C., Bugnicourt, E., Philippet, L., Rodriguez-Turienzo, L., Nettleton, D., Hoffmann, L., & Schlummer, M. (2021). Review on the photonic techniques suitable for automatic monitoring of the composition of multi-materials wastes in view of their posterior recycling. Waste Management and Research, 39(5), 631–651. https://doi.org/10.1177/0734242X21997908

Chakraborty, S., & Saha, A. K. (2022). Selection of optimal lithium-ion battery recycling process: A multi-criteria group decision making approach. Journal of Energy Storage, 55, 105557. https://doi.org/10.1016/j.est.2022.105557

Charles, R. G., Douglas, P., Dowling, M., Liversage, G., & Davies, M. L. (2020). Towards Increased Recovery of Critical Raw Materials from WEEE– evaluation of CRMs at a component level and pre-processing methods for interface optimisation with recovery processes. Resources, Conservation and Recycling, 161, 104923. https://doi.org/10.1016/j.resconrec.2020.104923

Chen, T., Zhang, T., & Li, H. (2020). Applications of laser-induced breakdown spectroscopy (LIBS) combined with machine learning in geochemical and environmental resources exploration, TrAC Trends in Analytical Chemistry, 133, 116113. https://doi.org/10.1016/j.trac.2020.116113

European Commission (2021). Critical Raw Materials Resilience: Charting a Path towards greater Security and Sustainability (COM(2020) 474). https://eur-lex.europa.eu/legal-content/EN/TXT/?uri=CELEX:52020DC0-474

Greenwood, M., Wentker, M., & Leker, J. (2021). A bottom-up performance and cost assessment of lithium-ion battery pouch cells utilizing nickel-rich cathode active materials and silicon-graphite composite anodes. Journal of Power Sources Advances, 9, 100055. https://doi.org/10.1016/j.powera.2021.100055

Guo, G., Niu, G., Shi, Q., Lin, Q., Tian, D., & Duan, Y. (2019). Multi-element quantitative analysis of soils by Laser Induced Breakdown Spectroscopy (LIBS) coupled with univariate and multivariate regression methods. Analytical Methods, 11(23), 3006–3013. https://doi.org/10.1039/c9ay00890j

Han, L., Liu, F., & Zhang, L. (2021). An Improved Sub-Model PLSR Quantitative Analysis Method Based on SVM Classifier for ChemCam Laser-Induced Breakdown Spectroscopy. Symmetry, 13, 319. https://doi.org/10.3390/sym13020319

Hu, J., Zhong, S., & Yan, T. (2021). Using carbon black to facilitate fast charging in lithium-ion batteries. Journal of Power Sources, 508, 230342. https://doi.org/10.1016/j.jpowsour.2021.230342

Jean-Noël, K. M., Arthurb, T. K., & Jean-Marcc, B. (2020). LIBS Technology and its Application: Overview of the Different Research Areas. Journal of Environmental Science and Public Health, 04(03), 134–149. https://doi.org/10.26502/jesph.96120090

Kabir, M. H., Guindo, M. L., Chen, R., Sanaeifar, A., & Liu, F. (2022) Application of Laser-Induced Breakdown Spectroscopy and Chemometrics for the Quality Evaluation of Foods with Medicinal Properties: A Review. Foods. 11(14), 2051. doi: 10.3390/foods11142051

Kappeler, M., Basler, C., Brandenburg, A., Carl, D., & Wöllenstein, J. (2022). Homogeneity Measurements of Li-Ion Battery Cathodes Using Laser-Induced Breakdown Spectroscopy. Sensors, 22(8816). https://doi.org/10.3390/s22228816

Karali, N., & Shah, N. (2022). Bolstering supplies of critical raw materials for low-carbon technologies through circular economy strategies. Energy Research & Social Science, 88, 102534. https://doi.org/10.1016/j.erss.2022.102534

Neumann, J., Petranikova, M., Meeus, M., Gamarra, J. D., Younesi, R., Winter, M., & Nowak, S. (2022). Recycling of Lithium-Ion Batteries: Current State of the Art, Circular Economy, and Next Generation Recycling. Advanced Energy Materials, 12(17). https://doi.org/10.1002/aenm.202102917

Olivieri, A. C. (2015). Practical guidelines for reporting results in single- and multi-component analytical calibration: A tutorial. Analytica Chimica Acta, 868, 10–22. https://doi.org/10.1016/j.aca.2015.01.017

Pamu, R., Davari, S. A., Darbar, D., Self, E. C., Nanda, J., & Mukherjee, D. (2021). Calibration-free quantitative analysis of lithium-ion battery (LiB) electrode materials using Laser-Induced Breakdown Spectroscopy (LIBS). ACS Applied Energy Materials, 4(7), 7259–7267. https://doi.org/10.1021/acsaem.1c01386

Pedrycz, W., Breuer, A., & Pizzi, N. J. (2004). Genetic design of feature spaces for pattern classifiers. Artificial Intelligence in Medicine, 32(2), 115–125. doi:10.1016/j.artmed.2004.01.005

Proposal for Regulation 2023/0079/COD. Establishing a framework for ensuring a secure and sustainable supply of critical raw materials and amending Regulations (EU) 168/2013, (EU) 2018/858, 2018/1724 and (EU) 2019/1020. European Parliament, Council of the European Union. https://eur-lex.europa.eu/legal-content/EN/ALL/?uri=CELEX:52023PC0160

Rifai, K., Özcan, L., Doucet, F., & Vidal, F. (2020). Quantification of copper, nickel and other elements in copper-nickel ore samples using laser-induced breakdown spectroscopy. Spectrochimica Acta Part B: Atomic Spectroscopy, 165, 105766. https://doi.org/10.1016/j.sab.2020.105766

Saldaña, G., San Martín, J. I., Zamora, I., Asensio, F. J., & Oñederra, O. (2019). Analysis of the Current Electric Battery Models for Electric Vehicle Simulation. Energies, 12(14):2750. https://doi.org/10.3390/en12142750

Se, K. W., Ghoshal, S. K., & Wahab, R. A. (2019). Laser-induced breakdown spectroscopy unified partial least squares regression: An easy and speedy strategy for predicting Ca, Mg and Na content in honey. Measurement, 136, 1–10. https://doi.org/10.1016/j.measurement.2018.12.052

Sita, L. E., da Silva, S. P., dos Santos, C. S., Parreira, P. S., & Scarminio, J. (2021). Rational analysis applied to calculate the unknown stoichiometry of Li-ternary oxides blended to Li-mono oxides in cathode material mixtures. Journal of Alloys and Compounds, 877, 160230. https://doi.org/10.1016/j.jallcom.2021.160230.

Sommerville, R., Zhu, P., Rajaeifar, M. A., Heidrich, O., Goodship, V., & Kendrick, E. (2021). A qualitative assessment of lithium ion battery recycling processes. Resources, Conservation and Recycling, 165, 105219. https://doi.org/10.1016/j.resconrec.2020.105219

Song, W., Afgan, M. S., Yun, Y. H., Wang, H., Cui, J., Gu, W., Hou, Z., & Wang, Z. (2022). Spectral knowledge-based regression for laser-induced breakdown spectroscopy quantitative analysis. Expert Systems with Applications, 205. https://doi.org/10.1016/j.eswa.2022.117756

Thompson, D. L., Hartley, J. M., Lambert, S. M., Shiref, M., Harper, G. D. J., Kendrick, E., Anderson, P., Ryder, K. S., Gaines, L., & Abbott, A. P. (2020). The importance of design in lithium ion battery recycling-a critical review. Green Chemistry, 22(22), 7585–7603. https://doi.org/10.1039/d0gc02745f

Thompson, D., Hyde, C., Hartley, J. M., Abbott, A. P., Anderson, P. A., & Harper, G. D. J. (2021). To shred or not to shred: A comparative techno-economic assessment of lithium ion battery hydrometallurgical recycling retaining value and improving circularity in LIB supply chains. Resources, Conservation and Recycling, 175, 105741. https://doi.org/10.1016/j.resconrec.2021.105741

Toro, L., Moscardini, E., Baldassari, L., Forte, F., Falcone, I., Coletta, J., & Toro, L. (2023). A Systematic Review of Battery Recycling Technologies: Advances, Challenges, and Future Prospects. Energies, 16(18), 1–24. https://doi.org/10.3390/en16186571

Weigl, D. (2022). Techno-Economic Impact of a Smart Battery Sorting System: Cooperative Research and Development. Final Report, CRADA Number CRD-21-17531. National Renewable Energy Laboratory. NREL/TP-5400-83532. https://www.nrel.gov/docs/fy23osti/83532.pdf.

World Economic Forum (2019). A Vision for a Sustainable Battery Value Chain in 2030: Unlocking the Full Potential to Power Sustainable Development and Climate Change Mitigation.

Yang, L., Xiang, Y., Li, Y., Bao, W., Ji, F., Dong, J., Chen, J., Xu, M., & Lu, R. (2023). Identification and classification of recyclable waste using laser-induced breakdown spectroscopy technology. AIP Advances, 13(7). https://doi.org/10.1063/5.0149329

Zhang, T., Tang, H., & Li, H. (2018). Chemometrics in laser-induced breakdown spectroscopy. Journal of Chemometrics, 32(11), 1–18. https://doi.org/10.1002/cem.2983

Zheng, P., Young, D., Yang, T., Xiao, Y., & Li, Z. (2023). Powering battery sustainability: a review of the recent progress and evolving challenges in recycling lithium-ion batteries. Frontiers in Sustainable Resource Management, 2. https://doi.org/10.3389/fsrma.2023.1127001

Refractory Sorting Using Revolutionizing Classification Equipment

Markus Dargel[1]*, Volker Mörkens[2], Alexander Leitner[3], Cord Fricke-Begemann[4], Reinhard Noll[5], Joachim Makowe[6]

1 LSA GmbH, Engineering, Aachen, Germany
2 LSA GmbH, Executive Management, Aachen, Germany
3 RHI Magnesita GmbH, Recycling Innovation & Technology, Leoben, Austria
4 Fraunhofer ILT, Laser Technology, Aachen, Germany
5 LSA GmbH, Senior Scientist, Aachen, Germany
6 LSA GmbH, Executive Management, Aachen, Germany

* Corresponding Author: Gewerbepark Brand 78, 52078 Aachen, markus.dargel@lsa-systems.de

Keywords: Refractory, Laser-induced Breakdown Spectroscopy (LIBS), LIBS-Sensor, Sorting, AI, CO_2-Reduction, EU-Project

Abstract

Sustainability and CO_2 reduction are becoming increasingly important. (EU 2023, Volkov et al. 2021). Technical solutions are therefore in demand, especially in the course of the current climate debate. In addition, raw material prices have been rising for years (Bragagni et al. 2021). Reducing CO_2 emissions by increasing recycling rates is therefore both ecologically and economically necessary. The EU-funded project ReSoURCE - Refractory Sorting Using Revolutionizing Classification Equipment - has therefore set itself the goal of increasing the recycling rate in the refractory industry by using advanced sensor equipment. Refractories must withstand high temperatures and stresses. Since the requirements vary widely from customer to customer and industry to industry, each application requires a unique, best-fit-lining concept. As a result, refractory materials contain a diverse mix of materials and additives. This versatile chemical composition makes subsequent

sorting or recycling complex and costly. Hence - at the present stage – recycling is only economically feasible for certain batches and grain sizes. The ReSoURCE project uses sophisticated sensors and a high degree of automation to exploit currently unusable feedstocks and finally to allow to increase the overall recycling rate. The entire recycling process is automated using artificial intelligence (AI) -assisted multi-sensor systems consisting of 3D object recognition, a LIBS sensor with an integrated 3D scanner and a hyperspectral camera. Achieving the project's goals will save up to 800 kilotons of CO_2 and 760 GWh of energy annually in the European Union. The increasing use of secondary raw materials will also decrease the need for extractive processing in the mining of raw materials, in this case saving approximately 1 million tons per year in the European Union. Two demonstrators will be set up. One demonstrator will be used to classify and sort single grains, while the second will handle and sort fine fractions. The refractory industry is not the only one to benefit from the development of this highly automated solution for classifying complex material compositions. A practically tested and validated system could be deployed in many industry sectors to significantly increase recycling rates, such as e.g., in the aluminum or steel sectors.

This project has received funding from the European Union's Horizon Europe research and innovation program under grant agreement No. 101058310 (ReSoURCE)

1 The Vision

The project aims to significantly reduce CO_2 emissions by increasing the recovery rate of refractory materials. The basis for this reduction is a fully automated sorting plant, which was developed by LSA GmbH in close cooperation with RHI Magnesita and will be made available for the project. As part of the project, measurement campaigns and adjustments to the system are being carried out with the aim of finding the best possible solution for the respective recycling applications in terms of the parameterization of the system and the design of the components used. The challenge here is the targeted use of sensor technology, which is based on a combination of several sensors, their synchronization, and the sorting technology, which must mechanically separate complex material geometries. In addition, the aim is to recycle fine material with a grain size of less than 5 mm, which cannot be recycled back into refractories to date. As a single grain, fine material can no longer be picked up by robots. The throughput of the blow-out unit would also be significantly lower. All in all, the system presented here would no longer be economically viable for sorting fines. In Demonstrator B, the fines are sorted by batch. This means that the fines are enriched rather than classically sorted.

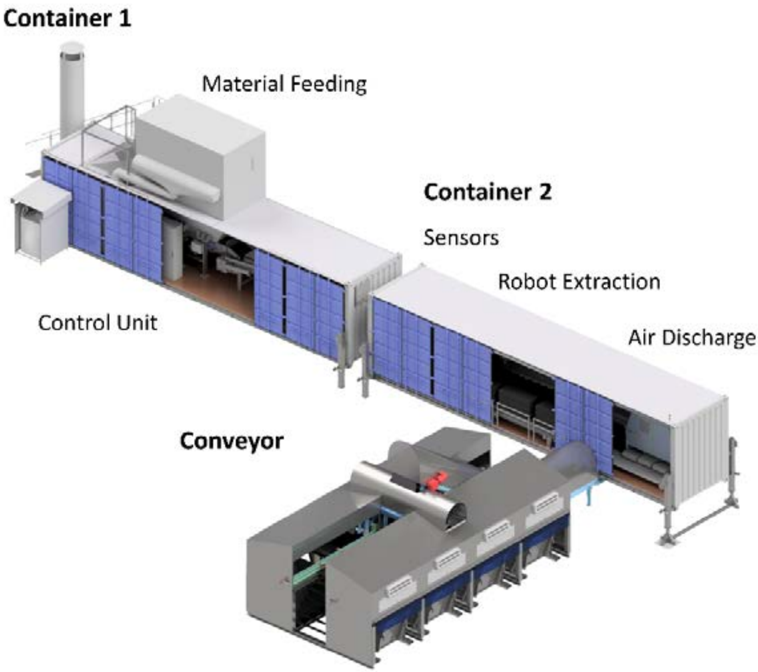

Fig. 1: 3D-CAD image of the automated processing line to identify and sort mixtures of spent refractory materials in a wide range of grain sizes.

2 The procedure

Every effort in the field of recycling must consider the economic efficiency of the process in operation. The recycling task is therefore different for every use case. For this reason, the relevant process sequences were examined for several use cases and representative material samples were procured; a key point here for refractories is the break-out character, which defines the geometry and also the composition of the material after practical use.

To achieve the project goal of reducing CO_2, a life cycle assessment and a techno-economic evaluation are carried out continuously. A holistic view of the ecological and economic situation covers the entire life cycle of the material. In this sense, the ReSoURCE project also includes an analysis of waste management, which comprises the examination of the individual waste stream collection, transportation, representative sampling, treatment, recycling, and disposal. Following this analysis, the information collected is summarized in a waste characterization report.

The sorting process is the heart of the value chain and is divided into various stages. Firstly, the fractions to be sorted must be identified and specified in detail by the end user. Concerning the sorting task, the latter essentially refers to the chemical composition. Following this specification, the detectors are selected, designed and, as a final step, integrated into the system and parameterized. This step is carried out as comprehensively as possible with regard to the sorting task, namely for as many variants of the highly diverse refractory material as possible. Different sorting tasks can sometimes mean very different chemical compositions. This not only leads to a new elemental footprint of each class. It can also lead to the use of different element lines for the evaluation of spectra. It can also mean that certain classes tend to break into larger or smaller grains when they hit the conveyor belt, which in turn affects the discharge unit. Knowing the exact nature of the feed material and the desired classes is essential to the quality of the sorting result. In addition to the synchronization of the various sensors, the design of the individual sensors is also important here. For the most accurate analysis possible, the sensors must be adapted to the material flow and microstructure, i.e. the different geometries of the objects on the conveyor belt or the coarse ceramic character must be taken into account. In the case of LIBS analysis, this means adapting the laser focus in real time; in the case of HSI cameras, it means adapting the camera optics.

3 The System

The entire automated processing line can be divided into three sub-areas. These individual assemblies each have a defined purpose and are explained below. The order of the individual assemblies in this text also represents the sequence of the material flow.

3.1 Feeding Unit

The feeding unit is housed in a CSC-certified overseas container. Doors and service panels are also provided across the full width of the hopper to allow for potential intervention and troubleshooting at any point in the process. This allows maximum mobility, allowing the system to be used anywhere in the world. Material is fed into the system from a hopper at the start of the process. It can be fed by a wheel loader or forklift and big bags. The material is then transported out of the hopper and separated. In addition to material handling, the bunker contains the necessary components such as compressed air generation and filtration. To prevent potential problems with dust pollution or environmental contamination, air is extracted at various points throughout the process and filtered. The filtered dust is then stored in big bags and emptied at defined intervals. The filtered air is released into the environment via a chimney fitted with silencers to prevent noise pollution. In addition, the entire containers are insulated and equipped with heaters to ensure safe operation in winter.

Figure 2 below shows the feeding unit. Starting from the left, one can see the chimney for discharging the filtered air, the container with a walk-on platform and the Big Bag for collecting the separated dust.

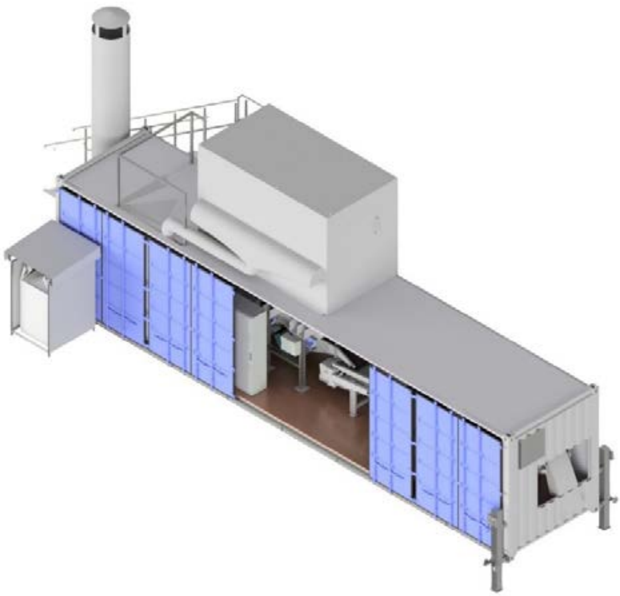

Fig. 2: 3D-CAD image of the feeding unit.

3.2 Sorting Unit

The sorting area is housed in an overseas container as well. Accessibility to the sorting container is important because of the sensor technology housed. In the event of a fault, all critical components must be easily accessible. The material is first passed under the measuring bridge. In this measuring bridge, the 3D topology of each sample on the belt is first determined. The samples are then analyzed with two different sensors. A hyperspectral camera captures the entire surface of the samples and automatically generates spectra of the measured data. A surface that is perpendicular to the laser is selected based on the 3D topology and the laser beam for the LIBS measurement is focused on the surface using a 3D scanner. Depending on the material, a different number of measurement points is set. These measurement signals are also converted into spectra in a spectrometer. With the help of AI, a chemical fingerprint can be obtained from each measured sample and assigned to the various material classes on this basis. The entire data gathered will be merged with the HSI data using AI to enable the samples to be analyzed as comprehensively as possible. The material is afterward sorted by three delta robots into intermediate collection bins. These bins are assigned to individual product classes by a measuring program. Smaller grain sizes are sorted by air discharge at the end of the belt.

A close-up of the Sorting Container is shown in Figure 3 below. The doors for maintenance purposes, the collecting bins and the air discharge unit are clearly visible.

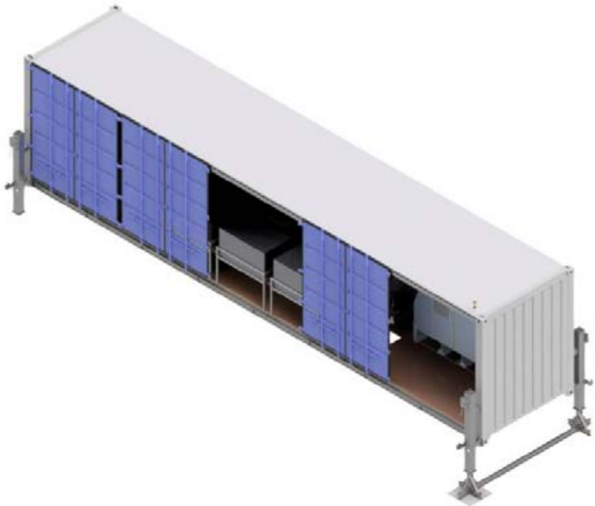

Fig. 3: 3D-CAD image of the sorting unit.

3.3 Conveying Unit

The conveyor unit distributes the individual product classes into large containers that can be emptied by forklift or front wheel loader. Up to eight different classes can be sorted.

A drawing of the conveying unit is shown in Figure 4 below.

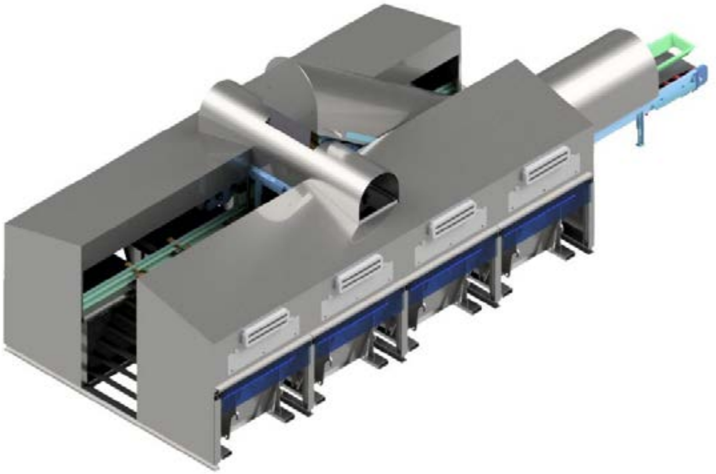

Fig. 4: 3D-CAD image of the conveying unit.

4 Conclusion and Outlook

The sorting plant design has been finalized and is currently under construction. The first LIBS measurement results are promising with regard to the finest possible classification of the material. In addition to the Demonstrator A presented here, the Demonstrator B for fine materials is being further developed. The combination of both systems can have a significant impact on CO_2 emissions in the refractory industry. In the future, the plant will also be further improved in terms of throughput. The project is already providing insight into which components can be considered bottlenecks and how to ensure greater scalability.

5 Acknowledgements

The project is funded in the European Union’s Horizon 2021 research and innovation programme under grant agreement No 101058310.

References

Reducing carbon emissions: EU targets and policies; European Parliament News Article; October 2023; https://www.europarl.europa.eu/news/en/headlines/society/20180305STO99003/reducing-carbon-emissions-eu-targets-and-policies

Volkov Husović, T., Simić, M., Martinović, S.,& Vlahović M. (2021); Recycling refractories for steelmaking processes; in Proceedings book - 2nd International Conference „The Holistic Approach to Environment“, May 28th, 2021, Virtual conference; Association for Promotion of Holistic Approach to Environment., 642-652; https://hdl.handle.net/21.15107/rcub_cer_5945

Bragagni Esq Obe, Maurizio & Xhaferraj, Lorenc. (2021). RAW MATERIAL PRICES INCREASE. 10.13140/RG.2.2.10320.43526.

Laser-Induced Breakdown Spectroscopy (LIBS) for Aluminium Alloy Sorting: A Journey from Research to Industry

Frank van de Winkel[1]*

1 TOMRA Sorting GmbH, Market Strategy, Metal, Mülheim-Kärlich, Germany

* Corresponding Author: Otto-Hahn-Straße 2-6, 56218 Mülheim-Kärlich, frank.vandewinkel@tomra.com

Keywords: LIBS, Aluminium, Alloys, Recycling, Scrap

Abstract

Laser-Induced Breakdown Spectroscopy (LIBS) is a powerful analytical technique that has evolved over the years to become a valuable tool for material analysis and sorting. This article explores the working principle of LIBS and its application in sorting aluminum alloys, tracing its development from early research projects to its current use in industrial scrap sorting.

LIBS utilizes a high-energy laser pulse to create a plasma on a material's surface. This plasma emits light as it cools, and this light contains information about the material's elemental composition. By analyzing the emitted light's spectral lines, researchers can identify and quantify the elements present in the sample, making LIBS an excellent tool for material analysis and sorting.

Aluminum alloys are widely used in various industries. Once turned into scrap, it is crucial to sort them accurately based on their composition for aluminum recycling. LIBS has proven to be an effective method for this purpose. The distinct elemental signatures of different aluminum alloys enable precise identification and separation, facilitating aluminum recycling, and ensuring material quality within scrap materials.

Development times for a new sorting technology can vary significantly based on complexity, available resources, and market demand. Simpler sorting methods may take a few months to years to develop, especially if there's high market demand for a particular solution. More advanced technologies, such as those incorporating sophisticated sensor technology like LIBS detection, might require several years of research, prototyping, and real-world testing due to their complexity. The development of LIBS based sorting for the scrap industry took more than two decades:

1 2002 – Research Project SILAS:

The journey of using LIBS for aluminum alloy sorting began in 2002 with the SILAS ("Schnelle Identifikation von Leichtmetallen mittels Automatischer Sortierung", Innonet Projekt) research project. Partners in this project – amongst others – were RWTH Aachen (former Department for Processing and Recycling [I.A.R.]), Fraunhofer Institute for Laser Technology (ILT) and TOMRA. This early effort laid the foundation for understanding the feasibility of using LIBS for sorting aluminum alloys.

2 2007 – Research Project LASORT:

Building upon the insights from SILAS, the LASORT project in 2007 aimed to refine the LIBS-based sorting process. Researchers focused on improving the speed and accuracy of alloy identification, making strides towards a practical sorting solution.

3 2010 – Research Project PARILAS:

The PARILAS project in 2010 marked a significant milestone in LIBS-based sorting. It aimed to optimize the LIBS system for industrial use, making it robust and reliable for continuous sorting operations.

4 2018 – TOMRA's Own Development:

In 2018, TOMRA embarked on its independent development of sorting machines for the scrap market, leveraging the advancements made in LIBS technology over the years. These machines now provide a solution for the recycling industry, allowing efficient sorting of aluminum alloys based on their composition.

The evolution of LIBS from early research projects like SILAS and LASORT to its integration into industrial sorting machines by TOMRA demonstrates the success of scientific innovation in practical applications. LIBS has proven to be a game-changer for the aluminum recycling industry, enabling precise sorting of alloys, promoting sustainability, and reducing waste. As technology continues to advance, LIBS-based sorting methods are likely to become even more efficient and widespread in various material sorting applications, contributing to a greener and more resource-efficient future.

Fast Inline Analysis of Aluminum with LIBS for High Precision Recycling

Dr. Christian Bohling*, Dr. Cassian Gottlieb, Andreas John,
Dr. Jens-Uwe Günther, Daniel Roessink, Amit Ahsan

SECOPTA analytics GmbH, Teltow, Germany

* Corresponding Author: Geschäftsführender Gesellschafter,mSECOPTA analytics GmbH, Rheinstrasse 15b, 14513 Teltow, Germany

Christian.bohling@secopta.de

Keywords: LIBS, elemental analysis, aluminum, recycling, inline analytics, chemometrics, artificial intelligence

Abstract

In recent years precise elemental analysis based on Laser-Induced Breakdown Spectroscopy (LIBS) has found its way from the laboratory into industrial applications. The availability of long-term stable and cost-effective laser beam sources, as well as high computing power for data analysis in real-time, enable applications such as sorting and control technology that were not possible a few years ago. In particular, the availability of fast evaluation algorithms as a combination of chemometric methods and artificial intelligence allows the use of LIBS as precise and long-term stable analysis devices in industrial inline applications.

Due to the large energy savings (up to 95%), the recycling of aluminum is an important step towards conserving resources. Especially in the field of aluminum alloy analysis, LIBS has advantages over other methods (e.g. XRF). Even light alloying elements can be analyzed quickly and precisely with LIBS. Recycling at the same step of the value chain is crucial for the realization of closed raw material cycles. Downcycling and increasing contamination by interfering elements in the material flow must be avoided.

Three solutions for the recycling of aluminum based on LIBS will be presented during the talk:

- Precision recycling into many subclasses
- Scrap sorting with high throughput
- Fast inline analysis of molten aluminum

Al recycling without downgrading requires a much higher purity of secondary raw materials. Contamination of the melt with unwanted or outright detrimental elements (e.g. Li) is a huge liability requiring costly dilution with clean raw materials, or in the worst case even rendering the entire melt useless. Therefore, the goal is to fine-grain sorting of the scrap metals to feed only such scrap metals back into melting which is close to the target melt. In this regard, the current state-of-the-art sensing techniques fall short in terms of analyzing alloying elements in the main metal mix. SECOPTA-developed MopalLIBS sensor with pre-ablation capabilities allows high purity sorting of Al into the main classes (1000-7000) as well as their subclasses. Thus allowing control over quality assurance and process efficiency while eliminating feed materials with detrimental elements that could contaminate the melt beyond tolerances. With high throughput and precise sorting of the feeding material (scrap, mix alloys), the customer is expected to save approx. **300 Eur/t** from process benefits.

In terms of inline melt analysis, the goal is to achieve the target melt composition as fast as possible. In this field, SECOPTA MeltLIBS sensor has been successfully implemented in a famous Al remelter facility in Austria to measure liquid Al melts at 600 degree. Positioned directly on the top of the furnace, it monitors alloying elements (e.g. Mg, Mn, Fe, Si, Cu, Zn) and report melt composition directly to the level 2 system. This allows for electing the proper corrective measures in the shortest time and achieving target melt composition as fast as possible. Additionally, it saves resources and time by omitting conventional spark analysis. With all the resulting process benefits customer has roughly estimated the amortization of the device within **less than 1 year**.

Precision Ore sorting System

Voloshyn Volodymyr[1*], Kulyk Yevhen[1], Denys Gryshan[2]

[1] LLC "SPE "Gamayun", CEO, Kryvyi Rih, Dezhneva lane 1A, Ukraine

[1] LLC "SPE "Gamayun", Technological department, Kryvyi Rih, Dezhneva lane 1A, Ukraine

[2] OFZ, a.s., Oravský Podzámok, Široká 381, Slovakia

* Corresponding Author: Kryvyi Rih, Dezhneva lane 1A, Ukraine 50000, vivatsteps@gmail.com

Keywords: paramagnetic ores, precision measurements, sensitivity, accuracy, digital processing.

Abstract

It concerns the sorting of paramagnetic ores. A special feature of the development is the processing of weak useful electrical signals from paramagnetic ores, which makes the problem of suppressing industrial electromagnetic interference to be relevant. Here is why the sorting system is called precision ore sorting system.

1 Introduction

Leading manufacturers of ore sorting equipment, such as TOMRA and STEINERT, are successfully developing in the strategic direction of using universal multisensory technologies. The Gamayun Company follows the well-known axiom that there is no single effective and universal technology for all types of ores. In this regard, the Company decided that it could compete with them by developing only individual sensor systems.

A wide range of technical solutions for the preliminary enrichment of ores is known (Tsypin, 2015). However, there are a number of difficult-to-enrich ores, such as iron-manganese (Mazhanov et al., 2021), ores with a very low concentration of useful components, which can only be enriched by indirect methods (by correlation with certain minerals) and others. For such mineral resource, it is advisable to develop special, narrowly targeted methods.

2 Method

The Company has analyzed a group of known sorting methods based on measuring the volumetric content of a useful component in a piece of ore, not just the part of component, visible on the surface of the piece. These are technologies based on X-ray transmission (XRT), thermal infrared spectroscopy (TIR) and others. The Company chose the electromagnetic (EM) technology because it has the greatest potential for development. Firstly, this method is one of the “oldest” used in sorters, and secondly, it can be significantly improved if to use it in combination with modern IT technologies and data processing.

Thus, the 3D-EM method was developed, in which the 3D laser is the controlling system, and the matrix of induction sensors of the EM system is the one which is controlled. Both systems operate in a consolidated manner, controlled by a main computer, which generates controlling operations based on two data arrays: the topology of the matrix of location the induction coils in the sensor block and the current geometric parameters of moving monolayer of fractionated raw materials. The method provides extremely high sensitivity and accuracy in measuring the parameters of pieces of ore, containing paramagnetic minerals, while working with high productivity in wide size classes.

2.1 Sensitivity

High sensitivity of the system of separation of lump ore mass with weak magnetic susceptibility of separating minerals is ensured due to:

- the use of special topology of matrix of induction coils, which parameters as well as electromagnetic parameters of the coils, are stored in the main computer;
- the use of 3D laser to create an array of initial data in order to identify each piece of ore mass according to the criterion of the coordinates of the geometric centers of the pieces relative to the centers of system of coils of the sensor block;

- the process of measuring of magnetic susceptibility of pieces is based on the pulse method, herewith the data array of 3D laser is the controlling one, on the basis of which the management of measurements is being fulfilled for individual sensors of the matrix;
- the measurement process is ensured by activating only one coil, located in a zone of absence of mutual influence from neighboring coils;
- each precision measurement operation is the result of subtracting the signal from a piece of ore and the electromagnetic background signal measured by the same coil in the absence of a piece;
- to reduce the electromagnetic background, the original algorithms of digital processing are implied, separately for the low-frequency and high-frequency sections of the noise spectrum;
- the measurement ends with the start of the auto generator and the formation of impulse, the duration of which is proportional to the magnetic susceptibility of the piece;
- then the generated impulse is filled with ultra-high frequency pulses, the number of which is a quantitative assessment of the magnetic susceptibility of a piece of paramagnetic ore.

2.2 Accuracy

High accuracy of magnetic susceptibility measurement is ensured by introducing correction functions on the measured value of the magnetic susceptibility parameter:

- the function of adjusting the measurement depending on the actual volume of the piece - is implemented according to a monotonically decreasing correlation to the measured volume of the piece, with normalization to the volume of the piece, which meets the maximum size;
- the function of adjusting the measurement depending on the deviation caused by the fact that the actual coordinates of the geometric center of the piece do not coincide with the coordinates of the center of the induction coil - is implemented according to a monotonically decreasing dependency to the

measured deviation, with normalization to the geometric location of the ideal coincidence of both centers;

- function of adjusting the measurement of dependency from the angle, formed by the lines: the geometric location of the longitudinal axis of the piece and the measuring axis of the coil;
- function of adjusting the measurement depending on the features of the geometric shape of a piece of ore.

2.3 Productivity

High productivity is already conditioned by use of function of adjustment based on the volume of the piece, which ensures the operation of the sorting system in a wide range of size fractions of ore pieces. An additional operation that provides a significant increase in productivity is an increase in the specific density of pieces location (their number per unit of area of the conveyor belt) by controlling the moment of activation of the coils.

3 Functioning of the 3D-EM method

The main computer contains necessary information on the topology of the sensor block according to Figure 1. High sensitivity of measurements in conditions of fluctuating electromagnetic interferences is achieved as the difference between two signals (the maximum from the measurement of the piece and the minimum from the measurement of the electromagnetic background) according to the formula:

$$\Delta U = U_s - U_b \qquad (1)$$

where:

U_s - maximum signal from measuring a piece of ore;

U_b - interference signal measured on the belt in the absence of the measured piece.

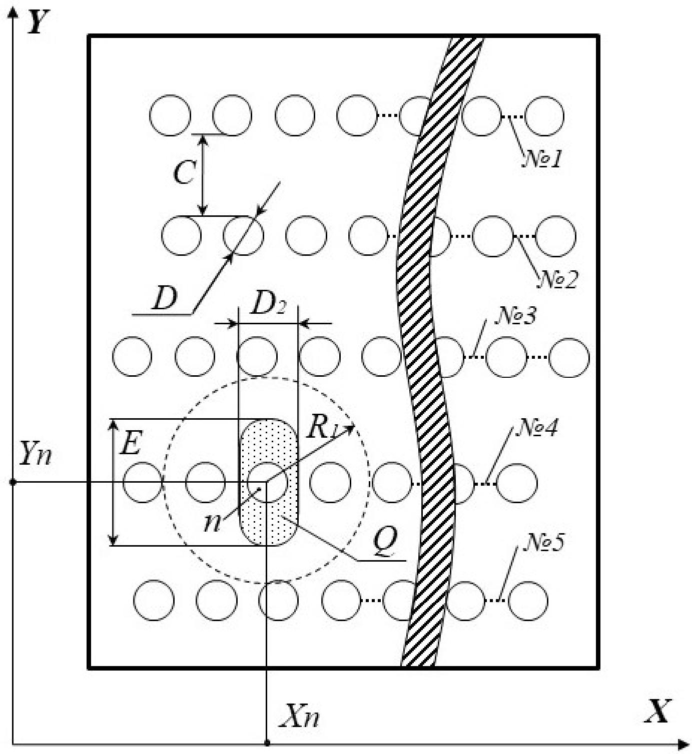

Fig.1. Geometric parameters of the matrix of placing induction coils in the sensor block.

The calculated coordinates of the geometric parameters of the pieces of ore in correlation to their spatial orientation relative to the coils using the example of an i-piece and a measuring n-coil are shown in Figure 2, which is a fragment of Figure 1. In this case, the signal consists of the sum of the influence of three factors:

$$U_b = U_c + U_l + U_e \qquad (2)$$

where:

U_c - a signal conditioned by the electromagnetic influence of other coils located near the *n*-coil, located in the same row within the radius R_1;

U_l - a signal conditioned by the influence of the magnetic properties of other pieces located near the *i*-piece within the *Q* zone;

U_e - a fluctuating interference signal, the spectral characteristic of which consists of low-frequency and high-frequency sections of the spectrum.

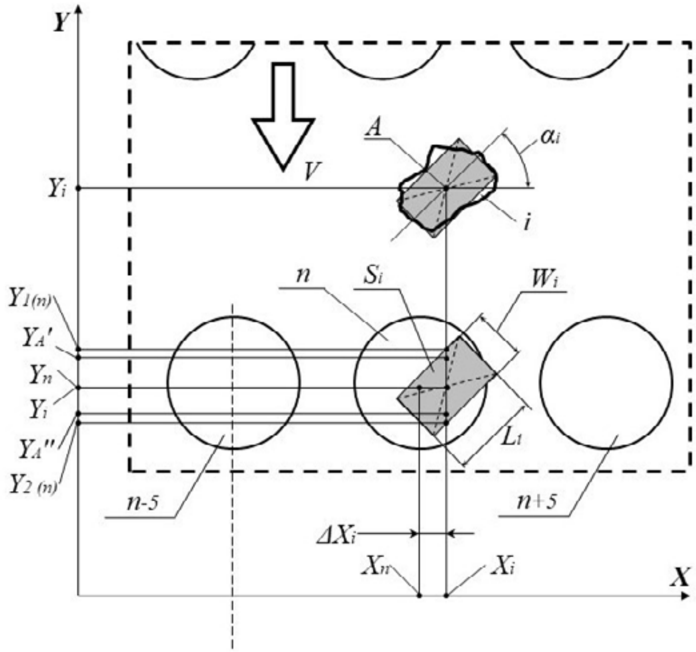

Fig. 2. Coordinates of the geometric parameters of the i-piece of ore when meas-ured by the n-coil.

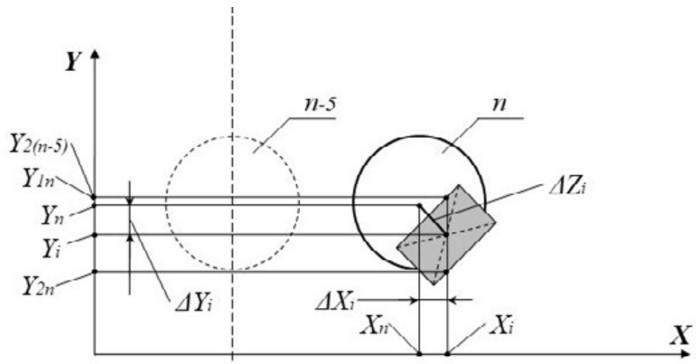

Fig. 3. Coordinates of the activation delay for the n-coil when the target control task is introduced.

When measuring the level of background U_b , for minimal influence of electromagnetic factors U_c and U_l , the following empirical conditions must be ensured:

U_c - there are no other activated coils within the radius $R_1=(D/2+C)$;

U_l - The measurement is being carried out within an area of area Q, which is formed by the movement of the conveyor belt above n-coil (Fig. 1), taking into account the active diameter of coil $D_2=1{,}3\times D$ (in this case, in the area of Q, except for the piece being measured, there should be neither any other whole piece of ore nor part of it)

For minimal influence of the low-frequency component U_e, the time between measurements of signals U_s and U_b should be minimal. For that, several measurements of U_b are performed along the coordinate x_n over the duration of segment ***E*** with coordinates from $Y=Y_n+(D+C)/2$ to $Y=Y_n-(D+C)/2$, while for calculations using formula (2), it is accepted the smaller of several measured background values.

For minimal influence of the high-frequency component U_e, a method of its suppression was used using an exponential filter. Its sense is to smooth out peak interference values with special digital signal processing algorithms.

The measurement of U_s signal is performing relative to the *n*-coil measuring axis with coordinate Y_n. An *i*-piece with a variable coordinate Y_i of the geometric center ***A*** moves along a constant coordinate X_i. When it reaches the position $Y_i=Y_{(1(n))}$, the *n*-coil is getting activated, which ends after a time τ_n when the position $Y_i=Y_{(2(n))}$ is reached. The total duration τ_n is functionally distributed into temporary operations: direct measurement $\Delta t=(Y'_A-Y''_A)/V$, starting the auto-generator $\Delta t_1=(Y_{1(n)}-Y'_A)/V$ and stopping the auto-generator $\Delta t_2=(Y''_A-Y_{(2(n))})/V$. The duration of the measurement depends on the size of the piece and the number of pieces per unit area of the belt. In addition, determining the value of Δt is an optimization problem, since its maximum value allows us to obtain maximum sensitivity of the system, and its minimum value allows us to obtain maximum productivity. The range $\Delta t=0{,}3\text{-}2{,}5$ milliseconds has been established empirically.

High measurement accuracy is achieved by introducing a number of empirical correction coefficients ***K*** for the measured signal U_s:

K_1 - provides compensation of geometric size of the piece F_i by correcting U_s according to a monotonically decreasing function depending on its size in the range F_{max}-F_{min}. The sense of the correction is as follows. Let us assume that two pieces of maximum sizes F_{max} and F_{min} contain the same mineral composition and are alternately placed at the same point (for example, $X_i=X_n$) on the measuring axis Y_n of the n-coil. In this case, the measured signal U_s for F_{min} will always be smaller than for F_{max}, although they consist of the same minerals. This fact can lead to an error in deciding on a piece (useful or waste). To compensate for a possible error, a correction coefficient K_1 is introduced:

$$U_{s(1)}=K_1 \times U_s$$

where: $K_1= f(F_i)$ – coefficient of a monotonically decreasing dependence on the size of the i-piece, its rationing is made to F_{max}.

K_2 - provides compensation of the output signal U_s of the sensor according to a monotonically decreasing function depending on the deviation of the geometric center of the piece from the center of the coil. The meaning of the correction is as follows. Suppose that the same piece is alternately placed at two different points with coordinates (for example, X_n and $X_n+\Delta X_i$) on the measuring axis Y_n. In this case, the measured signal is U_s for the coordinate $X_n+\Delta X_i$ will always be smaller than for the coordinate X_n, although the same piece is involved in the measurements. This fact can similarly lead to an error in making a decision on a piece. To compensate for a possible error, a correction coefficient K_2 is introduced:

$$U_{s(2)}=K_2 \times U_s,$$

where: $K_2= f(\Delta X_i)$ – coefficient of a monotonically decreasing dependence on the deviation of the geometric center of the *i*-piece from the center of the *n*-coil, its rationing is made to the position of the piece in coordinates $X_i=X_n$.

K_3 - provides compensation of the output signal U_s of the sensor according to a monotonically decreasing function depending on the angle α_i of inclination of the axis of the longitudinal dimension of the length L_i of the piece to the measuring axis Y_i. To compensate for a possible error from the geometric location of the piece, a correction coefficient is introduced K_3:

$$U_{s(3)}=K_3\times U_s$$

where: $K_3 = f(\alpha_i)$ - coefficient, which is a function of the angle $\alpha_i = |0° \pm 90°|$, its rationing is made from the position of the piece at $\alpha_i = 90°$.

K_4- provides compensation for the output signal U_s of the sensor depending on the features of the planar shape of the piece (the ratio of the length L_i and the width W_i of the piece) with an area S_i – const:

$$U_{s(4)}=K_4\times U_s$$

where: $K_4 = f(L_i/W_i)$, its rationing is made in the form of a piece, corresponds to a square $L_i = W_i$.

K_5 - provides compensation for the output signal U_s of the sensor depending on the characteristics of the volumetric shape of the piece (the ratio of the height H_i of the piece to its area S_i) with a volume V_i - const:

$$U_{s(5)}=K_5\times U_s$$

where: $K_5 = f(H_i/S_i)$, its rationing is made in the form of a piece, corresponds to a cube $L_i = W_i = H_i$.

The coordinates, size and shape of the *i*-piece in relation to the *n*-coil are random, and therefore the formula for the corrected sensor signal U'_s in the general case has the form:

$$U'_s = f(K_1, K_2, K_3, K_4, K_5) \times U_s \qquad (3)$$

High productivity is already conditioned by operation of the sorting system in a wide range of $Fmax$ - $Fmin$ piece sizes. An additional operation that provides increased productivity is the introduction of an additional shift along the Y axis of the moment of activation of the n-coil with subsequent additional correction of the K_2 coefficient. The essence of the operation is illustrated in Figure 3. Namely, with an increase in the number of pieces per unit area of the conveyor belt, the likelihood of a situation increasingly arises where, if it is necessary to activate the n-coil, for example the $n - 5$ coil is still in the active state. Simultaneous activation of both coils in a zone of radius R_1 leads to a violation of the condition for the parameter U_c of formula (2). In this case, the requirements of the condition for U_c are saved as follows. To maintain the condition for U_c, the active modes of n and n - 5 coils must be separated in time. Suppose the n - 5 coil at coordinate $Y_{2(n-5)}$ is already becoming deactivated. In this case, the n-coil must begin its activation process only at the Y_{1n} coordinate. In this regard, the geometric center of the i-piece turns out to be artificially shifted by the coordinate segment ΔY_i, while the deviation ΔX_i of the i-piece radially increases and takes on the absolute value ΔZ_i. Additional artificial operation entails a repeated correction of the K_2 coefficient:

$$K_2' = f\,(\Delta Z_i\,) \qquad (4)$$

where: $\Delta Z_i = \sqrt{\Delta X_i^2 + \Delta Y_i^2}$.

Thus, in the 3D-EM system, the following technological parameters have been achieved. The sensitivity of magnetic susceptibility reaches $\chi \sim 10^{-6}$ SI units. The measurement accuracy provides high resolution for the separated minerals (magnetic susceptibility contrast is $\geq 2{,}5$ relative units). And the range of sorted fractions is +10...-80 mm.

4 Equipment

The MLS equipment is produced in a modular design and assembled in 20-foot sea containers. Figure 4 shows a fragment of the layout of technological units inside the container. Such containers are especially relevant in mountainous and inaccessible locations. The structures can be used in both mobile and stationary versions. In each case, there is an individual configuration of the location of block structures. It is also possible to design stationary pre-concentration factories for high productivity, which is ensured using several units of MLS.

Fig. 4. Layout of technological units inside the container.

5 Orientation on preferred mineral resource

The precision 3D-EM sorting system has new qualities: extremely high sensitivity, high measurement accuracy and high productivity. The use of these qualities makes it possible to involve in the processing process a number of types of ores with weak magnetic susceptibility of constituent minerals, which were previously either not enriched at all, or the results of their enrichment were not effective:

The ores containing minerals with similar atomic masses, the sorting of which requires a tool with very high accuracy (resolution), for example, ferromanganese ores of massive texture.

The ores with an extremely low concentration of a useful component, which is correlated with non-magnetic or weakly magnetic separable minerals, for example, thin gold deposited in deposits with narrow quartz veins.

The ores containing separable minerals with a low atomic mass of the useful component, for example, this is a mineral resource for which X-ray methods show insufficient efficiency.

The rare earth metal (REM) ores, in which the useful component is correlated with the disseminated or vein texture of minerals dislocated in acidic or ultra-acidic waste rocks, the sorting of which requires an instrument with extremely high sensitivity, for example, rare earth metals in pegmatite ores. An example of a pegmatite vein occurring in granitoids is shown in Fig. 5.

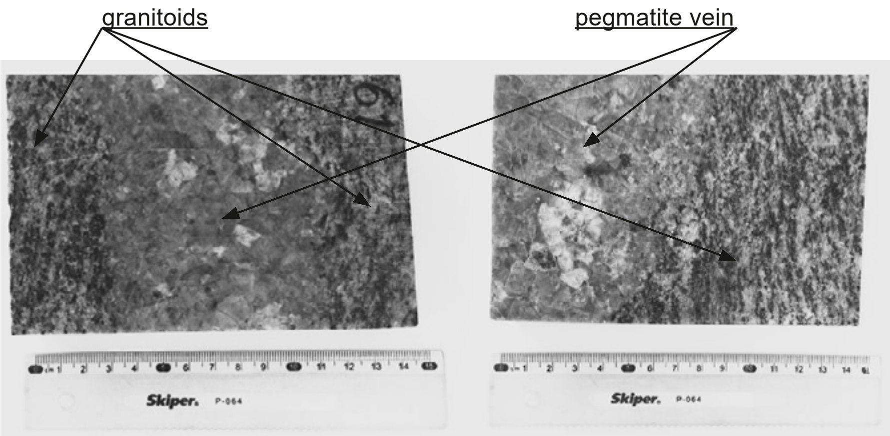

Fig. 5. Photo of a pegmatite vein located in granitoids.

6 Conclusion

The development that we offered is positioned by us as the theme of the conference “Development of sensor technologies”. The development is based on the 3D-EM method, which is a highly sensitive instrument with high resolution. The method is geared to precision sorting of ores containing minerals with weakly magnetic properties. The materials in this article explain the physical processes which are the subject of the development of the Company’s original software products.

References

Tsypin, E.F. (2015). Enrichment in the stages of ore preparation: Scientific monograph. Ural State Mining University (UGGU) Publishing House. 303.

Mazhanov, O.M., Evtekhov, V.D., Demchenko, O.S., Voloshyn, V.M., & Kulyk, O.M. (2021). Mineralogical justification for potentiality of producing marketable hematite products. Journal of Geology, Geography and Geoecology, 30(2), 334-343.

Optimized recycling of coarse fraction from copper alloy production residues using a XRF chute sorting system

Max Kölking[1*], Martin Jacob[1], Sabine Flamme[2],
Stefan Heinrichs[3], Nico Schmalbein[3]

1 Siegfried Jacob Metallwerke GmbH & Co. KG, Technology Development, Ennepetal, Germany
2 Institute for Infrastructure, Water, Resources and Environment, FH Münster - University of Applied Sciences, Münster, Germany
3 STEINERT GmbH, Köln, Germany

* Jacobstraße 41-45, 58256 Ennepetal, m.koelking@jacob-metall.de

Keywords: Copper, Copper alloys, Resource efficiency, X-ray fluorescence sorting systems, Foundry residues, Sorting by alloy specific components, Non-ferrous metal recycling, Life cycle assessment

Abstract

Byproducts from copper alloy production, such as dross, contain high amounts of valuable metals. Currently, the recovered coarse fraction of the dross requires an energy- and cost-intensive refining process due to its complex composition. This paper demonstrates that advanced sorting of the coarse fraction prior to the metallurgical stage using an industrial X-ray fluorescence chute sorting system can contribute to a more efficient recycling.

1 Introduction

With rising demands of copper and copper alloys for the renewable energy transition and electromobility (Elshkaki et al., 2016), the need for copper recycling is surging. The production of copper alloys such as brass, bronze and red brass generates valuable byproducts, such as dross, that are currently not sufficiently recycled. Dross contains proportionally high amounts of usable metals bound in metallic parts and in oxidized form (Hillmann & Lüning, 2023). In order to recover these valuable components and to separate the metallic parts and the non-metallic/ oxidic parts, the dross is usually processed by mechanical processing techniques, e.g. by crushing/ball milling and screening (Kilicarslan et al., 2014). However, the metallic coarse fraction removed by screening often consists of copper alloys from several melts and therefore must undergo extensive refining processes in which the alloying elements are lost (Schlesinger et al. 2022). An alternative approach is to **s**ort the material **b**y its **a**lloy **s**pecific **c**omponents (SBASC) to return the alloys to the original material cycle by remelting. SBASC requires a material differentiation based on chemical composition which is possible using spectrometric techniques, such as X-ray fluorescence (XRF). Using industrial XRF sorting systems for copper-based materials is not yet common practice. For this reason, this study investigates the potential on a mixed coarse fraction in large-scale trials. In addition, a comparison with the current refining scenario in terms of resource efficiency and environmental impact is made to identify the best available technique.

2 Sorting trials

A four-ton sample of a mixed coarse fraction with a grain size of 10 to 32 mm (image of the material in Fig. 1) was used for sequential sorting trials.

Fig. 1. Sample of the coarse fraction (10-32 mm)

After pre-sorting the material by magnetic and eddy current separation, the SBASC was carried out in several subsequent stages using an XRF chute sorting system (STEINERT CHUTEC® CSS 140 XF L) with upgraded classification software for copper-based material. As shown in Fig. 2, seven relevant sorting products were recovered in varying proportions.

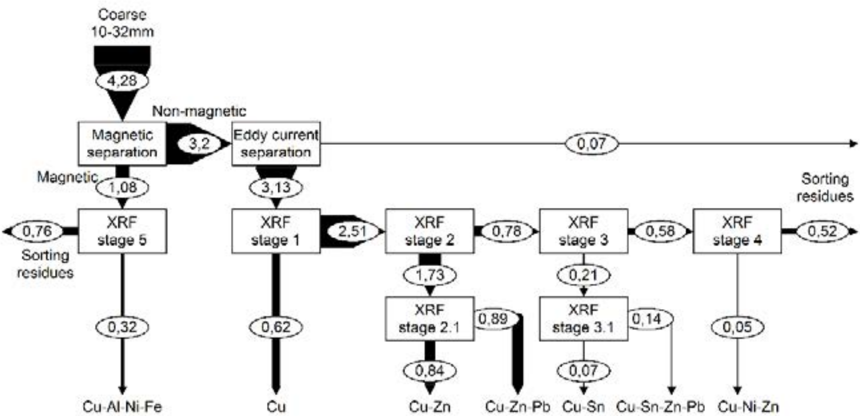

Fig. 2. Sorting stage order and mass flows (in tons) of the large-scale trials

The analysis results in Tab. 1 show that the characteristic alloying elements were successfully enriched in the products intended for remelting. In addition, a high purity copper product (>98% Cu) could be recovered.

Tab. 1: Composition of the sorting products (relevant elements are highlighted)

Sorting product	Chemical composition in (%)							
	Sn	Pb	Zn	Cu	Ni	Fe	Mn	Al
Cu-Al-Ni-Fe	0.10	0.08	0.57	**82.45**	**3.86**	**4.28**	0.81	**7.64**
Cu	0.40	0.27	0.43	**98.34**	0.19	0.07	0.02	0.11
Cu-Zn	0.26	1.35	**32.23**	**65.26**	0.14	0.19	0.09	0.14
Cu-Zn-Pb	0.60	**2.18**	**31.05**	**65.11**	0.19	0.28	0.12	0.18
Cu-Sn	**3.98**	**1.05**	**1.62**	**92.26**	0.68	0.06	0.01	0.09
Cu-Sn-Zn-Pb	**4.93**	**5.84**	**4.60**	**83.44**	0.62	0.09	0.02	0.17
Cu-Ni-Zn	0.63	0.91	**17.62**	**71.95**	**7.28**	0.29	0.41	0.56

Despite the overall good sorting performance, remelting the sorting products still requires different levels of dilution by the addition of virgin material or clean new scrap to meet alloy specifications. An example is the excess Pb content of 0.08% in the Cu-Al-Ni-Fe product, which is often limited to 0.03% for copper-aluminium alloys and thus must be lowered. In this context, there are some general physical limitations that need to be considered. Apart from the specific properties of the coarse fraction, excessive element contents could have been caused by misclassified and falsely sorted alloys. As the XRF sorter is designed for high throughput sorting, only short measurement times (<10ms) are possible, resulting in the elements being detected with less accuracy than, for example, when using a handheld/stationary spectrometer. Another limitation that can also affect detection accuracy and the sorting result is the air gap between the X-ray unit and the material being analyzed.

3 Environmental assessment

To make a scientifically based statement about whether the use of a XRF sorter is more resource efficient and has less environmental impact than refining the unsorted coarse fraction (reference scenario), a comparative life cycle assessment (LCA) was performed according to DIN EN 14040 (DIN, 2021).

3.1 Method and assumptions

The comparison requires consideration of the entire recycling chain, i.e. the mechanical and metallurgical stages. Besides the energy consumption of the individual recycling processes (sorting, remelting, refining etc.), also the additional material demand for alloy production is considered by extending the system boundary (cradle-to-gate). For the LCA, only the XRF stages 1, 2, 3 and 5 and their respective sorting products are observed: Cu-Al-Ni-Fe, Cu-Zn-Pb (incl. Cu-Zn), Cu-Sn-Zn-Pb (incl. Cu-Sn) and Cu. As this recycling system generates multiple outputs (Cu-Al-Ni-Fe is remelted to aluminium bronze alloy *CuAl11Fe6Ni6*, Cu-Zn-Pb is remelted to special brass alloy *CuZn32Al2Mn2Fe1*, Cu-Sn-Zn-Pb is remelted to red brass alloy *CuSn5Zn5Pb5*, Cu and the sorting residues are refined to copper cathodes), the LCA refers to a combined functional unit. To ensure comparability, it is assumed that the same amount of copper alloys is also produced in the reference scenario.

3.2 Results

Under the assumptions made, SBASC of the coarse fraction using an XRF sorter reduces the cumulative energy demand (CED) by about 25% and the global warming potential (GWP) by about 21% compared to the reference scenario, in which the entire material is refined (see Fig. 3).

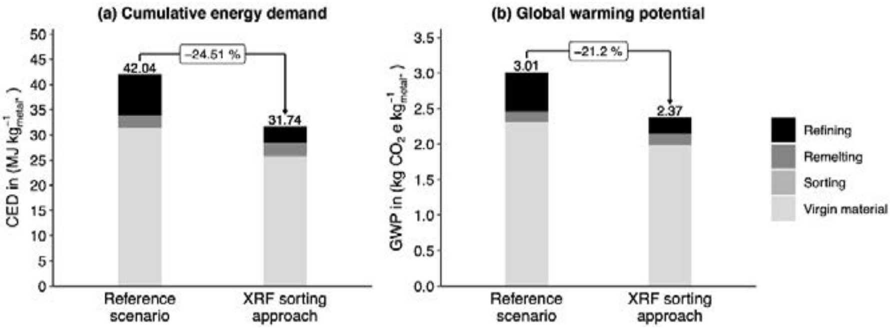

*Fig. 3. Results of the comparative LCA (*1 kg metal consists of 0.856 kg Cu, 0.078 kg Zn, 0.015 kg Sn, 0.010 kg Al, 0.011 kg Fe, 0.004 kg Ni, 0.023 kg Pb & 0.003 kg Mn (equal to 0.35 kg copper cathodes & 0.65 kg copper alloys)*

The major savings are achieved by remelting the three alloyed sorting products and therefore direct recycling of the alloying elements (Zn, Sn, Ni, Mn, Al, etc). At the same time, less refining is needed which results in a significantly lower energy demand and thus less emissions. The impact of the energy consumption needed for the mechanical sorting stage (operation of sorting machines, wheel loader, etc.) is negligible.

4 Conclusions and outlook

In light of decarbonization ambitions, increasing scarcity of resources and/or rising regulatory requirements, optimization of recycling processes and thus more sustainable metal production is inevitable. Using the mixed coarse fraction from copper alloy production residues as an example, the results of the comparative LCA confirm the environmental benefits of using XRF sorting systems prior to metallurgical recycling processes. By enabling more direct recycling through remelting, XRF sorting contributes to increased resource efficiency, a reduced CO_2 footprint and an increased security of metal supply. A detailed evaluation of this optimized recycling approach for the coarse fraction, including economic aspects, is part of ongoing research.

References

Deutsches Institut für Normung (2021). Environmental Management – Life Cycle Assessment – Principles and framework (ISO 14040:2006 + Amd 1:2020; German version EN ISO 14040:2006 + A1:2020. ICS 13.020.10; 13.020.60. Beuth Verlag.

Elshkaki, A., Graedel, T. E., Ciacci, L. & Reck, B. K. (2016). Copper demand, supply, and associated energy use to 2050. Global Environmental Change 39, 305-315. Elsevier. http://dx.doi.10.1016/j.gloenvcha.2016.06.006

Hillmann, C. & Lüning, J. (2023). Utilization of residues from the non-ferrous industry for secondary Cu/Zn concentrate. Proceedings European Metallurgical Conference 2023 (Band 1). GDMB Gesellschaft der Metallurgen und Bergleute e.V. 2023. ISBN: 978-3-935797-35-1

Kilicarslan, A., Saridede, M. N., Stopic, S. & Friedrich, B. (2014). Use of ionic liquid in leaching process of brass wastes for copper and zinc recovery. International Journal of Minerals, Metallurgy, and Materials (21), 138–143. https://doi.org/10.1007/s12613-014-0876-y

Schlesinger, M. E., Sole, K. C., Davenport, W. G. & Alvear Flores GRF (2022). Extractive Metallurgy of Copper (Sixth Edition). Elsevier. https://doi.org/10.1016/B978-0-12-821875-4.00011-0

Unlocking the Potential of Sensor-Based Sorters using Data-Driven Insights

Christian Korsten[1]

1 TOMRA Sorting GmbH, Product Management Mining Digital, Wedel, Germany

* Corresponding Author: christian.korsten@tomra.com

Keywords: Data analytics, Optimization, anomalies, customer value, cloud-based service

Abstract

Sensor-based sorters have revolutionized the way industries handle mineral processes, offering increased efficiency, precision and reduced operational costs. This abstract explores the pivotal role of data in maximizing the potential of these sorters and ensuring optimal performance. Their effectiveness of the various sensors relies on data collection, analysis, and interpretation, influencing every stage of the sorter's operation. Data-driven techniques calibrate and configure sorters during installation for accurate sorting, with real-time data continuously collected and processed for instant reactions to changing conditions. Data analytics identify sorting process patterns, allowing customers to fine-tune for improved efficiency. Historical data analysis predicts maintenance needs, reducing downtime and costs. Remote monitoring and control systems, empowered by data, enable customers to manage their sorter operations from anywhere. Real-time alerts and notifications ensure prompt responses to anomalies or breakdowns, further minimizing downtime and maximizing productivity. In conclusion, data is crucial for sensor-based sorter success, ensuring optimal sorting accuracy, cost reduction, and sustainability. Future advancements in sensor technology and data analytics promise even greater optimization opportunities. Integrating data-driven solutions like TOMRA Insight into sorters is critical for achieving operational goals effectively.

1 Introduction

Sensor-based sorting is attracting increasing interest in various industries. In recent years, more and more equipment has been installed in high-capacity production environments (Robben & Wotruba, 2019). The various suppliers of sensor-based sorting systems are integrating these sorters into complex processes where optimal operation depends on experience, such as in recycling and mining (Jacoby, 2022). Customers are getting used to the operation of sensor-based sorting systems and are starting to gain experience in operating them. It is possible to integrate the systems into the plant control using standard industry interfaces like Open Platform Communications (OPC) and Modbus. But is this data transfer sufficient to operate the systems optimally? Can it be used for plant optimization? Sensor-based sorting systems generate an unprecedented amount of data, including material characteristics, sorter health information and equipment performance. Operational effectiveness depends heavily on the analysis and interpretation of this machine data.

Throughout the history of sensor-based sorting, the focus has been on the sorting decision. A lot of data was broken down to a yes or no result, eject or non-eject. This was necessary to make a decision in milliseconds with the computing power available at the time. As a result, only limited machine data and information was made available to customers. With the development of computing power and additional software tools, this is now changing without neglecting sorting. It is now possible to use data in parallel to make processes visible and transparent. It must now be used. Data plays a key role in every stage of the sorter's operation, from initial setup to ongoing maintenance and optimization. During installation, sensor-based sorters are calibrated and configured using data-driven techniques to ensure accurate sorting. In addition, real-time data is continuously collected and processed as materials pass through the sorter, allowing immediate response to changing conditions.

The following sections summarize the types of data and measurements that are necessary to assist our customers in the use of our sensor-based systems.

2 How to unlock the potential

One way to unlock the potential of a sensor-based sorter is to integrate it with a cloud-based customer portal to make the data transparent and accessible to all stakeholders. At TOMRA, we have our cloud-based customer portal, called TOMRA Insight, to give our customers secure, easy, and fast access to the data their equipment generates during operation, but also to give them access to additional services and information around their sorters. TOMRA Insight provides the customer with unprecedented near real-time visibility into the sorting process (TOMRA eBook, 2023). This visibility is invaluable, allowing authorized personnel to remotely monitor their operation and make timely decisions based on live data from anywhere, at any time. Whether tracking throughput, identifying bottlenecks, or monitoring sorting accuracy, customers gain a comprehensive understanding of the sorter's performance. Remote teams and TOMRA experts can seamlessly collaborate, share data, and gain insight into the efficiency of the sorting process, by looking on the near-real time data and historical data.

3 The type of data is important

Data at Rest and Data in Motion refer to different states of data within a system, and understanding these concepts is critical to ensuring the security and functionality of a sensor-based sorter in a cloud-based customer portal (cf. Fig. 1).

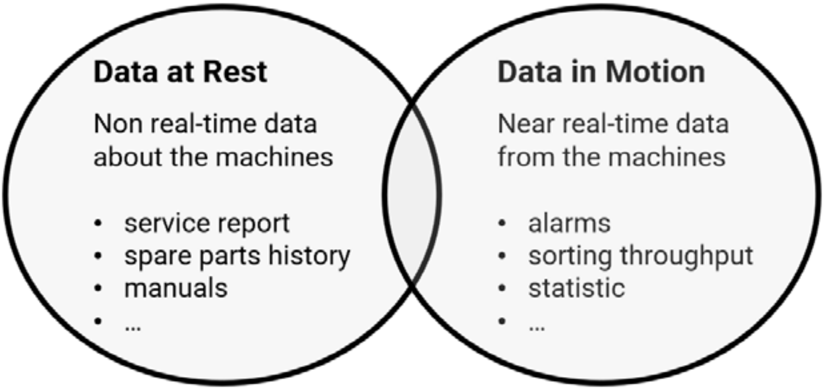

Fig. 1: Types of digital data, differences between Data at Rest and Data in Motion [TOMRA eBook, 2023]

Data at rest (non-real-time data) or machine-related data often includes documentation, service, and operator manuals. Operators and technicians no longer need to waste time searching for the right machine documentation because it is digitally available on their mobile devices.

On the other hand, *data in motion* refers to information that is actively being transmitted or moved between systems, networks, or components. In the context of a sensor-based sorter in a cloud-based customer portal, this includes real-time data from sensors.

Currently, at TOMRA, we have categorized the data in motion for our systems into the following categories [3]:

- Material composition statistics,
- Analytical statistics,
- Production statistics, and

Machine health data.

3.1 Material Composition Statistics

This information allows users to monitor trends, e.g., in the composition of incoming material (Fig. 2), showing purity levels and detected defects (TOMRA eBook, 2023). Accurate material composition data ensures that the final product meets specified requirements. It allows continuous monitoring of the sorting process. Any deviations or anomalies can be quickly identified, allowing timely adjustments and minimizing production downtime.

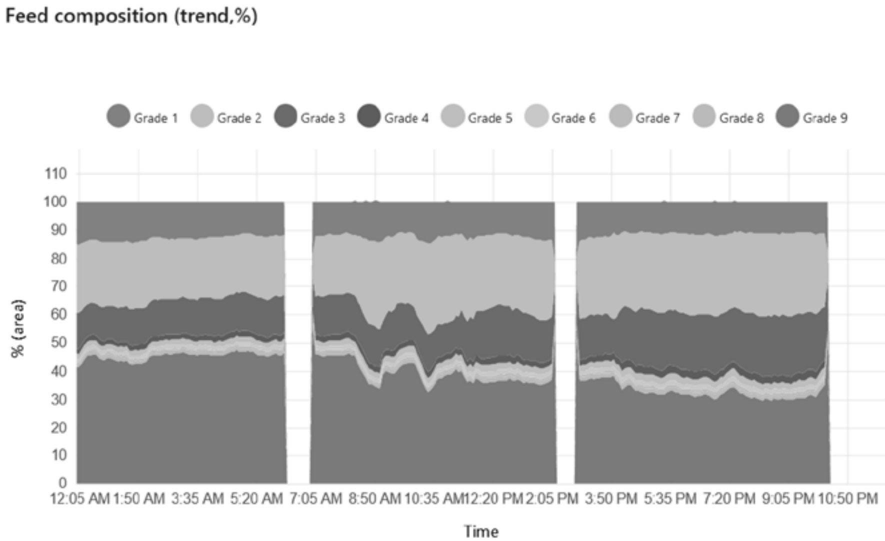

Fig. 2: Exemplary visualization of Feed Composition (TOMRA Insight portal). Changes over time in the composition gives feedback on the feed quality.

3.2 Analytical statistics

This type of statistics helps the user optimize the use of the sensor-based sorter. For example, particle size distribution statistics (Figure 3) can be used to identify material preparation challenges. Belt occupancy information (Fig. 4) can be used to identify infeed blockages or to optimize material distribution across the full sorting width. These metrics are an excellent tool for monitoring whether your machines and processes are running optimally (TOMRA eBook, 2023).

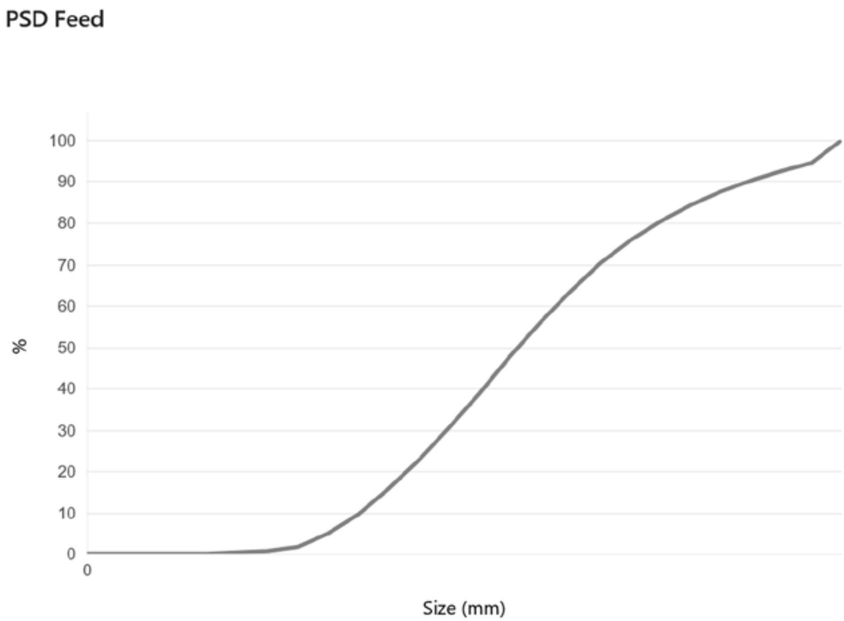

Fig. 3: Exemplary visualization of a PSD (Particle Size Distribution) (TOMRA Insight portal)

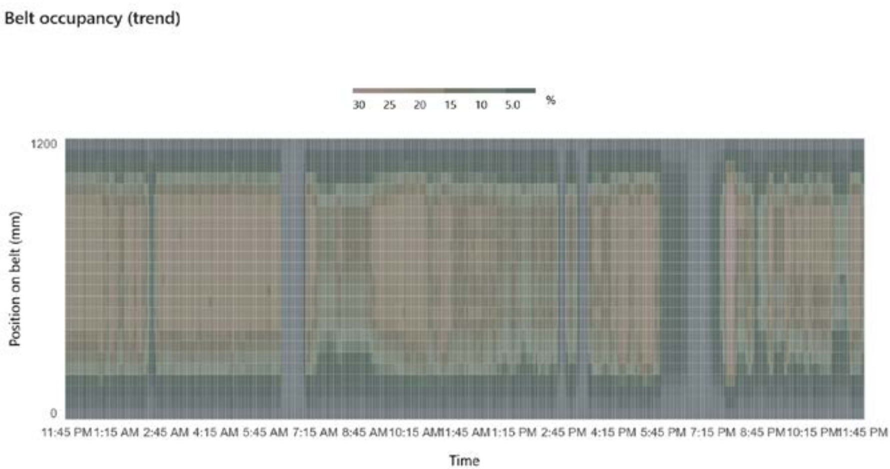

Fig. 4: Exemplary visualization of belt occupancy visualized as heatmap (TOMRA Insight portal)

3.3 Production Statistics

Actual sort statistics visualize calculated sort fractions in different metrics. Examples include:

- Monitoring of trends in capacity (Fig. 5),
- Monitoring of changes in ejection over time based on different input materials,
- Summary of production data for selected periods (Fig. 6).

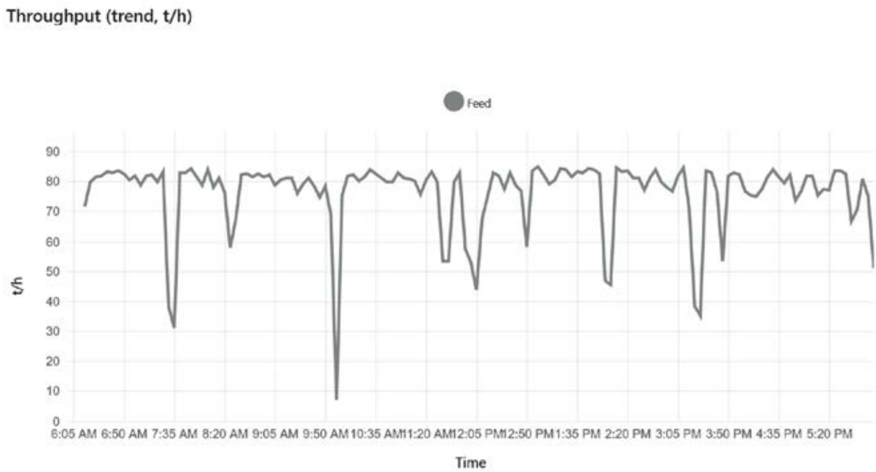

Fig. 5: Exemplary visualization of throughput changes over time (TOMRA Insight portal)

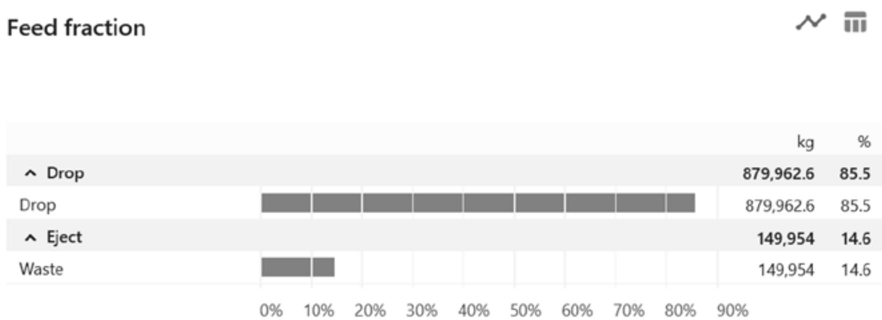

Fig. 6: Exemplary visualization of a feed fraction as a mass balance (TOMRA Insight portal)

3.4 Machine health data

While a sorter is running, it generates data not only about the product being sorted, but also about its own operating status, availability, and condition. Collected data such as vibration, temperature, air pressure (Fig. 7), and light intensity, combined with machine alarms and warnings, allows for machine performance and prediction of machine part failure (TOMRA eBook, 2023). This type of data helps prevent unnecessary downtime.

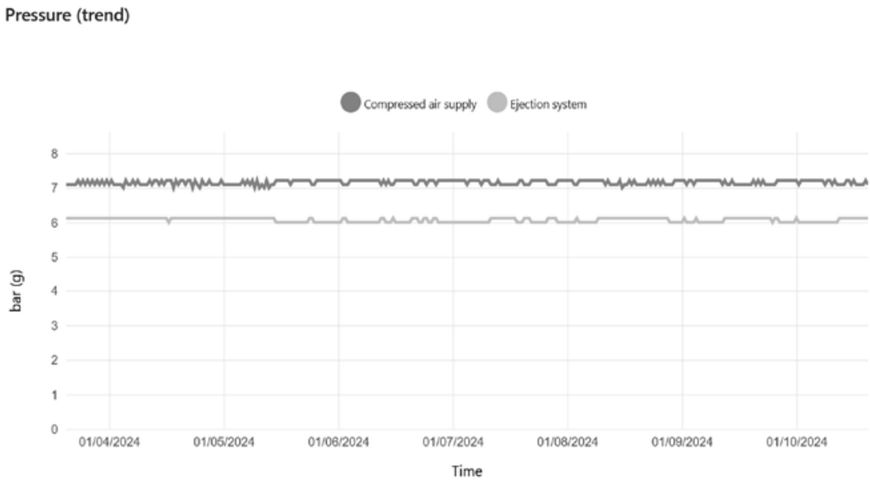

Fig. 7: Exemplary visualization of Air Pressure (TOMRA Insight portal)

Overall Equipment Effectiveness (OEE) is a key performance indicator used in manufacturing and other industries to assess the efficiency and productivity of equipment and processes. The importance of OEE lies in its ability to provide a comprehensive view of how well a production system is performing. Using information from the sorter, it is possible to provide feedback to the customer on availability, performance, and quality. It provides a single, easy-to-understand metric to evaluate how well a machine or process is running. In particular, the visualization of losses helps to identify specific areas for improvement (Fig. 8).

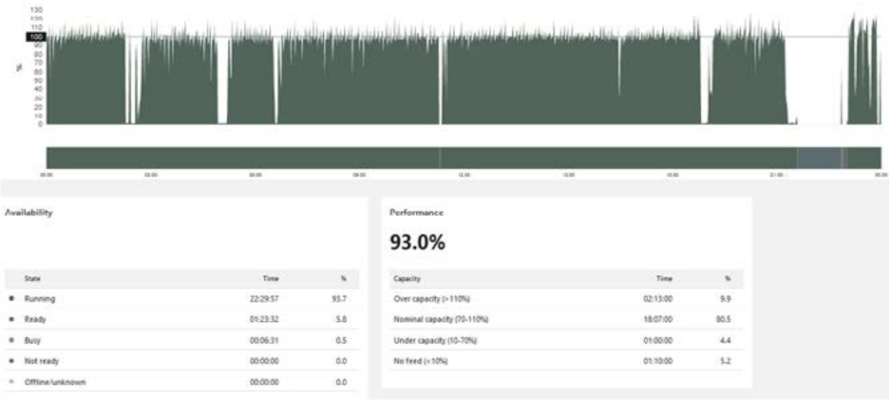

Fig. 8: OEE (Example for Availability and Performance in TOMRA Insight Portal)

4 Anomaly Detection for Early Problem Solving (Rapid Response Mechanisms)

The combination of the above-described information the machines can deliver and the use of intelligent notifications and other visual alarms helps our customer in the daily use of the sorters. It is important to take faster action when a problem occurs. Timely detection and reaction of anomalies is critical to prevent downtime and optimize production in mining operations. Anomaly detection algorithms, when integrated with sensor-based sorting technologies, enable rapid response to equipment malfunctions, process deviations or material inconsistencies. This proactive approach increases overall reliability and maintains consistent output quality.

5 Conclusion & Summary

In conclusion, combining sensor-based sorters with advanced data-driven solutions has made material sorting in various industries more efficient, accurate and cost-effectiveness. The technologies itself have significantly changed how we recycle, mine, and process food. Various sensors play a crucial role in detecting and separating materials based on their properties. From initial calibration and configuration to ongoing maintenance and optimization, data-driven techniques ensure accurate sorting. Real-time data collection and processing enables immediate responses to change conditions, promoting adaptability and improving overall system performance.

Today, however, it is important to make the data visible and to work closely with the customer when dealing with sensor-based sorters. With today's capabilities, it is possible to make much more data available to all parties involved in near-real time from the initial yes/no decision, and our TOMRA Insight solution is a great platform to present the now available additional information to the customer.

Beyond the operational aspects, data analysis is proving to be a powerful tool for customers. Identifying patterns and trends in sorting processes enables continuous improvement in accuracy and efficiency. Historical data analysis helps predict maintenance needs, reduce downtime, and optimize operating costs. In addition, data-driven strategies reduce environmental impact by promoting waste reduction, recycling optimization, and resource recovery.

To unlock the full potential of sensor-based sorters, integration with cloud-based customer portals is key. The TOMRA Insight platform example this approach, providing secure access to machine data and additional services. Transparency into the sorting process provides unparalleled visibility, enabling remote monitoring and informed decision-making in real time. The categorized data, which includes material composition statistics, analytical statistics, production statistics, and machine health data, provides a comprehensive understanding of sorter performance.

Overall Equipment Effectiveness emerges as a critical performance indicator, providing a holistic view of equipment and process efficiency. Visualization of losses helps identify specific areas for improvement, enhancing the overall assessment of machine performance.

In the quest for operational excellence, anomaly detection becomes paramount. Rapid response mechanisms, facilitated by intelligent notifications and alarms, ensure early problem solving. This proactive approach not only increases reliability, but also maintains consistent output quality, which is critical to the success of sensor-based sorting technologies.

Looking ahead, the future holds exciting prospects as sensor technology and data analytics continue to advance. The integration of data-driven solutions, such as

TOMRA Insight, will play a key role in helping customers achieve their operational and sustainability goals.

References

Robben, C.; Wotruba,H. (Germany, August 2019). Sensor-Based Sorting Technology in Mining – PAST, Present and Future, https://www.mdpi.com/2075-163X/9/9/523

Jacoby, J., (Aachen, March 2022). Circular Economy Empowered by Data. In Proceedings of the Sensor-Based Sorting Conference

TOMRA eBook (2023). When sorters become data generating machine – https://www.tomra.com/en/mining/media-center/download/2022/ebook

The RockDataAcademy: an open-access knowledge base covering the ins and outs of using sensors to scan ores and rocks

Marinus Dalm[1*]

1 RockDataWorks, Rijswijk, The Netherlands

* Corresponding Author: m.dalm@rockdataworks.com

Keywords: Sensor-based sorting, ore sorting, real-time sensing, mining, knowledge base, learning

Abstract

In current mining procedures a relatively small percentage of the mined material is sampled and chemically assayed, and the results are only representative on volumes produced over multiple days to months. On shorter time scales, this could lead to incorrect decisions on for example ore-waste designations, meaning that ore grade materials are sometimes dumped on waste piles. The issue of sampling representativity is significantly reduced if real-time sensors would be used to scan a much larger part of the mined material. It is expected that such an approach can significantly improve resource efficiency, which is critical in securing a mineral resource supply for future generations.All sensor technologies have restrictions on the minerals and/or elements that can be detected of inferred. This is caused by the physical mechanisms behind the technology and depends on mineral concentration and compositional heterogeneity of the ore. Since nearly every ore deposit in the world is unique in composition and characterized by different geological features that drove mineralization, no one-size-fits-all sensor solution is available. This makes it difficult for mining professionals to find suitable sensing technologies that can help them solve problems and improve processes for their specific ore types. To bridge the gap between ore sensing research, sensor technology providers, and mining industry, an open-access knowledge base is being developed covering all

the ins and outs of using sensors to scan ores in mining. The goal is to support development and integration of ore sensing applications and thereby contribute to a more sustainable utilization of mineral resources.

1 Introduction

More and more mining companies are becoming aware of the potential benefits of sensor-based ore sorting and process optimization. This is reflected by a growing number of sensor systems that are available on the market for applications such as drill hole logging, conveyor belt scanning, sensor-based ore sorting, mine wall scanning, etc.. In order to evaluate and compare the potential benefits of these systems for a specific mining operation, it is important to understand what kind of information is supplied by the sensor and how it can be used to improve mining processes. Regarding the sensor this requires knowledge on how information is derived from the raw sensor data, how the measurements represent the material, and which limitations apply. For process improvement understanding is required on what the current source of information is on the composition of mined materials and how this represents the mined ore volumes.

Little information is currently available for mining professionals on how to evaluate and benchmark sensor technologies and applications for scanning ores. Instead, they need to rely on technology suppliers to correctly inform them on the feasibility of sensor systems for their specific ore types and problems. However, technology suppliers may be biased in their evaluations and may not fully understand the implications associated with scanning ore materials with variable and heterogeneous composition.

In order to support further development and integration of ore sensing applications, there is a need for an independent platform where mining professionals can acquire more information and knowledge on real-time sensing opportunities. This paper aims to address some of the key concepts associated with using sensors to scan ores in mining and launches an initial version of such a platform.

2 Current source of ore grade information

In metal mining excavated materials are usually designated as ore or waste based on inspection by a geologist, resource model estimations, and grade control samples. The resource model is produced by mapping the geology and performing geochemical analysis on samples that are commonly collected through drilling. In the model, an ore deposit is often represented as a three-dimensional array of blocks and the characteristics of each block are estimated from the samples by using a geostatistical approach (Sinclair & Blackwell, 2002; Rossi & Deutsch, 2014). The appropriate size and shape of the blocks mainly depends on the spacing of the samples, the size of geologic features, and the required precision of the block estimates. Additionally, mine engineering requirements such as bench height and equipment size can affect the chosen block size (Rossi & Deutsch, 2014).

A large portion of the samples that are used to create the model are collected during the exploration of an ore deposit. Sampling is aimed at determining the quantity and distribution of metals that define ore value and potential mining profitability. Collecting samples is an expensive process since it often requires drilling in environments that are not easily accessible. Because of this, the number of samples is gradually increased and carefully balanced against the precision of the resource model (Sinclair & Blackwell, 2002; Koppe et al., 2017; Drumond et al., 2020). The goal is usually to permit classification of the deposit for reporting as a certain type of ore resource or reserve, as defined by mining standards and codes such as JORC (JORC, 2012). Sample number requirements to obtain a certain precision heavily depend on the geologic complexity and continuity of the mineralization that formed a deposit, and therefore differs between deposit types.

When a mine is in early production, resource models are often based on thousands of samples collected from a regular grid of drill holes at a spacing that is usually in the order of tens of meters. Analyses are performed to proof that the models provide reliable estimates of the entire mineral resource, and can be used to develop a long-term mine planning. However, precision of the estimates of the individual blocks of a model is usually poor and unrepresentative of ore grade variations at scales below monthly mined volumes (Sinclair & Blackwell, 2002; Rossi & Deutsch, 2014). For many mining operations such modelling performance is sufficient since it permits production planning and reconciliation on a monthly or quarterly basis, which meets their reporting periods to investors.

As mining progresses, resource models are usually updated with production data and additional grade control samples. These grade control samples are obtained by additional drilling or by sampling cuttings from so called blast holes that are drilled for charging with explosives. Updating the model with grade control samples allows the block size to be reduced and increases model precision to permit representative estimation of daily to weekly mined volumes (Rossi & Deutsch, 2014). The improved model based on grade control samples is often also referred to as the grade control model.

Since grade control sampling is performed while the mine is operating and required to meet certain production targets, there are strict time constraints on the collection of these samples. Additionally, the geochemical analysis of samples by laboratories is also under pressure because the results need to be available as soon as excavation of the targeted blocks starts. Because of these time constraints, the number of collected grade-control samples does not always meet the requirements for obtaining representative block estimates. Investments in grade control may also depend on the performance of the mining operation and the need to improve production rates.

The significance of grade control sampling also depends on the characteristics of the portion of the deposit that is being mined. If mining is taking place in a zone where the resource model indicates a high confidence that ore grades are well above or below the economic cut-off grade that defines ore and waste, grade control sampling probably won't affect decisions on ore-waste designations. However, apart from distinguishing between ore and waste many mines also distinguish different ore types based on grade, the presence of toxic components, oxidation state, or the occurrence of deleterious minerals that affect metal extraction. In this case, grade control also plays an important role in providing mineral processing facilities with the correct ore types in order to operate efficiently. Grade control is sometimes also performed during or after excavation by sampling of blasted ore piles, truck loads, conveyor belts, or stockpiles. In this case, ore grades can no longer be estimated by geostatistical approaches based on geological features and ore grade continuity because no spatial information is available for the selected samples. Instead, the principles of sampling theory to obtain representative results for bulk material volumes are important here (Abzalov, 2016). If properly executed, bulk grade information can still be fed back into the resource model for reconciliation purposes and improvement of future estimates.

3 Real time sensing techniques and applications

Sensors can be used at all stages of the mining value chain to assist in the rapid characterization of the composition of ore materials. Figure 1 presents an overview of this value chain and the various sensor opportunities that exist. Certain mines already use some of the applications in this figure or are developing them together with technology providers. However, all mines can likely further improve their processes by implementing more sensor applications.

Real-time sensing applications are defined here as those that acquire information about the properties of a material without physically removing samples or sample preparation and within a time period that allows the information to be used for decision making (Dalm, 2018). The “real-time” scanning speed in this context depends on the target of decision making. This can vary from scanning ore particles within several milliseconds for particle-by-particle sorting to mapping a rock pile within a few hours to allow the information to be used for grade control and production planning.

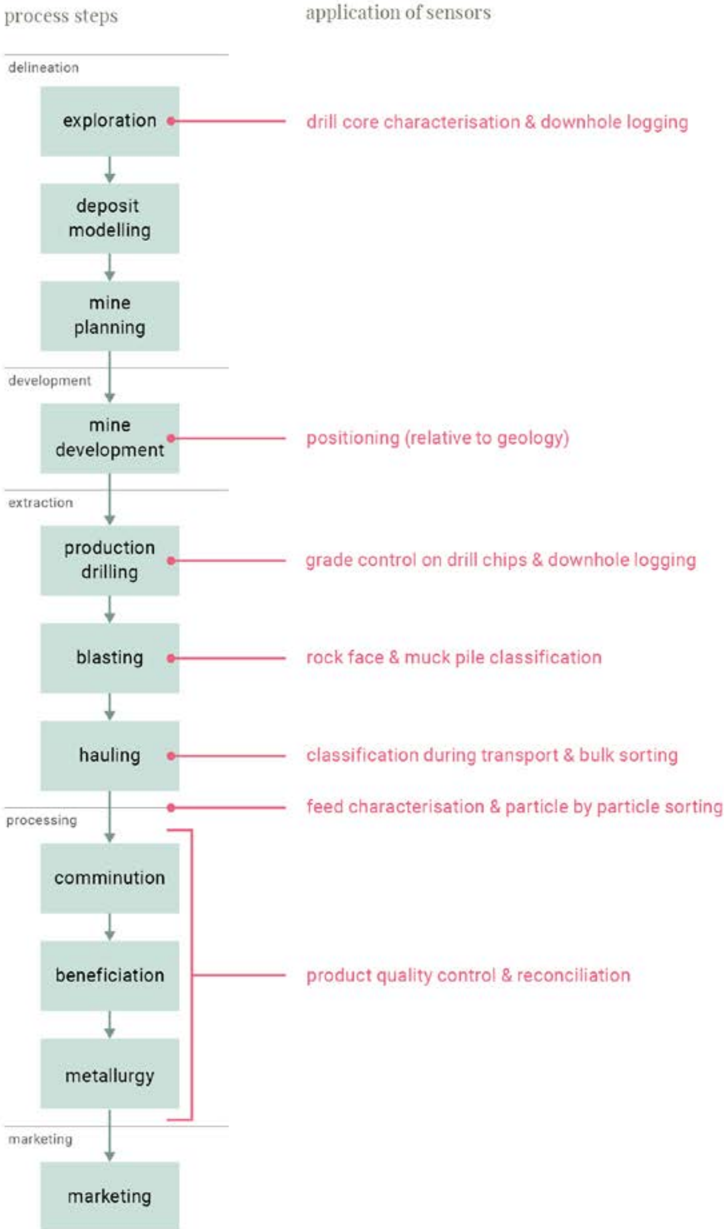

Fig. 1: Opportunities for sensor applications in the mining process (Dalm, 2018).

A variety of sensor systems is currently available on the market for the applications shown in figure 1. All of these systems rely on a specific sensing technology that can be used to detect a material property such as colour, density, mineralogy, or chemical elements. Table 1 presents an overview of material properties that can be detected with the sensing technologies on which most commercially available scanning systems rely.

All of the technologies shown in table 1 have restrictions on the minerals and/or chemical elements that can be detected of inferred. This is caused by the physical mechanisms behind the technology and depends on mineral concentration and compositional heterogeneity of the ore. The X-ray fluorescence (XRF) technology for example can be used to detect the concentration of chemical elements in a material. The ability to detect a certain element is first of all limited by the concentration, since a minimum quantity is required in order to receive a signal from that element. This phenomenon is also referred to as the detection limit. The detection limit is not the same for all elements, meaning that certain elements can be detected at lower concentrations than others. Additionally, all elements with atomic weights that are lighter than magnesium cannot be detected with XRF at all (Beckhoff et al., 2007).

The detection limit of an XRF sensor is also affected by the spot size on which measurements are performed in relation to the crystal or grain size distribution of the individual minerals within the rock. If this spot size is small (e.g. several millimetres in diameter), it is likely that elevated concentrations of certain minerals occasionally occur within that spot. This means that very low concentrations can sometimes still be detected by taking a sufficient number of measurements at different positions throughout the surface of a rock or ore pile.

Another effect that influences the detection capabilities of an XRF sensor is the so called matrix effect. The matrix effect is a phenomenon in which the measured signal of a certain element depends on the overall composition of the material. For a fixed concentration of 1% copper for example, a different signal intensity is measured when it is within a mixture of sulphide minerals than when it is in a mixture of oxide minerals. Such a dependency on overall composition can be accounted for through calibration of the sensor on representative samples. However, this may require a significant amount of work to be done before the sensor can be used for measuring composition of any ore material. This is especially the case when many different rock types occur at a certain mineral deposit since all compositional variability should be included in the sample set on which calibration is performed.

All mineralogical and chemical sensor technologies listed in table 1 are affected by detection limits and matrix effects. Because of this, feasibility studies are always needed to determine whether a certain sensor can be used to detect the material properties of interest for a specific ore deposit. Additionally, it needs to be investigated if sufficient precision can be achieved in order to improve material classification and decision making.

Physical property	**Sensor technology**	**Measured effect**	**Detected material property**
Reflectance	Reflectance spectrometry (UV-VIS-NIR-SWIR-MWIR-LWIR-FIR)	Mineral absorption features	Mineralogy
	RGB imaging	Visible appearance	Visible appearance
Luminescence (emission)	LIF & XRL	Mineral fluorescence	Mineralogy
	Raman	Raman scattering	Mineralogy
	XRF & LIBS	Atomic fluorescence	Chemistry
	PGNAA & Natural radioactivity	Atomic radioluminescence	Chemistry
Incandescence (emission)	TI	Blackbody radiation	Heat capacity & transfer
	MWTI	Blackbody radiation after microwave heating	Heat capacity & transfer
Transmitted radiation	DE-XRT & DE-γRT	Transmitted X-rays / γ-rays	Density
	MWT	Transmitted microwaves	Moisture content
	Thz-TDS	Transmitted terahertz radiation	Absorption & refraction index
Electric conductivity	Inductive	Changes in electromagnetic field	Electric conductivity

4 Considerations on data precision

4.1 Current practice

For both the generation of resource models as well as the sampling of excavated bulk ore volumes, theories exist that link sampling procedures to the precision of the obtained results. For the generation of resource and grade control models, the uncertainty of block estimates can be related to drill hole spacing and the used block geometry (Koppe et al., 2017; Afonseca & Miguel-Silva, 2022). Considering resource models, it is usually acceptable if the estimates of ore grade and tonnage are ±15% at a 90% confidence interval over a monthly or quarterly period (Afonseca & Miguel-Silva, 2022). For grade control models, it is more common to balance the costs associated with the misclassification of ore and waste blocks to the costs of acquiring more samples (Afonseca & Miguel-Silva, 2022; Martínez-Vargas, 2017). Single block misclassification rates of around 10% are normal in this case.

Overall, the precision of ore grade information depends strongly on the sampling density and the geologic complexity of the ore deposit. The combined volume of all samples that are gathered during the life of a mine usually represents only 0,001% to 0,0001% of the entire deposit (Sinclair & Blackwell, 2002). When ore volumes in the order of monthly or yearly productions are considered, such a low representativity is acceptable because the drill holes from which samples are acquired are well spread throughout the entire volume. For smaller volumes though, accurate ore grade estimations become increasingly more difficult because the distribution of samples is less representative. This can be mitigated through a well-defined grade control strategy, which can provide representative estimations for volumes produced over one or several days. However, for hourly mine productions the uncertainty of ore grade information is considered to be relatively high. This is especially the case for deposits with a high degree of heterogeneity where the geological features that drove mineralization are smaller than the drill hole spacing at which samples are collected. This is common for many hydrothermal ore deposits where mineralization takes place along veins and fractures with widths in the order of several centimetres, while the drill hole spacing is multiple meters (Pirajno, 1992; Afonseca & Miguel-Silva, 2022). This means that when mining takes place in a zone where grades are close to the cut-off grade, frequent misclassification of ore and waste likely takes place for small batches such as truck loads or hourly productions.

In the case of bulk ore sampling, the relative sampling variance due to fundamental sampling error can be related to the mass, mineralogy, particle size distribution, and heterogeneity of the ore (François-Bongarçon & Gy, 2002; Minkkinen & Esbensen, 2019; Abzalov, 2016). A relative standard deviation <10% on the obtained results is often considered acceptable (Abzalov, 2016; Thompson & Howarth, 1978).

4.2 Potential improvements with real-time sensing

The improvement on data precision that real-time sensors can provide is related to the high speed at which data can be gathered with the currently available sensing technologies. This provides opportunities to greatly enhance sampling representativity on large volumes of ore material, which is considered to significantly decrease sampling errors. An example of how sensors can improve data precision is on the sampling of blast holes in open pit mining for the generation of grade control models. This is currently performed by physically taking a sub-sample of the cone of cuttings produced from drilling in order to determine ore composition along the entire depth of the drilled hole. However, it is also possible to use sensors to measure the chemical or mineralogical composition of cuttings while drilling is taking place (Timegate, 2022). Such an application can likely provide this information at intervals of several tens of centimetres of drilled depth. Considering that these blast holes are usually around 10 to 15 meters deep, this may increase the number of data points along the depth of the hole by a factor of 30 to 80. This means that more information is provided on the compositional variability of the ore within a mining block due to the occurrence of relatively small geological features, which can be used to improve the representativity of the grade control model. Additionally, the information is instantly available and it is no longer needed to wait several days until samples have been processed and analysed in a laboratory.

Another example where sensors can improve the precision of information about ore composition is conveyor belt scanning. On a conveyor belt, the surfaces of particles originating from a mining block will be exposed and can be scanned with various sensor technologies. A typical mining block in open pit mining of 25 x 25 x 15 meter represents a volume of 9 375 m^3 and a weight of around 25 000 tonnes at a common rock density of around 2,7 g/cm^3. At large open pit operations conveyor belt transport speeds can typically reach 5000 tonnes per hour, meaning that it takes around 5 hours to transport the entire block. Certain sensing technologies, such as laser-induced breakdown spectroscopy (LIBS), can be used to take up to 100 measurements per second (e.g. Elemission, 2023). This means that over a 5 hour period, a LIBS conveyor belt scanner can acquire 1,8 million measurements that are randomly distributed throughout the volume of the mining block. Considering that a single estimate with a relatively low precision for a block results from conventional grade control models, such a conveyor belt scanning application can likely provide significant improvements in data precision.

Even though the precision of single sensor measurements is usually not as high as those of geochemical analyses performed in a laboratory, the averaging of many sensor measurements will compensate for this. Only when a bias occurs between the sensor data and the actual composition of the ore, a lower precision of the sensor data may result. However, any bias can be eliminated through well-defined calibration procedures. This is also the reason that proper calibration of sensors is extremely important when developing real-time sensing applications. Calibration needs to be performed on samples that represent all the variability of rock types that occur at a certain mine in order to account for any matrix effects that influence the sensor detections.

5 Benefits of utilizing sensors

Apart from improving the precision of currently available data on the composition of mined ores, sensors also provide more information about the compositional variability of the ore. Smaller material volumes can be characterized, which can be used for optimizing downstream metal extraction processes and bulk ore sorting to eliminate waste or separate ore types (e.g. high vs low sulphur, deleterious minerals, etc.). Additionally, data can be fed back into grade control models to enhance the precision of these models and improve the future planning of resource extraction (Dalm, 2018).

Certain sensor technologies are able to acquire data so fast that they can be used for particle-by-particle sorting on sensor-based sorting machines. On such machines, individual rock particles are scanned by sensors and are subsequently sorted by using jets of compressed air. These machines can therefore be used as a pre-concentration or pre-processing step to eliminate waste or contaminants from the feed to mineral processing facilities (Lessard et al., 2016).

The potential benefits of real-time sensing applications in mining depend heavily on the geologic complexity and grade distribution of an ore deposit. Considering the low representativity of current grade control models for relatively small material volumes, it is expected that significant improvements in material classifications and ore-waste designations are possible. This is also shown by the work of Buxton & Benndorf (2013), who present a semi-quantitative analysis of the potential economic benefits of various sensor applications. However, apart from economic benefits there are also potential benefits in terms of resource utilization. This is because improvements in ore-waste designations results in a lower amount of ore being dumped on waste piles, and therefore increases the total metal recovery from ore deposits. Such improvements in resource utilization are likely critical in securing a mineral resource supply for future generations.

6 Conclusions

Compositional information about the materials that are being excavated at most metal mines around the world is only representative on scales ranging from multiple days to monthly produced volumes. On smaller scales such as hourly production rates or truck load volumes, uncertainties on the available information such as ore grade are high. This likely leads to regular misclassification of small batches as ore or waste, resulting in metal losses and wasted energy on processing barren materials.

Various sensor applications are available nowadays that are able to significantly improve the precision of compositional data for relatively small ore volumes. All of these systems rely on a certain sensing technology such as the ones presented in table 1. The feasibility of each of these technologies to detect a specific material property of interest such as ore grade strongly depends on the characteristics of the ore deposit at which they are applied. Since nearly every ore deposit in the world is unique in composition and associated with different geological features that drove mineralization, no one-size-fits-all sensor solution is available. This makes it difficult for mining professionals to find sensing technologies that can help them solve problems and improve processes for their specific ore types.

To bridge the gap between ore sensing research, sensor technology providers, and mining industry, an open-access knowledge base is being developed covering all the ins and outs of using sensors to scan ores in mining. It aims to address topics such as the benefits of ore scanning and sorting, selecting suitable sensing technologies for specific ore types, investigating analyser and sorter feasibility, sensor data analytics and calibration, and data-driven process optimization. It will also list and categorise sensor equipment suppliers by scanning application and type of sensor technology. The platform will be completely free and accessible for everyone. The goal is to support development and integration of ore sensing applications in mining and thereby contribute to a more sustainable utilization of mineral resources.

The first version of the knowledge base is available at:

https://rockdataworks.com/rockdataacademy/.

References

Abzalov, M. (2016). Applied mining geology (Vol. 12). Switzerland: Springer International Publishing.

Afonseca, B. C., & Miguel-Silva, V. (2022). Defining optimal drill-hole spacing: A novel integrated analysis from exploration to ore control. Journal of the Southern African Institute of Mining and Metallurgy, 122(6), 305-315.

BECKHOFF, B., KANNGIEßER, B., LANGHOFF, N., WEDELL, R. & WOLFF, H. 2007. Handbook of practical X-ray fluorescence analysis, Springer Science & Business Media.

Buxton, M & Benndorf, J. (2013). The use of sensor derived data in optimization along the mine-value-chain. Proceedings of the 15th International ISM Congress, Aachen, Germany.

Dalm, M. (2018). Raw material beneficiation in mining: sensor-based sorting opportunities for hydrothermal ore deposits (PhD thesis). Available at: https://doi.org/10.4233/uuid:70a1e180-ef0c-4226-9af3-7e9dc3938c7f (accessed Nov 2023)

Drumond, D. A., Amarante, F. A. N., Koppe, V. C., & Costa, J. F. C. L. (2020). A chart for judging optimal sample spacing for ore grade estimation: Part II. Natural Resources Research, 29, 551-560.

Elemission (2023). COBRA laser process analyzer (Online). Available at: https://www.elemission.ca/cobra (accessed Nov 2023).

François-Bongarçon, D. & Gy, P. (2002). The most common error in applying'Gy's Formula'in the theory of mineral sampling, and the history of the liberation factor. Journal of the Southern African Institute of Mining and Metallurgy, 102(8), 475-479.

HUNT, G. R. (1977). Spectral signatures of particulate minerals in the visible and near infrared. Geophysics, 42, 501-513.

JORC (2012). Australasian Code for Reporting of Exploration Results, Mineral Resources and Ore Reserves (Online). Available at: https://www.jorc.org (accessed Nov 2023).

Koppe, V. C., Rubio, R. H., & Costa, J. F. C. L. (2017). A chart for judging optimal sample spacing for ore grade estimation. Natural Resources Research, 26, 191-199.

Lessard, J., de Bakker, J., & McHugh, L. (2014). Development of ore sorting and its impact on mineral processing economics. Minerals Engineering, 65, 88-97.

Martínez-Vargas, A. (2017). Optimizing grade-control drillhole spacing with conditional simulation. Minería y Geología, 33(1), 1-12.

Minkkinen, P. O., & Esbensen, K. H. (2019). Sampling of particulate materials with significant spatial heterogeneity-theoretical modification of grouping and segregation factors involved with correct sampling errors: fundamental sampling error and grouping and segregation error. Analytica Chimica Acta, 1049, 47-64.

Pirajno, F. (1992). Hydrothermal mineral deposits: principles and fundamental concepts for the exploration geologist. Berlin Heidelberg, Springer-Verlag.

Rossi, M. E. & Deutsch, C. V. (2014). Mineral resource estimation. Dordrecht: Springer. doi: 10.1007/978-1-4020-5717-5.

Sinclair, A. J. & Blackwell, G. H. (2002). Applied mineral inventory estimation. Cambridge: Cambridge University Press.

Timegate (2022). Mineralogical information with Timegated Raman in the GoldenEye project (Online). Available at: https://www.timegate.com/news/mineralogical-information-with-timegated-raman-in-the-goldeneye-project (accessed Nov 2023).

We would like to thank the following sponsors for their support:

Sponsors

Media Partners